DESIGN, SYNTHESIS AND EVALUATION OF NEW PACE4 INHIBITORS FOR PROSTATE CANCER TREATMENT

By

Vahid Dianati

Thesis presented in the chemistry department for obtaining the degree of
Doctor of Science (Ph.D.)

FACULTY OF SCIENCE
UNIVERSITY OF SHERBROOKE

Sherbrooke, Québec, Canada, January 2019

CONCEPTION, SYNTHESE ET EVALUATION DE NOUVEAUX INHIBITEURS DE PACE4 POUR LE TRAITEMENT DU CANCER DE LA PROSTATE

par

Vahid Dianati

Thèse présentée au Département de chimie en vue
de l'obtention du grade de docteur ès sciences (Ph.D.)

FACULTÉ DES SCIENCES
UNIVERSITÉ DE SHERBROOKE

Sherbrooke, Québec, Canada, Janvier 2019

Le 24 janvier 2019

le jury a accepté la thèse de Monsieur Vahid Dianati
dans sa version finale.

Jury Members

Professor Yves L. Dory
Research Director
Department of chemistry

Professor Robert Day
Research Codirector
Department of Surgery/Urology

Professor William Lubell
External evaluator
University of Montreal

Professor Jean Lessard
Internal Evaluator
Department of chemistry

Professor Claude Legault
Internal Evaluator
Department of chemistry

Professor Patrick Ayotte
Committee President
Department of Chemistry

SOMMAIRE

Le présent mémoire s'intéresse à la conception, la synthèse et l'évaluation pharmacologique d'inhibiteurs peptidomimétiques de PACE4, une pro-protéine convertase. Ces composés sont étudiés comme traitement potentiel du cancer de la prostate. Le cancer de la prostate (PCa) et les traitements actuels pour le PCa sont donc passés en revue. L'introduction se poursuit par une brève évaluation des thérapies ciblées vers le PCa qui démontre que les pro-protéines convertases sont des enzymes importantes de la voie de transmission. Les inhibiteurs actuels des pro-protéines convertases ont finalement été examinés. Des études de relation structure-activité (SAR) ont été réalisées sur un octapeptide (appelé Multi-Leu; séquence: Ac-Leu-Leu-Leu-Leu-Arg-Val-Lys-Arg-NH_2) qui s'est révélé être un prototype d'inhibition de l'enzyme PACE4. Ce composé a ensuite évolué par le remplacement du résidu Arg en position C-terminale par un résidu Amba (4-amidinobénzylamide) d'une part et par l'introduction d'une DLeu au lieu d'une l-Leu en position P8 d'autre part. Le nouvel inhibiteur appelé C23 (séquence: Ac-DLeu-Leu-Leu-Leu-Arg-Val-Lys-Amba) présentait une activité améliorée vis-à-vis de l'enzyme PACE4 et de bons résultats *in vitro* dans des essais cellulaires antiprolifératifs. Le but du travail présenté dans ce document est l'amélioration de l'affinité enzymatique pour l'enzyme PACE4, l'accroissement de la sélectivité par rapport à d'autres membres de la famille, en particulier la furine, et l'augmentation de l'activité cellulaire des composés prototypes en modifiant les résidus aux positions P3, P1 et P1'.

Le premier chapitre concerne les études SAR sur les résidus de P3. L'amélioration de la sélectivité et de la puissance de l'inhibiteur est l'objectif de ce chapitre. L'acide aminé Val en position P3 du peptide Multi-Leu a été remplacé par des résidus basiques pour créer des interactions supplémentaires avec un résidu Asp dans la poche S3. Un résidu basique β-ramifié dans cette position améliore la sélectivité pour PACE4 jusqu'à 40 fois (K_i = 2.7 nM).

Le deuxième chapitre traite des modifications de la position P1 du peptide prototype C23. Malgré que l'inhibiteur C23 ait une affinité, une stabilité et une activité cellulaire supérieures pour l'enzyme PACE4 par rapport à son précurseur Multi-Leu, il n'est que deux fois plus sélectif pour la convertase PACE4. La plus grande partie de cette perte de sélectivité est due aux interactions plus favorables du résidu Amba en position P1 de la furine. Par conséquent, d'autres mimétiques de l'acide aminé Arg ont été testés dans cette position pour retrouver la sélectivité perdue.

Dans le troisième chapitre, l'acide aminé en position P1' a été exploré pour discriminer les enzymes PACE4 et furine. L'addition de résidus naturels dans cette position, cependant, n'a amélioré ni la sélectivité ni l'affinité. Par ailleurs, l'évaluation cellulaire a montré que les résidus hydrophobes et basiques amélioraient l'activité cellulaire. En utilisant des acides aminés non naturels aux positions P1 et P1', l'activité antiproliférative cellulaire des inhibiteurs résultants est sensiblement améliorée. Il a été prouvé que cette meilleure activité cellulaire était due à la pénétration accrue des inhibiteurs résultant d'une hydrophobicité élevée dans la région de l'extrémité C-terminale.

En conclusion, l'affinité et la sélectivité envers la pro-protéine convertase PACE4 des inhibiteurs ont été améliorées par des modifications aux positions P3 et P1. Les résidus hydrophobes en position P1' augmentent la perméabilité cellulaire et donc l'activité antiproliférative des cellules PCa. Dans cette perspective, la combinaison de ces modifications pourrait conduire à une amélioration du profil pharmacodynamique des composés.

ABSTRACT

This thesis deals with the design, synthesis and pharmacological evaluation of peptidomimetic inhibitors of PACE4, a pro-protein convertase. These compounds are studied as a potential treatment for prostate cancer. Prostate cancer (PCa) and current treatments for PCa are therefore reviewed. The introduction continues with a brief evaluation of targeted therapies for PCa that demonstrates that pro-protein convertases are important enzymes in the secretory pathway. Current inhibitors of pro-protein convertases are reviewed at the final part of introduction.

Structure-activity relationship (SAR) studies were performed on an octapeptide (called Multi-Leu; sequence: Ac-Leu-Leu-Leu-Leu-Arg-Val-Lys-Arg-NH_2) which was found to be a prototype of inhibition of the enzyme PACE4. This compound then evolved by replacing the Arg residue in the C-terminal position with an Amba (4-amidinobenzylamide) residue on the one hand and by introducing a DLeu instead of a l-Leu in position P8 on the other hand. The new inhibitor called C23 (sequence: Ac-DLeu-Leu-Leu-Leu-Arg-Val-Lys-Amba) exhibited improved activity with respect to the PACE4 enzyme and good *in vitro* results in antiproliferative cell assays. The purpose of the work presented in this document is to improve the enzymatic affinity for the enzyme PACE4, increase selectivity over other members of the family, particularly furin, and increase the cellular activity of the prototype compounds by modifying the residues at positions P3, P1 and P1'.

The first chapter concerns SAR studies on P3 residues. Improving the selectivity and potency of the inhibitor is the goal of this chapter. The amino acid Val at the P3 position of the Multi-Leu peptide has been replaced by basic residues to create additional interactions with an Asp residue in the S3 pocket. A basic β-branched residue in this position improves the selectivity for PACE4 up to 40-fold (Ki = 2.7 nM).

The second chapter deals with the modifications of the position P1 of the prototype peptide C23. Although the C23 inhibitor has higher affinity, stability, and cell activity for the PACE4 enzyme than its Multi-Leu precursor, it is only twice as selective for the PACE4 convertase. Most of this loss of selectivity is due to the more favorable interactions of the Amba residue at the P1 position of furin. Therefore, other Arg amino acid mimetics have been tested in this position to recover the lost selectivity.

In the third chapter, the amino acid at position P1' was explored to discriminate between PACE4 and furin enzymes. The addition of natural residues in this position, however, improved neither selectivity

nor affinity. In addition, cell evaluation showed that hydrophobic and basic residues improved cellular activity. By using unnatural amino acids at the P1 and P1' positions, the cell antiproliferative activity of the resulting inhibitors is substantially improved. This improved cell activity has been shown to be due to increased penetration of inhibitors resulting from high hydrophobicity in the C-terminal region.

In conclusion, the PACE4 affinity and selectivity of inhibitors were improved by modifications in P3 and P1 positions. Hydrophobic residues in P1' position enhanced the cell permeability and thus the PCa cell antiproliferative activity. In this perspective, combining such modifications could lead to compounds with improved pharmacodynamic profiles.

ACKNOWLEDGEMENTS

I want to appreciate all the members of Yves Dory's lab since 2014 for providing such a motivating and pleasant environment which made my PhD years enjoyable and unforgettable. The main part of this unbelievable social experience was related to professor Yves Dory who supervised the present dissertation. He was not only an incredible organic/medicinal chemist but also a great mentor and a reliable friend. He was always present, and his precise advice was critical in the development of the project. I was very fortunate to have professor Robert Day as my co-supervisor as one of the greatest scientists in the field of proprotein convertases. The current study have reached this level because of his wise thoughts and comments. I want to acknowledge the writing skills of both my supervisors who revised the manuscripts of the three published research articles I wrote. My sincere gratitude goes to my supervisors for giving me the confidence and freedom in research which enabled me to show my best performance.

I want to express my gratitude to the external evaluator of this thesis Pr. William Lubell, the members of my committee Pr. Jean Lessard, Pr. Claude Legault and Pr. Patrick Ayotte for reviewing my thesis.

I would like to acknowledge the contribution of the hardworking Day lab's members in the biological evaluation of synthesized compounds. Anna Kwiatkowska, Frederic Couture and Roxane Desjardins had a major role in this regard. I had impactful scientific conversations with Anna and Fred which improved my understanding of the biology of proprotein convertases. Anna's experience and skills in peptide chemistry and HPLC systems is astonishing. She also helped me to develop my scientific writing skills. I also thank Sandra Gagnon, Anthony Dame and Nicolas Dory for their participation in performing the biological assays.

I share lots of memories inside and outside of lab with Thi Than Há Dao, Sophie Beauchemin, Thomas Marmin, Jean-Louis Beaudeau, Hojjat Seyedjamali, Yanan Zhu, Dominique Bella NDong, Pauline Navals, Alexander Foh-Dion, Laura Mourot, Niousha Nazari, Trần Minh-Huệ and Victoria Lépante. I had fruitful scientific discussions with Há, Hojjat, Sophie and Jean-Louis. I thank Niousha for English editing of the introduction and of the two last chapters. I am grateful to Pauline for the synthesis of one of the P1-modified compounds and its Arg-mimetic, and Sophie for her assistance in the synthesis of P1'

peptide library. My great appreciation goes to the other members of Dory's lab who made the work atmosphere more joyful and inviting.

I would like to thank the IPS technical staff, Marc-André Bonin for his assistance in automated peptide synthesis, Eric Marsault and his lab especially Annie Doucet, Antoine Le-Roux and Alexandre Murza for UPLC and preparative HPLC facilities and Luc Tremblay, Pierre-Luc Boudreault and Danny Létourneau for NMR assistance. I acknowledge Hugo Gagnon and Jean-Philippe Couture (PhenoSwitch Biosciences Inc.) for HRMS analysis. I also appreciate the Department of chemistry professors and staff especially Jean-Marc Chapuzet, Dr. Isabelle Dion, Lise Charbonneau, René Gagnon, Dr. Nicole Wilb and Philip Richter. This research was not possible without the financial support of Canadian Cancer Society Research Institute (701590 to R.D. and Y.L.D.) and Prostate Cancer Canada (TAG2014-02 to R.D.) and University of Sherbrooke (Faculty of science).

My deep appreciation goes to my family especially my parents whose financial and emotional support pave the way towards where I am today. I want to appreciate my wife Azar who helped me to have the opportunity of pursuing my PhD studies at University of Sherbrooke. She was not only my wife but also a friend and a good colleague. She performed the molecular dynamic simulation in chapter one under the supervision of Pr. Armand Soldera. I want to dedicate this thesis to my daughter Baran who shed a new light in our life.

TABLE OF CONTENTS

LIST OF ABBREVIATIONS

6-Cl-HOBt	6-Chloro-1-hydroxybenzotriazole
α_1-PDX	α_1-Antitrypsin Portland
Aca	(*S*)-2-Amino-3-(4-carbamimidoylphenyl)acetic acid
Acpa	(*S*)-2-Amino-3-(4-carbamimidoylphenyl)propanoic acid
ADAM	A disintegrin and metalloproteinase
ADT	Androgen deprivation therapy
AEBA	4-(2-Aminoethyl)benzimidamide
Agb	2-Amino-4- guanidinobutyryl
Agp	2-Amino-3-guanidinopropionyl
Amba	4-Amidinobenzyl amine
AMC	7-Amido-4-methylcoumarin
Ampa	5-(Aminomethyl)picolinimidamide
Apa	4-Aminophenylalanine
AR	Androgen receptor
ASIR	Age-standardized incidence rates
CP/CPPS	Prostatitis/chronic pelvic pain syndrome
CPP	Cell penetrating peptide
CRPC	Castration-resistant prostate cancer
Dab	2,3-Diaminobutyryl
Dap	2,3-Diaminopropionyl
Dec	Decanoyl
DHT	Dihydrotestosterone
DIAD	Diisopropyl azodicarboxylate
DIC	*N*,*N*'-Diisopropylcarbodiimide
DIPEA	*N,N*'-Diisopropylethylamine
DRE	Digital rectal examination
EDCI	1-Ethyl-3-(3-dimethylaminopropyl)carbodiimide;
FBS	Fetal bovine serum
ER	Endoplasmic reticulum

FACS	Fluorescence activated cell sorter
FBS	Fetal bovine serum
FITC	Fluorescein isothiocyanate
FSH	Follicle-stimulating hormone
GDF-15	Growth differentiation factor-15
Gpa	4-Guanidinophenylalanine
GnRH	Gonadorelin releasing hormone
GS	Gleason Score
HATU	1-[Bis(dimethylamino)methylene]-1*H*-1,2,3-triazolo[4,5-*b*]pyridinium 3-oxide hexafluorophosphate
HFIP	Hexafluoro-2-propanol
IGFR	Insulin-like growth factor 1 receptor
LH	Luteinizing hormone
LHRH	Luteinizing hormone-releasing hormone
MD	Molecular dynamics
MHC	Major histocompatibility complex
ML	Multi-Leu
MMP	Matrix-metalloproteases
MTT	3-(4,5-Dimethylthiazol-2-yl)-2,5-diphenyltetrazolium bromide
NMM	*N*-methylmorpholine
NOTA	1,4,7-Triazacyclononane-triacetic acid
PSA	Prostate specific antigen
PCa	Prostate cancer
SAR	Structure activity relationship
PACE4	Paired amino acids cleaving enzyme 4
PARP 1	Poly(ADP-ribose) polymerase 1
PC	Proprotein convertase
PCSK9	Proprotein convertase subtilisin/kexin type 9
PDGF	Platelet-derived growth factor
PEG	Polyethylene glycol
PET	Positron emission tomography

Phac	Phenylacetyl
PI	Propidium iodide
POPC	1-Palmitoyl-2-oleoyl-SN-glycero-3-phosphocholine
PPII	Poly-proline helix II
Pro-GDF-15	Pro-growth differentiation factor-15
PS-SPCL	Positional scanning-synthetic peptide combinatorial libraries
PTM	Post translational modifications
PyBOP	Benzotriazol-1-yl-oxytripyrrolidino-phosphonium hexafluorophosphate
R-*i*-Dab	2*S*,3*R*-Diaminobutyryl.
SRP	Signal recognition particle
SFTI-1	Sunflower trypsin inhibitor-1
S-*i*-Dab	2*S*,3*S*-Diaminobutyryl
S-*i*-Agb	2*S*-Amino-3*S*-guanidinobutyryl
SKI-1	Subtilisin/kexin isozyme-1
SPPS	Solid-phase peptide synthesis
Tle	*tert*-Leucine
TGFβ-1	Transforming growth factor beta 1
TGN	Trans-Golgi network
TRYP	Tryptamine
VEGFR	Vascular endothelial growth factor receptor
VEGF	Vascular endothelial growth factor

LIST OF TABLES

LIST OF FIGURES

LIST OF SCHEMES

INTRODUCTION

The roots of word “cancer” come from a Greek “karkinos”, as described by the Greek physician, Hippocrates (460–370 B.C). However, the earliest recorded evidence of human cancer was found in mummies in ancient Egypt about 1600 B.C.[1] The ancient Egyptians were treating surface tumors by surgically removing them with similar methods that are still under practice. According to Statistic Canada, cancer is the first cause of death in Canada followed by cardiovascular diseases.

In medicine, cancer is the accepted name for a group of diseases associated with abnormal growth of eukaryotic cells. Although many types of cancer cause the growth of solid tumors, some others such as blood carcinomas are not intrinsically solid tumors. Cancer could initiate in any organ and then spread to others by translocation of cancerous cells through the blood or lymph system. Unlike benign tumors, malignant cancerous tumors are associated with high risk of fatality usually after cells migrate to foreign tissues. Cancer cells have similarities with stem cells (non-differentiated cells) and they can begin a new tumor wherever they migrate, which is termed as *metastasis*. For instance, a breast cancer cell could migrate to the liver and grow a new tumor, but will still be called breast cancer.[2]

In general, cancerous cells develop from normal cells with a damaged DNA. Two main groups of genes which are crucial in cancer development are *oncogenes* and *tumor suppressor genes*. Oncogenes are formed by the mutation of genes of normal cells called protooncogenes. Protooncogenes control cell division and growth, hence their malfunction inevitably leads to a non-controlled cell division and growth.[2]

Eukaryotic cells have several mechanisms to repair DNA mismatches after division. Abnormal cells undergo a programmed cell death called *apoptosis*.[3] Apoptosis is initiated by certain intra- and extracellular biochemical signals. A cascade of events and reactions then results in distinctive morphological changes in the cell which are terminated by cell death. On the other hand, tumor suppressor genes control the cell division, DNA repair and regulation of apoptosis. An impairment in tumor suppressor genes function can produce a cancerous cell. Many factors such as chemicals including foods, radiation, air pollution or even certain viruses are associated with mutations or damages of tumor suppressor genes or oncogenes.[2]

Historically, the first practical treatment for cancer has been the surgical removal of tumor, but even ancient physicians had noticed the post-surgery recurrence of tumors. With the development of surgical techniques, radiotherapy emerged as a complementary therapy for cancer treatment in the early 20th century.[4] Subsequently, nitrogen mustards were discovered accidentally to serve as the first cancer chemotherapeutic agents. Nitrogen mustards were used as warfare during World War II.[5] Since then, a large number of chemotherapeutic agents has been developed. Parallel to these achievements, hormone therapy was also established for treating gender related organs tumors such as breast, ovarian and prostate cancer.

I.1. Prostate cancer

I.1.1. Prostate anatomy

The prostate is a walnut-sized gland, the main function of which is to secrete prostate fluid, a semen component (one-third of the total volume of semen). This fluid provides nutrients for sperms and facilitates their movement. During ejaculation, the muscles of the prostate gland squeeze this fluid into the urethra. The prostate gland weighs about 20 grams and is placed just beneath the bladder.

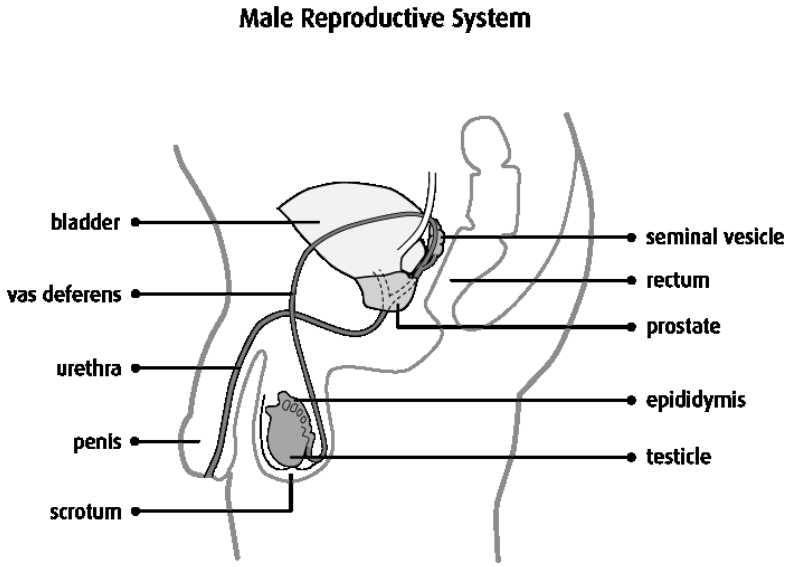

Figure 1. Male urogenital anatomy with permission from Canadian Cancer Society.[6]

Semen is a viscous gel at the time of ejaculation and eventually liquefies 20-30 min after ejaculation, enabling the sperms to swim.[7] A group of structural proteins, including semenogelin I and II that are components of semen coagulum, disappear after liquefaction. Prostate specific antigen (PSA), a protease

present in the prostatic fluid, is considered to be responsible for this transformation.[8] The prostatic fluid contains high levels of citrate anions which are electrochemically balanced by high concentrations of cations such as Zn^{2+}, Ca^{2+}, Mg^{2+}, K^{+} and Na^{+}.[9] Zinc inhibits PSA proteolytic activity with tight binding kinetics; it is itself regulated by citrate levels in the healthy prostate.[10]

I.1.2. Statistics

Prostate cancer (PCa) is the most common cancer in men responsible for about 1 in 4 cases of male cancers. [11] About 15 % of Canadian men will be diagnosed with PCa during their lifetime. PCa was attributed as the cause of death of 4100 Canadian men in 2017 and another 21300 men were diagnosed with PCa tumors. Responsible for 21% of all diagnosed cancer cases in Canadian men and 10% mortality rate in 2017, PCa has emerged as a serious healthcare issue which necessitates development of new treatments and therapeutics (**Figure 2**). [10]

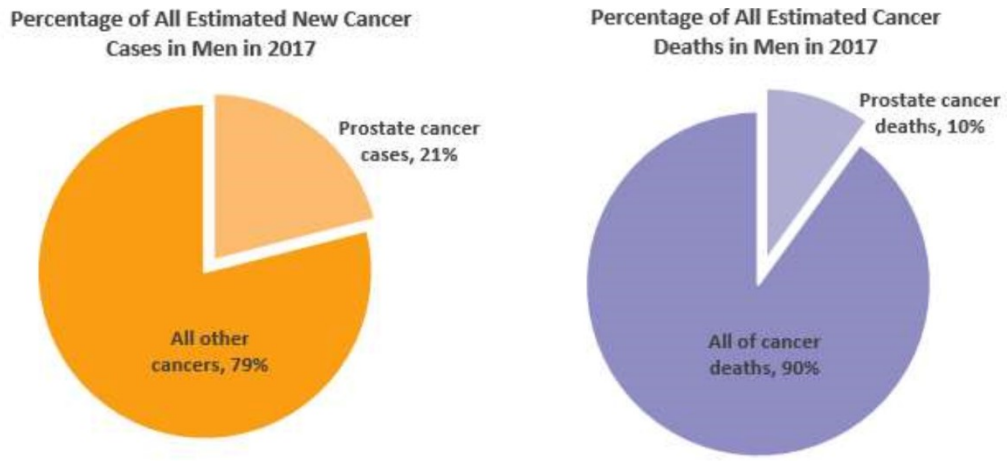

Figure 2. Diagnosed prostate cancer and related death cases in Canada 2017.[10]

I.1.3. Prostate cancer at cellular level

The prostate gland is comprised of a variety of cell populations: an organised epithelial lineage, a fibro-muscular stromal network, an endothelial vasculature and immune cells.[12] About 95% of all prostate cancer cases are adenocarcinoma which is a type of neoplasia of the epithelial tissue of glandular organs.[13] The remaining types of prostate tumors are urothelial carcinoma (also called transitional cell carcinoma), sarcoma, small cell carcinoma, carcinoid tumours, and squamous cell carcinoma.

Several *in-vitro* cellular models have been developed for PCa cellular investigations. The gold standard model contains three cell lines: DU145, LNCaP and PC3.[14] All of these cell lines are derived from metastatic prostate cancers. The DU145 and PC3 cells are hormone independent while LNCaP cells are androgen responsive and express androgen receptors and PSA.[14]

I.1.4. Risk factors

The principal risk factors for prostate cancer as well as many types of cancer is age. The number of reported cases under the age of 40 is low and increases thereafter.[15] However, the mortality rate for non-metastasized prostate cancer decreases in senior men, due to greater risk of other competing causes of death.[16] Genetics is the second major factor. Certain gene mutations are observed in 5-10% of people who have PCa. For instance, BRCA1/2 mutations have been reported as risk factor in 2% PCa cases.[17] Men with a first-degree relative diagnosed with PCa are two to three times more likely to develop the disease. This factor increases if patient's relatives have diagnosed with PCa before the age of 60. Race is being identified as another prognostic factor for PCa survival. African Americans are at higher risk of diagnosis with PCa while indigenous Australians display lower rates compared to Caucasian people.[18] The lifestyle also affects the PCa incidence. Cigarette smoking might increase the risk by changing the hormone levels or through increased exposure to carcinogens.[19] A vegan diet was associated with a lower risk of prostate cancer, while diets rich in animal fats were favorable for PCa, probably because of the usually high-bound obesity.[20]

I.1.5. Symptoms and diagnosis

Most prostate tumors are diagnosed without symptoms. However, there are some unspecific symptoms patients experience including: difficulty in urination, observation of blood in urine and pain in the genital areas. The current PCa diagnosis employs screening tests for the PSA levels. Although false positive results raise some concerns, the PSA test remains the front-line examination of the PCa. This test is a non-invasive and affordable examination which has been used routinely for several years.[21] In addition, *digital rectal examination* (DRE) is used as a diagnostic tool complementary to the PSA test for evaluation of PCa. The DRE test evaluates the size of the prostate by examining it through the rectum using a gloved finger. Ultimately, these tests are not sufficient, and a prostate biopsy is often necessary for a confirmatory PCa diagnosis. After biopsy, the prostate tissue samples are evaluated under the microscope, and the aggressiveness of the tumor is recorded using the Gleason scoring system.[22] The Gleason score indicates the malignancy of the prostate tumor by a score which represents clinical stage,

progression to metastatic disease, and survival chance.[23] A grade 1 PCa (Gleason score (GS) 6 or lower) is considered as low risk prostate tumor. The cells are well differentiated (not like stem cells) and rather look like normal prostate cells. Tumors with GS 7 (grade 2 or 3) are moderately differentiated which indicates an intermediate risk. Highest risk PCa tumors are allocated to grade 4 or 5 with GS 8-10 which are usually metastasized, and the cells are poorly differentiated. A gradual increase in the PSA levels with the grade of PCa is often observed.

Globally, randomized screening of a large population with the PSA test is used as a common practice. The aim of such screening is to increase the survival rate of patients by early diagnosis of the prostate tumor. Early diagnosis enables disease treatment before it advances to the unstoppable metastatic stages. However, recent findings brought some doubt about the efficacy of the PSA test on reducing the mortality of PCa patients.[24-25] High levels of PSA could be due to other non-malignant prostate diseases which will result in overdiagnosis and unnecessary biopsy and further inconvenience for false-positive cases. As represented in **Figure 3**, the peaks in 1992 and 2001 are due to large national screenings which were associated with over-diagnosis of PCa.

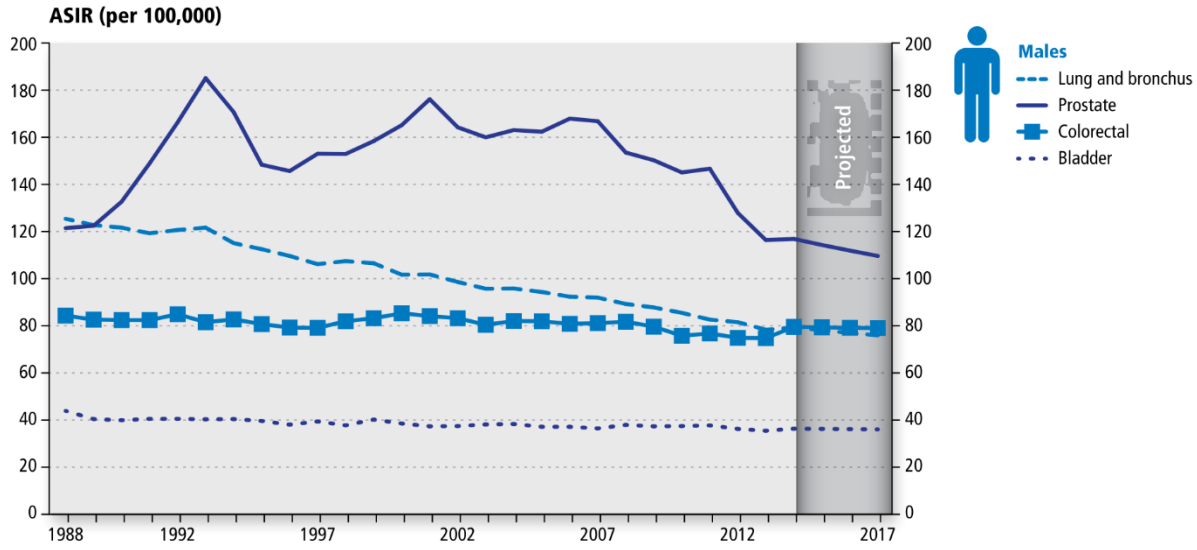

Figure 3. Age-standardized incidence rates (ASIR) for selected cancers, males, Canada, 1988–2017.[10]

I.1.6. Other common prostatic conditions

Prostatitis is a common prostatic condition which is sometimes caused by bacteria and is associated with inflammation and swelling of the prostate gland. Mostly, it comes with painful and difficult urination. Three main versions of this disease are acute bacterial prostatitis, chronic bacterial prostatitis and chronic

non-bacterial prostatitis/chronic pelvic pain syndrome (CP/CPPS) amongst which the former is the most common.

Benign prostatic hyperplasia or prostate enlargement is caused by an overgrowth of cells which put pressure on the urethra and discomforts urination. The condition is considered as benign and doesn't increase the prostate cancer risk. According to Canadian Cancer Society, it is not a health issue until it reflects other potential symptoms.

I.2. Current prostate cancer treatments

Choosing a treatment for prostate carcinoma is highly dependent on the risk level of PCa, patient age, preferences and overall health. The tumor can grow at different rates based on the malignancy and stage of cancer. For less invasive tumors, doctors may prescribe active surveillance, which means patients would be closely monitored periodically using diagnostic tools. For more malignant cases, the treatments could be initiated with more radical treatments, i.e. surgical removal of the prostate gland (prostatectomy) and radiation therapy. Surgery can be followed by hormone therapy then chemotherapy as second and third lines of treatment.

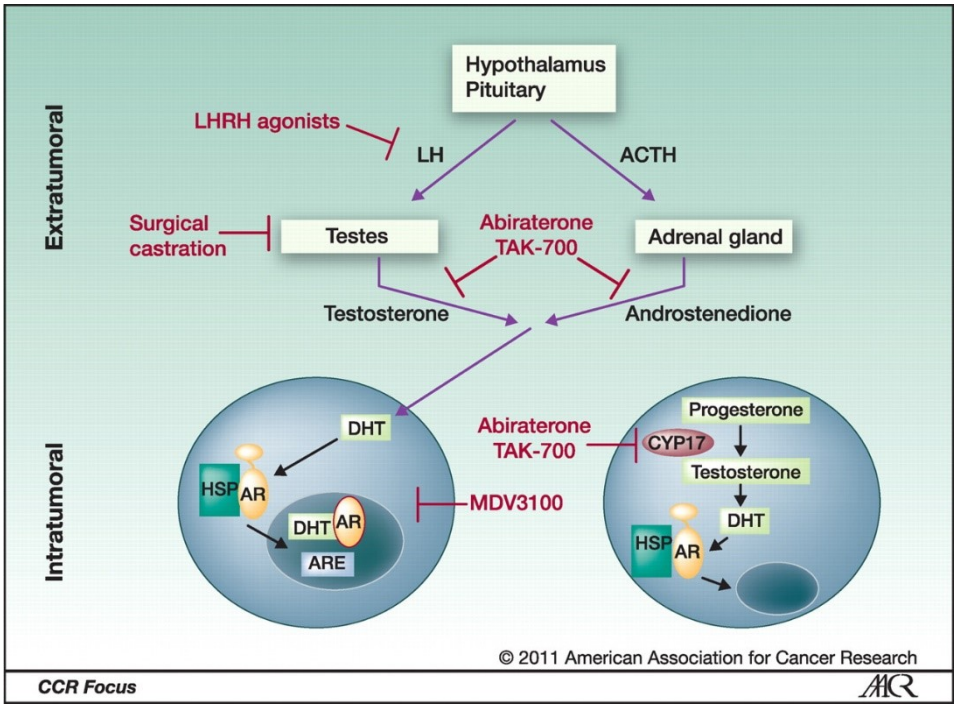

Figure 4. Androgen deprivation therapy with permissions from American Association for Cancer Research.[26]

I.2.1. Hormone therapy

Hormones are among the first approved medications for prostate and breast cancers (see section I.2.3). Androgen hormones such as testosterone and its active metabolite, dihydrotestosterone (DHT), are responsible for the male characteristics viz. muscle growth, facial hair and sexual behaviour including prostate cell function and growth.[27] DHT has 10-fold higher affinity for the androgen receptor compared to testosterone, making it the main androgen hormone in the prostate gland.[27] In the early stages of PCa, the cell proliferation and regulation (apoptosis) are usually androgen dependent. Thus, *androgen deprivation therapy* (ADT) is used as a tool for combating prostate tumors for early diagnosed patients. Small molecules are utilized to lower the levels of testosterone in the whole body as well as tumorous cells to reduce tumor growth and proliferation. ADT is effective in extending the life of patients and slowing down the progress of tumor but cannot cure PCa. Tumors normally adapt to androgen deprivation and this leads to the gradual ineffectiveness of the hormone therapy.[26] Several approaches in different levels of androgen homeostasis have been used to achieve ADT including orchidectomy (surgical remove of testicles) and medications such as luteinizing hormone-releasing hormone (LHRH) agonists, anti-androgens, estrogens and more recently gonadotrophin-releasing hormone antagonists (**Figure 4**).[28] *LHRH Agonists*. Luteinizing hormone-releasing hormone (LHRH, **1**) or Gonadotropin-releasing hormone (GnRH) is a hormone released by the hypothalamus which trigers the secretion of follicle-stimulating hormone (FSH) and luteinizing hormone (LH) from the anterior pituitary. After initial doses of LHRH agonists, the testosterone levels rise slightly in a condition known as *flare.*[29] Continuing the LHRH agonist treatment, the outcome is the reduction in the number (downregulation) of LHRH receptors. This results in reduction of circulating FSH and LH levels, along with downregulation of LHRH receptors, which cause a sharp decrease in gonadal testosterone production termed as *chemical castration*.[30] The structures of LHRH agonists in clinic are presented in **Figure 5**; leuprolide **2**, goserelin **3**, triptorelin **4** and histrelin **5**.[31] These compounds were developed by structure activity relationship (SAR) studies of the gonadorelin hormone. Chemical castration is associated with the shrinkage of testicles. Most patients prefer medications over orchiectomy due to emotional and psychological effects of removing testicles.[32]

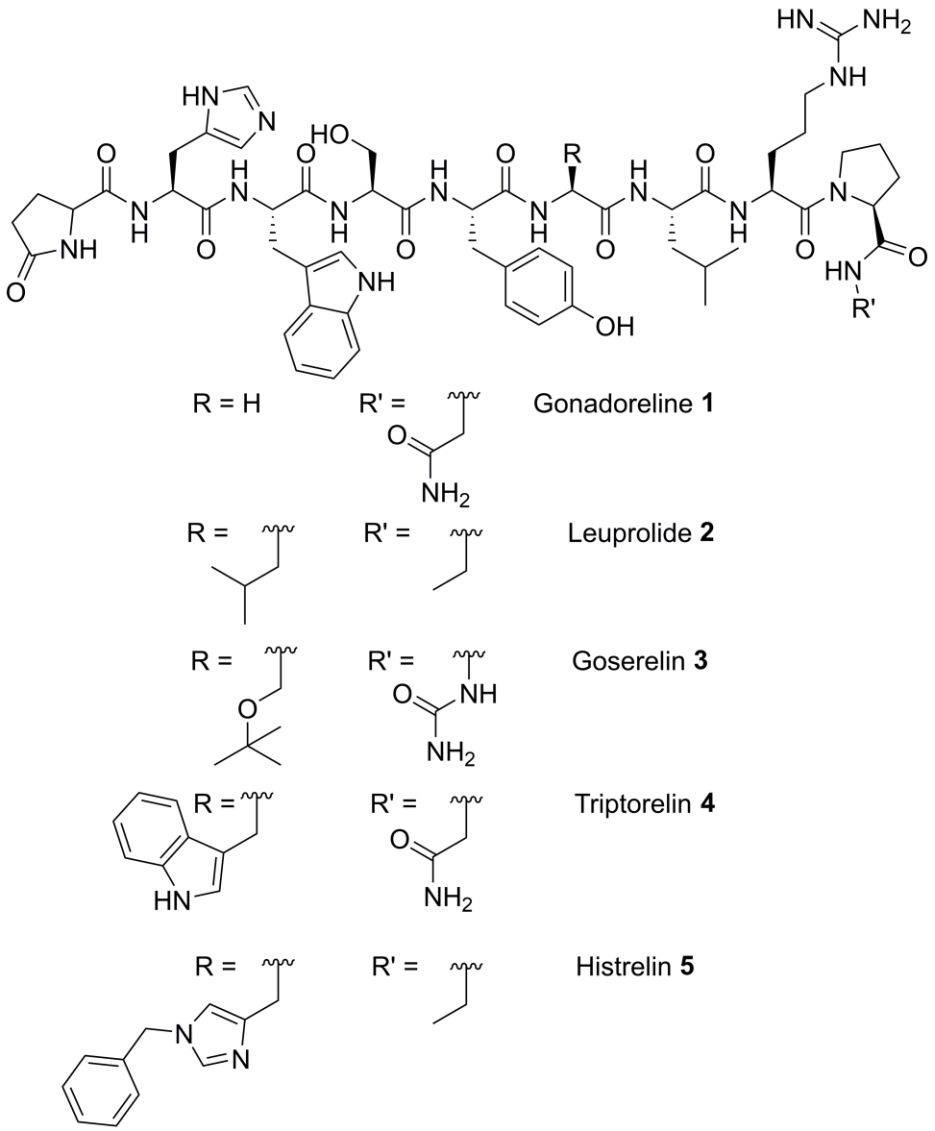

Figure 5. Representative chemical structures of gonadorelin and LHRH agonists that are used in prostate cancer treatment.

Androgen receptor antagonists. The anti-androgen drugs block the androgen receptor (AR) to prevent endogenous androgens such as testosterone and dihydrotestosterone from exhibiting their biological effects. The AR antagonists are mainly used as co-therapy with LHRH agonists to reduce the flare effect (**Figure 6**). Steroidal anti-androgens like cyproterone acetate (**10**) are structurally related to testosterone and DHT. Cyproterone acetate is an antagonist for AR and suppresses the gonadal androgen production.[33] The main class of AR antagonists are nonsteroidal and have a substituted anilide as core of the structure. The earlier nonsteroidal AR antagonists such as flutamide (**6**) and nilutamide (**7**) have been replaced with

newer agents like bicalutamide (**8**) and enzalutamide (**9**) in clinic. The hepatotoxicity of compounds **6** and **10**, and the interstitial pneumonitis associated with nilutamide (**7**) were the main side effects that led to their replacements.[34-35]

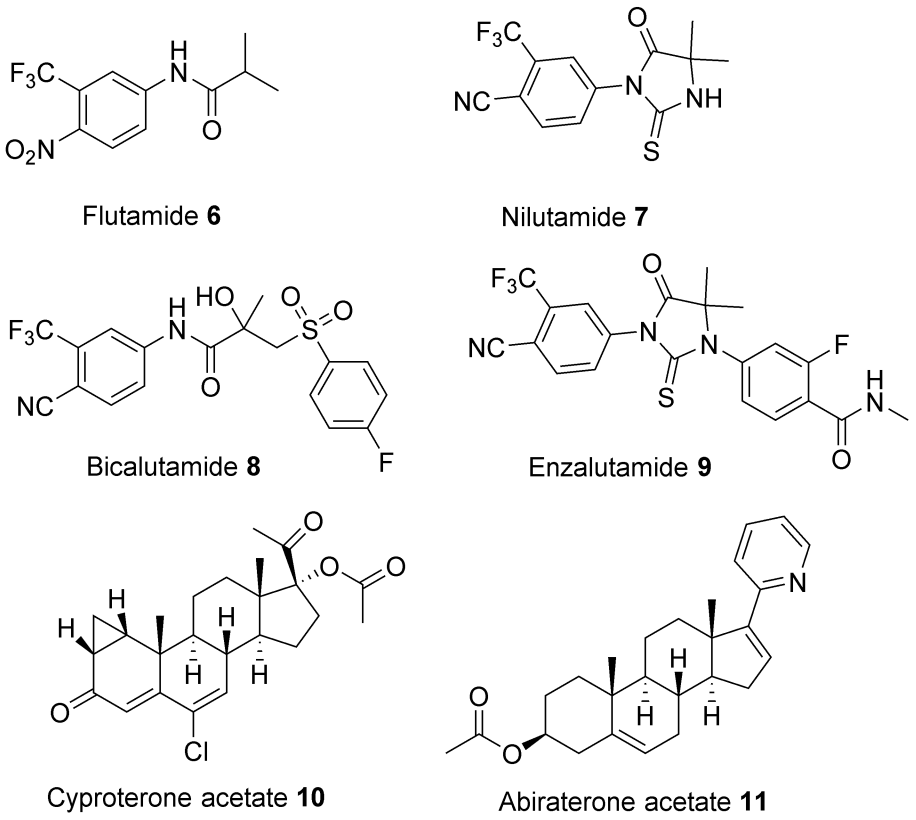

Figure 6. Representative chemical structure of anti-androgen agents.

Androgen biosynthesis inhibitors. Patients with a castration-resistant prostate cancer (CRPC) are still able to produce androgens in the adrenal gland and within the tumor. They do not respond to first line LHRH agonists and AR antagonists. The recently approved abiraterone acetate (**11**) is a CYP17 cytochrome P450 inhibitor interfering with the biosynthesis pathway of testosterone and DHT from cholesterol.[36] Abiraterone acetate (**11**) is also useful in the treatment of metastatic high-risk castration-sensitive prostate cancer.[37]

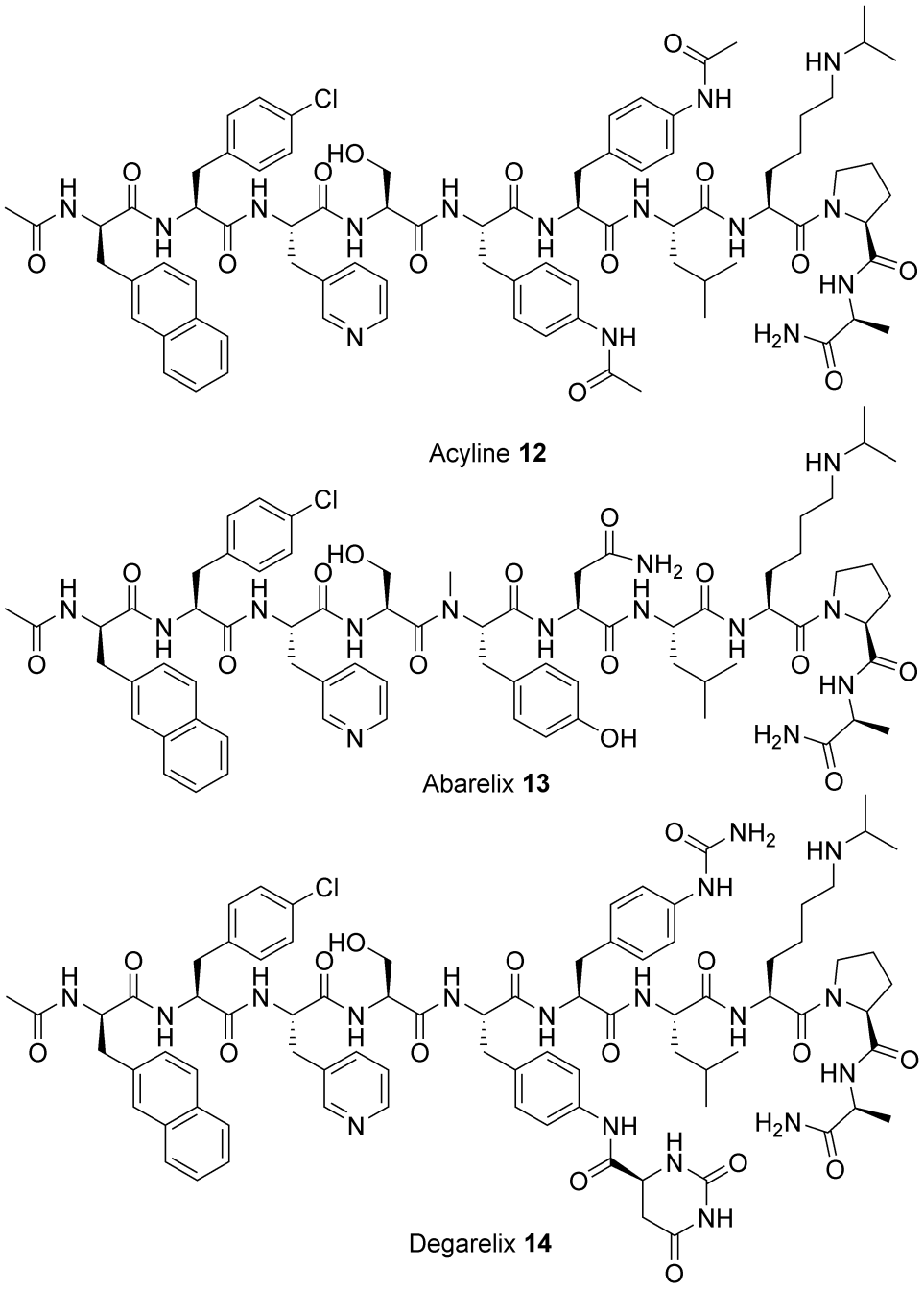

Figure 7. Representative chemical structure of GnRH antagonists.

GnRH antagonists. GnRH antagonists mediate their biological effects by binding to the GnRH receptors in the pituitary gland avoiding natural gonadorelin to activate the receptor. Unlike LHRH agonists, the antagonism action results in immediate suppression of LH release and consequently reduces the androgen release from testicles.[38] Due to their immediate onset of action, GnRH antagonists are valuable therapeutics for PCa patients who need a quick androgen control. Acyline (**12**), one of the first discovered

GnRH antagonists, readily forms gels in aqueous solutions preventing its formulation as a drug (**Figure 7**).[39] The other member of this class, abarelix (**13**), has been discontinued due to severe histamine release and allergic side effects.[40-41] Further inclusion of urea and carbamoyl functionalities led to the discovery of degarelix (**14**) which is currently available as the only GnRH antagonist on the market.[42] Degarelix (**14**) has a long duration of action compared to former agents like acyline (**12**) and abarelix (**13**).

I.2.2. Chemotherapy

Chemotherapy is the practice of using chemicals to treat any disease; however, in cancer terminology, it is used for administration of certain cytotoxic chemicals that block the growth and division of malignant cells. Different classes of chemotherapeutic agents have been introduced to treat cancer but only the ones which are administered particularly for prostate cancer are discussed herein.

Taxanes. Taxanes are a class of natural products originally obtained from pacific *Taxus* (yews) and discovered during a U.S. National Cancer Institute-funded screening program.[43] Paclitaxel (**15**) and its semisynthetic derivatives docetaxel (**16**) and carbazitaxel (**17**), are the most common taxanes used in PCa chemotherapy, all sharing a taxadiene core (**Figure 8**). Taxanes interfere with the normal function of microtubules during the process of cell division; thus, they are considered as mitotic inhibitors. Several groups have reported total syntheses of members of the taxane family,[44] but all the commercial routes employ semi-synthesis from yew extracts.[45]

Nitrogen mustards. The first developed chemotherapeutic agents for cancer were the nitrogen mustards which share a bis-2-chloroethyl amine moiety and are still in clinical use. Their main function is to alkylate DNA twice, through intramolecular aziridinium ion intermediates and to connect covalently DNA strands together (inter-strand cross-link). The DNA double-strand needs to be opened up during cell division and as a consequence of nitrogen mustard reaction, the cell division is hampered.[46] The common nitrogen mustard in PCa treatment is estramustine phosphate (**18**) which has a dual hormonal (estrogen) and alkylating neoplastic (nitrogen mustard) action. Phosphate **18** is a prodrug and its active metabolites are normustine (a.k.a. bis(2-chloroethyl)carbamic acid) and estradiol.

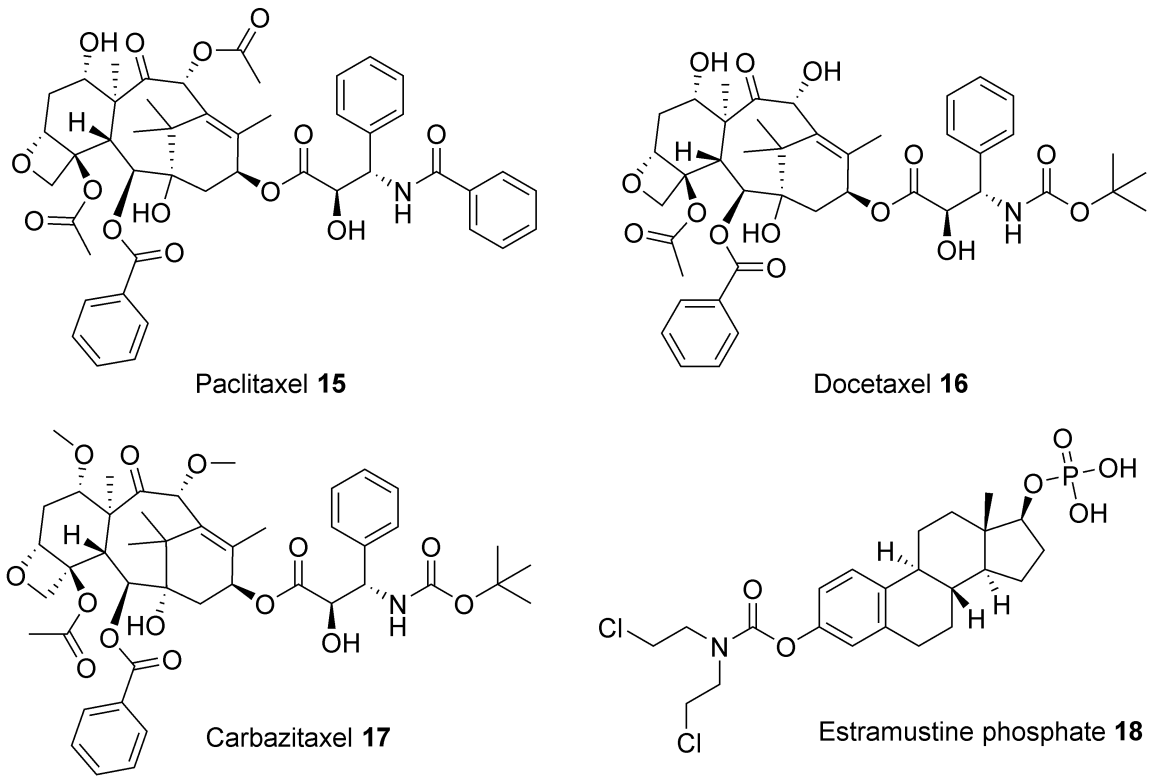

Figure 8. Representative chemical structure of taxanes and estramustine phosphate.

Anthracyclines. Another important class of chemotherapeutics is the anthracycline antibiotics which share an anthraquinone skeleton. They were first isolated from *Streptomyces* bacterium extracts as and examined as antibiotics; however their potent cytotoxicity led to their employment as anti-neoplastic agents.[47] The main function of anthracyclines is to intercalate between DNA bases and hamper cell division. Moreover, they are good inhibitors of topoisomerase II, a vital enzyme in DNA transcription and replication processes.[48] Anthracyclines are involved in iron-mediated generation of free oxygen radicals (quinone radicals) which cause DNA alkylation and damage.[49] Doxorubicin (**21**) and its safer diastereomer epirubicin (**22**) are widely used in PCa as well as other malignant situations (**Figure 9**). Another intercalating agent is mitoxantrone (**19**) which is also an anthraquinone and has a similar mechanism of action as the anthracyclines.

Most of the chemotherapeutic agents including taxanes and anthracyclines are administered jointly with prednisone, a corticosteroid anti-inflammatory medication, to reduce the pain and increase the quality of life of patients.[50] The other beneficial effects of prednisone in PCa are the reduction of androgen levels and tumor growth by downregulation of adrenal androgens, transcription factors, and cytokines.[51]

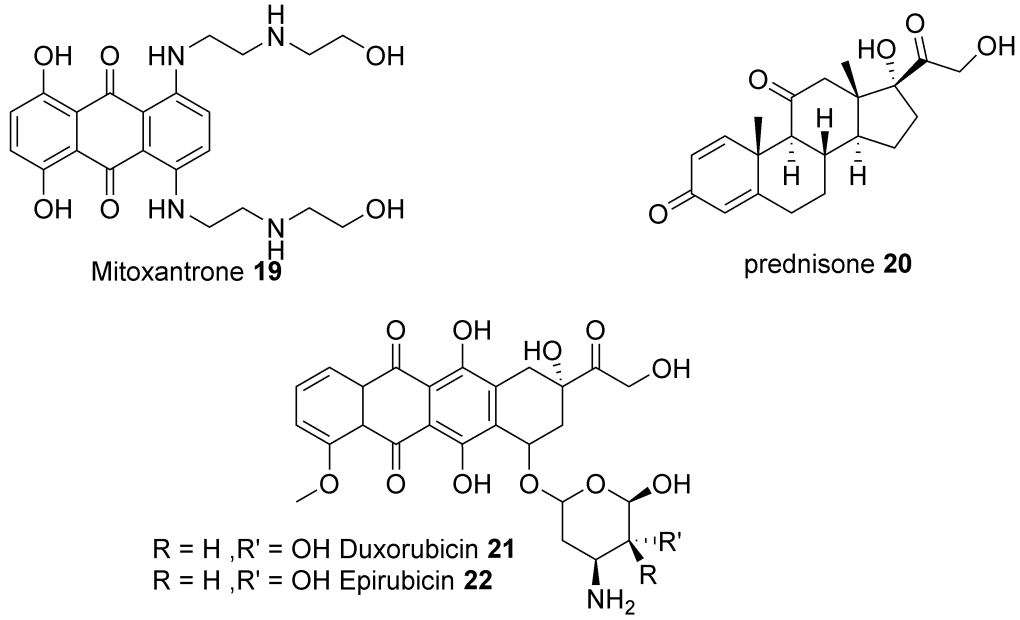

Figure 9. Representative chemical structures of anthracycline antibiotics and prednisone as a corticosteroid.

I.2.3. Targeted therapy

Cancer is a complex disease due in part to the various factors regulating human cells such as signalling, protein translocation, growth, division, protein synthesis, DNA replication and epigenetics. The undifferentiation of cancerous cells increases the possibility that each cell within the tumor has a different mutation compared to the adjacent cells. Tumors may thus adapt during treatment reducing the efficiency of medications. Cancer may vary from patient to patient and during the progression of the tumor. This huge level of complexity makes cancer one of the most challenging problems which humans have ever faced. Despite many efforts and investments, there is still no universal cure for cancer. Blocking only one pathway or target is usually not sufficient for curing tumors especially for more malignant ones, such that multiple targeted therapy has become a mainstay for treating cancer.

In the last two decades, owing to the completion of human genome map, targeted therapy received more attention from cancer scientists. Targeted cancer therapy utilizes small molecules or antibodies to block specific proteins or genes, *molecular targets*, that are responsible for tumor growth, progression, and cancer metastasis. The advantage of targeted therapy over current chemotherapy is due to their specificity for cancerous cells in contrast to chemotherapeutics that kill almost every rapidly-growing cell. Chemotherapeutics are cytotoxic agents. Targeted medicines are usually cytostatic and slow down or stop cell growth and proliferation rather than killing the cancerous cells. Targeted therapy along with

immunotherapy (modifying immune system for combating cancer) are considered as the future of cancer treatment.

Table 1.New targeted medications in clinical trials. Updated from ref. [52]

Pathways	Drug targets	Drugs	Drug development stage
AR PATHWAY	AR	Enzalutamide Apalutamide Darolutamide	Approved Approved Phase III
	AR cofactors		
	Androgen synthesis enzymes: CYP17	Abiraterone	Approved
ETS transcription factors	Transmembrane protease serine 2	PARP inhibitors: Veliparib, Talazoparib	Phase II
Growth factor receptors	EGFR	Afatinib, Lapatinib,	Phase II
	MET	Cabozantinib, Tivantinib, Onartuzumab	Phase II, III
	IGFR	Cixutumumab/IMC-A12, PLX3397	Phase II
	FGFR	Dovitinib/TKI258	Phase II
	VEGFR	Dovitinib/TKI258, Axitinib (AG013736), PLX3397	Phase II
PI3K	PIK3	BKM120, GDC0980, GSK2636771, BEZ235	Phase I. II
	AKT1	MK2206, GDC0068	Phase II
	mTOR	Temsirolimus, Everolimus, DS-3078a	Phase II
Other kinases	SRC	Dasatinib/Sprycel/ BMS-354825	Phase II
Cell Cycle	CDKs	Dinaciclib	Phase I
	Aurora A kinase	MLN8237 (Alisertib)	Phase II
Protein Chaperons	HSP90	AT13387, STA-9090	Phase I, II
	HSP27	OGX-427	Phase II
	Clusterin/TRPM2	OGX-011/custirsen	Phase III
Histone acetylation (transcriptional repression)	HDAC (EZH2, CHD5, MLL2)	Pracinostat SB939 Panobinostat Vorinostat	Phase III
DNA damage repair	PARP	PARP inhibitor Veliparib	Phase II
Angiogenesis	VEGFR	Dovitinib/TKI258, Axitinib (AG013736	Phase II
	Angiopoietin 1, 2	AMG 386/Trebananib	Phase II
Developmental pathways: NOTCH. SHH, WNT	gamma secretase	RO4929097	
	PTCH/SMOO	Vismodegib/GDC-0449, LDE-225, itraconazole	
	Wnt-5a, Fzd8	OMP-54F28, Foxy-5	Phase II

The available medications for PCa on the market are limited to hormonal therapy and chemotherapy for depriving the androgen levels and increasing the patient survival rates. Currently, many compounds are under development to target pathways other than the AR pathway (**Table 1**). DNA damage repair is

impaired in 90% of PCa cases, thus, inhibition of poly(ADP-ribose) polymerase 1 (PARP1) displayed benefits in the treatment of patients.[53] PARP inhibition is also beneficial for tumors with a mutant ETS gene (a protooncogene transcription factor).[54] The growth factor receptors are other important targets for prostate cancer which activate the tumor proliferation and differentiation by initiating the growth signal cascades. PI3K pathway kinases and other kinases which are involved in cell proliferation and apoptosis signaling as well as cell cycle homeostasis, are also targeted to treat PCa.[55-57] Targeting histone deacetylase, as DNA accessibility regulators for replication is under investigation in phase III clinical trials.[58] Proteins need to have their unique tertiary and quaternary structures for performing their functions. Targeting protein chaperones which assist in folding to the correct 3D structure has been pursued to decelerate the protein synthesis machinery of tumors.[59-60] Tumor growth requires more nutriments and consequently more blood vessels, leading to up-regulation of genes responsible for angiogenesis. Suppression of angiogenesis by inhibition of vascular endothelial growth factor receptor (VEGFR), and angiopoietin 1 and 2 has been found useful in patients with bone metastatic PCa.[61-62] Developmental pathways cooperating with the AR pathway are heavily involved in PCa, and mutations in these pathways may lead to malignancy and castration resistance PCa.[63]

Among candidate therapies in clinical trials, the monoclonal antibody bevacizumab (an anti-VEGF), aflibercept (an anti-VEGFR), dasatinib (an inhibitor of Src), custirsen (antisense against clusterin) and tasquinimod (an anti-angiogenesis factor)[64] are under investigation in different phases (**Table 1**).[52]

A revolutionary step towards greater involvement of targeted therapy (called *precision oncology* or personalized cancer treatment)[65] is to study the molecular alterations that occur in neoplasms. Such alterations include mutations responsible for tumor proliferation and are specific to the individuals. This study may ultimately lead to targeted treatment to combat these deleterious mutations.

I.3. Proprotein convertases

I.3.1. Secretory pathway

The secretory pathway consists of the endoplasmic reticulum (ER), the Golgi apparatus organelles and the secretory vesicles. Considerable differences exist between the chemical environment inside (lumen) and outside (cytosol) of the secretory pathway. While the cytosol is reductive, the ER, Golgi apparatus and extracellular environment are oxidative. Therefore, certain oxidation reactions such as disulfide bond formation are favorable in the secretory pathway, and different types of protein are found in the lumen

and the cytosol. During the synthesis of proteins in a ribosome (translation), if the protein possesses a special 16–30 residue sequence called the *signal peptide* in its N-terminal region, it can be recognized by the signal recognition particle (SRP) on the surface of the ER. The ribosome is then connected to the ER and the protein is translocated into the ER through its N-terminal part. Once the protein synthesis is terminated, a signal peptidase enzyme removes the signal peptide and releases the protein inside the lumen. The translocated proteins in the secretory pathway could live all their life inside the secretory pathway or be moved to other places of the cell such as the membrane, or sometimes be secreted to the extracellular matrix. Some post translational modifications (PTM) are typically necessary for further translocation, activation, localization, turnover, or interactions with other proteins which are normally mediated by enzymes.[66] These covalent modifications include protein cleavage, carboxy terminal amidation, disulfide bond formation, addition of fatty acids, lipids, glycosides, ubiquitin or cofactors as well as the addition of phosphate, sulfate, methyl, hydroxyl or acyl groups to one or several amino acid residues or proteins. Addition of hydrophobic groups such as palmitoyl and farnesyl are crucial for membrane localization. Phosphorylation is particularly important in cell signal transduction because certain signaling kinases could be switched on or off with single phosphorylation or dephosphorylation.

I.3.2. The discovery of proprotein convertases

A significant group of proteins are synthesized as protein precursors (proproteins) and further activation is necessary for their biological functioning. Availability of inactive proproteins in large amounts allows the fast release of the active protein at short notice, which is especially important for hormones, clotting proteins, toxins (in poisonous animals), digesting enzymes (trypsin and chymotrypsin), caspases, collagen, and the like. The processing of proteins by amide bond lysis is one of the most imperative PTMs, which is normally mediated by proteases at a specific peptide bond. The subtilisin/kexin enzymes are one of the primary families of proteases in the activation of proproteins.

The discovery of proinsulin and proopiomelanocortin led to the development of what was later mentioned as the prohormone theory by the Steiner and Chretien groups.[67-68] It was followed by the identification of the yeast kexin, a protease related to bacterial subtilisin that proteolytically cleaves its substrates at the C-terminal of paired basic residues.[69] Further studies pertaining to the proteolytic activity of yeast kexin revealed its ability to process mammalian proopiomelanocortin, the precursor of ACTH and β-endorphin.[70] These early findings led to the discovery of furin as the first human subtilisin/kexin related protease, which is the most ubiquitous proprotein convertase (PC) in human tissues.[71] The second enzyme

was called PC1 (later named PC1/3) and was found simultaneously by different groups.[72-73] Other similar family members were discovered at the beginning of the 90s and now are known as PC2, PC4, PACE4, PC5/6 and PC7. They cleave their substrates at paired or single basic residues with a consensus sequence (R/K)-$[X]_{0,2,4,6}$-(R/K)-↓-P1'-P2', where ↓ represents the cleavage site. For most PCs, Arg is preferred over Lys as the basic residue. Their catalytic activity is highly Ca^{2+}-dependent, as later confirmed by the disclosure of the furin crystal structure in 2003.[74]

The subtilisin/kexin isozyme-1 (SKI-1, also called site-1 protease) and proprotein convertase subtilisin/kexin type 9 (PCSK9) being the last two PC enzymes to be discovered are slightly different compared to the other seven members because they cleave their substrates at non-basic residues. Unlike other members of the family, calcium is not essential to the proteolytic activity of SKI-1 and PCSK9.[75] SKI-1 and PCSK9 are only homologous in their catalytic domain in comparison with other PCs.[76-77] The self-activation by proteolysis is the only reaction that the PCSK9 catalyzes. After removal of its prodomain, PCSK9 loses its proteolytic activity.

I.3.3. Structure of proprotein convertases

As illustrated schematically in **Figure 10**, PC enzymes share some similar domains in their structures including the ones listed below:

Signal peptide. A short sequence of residues in the N-terminal of PCs that is recognized by secretory pathway for translocation into the ER.

Prodomain. The prodomain acts both as an intramolecular chaperone and inhibitor of enzymatic activity.[78-79] Some prodomain residues engage in direct interactions with the active site cleft and inhibit the catalytic activity of PC enzymes. The variation of pH and Ca^{2+} during translocation from the ER to the trans-Golgi network (TGN) and the secretory vesicles initiates the auto-catalytic removal of the prodomain in PC enzymes.[80]

Catalytic domain. The catalytic domain is responsible for catalyzing the cleavage of the peptide bond at a consensus motif with paired basic residues. The mechanism of catalytic activity in PCs as in serine proteases relies on the catalytic triad (three residues of Asp, Ser and His). The details of the catalytic mechanism are discussed in section I.4.1.

P-domain. The P-domain plays a crucial structural role in the strong calcium and pH dependence of PCs.[81-82] PCs lose their catalytic activity without P-domains. A conserved RGD motif within the P-domain has a critical role in the cellular and subcellular trafficking of PCs.[83-85]

Cys-rich domain. This domain has many Cys residues and contains some extra transmembrane or cytoplasmic regions in some PCs (furin, PC4, PC5/6, PC7 and SKI-1).[77, 83]

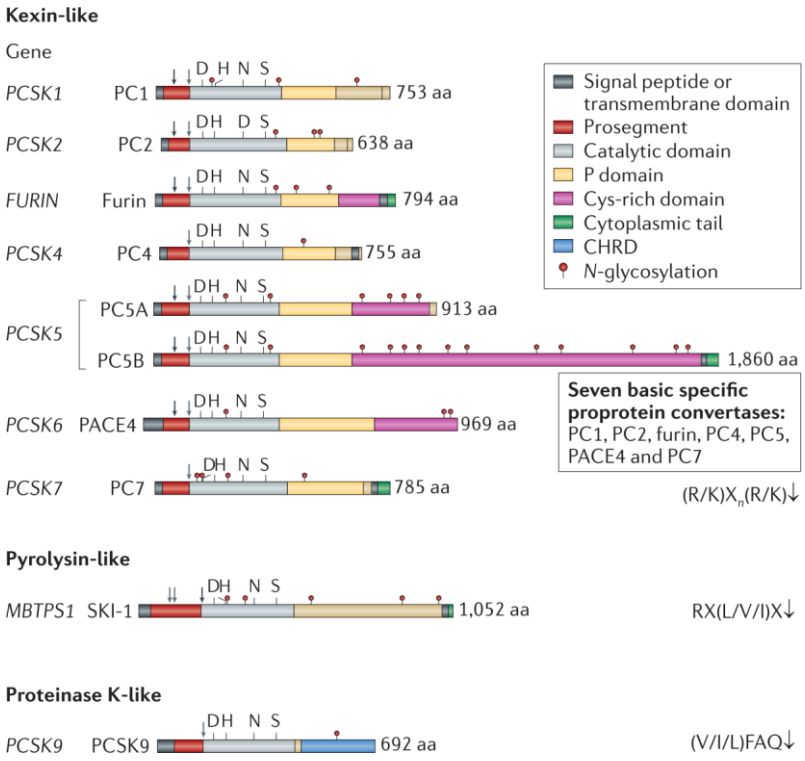

Figure 10. Schematic representation of sequences of human proprotein convertase family members. Reproduced with permission from Springer Nature publishing group.[86]

The active site residues are highly conserved among PCs, except for PCSK9 and SKI-1. This high level of homology is reflected on the consensus sequence that they recognize in their substrates. Consequently, some PCs can recognize the substrates of other PCs although with lower affinity (this function is called redundancy). Among PCs, only crystal structures of furin have been solved untill now.[74] The demonstrated homology models for other PCs based on furin crystal structure revealed a high degree of homology around the active site.[87] The disparities between PCs can be made distinguishable to a greater extent by receding from the active site region.

I.3.4. Cellular and tissue distributions of PCs

The tissue distribution of PCs varies considerably between family members. Furin is ubiquitously found in the whole human body and plays a vital role in embryogenesis. PC1/3 and PC2 process most of the prohormones such as proopiomelanocortin, proglucagon and proinsulin and are thus located mostly in neural system, hypothalamus and endocrinal tissues.[88-89] PACE4, PC5/6, PC7 and SKI-1 are widespread and found in several tissues. On the other hand, PC4 is only expressed in reproductive tissues such as the testicles and ovaries.[89] PCSK9 is largely expressed in the liver and regulates the LDL receptor recycling and consequently the levels of fatty acids and cholesterol.[90] In most human tissues, multiple PCs are expressed, and process diverse substrates indicating their unique role at the cellular level.

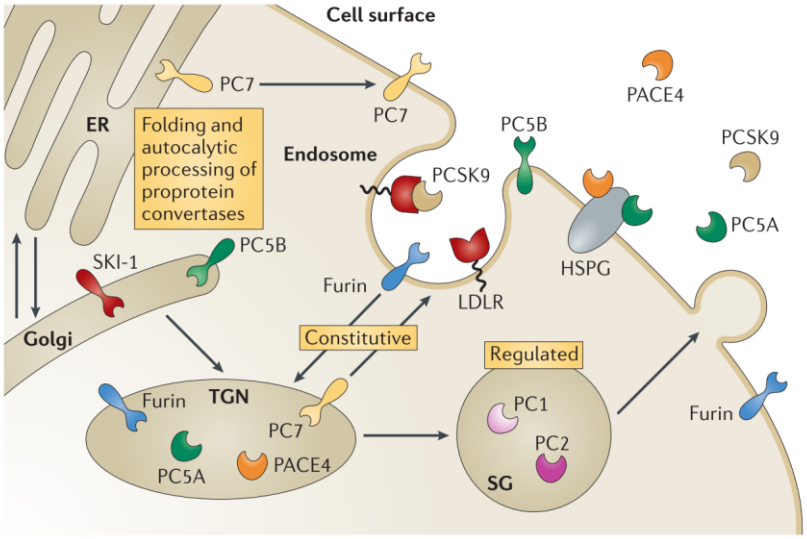

Figure 11. Subcellular trafficking of proprotein convertases. Reproduced with permission from Springer Nature publishing group.[86]

The PCs are synthesized and folded similarly in the ER as described in section I.3.1 for secretory proteins. The differences between PCs appear when they leave the ER for the Golgi apparatus. The unique profile of each PC for processing their substrates is related to where they are active (TGN, secretory granules, cell surface, endosomes or extracellular matrix; **Figure 11**).[86] The higher efficiency of PC1/3 and PC2 in acidic pH allows them to process their substrate within the secretory granules of neuroendocrine cells, where the pH is 5 to 6. The endosomal pathway assists the journey of transmembrane furin and PC7 from the TGN to the cell surface and their return into the TGN.[86]

PACE4-FL (PACE4-A) and PACE4-altCT (the malignant isoform) are two alternative spliced versions of PACE4. The former is either secreted or is observed at the cell surface, while the latter is predominantly found within the Golgi apparatus and the endosomes.[91] Some other spliced versions of PACE4 are also produced, but they remain primarily in the ER as inactive zymogens.[92] A similar pattern has been noted for alternative splicing of PC5/6.[93] The soluble 913-residue PC5/6A is secreted into the extracellular matrix through endosomes, while the 1860-residue PC5/6B has a transmembrane domain. Similar to furin and PC7, PC5/6B is able to localize between the cell surface and the Golgi apparatus.

I.3.5. Proprotein convertases and cancer

A large body of evidence has confirmed the involvement of PCs in various levels of cancer such as carcinogenesis, tumor growth, angiogenesis and metastasis.[94] The malignant overexpression of different PCs has been documented for several types of cancer.[94] The significance of PCs is due to the processing of cancer-related substrates in the pathologic conditions. Numerous essential malignant proteins and enzymes are shown to be processed by PCs or at least they have the consensus motif for proteolytic cleavage by PCs. PC1/3 and PC2 are mostly present in neuroendocrinal tissues and they are entangled in tumors with the neuroendocrinal origin.[95-96] The abnormal activity profile of both PCs is revealed to be important in the metastasis of colorectal cancer to the liver.[97] The high expression of 7B2 protein (a neuroendocrine chaperone for PC1/3 and PC2) was counted as evidence of such role.[98] PC1/3 and PC2 mRNA are also largely expressed in small-cell lung carcinomas.[99]

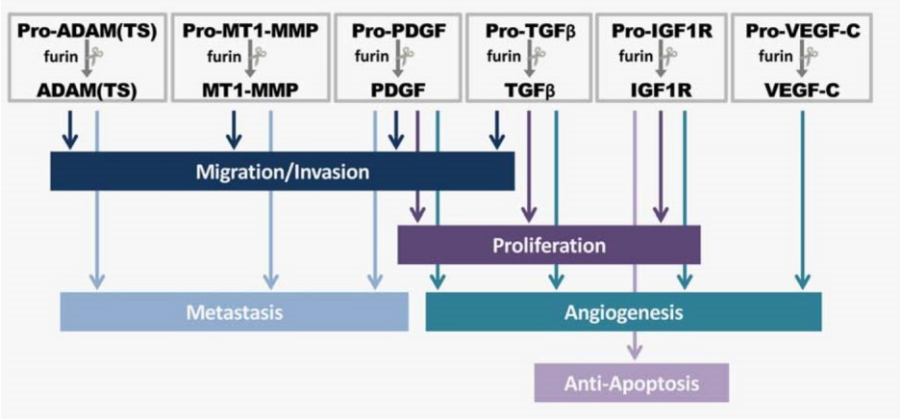

Figure 12. Influence of proproteins processed by furin in cancer development. Reproduced with permission from John Wiley and Sons.[100]

PACE4 and furin are the most studied PCs in relation to cancer and have extensive links with various pathologic and malignant conditions.[94] Furin is found to be overexpressed in several tumors, including

lung, head and neck carcinomas as well as endometrial, cervical and ovarian, breast, skin, gastro-intestinal tract, brain and central nervous system cancers.[100] In some cases, furin tends to be a marker for aggressiveness of neoplasms and cancer progression.[100] The proteolytic activity of furin mediates the processing of substrates such as Pro-ADAM(TS) and Pro-MT1-MMP, which results in increased aggression, migration and metastasis of tumors by release of proteases from ADAM (a disintegrin and metalloproteinase**)** and MMP (matrix-metalloproteases) families. Moreover, furin-mediated processing is necessary in the activation of some key growth factors and their receptors such as platelet-derived growth factor (PDGF), transforming growth factor beta 1 (TGF-β1), vascular endothelial growth factor-C (VEGF-C) and insulin-like growth factor 1 receptor (IGF1R) (see **Figure 12**).[101] The growth factors stimulate the tumor progression by enhancing cell proliferation, angiogenesis and anti-apoptosis effects. Furin also processes integrin α-subunits, E-cadherin and N-cadherin (cell adhesion molecules) that are instrumental in the migration of cells through lymph nodes (a.k.a. metastasis).[102-105]

A growing body of reports implicate the role of PACE4 in pathologic conditions. The overexpression of PACE4 is associated with tumor growth and malignancy.[106] Breast cancer MDA-MB-231 cells were observed to be less aggressive (i.e. low expression of genes involved in cell growth, invasion and adhesion) when PACE4 mRNA was silenced, and most cell cycles were arrested in the G0/G1 phase.[107] Administration of PACE4 inhibitors decreased the proliferation of estrogen-receptor-positive breast cancer cell line ZR-75-1 and tumor progression.[108] PACE4 mediates the collagenase type IV activation through the processing of pro-MMPs in non-melanoma skin cancers.[109] Consequently, the increase in MMP levels leads to more vulnerability of cells to carcinogens (e.g. benzopyran) and accelerated metastasis.[109-110] PACE4 overexpression was also detected in non-small cell lung cancer and ovarian cancer at both tumor cell lines and patient's tissues.[111-113] PACE4 also exhibits a unique role in the development of prostate cancer. This will be described in more detail in the following section.

I.3.6. Validation of PACE4 as a target in prostate cancer

The PACE4 enzyme has been proven to play a critical role in the progression and the malignancy of prostate. The PACE4 mRNA in DU145 cell lines was targeted and silenced using a special biochemical tool (i.e. on/off switch adapter-hepatitis delta virus ribozyme).[114] The resulting cell line, called 4-2, displayed slower proliferation. That study proposed that PACE4 has a high impact on the metastasis and malignancy of prostate tumor through processing of growth factors. More recently, pro-growth differentiation factor-15 (pro-GDF-15) was discovered as a specific substrate for PACE4.[91] However,

further investigations are essential for discovering other cancer-related substrates of PACE4. It was also observed that PACE4, especially its malignant spliced version PACE4-altCT, is overexpressed in prostate cancer tissues compared to normal prostate tissues (**Figure 13-A**, **E** and **F**).[91, 114] The abnormally high levels of PACE4 in more than 90% of prostate adenocarcinoma was projected as a biomarker for prostate cancer.[115-116]

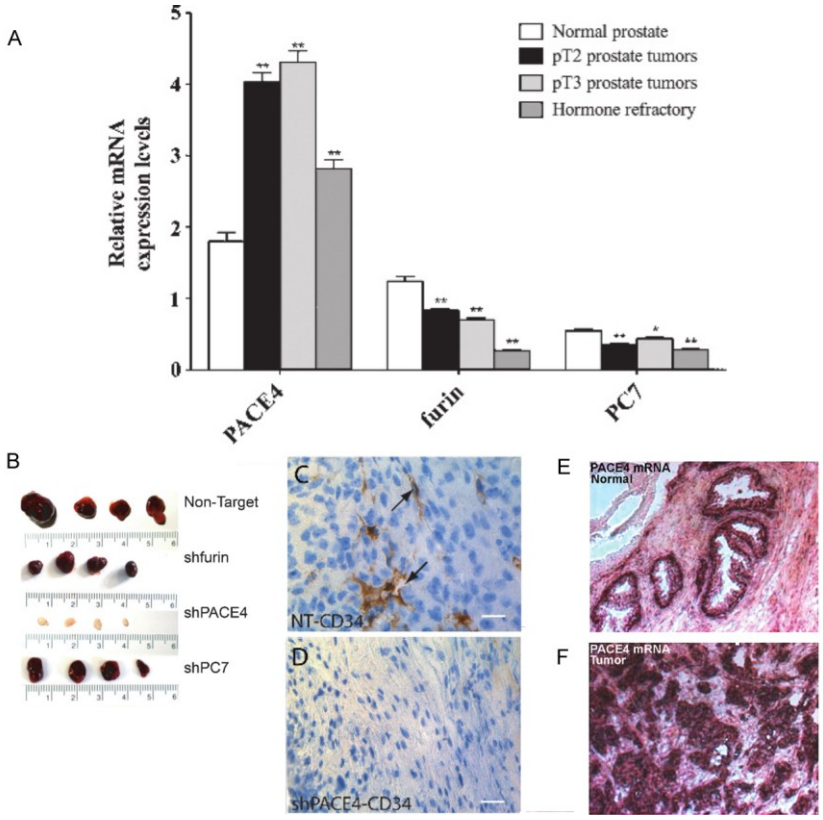

Figure 13. Expression of PACE4 in prostate tissue and its silencing in tumor xenograft. A) Comparison of PACE4 with other PCs in normal and tumorous prostate. B) Representation of LNCaP tumor xenografts with different PCs silenced mRNA. CD34 staining of C) non-treated (arrows show the lumen of micro vessels) and D) PACE4-silenced tumor. PACE4 mRNA in E) Normal, and F) tumorous prostate tissues (purple indicates the presence of PACE4 mRNA). Figure adapted with permissions from Elsevier.[114, 117]

The xenografted model that is defined by transplanting human tumor cells under skin or inside the organ of a nude mouse (a genetically modified mouse with an inhibited immune system) is widely used as *in vivo* tumor model. LNCaP xenografted tumors normally exhibit a dark red color due to the pervasive presence of vessels, but the color was pink in PACE4 mRNA silenced tumors, indicating less neovascularization (**Figure 13-B**).[117] The density of the micro vessels was reduced by 80% by PACE4-

silencing in tumors (**Figure 13-C** and **D**), which indicated the impact of PACE4 on vascularization of prostate tumors.[117] Furthermore, the tumor growth was inhibited only by silencing PACE4 mRNA and neither furin nor PC7 mediated tumor growth (**Figure 13-B**). PACE4 knocked-down tumor cells were observed to be arrested in G0/G1 state of the cell cycle.[117]

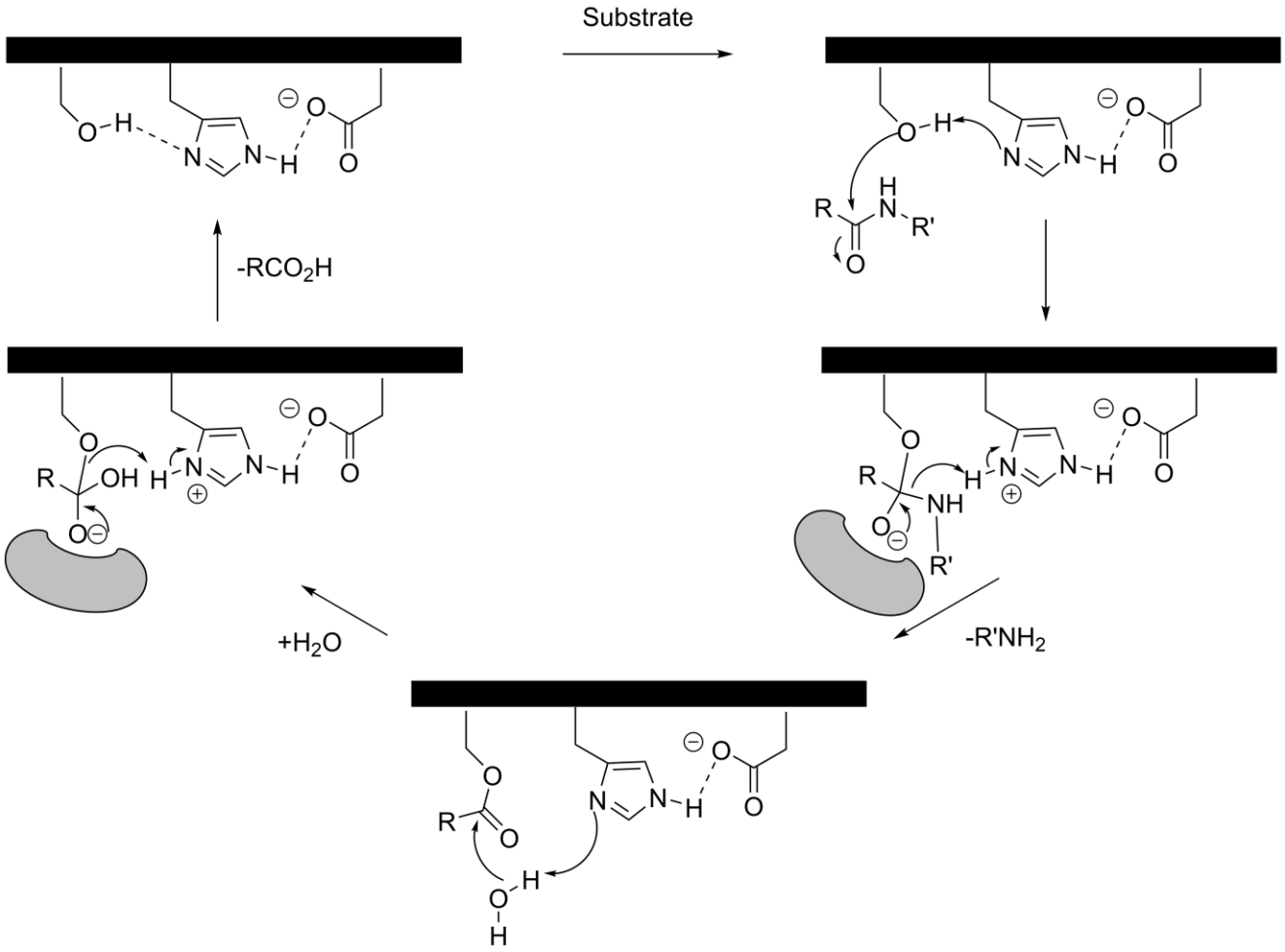

Figure 14. Mechanism of proteolysis catalyzed by serine proteases

I.4. Inhibition of proprotein convertases

I.4.1. Proprotein convertases are serine proteases

Proteases are hydrolase enzymes that catalyze the hydrolysis of the peptide bonds in their substrates. Proteases are categorized based on their catalytic mechanisms and the key amino acid residues involved in proteolysis. The seven major groups of proteases include serine, cysteine, threonine, aspartate, glutamate proteases as well as metalloproteases and asparagine peptide lyases.

Serine proteases have been classified in three clans: SA (chymotrypsin-like), SB (subtilisin-like) and SC (α/β-hydrolase fold). Their catalytic Ser, His and Asp residues are firmly conserved with a special geometry despite the differences in clans.[118] The other classification is based on the genetic codon of catalytic Ser being either TCN or AGY.[119] Proprotein convertases, as they are related to subtilisin, are classified in the clan SB of serine proteases.

The mechanism of peptide bond hydrolysis in serine proteases is illustrated in **Figure 14**. The reaction is initiated with a proton transfer between Ser and Asp residues, which is mediated by a His residue. The resulting alkoxide is now nucleophilic enough to attack the carbonyl of the amide bond. The tetrahedral intermediate is stabilized by the interaction with the *oxyanion hole* residue, which is usually an Asn in PCs (only in PC2 is an Asp). Another proton transfer releases the amine part of the substrate and leaves the enzyme to be acylated at Ser. Finally, the hydrolysis of the acyl-enzyme produces the acid part of the substrate and the enzyme returns to the initial state to continue the catalytic cycle.

The substrates of proteases have a special nomenclature. Starting from the fragile peptide bond towards the N-terminus, the residues are named …, P1, P2, P3 and towards the C-terminus as P1', P2', P3', ... The interrelated sub-pocket that each residue occupies in the enzyme is indicated with …, S3, S2, S1, S1', S2', S3', …

I.4.2. Peptide inhibitors of proprotein convertases

The initial inhibitors of PCs were synthesized based on the consensus sequence of their substrates. The first PC inhibitor, Dec-RVKR-Cmk **22** (where Dec and Cmk stand for decanoyl and chloromethylketone, respectively) is a non-specific irreversible inhibitor of proprotein convertases.[120-121] The crystal structure of **22** in the active site of mouse furin shows the chloromethylketone moiety covalently attached to the catalytic Ser and His residues (**Figure 15**).[74] The Arg residues occupy the P1 and P4 having the most important non-covalent interactions (an Ala, two Asp and a Pro in S1 subsite; two Asp and a Tyr in S4 subsite). A Lys residue interacts with an Asp and an Asn in S2 subsite of enzyme and P3-Val backbone introduce a β-sheet-like interaction with the backbone of a Gly residue. These interactions are significantly similar among seven members of the PC family, namely PC1/3, PC2, PC4, PACE4, PC5/6, PC7 and furin. Despite the wide use of compound **22** as a biochemical tool in inhibiting PC activity, its extended cytotoxicity, due to its alkylating nature, prevents it from being a viable molecule for drug discovery purposes.[122]

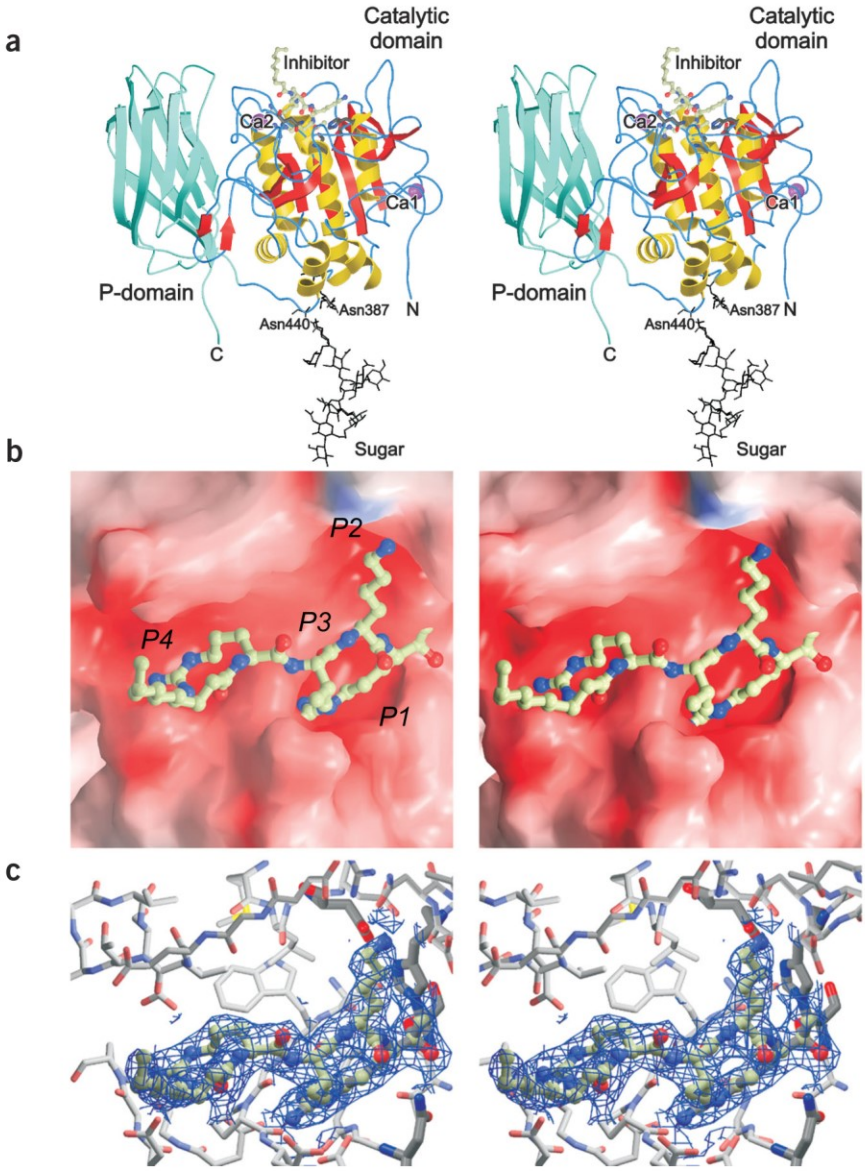

Figure 15. The relaxed-eyes stereo views of crystal structure of mouse furin. a) The 3D structure of furin with inhibitor **22** in the active site shown as ribbon b) The solid surface representation of furin with inhibitor represented as ball-and-sticks c) The stick model of active site residues interacting with inhibitor **22**. Reproduced with permission from Springer Nature publishing group.[74]

Meanwhile, a fluorometric assay was developed for determining the inhibitory constant (K_i) of PC inhibitors using RXKR-AMC (where X usually is S, T or V and AMC stands for 7-amino-4-methylcoumarin) as substrate (**Figure 16**).[121] PC enzymes cleave this fluorogenic substrate's amide bond between Arg and AMC, and the free AMC emits fluorescence (λ_{EM}, 460 nm; $\lambda_{EX.}$, 370 nm). A competitive

inhibitor interferes with the hydrolysis reaction and competes with the substrate to occupy the active site of the enzyme. The concentration of the inhibitor that disables the processing of RXKR-AMC substrate by enzyme defines the inhibitor's affinity. The concentration that shows half of the maximum activity of the inhibitor is called IC_{50}. The IC_{50} is used to calculate the K_i using either the Cheng-Prusoff or Morison equations. When $E_0 < K_i$ (initial concentration of enzyme), Cheng-Prusoff equation provides a good approximation for K_i.[123] Once $E_0 \geq K_i$, tight binding kinetics is involved and Morison equations is recommended for K_i calculation.[124]

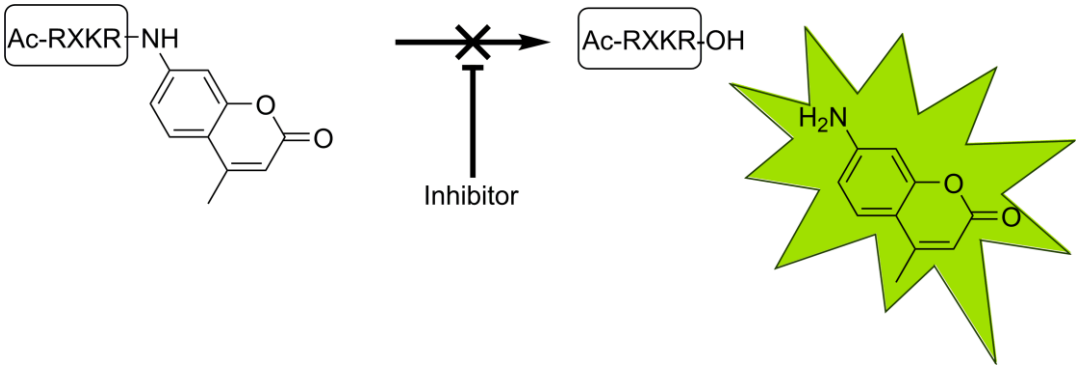

Figure 16. Fluorometric assay for determination of inhibitory constant

The Dec-Arg-Val-Lys-ArgCH_2-Ala-Val-Gly-NH_2 **23** (furin K_i = 3.4 nM, ArgCH_2 is the reduced amide bond, **Table 2**) is identified as the first reversible peptide inhibitor for furin with tight binding kinetics.[125] Short multi-arginine peptides are also non-specific potent inhibitors of PCs.[126] For example, compound **25** is a very potent inhibitor of PCs and together with **22** have been used as non-specific PC inhibitors in biochemical investigations. Other multi-basic cell penetrating peptides such as [W5R4C] and [W4R4] were observed to be micromolar inhibitors of PCs.[127] The furin inhibitors are the most studied among proprotein convertase inhibitors, with a focus on the role of furin in the processing of viral envelope glycoproteins (e.g. hemagglutinin in influenza virus, HBeAg precursor in hepatitis B virus and gp160 in HIV), bacterial toxins (e.g. in anthrax) and cancer-related proteins.[128-132] For instance peptide **38** (DTyr-KE**RSKR**-Tic-VQKD, where Tic is (*S*)-*N*-Fmoc-1,2,3,4-tetrahydroisoquinoline-3-carboxylic acid) that subsequently evolved to the nanomolar PC inhibitor **39**, is synthesized based on the hemagglutinin protein.[122, 127]

Table 2. The K_i (nM) of known peptide inhibitors of proprotein convertases.

Inhibitor structure	Furin	PACE4	PC1/3	PC5/6	PC7	Source
Dec-**RVKR**-Cmk (**22**)	1	3.6	-	0.12	0.12	Synthetic
Dec-**RVK-ArgCH$_2$**-AVG-NH$_2$ (**23**)	3.4	-	-	-	-	Synthetic
Hexa D-Arginine (D-Arg)$_6$ (**24**)	106	580	13200	206	1875	synthetic [126, 133]
Nona D-Arginine (D-Arg)$_9$ (**25**)	1	-	-	19	81	synthetic [133-135]
Complete hpro-furin (**26**)	1.7	0.4	-	-	150	hPro-furin[80]
Complete hpro-PC2 (**27**)	> 1000	> 1000	-	-	131	hpro-PC2[80]
Complete hpro-PC1/3 (**28**)	1.4	1.1	-	-	25	hpro-PC1/3[80]
Complete hpro-PACE4 (**29**)	5.3	2	-	-	117	hpro-PACE4[80]
Complete hpro-PC4 (**30**)	9	7	-	-	-	hpro-PC4[80]
Complete hpro-PC5/6 (**31**)	2.9	1.3	-	-	16	hpro-PC5/6[80]
Complete hpro-PC7 (**32**)	12.4	0.34	-	-	1.3	hpro-PC7
^{64}SDDDRVTWAEQQYEKE**RSKR**^{83} (**33**)	-	-	600	-	-	pro-PC1/3 [136]
^{50}RRSRRSALHITKRLSDDDRVTWAEQQYEKE**RSKR**^{83} (**34**)	4800	-	700	-	-	pro-PC1/3 [136]
$^{25-107}$hPro-furin (**35**)	107	-	-	-	-	pro-furin
DSHAKRHHGYKRKFHEKHHSHRGYRSNYLYDN (**36**)	1980	-	-	-	2400	His- rich salivary peptides[137]
^{235}VLGALL**RVKR**LE^{246} (**37**)	246	-	9	317	940	pro-SAAS[138]
DTyr-KE**RSKR**-Tic-VQKD (**38**)	790	-	1400	-	-	synthetic [139]
TPRARR**RKKR**T-NH$_2$ (**39**)	23	162	-	232	142	influenza H5N1 hemagglutinin[131]
8-Amino-octanoyl-RARR**RKKR**T-NH$_2$ (**40**)	8	3	-	3	430	influenza H5N1 hemagglutinin[122]
Ac-LL**RVKR**-NH$_2$ (**41**)	1400		3.2			synthetic[140]
Monocyclic K**RCKK**SIPPICF-NH$_2$ (**42**)	0.49	-	-	-	-	sunflower trypsin inhibitor 1[141]

The complete prodomains of proprotein convertases inhibit PCs with inhibitory constants in the nM range (**Table 2**, compounds **26**–**32**).[80] However, the peptide derived from pro-furin and pro-PC1/3 were shown to be less active compared to full prodomains (**Table 2**, compounds **33**–**35**).[136] His-rich salivary peptides (e.g. **36**) also inhibit furin and PC7 in the μM range.[137] Pro-SAAS is another secretory protein precursor that needs PC processing for maturation. A peptide segment of pro-SAAS (**37**) is shown to inhibit PC1/3 with good selectivity over other PCs.[138] A positional scanning conducted over 52 million hexapeptides resulted in compound **41,** which was 28-fold selective for PC1/3 over furin.[140] Peptide **42**, an engineered

monocyclic peptide derivative of sunflower trypsin inhibitor-1 (SFTI-1) was found to be a potent furin inhibitor (K_i = 0.49 nM) with tight binding kinetics.[141]

Bioengineered proteins have been used to inhibit PCs. The most well-known example is α_1-antitrypsin Portland (α_1-PDX) and its analogues as a serpin (an endogenous protease inhibitor protein) variant that inhibits furin (K_i = 600 nM) and other PCs. The engineering was performed by the replacement of a native AIPM motif by a PC recognizable motif (RIPR).[142-143] However, its application remained limited only to the biochemical investigations. Other protein inhibitors including eglin c, turkey ovomucoid third domain and α2-macroglobulin mutants inhibit furin proteolytic activity.[144-148]

The PC2 active site has some differences compared to other PCs, which renders the synthesis of its specific inhibitors easier. Peptide fragments of 7B2 CT protein are also potent and specific inhibitors of PC2.[149] The smallest CT derived peptide with specific PC2 inhibition abilities is the CT 1-18 which its sequence is SVNPYLQGQRLDNVVAKK-NH_2 (PC2 K_i = 23 nM).[150]

I.4.3. Small molecule and peptidomimetic inhibitors of proprotein convertases

Due to the dependence of PCs on Ca^{2+}, some calcium chelating agents have been proposed as inhibitors of PCs. Their low affinity and the involvement of Ca^{2+} over a wide range of biochemical reactions in the human body are obstacles for further development of this class of inhibitors.[151-152] The diterpene compounds extracted from the *Andrographis paniculata* plant were found to be micromolar inhibitors of PC1 and PC7.[153]

Despite all efforts to find non-peptide-based PC inhibitors, only compounds with the 2,5-dideoxystreptamine scaffold exhibited nanomolar potency in the inhibition of PCs.[154] The multi-guanylated compound **43** inhibits furin with K_i = 6 nM (**Figure 17**).[154] However, further cellular analysis indicated that compound **43** has moderate cytotoxicity and low interaction with intracellular furin.[155] Optimization of this compound resulted in compounds **44** (furin K_i = 12 nM) and **45** (furin K_i = 400 nM) with higher capacity for treatment of pathogenic bacterial infections (e.g. *Pseudomonas aeruginosa* or *Bacillus anthracis*) despite their lower potency for furin. More recently, crystallographic studies of compound **43** in furin active sites indicated that the high affinity for furin is the result of the interactions of two molecules of **43** in the catalytic cleft.[156] One molecule interacts directly with the S4 pocket and interferes with the catalytic triad, while the other molecule is bound loosely at a remote location near the active site.[156]

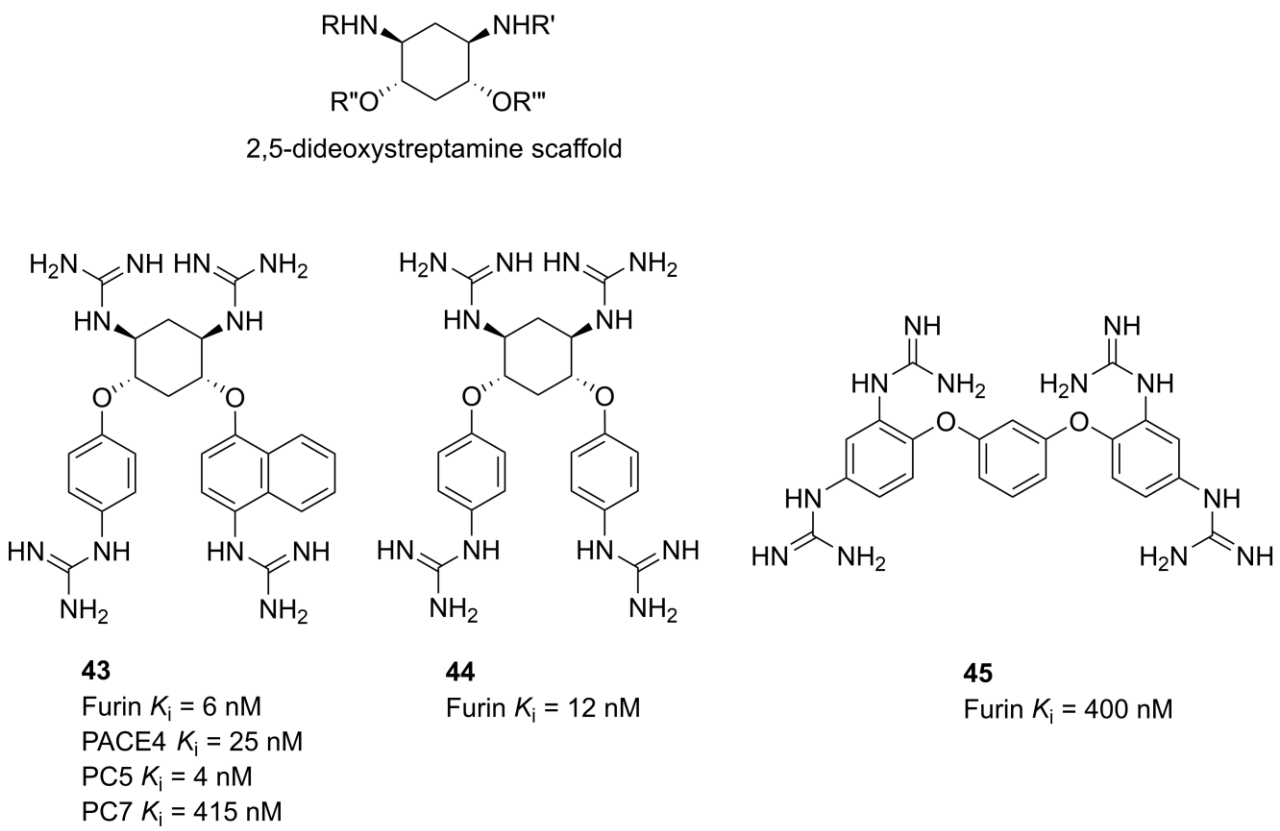

Figure 17. Structure of 2,5-dideoxystreptamine scaffold and its derivatives as potent furin inhibitors.

Becker et al. built libraries of peptidomimetic based on the RVKR motif and early findings on compound **23** (**Table 2**).[157] By screening arginine mimetics in P1, they found that 4-amidinobenzyl amine (Amba) can replace Arg advantageously at that position. Thus, compound **46**, which is the best furin inhibitor in that study (furin K_i = 0.81 nM), has phenylacetyl (phac) and Amba residues at positions P5 and P1 respectively (**Figure 18**). This peptide analogue was a starting point for further exploration beyond the P4 residue which yielded guanidine **47**.[158] The presence of a basic P5 residue (3-guanidinomethyl-phenylacteyl) in **47** increased the affinity for furin by a magnitude of two (K_i = 0.008 nM, **Figure 18**). A crystal structure of protonated **47** in physiological pH bound to furin showed that the additional positive charge interacted with negative charges of the furin active site located in the S4 subsite and an alternative S5 subsite.[159] The P5 residue interacts unexpectedly with a region only 4 Å apart from the S4 subsite. Further modifications of P3-Val with natural amino acids did not improve affinity, but the inclusion of *tert*-leucine (Tle) in this position and 4-guanidinomethyl-phenylacetyl in P5 led to compound **48** (furin K_i = 0.005 nM), the most potent inhibitor of furin discovered to date.[160] In a more recent study, the same group found that the modification of P2-Arg with Lys residue was associated with reduction in acute

toxicity on mice and thus improved the therapeutic index, but with a diminished furin affinity compared to **48**.[161]

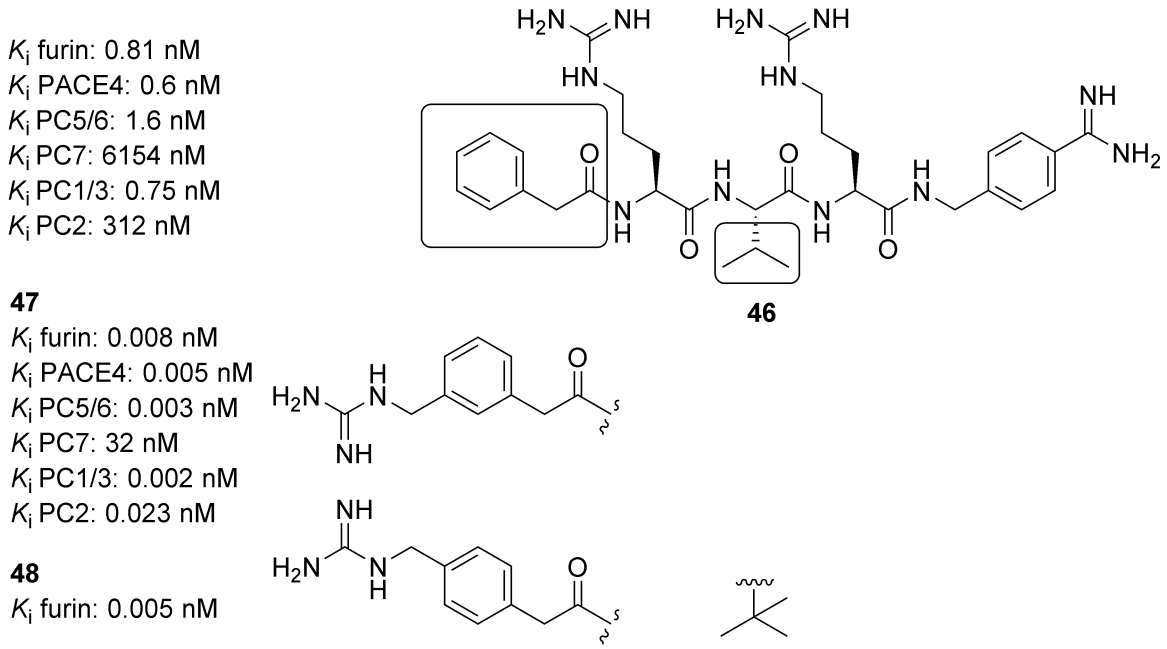

Figure 18. Representative chemical structure and affinity of peptidomimetic furin inhibitors

Other crystal structures of furin with and without ligand **47** and molecular dynamic studies demonstrated that the shape of the enzyme changes as the inhibitor approaches the active site cleft (**Figure 19**).[162] Free furin has a stable off-state conformation which transits to an on-state active conformation ready to accept the inhibitor. Once the inhibitor approaches the active cleft, the newly formed interactions introduce a favorable negative ΔG_{bind}. The new on-state inhibitor bound conformation is more stable than the off-state inhibitor-free conformation. A common feature of proteases including PCs is that peptide ligands adopt a β-sheet conformation (usually an antiparallel β-sheet) stabilized by residues in the active site (typically a Gly is involved).[163] The formation of this β-sheet-like interaction with Gly255 of furin along with deep S1 subsite interactions are found to be responsible for the spatial proximity of the catalytic serine in the catalytically active conformation (on-state) of furin.[162] The other important factors in the conformation of furin were chelation of two Ca^{2+} ions, which were shown to be instrumental in the structural integrity of furin.[162]

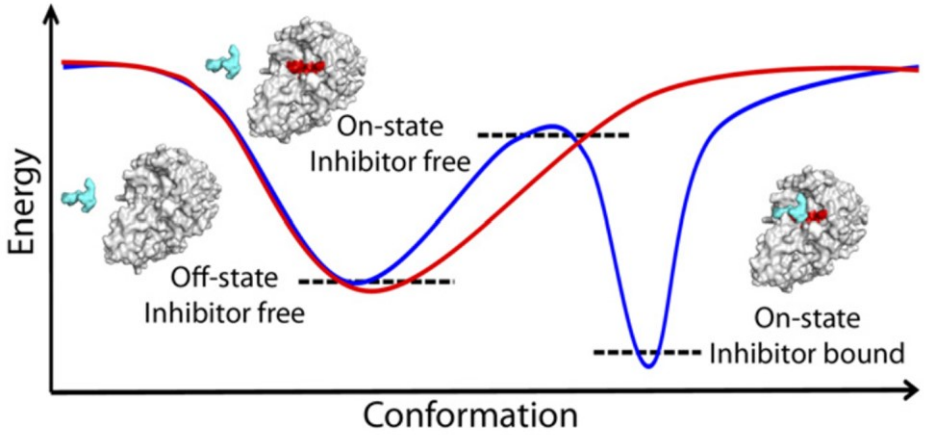

Figure 19. Schematic representation of inhibitor-induced conformation alteration in furin crystal structures. Figure reproduced from Dahms et al.[162]

I.4.4. Inhibitors of PACE4

Designing specific competitive inhibitors for PCs is challenging and laborious due to the high levels of homogeneity between the PC family in the S1–S4 subsites.[164] However, some differences appear beyond the S5 subsite as disclosed by the new crystallographic studies of some furin inhibitors.[165]

a)

Prodomain	K_i (nM)		specificity ratio
	PACE4	**Furin**	
hFurin	0.4 ± 0.1	1.7 ± 0.4	4.2
mPC1/3	1.1 ± 0.5	1.4 ± 0.3	1.3
hPC2	>1000	>1000	1.0
mPC4	7 ± 2	9.0 ± 0.7	1.3
hPC5/6	1.3 ± 0.1	2.9 ± 0.5	2.2
hPC7	0.34 ± 0.02	12.4 ± 0.6	36
hPACE4	2.0 ± 0.1	5.3 ± 0.1	2.7

b)

	P7	P6	P5	P4	P3	P2	P1
hFurin	**A**	K	R	R	T	K	R
mPC1/3	E	K	E	R	S	K	R
hPC2	G	F	D	R	K	K	R
mPC4	**L**	R	R	R	**V**	K	R
hPC5/6	**V**	K	K	R	T	K	R
hPC7	**L**	**L**	R	R	**A**	K	R
hPACE4	**V**	K	R	R	**V**	K	R
Consensus	-	K	R	R	-	K	R

Figure 20. a) The inhibition of PACE4 and furin by PC prodomains and b) the active site interacting residues. Reproduced with permission from the American Chemical Society.[166]

As discussed in section I.4.2 (**Table 2**), PC prodomains **26-32** are potent (nM range) inhibitors of PCs. While most prodomains inhibit PACE4 and furin in a similar range of concentrations, a PACE4 preference was noticed for PC7 prodomain **32** (**Figure 20-a**).[166] This was a starting point for further research on PC7 prodomain-derived peptides endowed with PACE4 specificity. Comparison of P7-P1 residues in the PC7 prodomain primary cleavage site with prodomains from other PCs revealed that two Leu at positions P6 and P7 are a unique feature of the PC7 prodomain. (**Figure 20-b**).[166]

In parallel, Positional Scanning-Synthetic Peptide Combinatorial Libraries (PS-SPCL) of 6-mer peptides having the RVKR consensus sequence at positions P4–P1 resulted in the strong and selective inhibitor Ac-LL**RVKR**-NH_2 (furin K_i = 900 nM and PACE4 K_i = 49 nM),[166] a peptide whose sequence is very similar to that of the PC7 prodomain-derived peptide (LLR**RAKR**). Sequential addition of Leu residues to the N-terminal of RVKR was associated with an in increase in selectivity. The peptides with three and four Leu showed the best potency and selectivity. However, the octapeptide displayed better antiproliferative activity on prostate cancer cell lines and thus, was chosen for further investigation and SAR analysis. This octapeptide, which was named Multi-Leu (ML) peptide, was 20 times more selective for PACE4 over furin (furin K_i = 430 nM and PACE4 K_i = 22 nM; **Figure 21**).[166]

Peptides Sequences	K_i (nM)		specificity
P10 P9 P8 P7 P6 P5 P4 P3 P2 P1	**PACE4**	**Furin**	ratio
Ac- R V K R - NH_2	1600 ± 400	1300 ± 100	0.81
Ac- L R V K R - NH_2	1600 ± 300	1200 ± 100	0.75
Ac- L L R V K R - NH_2	240 ± 40	900 ± 70	3.8
Ac- L L L R V K R - NH_2	18 ± 1	400 ± 10	22
Ac- L L L L R V K R - NH_2	22 ± 6	430 ± 10	20
Ac- L L L L L R V K R - NH_2	70 ± 10	1000 ± 30	14
Ac- L L L L L L R V K R - NH_2	300 ± 100	4100 ± 300	14

Figure 21. Optimizing the number of Leu residues in the tail of the RVKR warhead leading to the discovery of Multi-Leu peptide. Reproduced with permission from the American Chemical Society.[166]

In the MTT antiproliferative assay, the metabolic activity of cells is evaluated based on the ability of mitochondrial oxidoreductases to reduce yellow MTT (3-(4,5-dimethylthiazol-2-yl)-2,5-diphenyltetrazolium bromide) to purple formazan (**Figure 22**). Treatment of cells with different concentrations of PACE4 inhibitors affects their metabolic activity (response). The related dose-response curves are used to determine the IC_{50} (the concentration that shows half of maximal inhibitory effect) of the corresponding inhibitors. The cellular antiproliferative activity (IC_{50}) of ML peptide on DU145 and LNCaP prostate cancer cells was calculated to be 100 µM and 180 µM respectively (**Figure 23**).

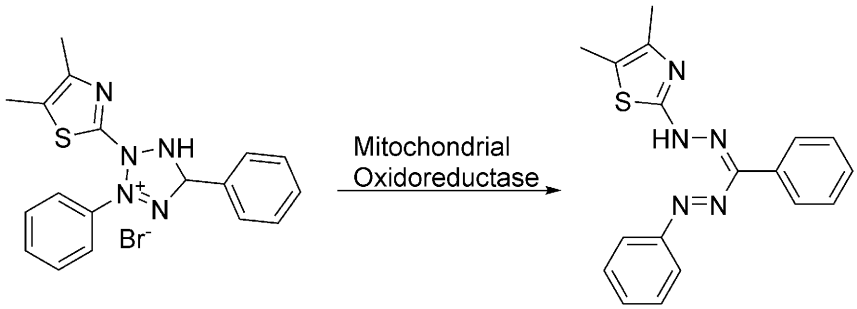

Figure 22. Conversion of MTT to formazan in mitochondria of metabolically active cells

Because the sequence of the ML peptide contains only natural residues, it can be easily cleaved by human plasma proteases. Therefore, SAR studies were performed on this lead peptide using peptidomimetic strategies to improve its short half-life ($t_{1/2}$). These efforts led to the discovery of compound C23 with enhanced affinity for PACE4 and improved cellular activity (**Figure 24**).[167-168] Compound C23 is armed with 4-amidinobenzylamide (Amba) in P1 and DLeu in P8. Inclusion of these two unnatural residues increased the half-life from a few minutes in ML to 1.7 h in C23.[169] As for furin inhibitors, Amba displayed stronger interactions in P1 compared to Arg, which led to higher PACE4 affinity of C23 compared to the ML peptide (K_i = 4. 9 nM, **Figure 24**). The antiproliferative activity of C23 was also improved (DU145 IC_{50} = 25 µM and LNCaP IC_{50} = 45 µM; **Figure 23** and **24**).

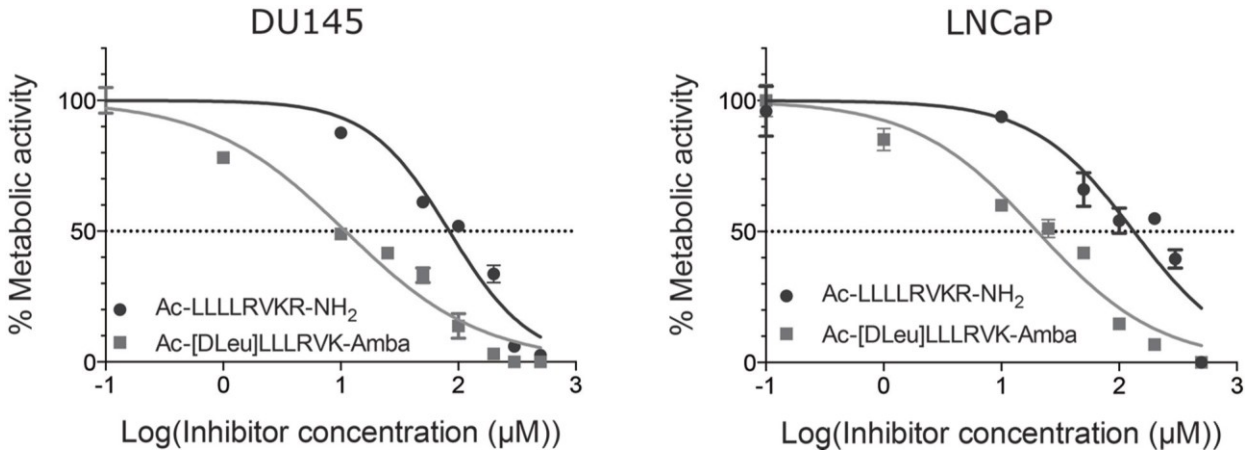

Figure 23. Dose-response curves in MTT assay for ML and C23 compounds on prostate cancer cell lines. Reproduced with permission from Levesque et al.[170]

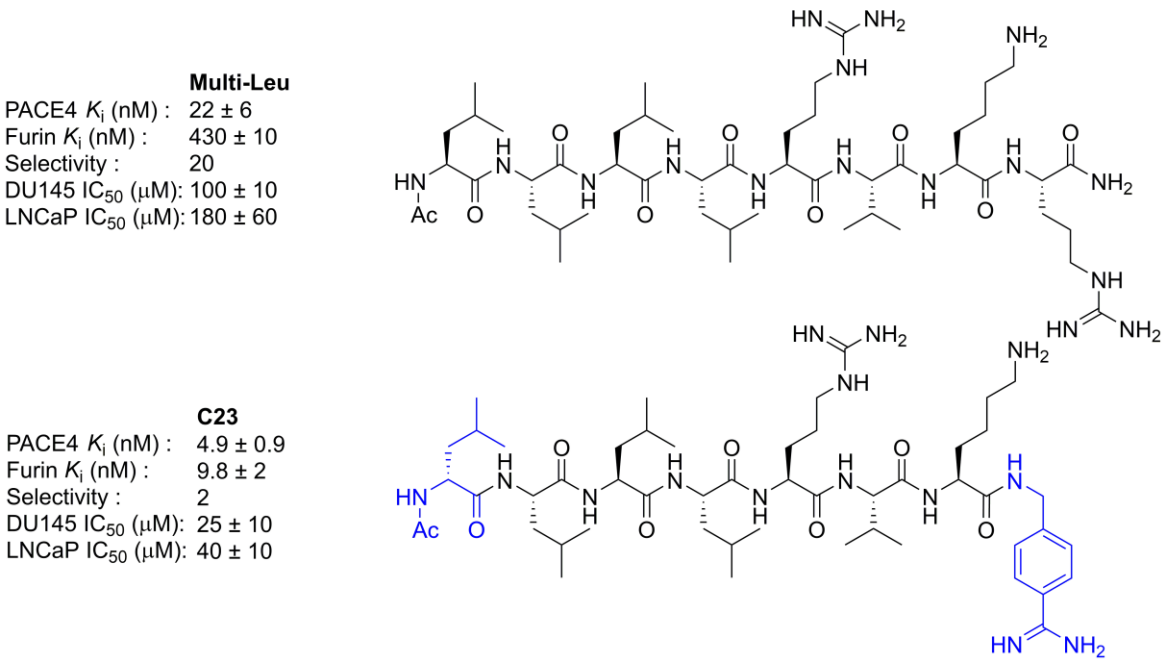

Figure 24. Chemical structures, enzymatic and cellular potencies of ML and C23.

Studies focused on the ML peptide indicated that the penetration of this peptide into the cell is essential for cellular antiproliferative activity.[166] N-terminal extension of ML or C23 peptides with polyethylene glycol (PEG) chains of various lengths reduced the cell permeability of the resulting inhibitors. The lower cell permeability of PEGylated inhibitors was identified as the reason for attenuated cellular activity.[166, 168] The cell permeability of PACE4 inhibitors was assessed by treating the DU145 cells with FITC (fluorescein isothiocyanate) labeled peptides followed by counting the number of cells that emit fluorescence using a FACS machine (fluorescence activated cell sorter). More recently, PACE4-altCT, an alternatively spliced version of PACE4, has been identified as the enzyme responsible for the appearance of malignant metabolites in pathologic conditions.[91] This spliced version is located inside the TGN endosomes and thus the cell penetration of the inhibitor is necessary to reach it. PACE4 mediates its effects on PCa by processing pro-GDF-15 to GDF15, which is an important factor for cell growth.[91] GDF15 also protects cancer cells against radiation-therapy and is involved in tumor neovascularization.[91] By inhibiting PACE4, C23 was shown to inhibit the processing of pro-GDF-15 to its mature protein as well as some other undiscovered substrates.[91]

Both C23 and ML peptides have four leucines in P5–P8 positions. A systematic scan of these positions of C23 compound with all the natural residues, except Cys, revealed that these residues should be

essentially hydrophobic[171] and that inhibitors must therefore be amphipathic to be active *in cellulo*. Cell permeability is the primary issue in this regard.

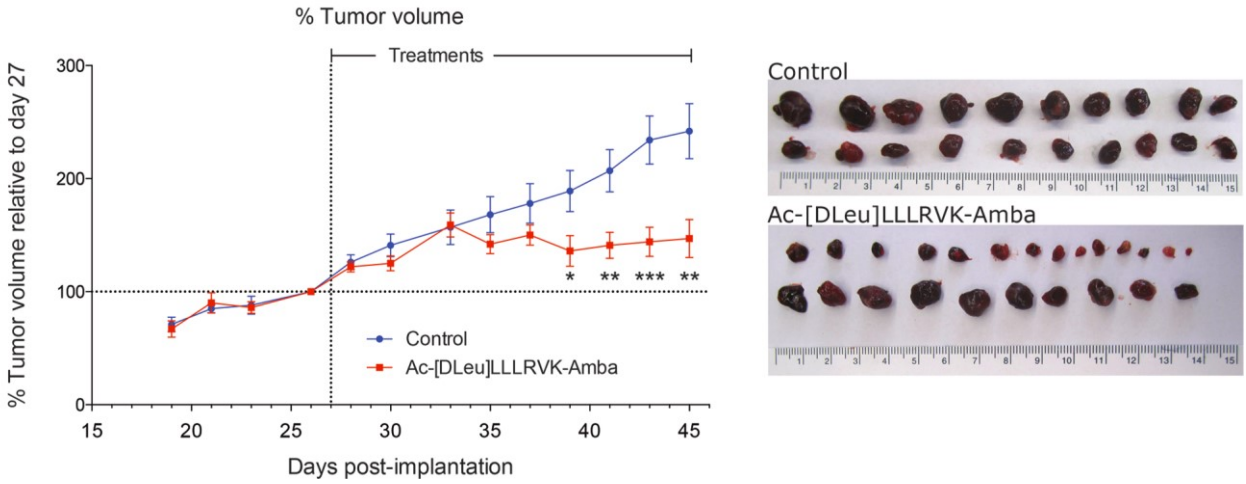

Figure 25. Tumor progression following 2 mg/kg/day treatment with C23 compound. Reproduced with permission from Levesque et al.[170]

N-terminal lipidation of ML or C23 preserves or improves the antiproliferative activity. However, the acute toxicity of lapidated inhibitors on healthy CD1 mice was significantly higher than non-lipidated compounds.[168]

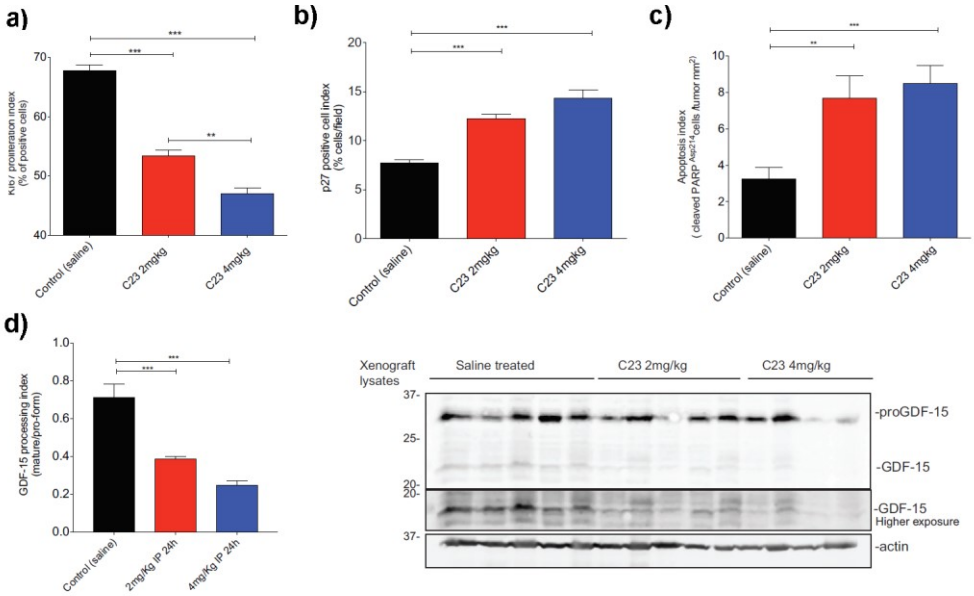

Figure 26. The dose-dependent effect of PACE4 inhibition by C23 on cell proliferation, cell quiescence, apoptosis and pro-GDF-15 processing *in vivo*. Reproduced with permission from American Association for Cancer Research.[91]

With improved stability in human plasma and increased cellular activity, C23 was tested *in vivo* using a LNCaP xenografted tumor mice model. When administered systematically in 2 mg/kg/day doses, C23 inhibited the tumor growth by 60% compared to non-treated controls over a period of 18 days of treatment (**Figure 25**).[170] The PSA levels during the period of treatment followed the same pattern with 47% reduction for treated animals at the completion of the experiment (170 ± 40 ng/mL for control and 90 ng/mL for C23 treated animals).[170] The analysis of the tumors revealed that the number of cells progressing through cell cycle were significantly reduced (20%) after administration of C23 (cell quiescence at Go/G1 state).[170] The rate of apoptotic cells within control tumor raised from 2.4% to 6% in treated tumors, which indicated a 250% increase. In addition, the angiogenesis and micro-vascularization was considerably reduced in tumor tissues (40%).[170] In another study, a 28 days intraperitoneal administration of LNCaP xenografted tumors with 2 and 4 mg/kg/day doses of C23 was shown to affect cell proliferation, cell quiescence and apoptosis markers in a dose-dependent manner (**Figure 26-a** to **26-c**).[91] The levels of GDF-15, a PACE4 metabolite, was also reduced after 28 days of treatment with C23 (**Figure 26-d)**, which provided evidence of PACE4-mediated pharmacodynamics of C23.[91]

The ML peptide and C23 was radiolabeled with ^{64}Cu by addition of NOTA (1,4,7-triazacyclononane-triacetic acid, a bifunctional chelating group, **Figure 27**) in its N-terminus to investigate its *in vivo* uptake.[172] Positron emission tomography (PET) scanning of ^{64}Cu/NOTA-DLeu-LLLRVK-Amba and ^{64}Cu/NOTA-LLLLRVKR-NH_2 showed a rapid uptake of the peptides by LNCaP xenografted tumor suggesting a significant tissue penetration of PACE4 inhibitors.[170, 173] The uptake of inhibitors by tumor was shown to follow a PACE4-dependent mechanism. Although C23 and its radiolabeled version were rapidly eliminated from the plasma, the study confirmed efficient distribution and significant tumor uptake of these PACE4 inhibitors.[170]

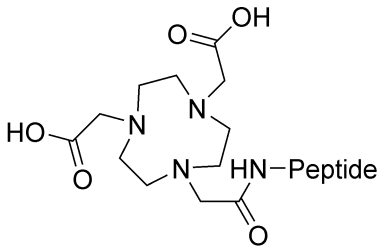

Figure 27. General structure of NOTA-labeled peptides

I.5. Thesis objectives

Despite the advantages of C23 as an inhibitor of PACE4 for the treatment of PCa, there is still room for improvement in selectivity, cellular activity and stability. The primary drawback of the C23 compound is its fairly low PACE4 selectivity. As represented in I.4.4 section, the PACE4 affinity of C23 compared to ML peptide was improved by more than 4-fold (PACE4 K_i = 22 nM and 4.9 nM for ML and C23, respectively). Unfortunately, at the same time, the PACE4 selectivity was reduced from 20-fold for ML to only 2-fold for C23. Furin inhibition is a concern because it is ubiquitously expressed in all human tissues. Consequently, its inhibition may potentiate side effects in off-target tissues.[100] As a result, the quest of PACE4 inhibitors devoid of residual furin inhibition is still on.

Based on PC mRNA silencing studies (section I.3.6), PACE4 is indeed the key PC in proliferation and homeostasis of prostate tumor. By inhibiting PACE4, C23 was shown to block the processing of pro-GDF-15 to its mature protein.[91]

Further SAR investigation of C23 and ML are addressed in the following chapters. The primary objective of the current thesis is to improve the selectivity and affinity of PACE4 inhibitors over furin. This goal is pursued by modifications in the P3, P1 and P1' positions of the ML and C23 compounds.

In the P3 position, basic residues were investigated for replacement of Val to establish new interactions with Asp160 of PACE4. Asp160 was identified as the only different residue in the active site region of PACE4 compared to furin. The results of this study were published in ChemMedChem as a communication and are presented in the first chapter of the current thesis.

Despite similarities of the S1 subsites in PACE4 and furin, Amba-bearing inhibitors such as C23 typically display low selectivity for PACE4. This is due to the higher affinity of Amba for furin's S1 subsite compared to PACE4's. Therefore, previously not-tested Arg mimetics were evaluated in the P1 position of C23 pursuing selectivity. This study, published in the Journal of Medicinal Chemistry as a full article, is presented in the second chapter.

Exploiting the P1' position of PACE4 inhibitors for selectivity, surprisingly, resulted in an improvement of other aspects as well. Thus, screening of natural residues at this position further led to the rational design of some unnatural residues providing more PCa cellular penetration and antiproliferative activity.

The results of this investigation are published in the Journal of Medicinal Chemistry as a full article and are presented in the third chapter.

Overall, different strategies including optimization of P3 (Chapter 1), P1 (Chapter 2) and P1' positions (Chapter 3) are exploited to enhance the selectivity and antiproliferative activity profile of PACE4 inhibitors. The current thesis offers new conceptual knowledge and leads for developing next generation PACE4 inhibitors as candidates for targeted therapy of prostate cancer.

CHAPTER 1 : RATIONAL DESIGN OF A HIGHLY POTENT AND SELECTIVE PEPTIDE INHIBITOR OF PACE4 BY SALT BRIDGE INTERACTION WITH D160 AT POSITION P3

The current chapter was published in *ChemMedChem* 2017, **12**, 1169 – 1172 (DOI: 10.1002/cmdc.201700300) with the following title, authors and affiliations;

Rational Design of a Highly Potent and Selective Peptide Inhibitor of PACE4 by Salt Bridge Interaction with D160 at Position P3

Vahid Dianati,[a] Azar Shamloo,[b] Anna Kwiatkowska,[c] Roxane Desjardins,[c] Armand Soldera,[b] Robert Day,[c] and Yves L. Dory*[a]*

[a] Institut de Pharmacologie de Sherbrooke, IPS, Département de Chimie, Faculté des Sciences, Université de Sherbrooke, 3001 12e Avenue Nord, Sherbrooke, Québec J1H 5N4 (Canada)

E-mail: Yves.Dory@usherbrooke.ca

[b] Département de Chimie, Centre Québécois sur les Matériaux Fonctionnels, Université de Sherbrooke, Sherbrooke, Québec J1K 2R1 (Canada)

[c] Institut de Pharmacologie de Sherbrooke, Département de Chirurgie/Urologie, Université de Sherbrooke, 3001 12e Avenue Nord, Sherbrooke, Québec, J1H 5N4 (Canada)

E-mail: Robert.Day@USherbrooke.ca

1.1. Author contributions

This work was done in the Institut de Pharmacologie de Sherbrooke under the supervision of Pr. Robert Day and Pr. Yves L. Dory in collaboration with Pr. Armand Soldera's lab at the Département de Chimie, Centre Québécois sur les Matériaux Fonctionnels in Université de Sherbrooke. The original research article was published by Vahid Dianati, Azar Shamloo, Anna Kwiatkowska, Roxane Desjardins, Armand Soldera, Robert Day, and Yves L. Dory in ChemMedChem 2017, **12**, 1169 – 1172. Vahid Dianati and Yves L. Dory designed the compounds. Vahid Dianati synthesized all the compounds and performed the kinetic assays. Roxane Desjardins purified the recombinant enzymes for kinetic assays. Azar Shamloo

did the MD simulations under supervision of Armand Soldera. Anna Kwiatkowska contributed in performing the kinetic assays. Vahid Dianati, Robert Day and Yves L. Dory analyzed the data. Vahid Dianati wrote the manuscript with revisions from Anna Kwiatkowska, Robert Day and Yves L. Dory.

1.2. Abstract

PACE4, a member of the proprotein convertases (PCs) family of serine proteases, is a validated target for the treatment of prostate cancer. Our group has developed a potent and selective PACE4 inhibitor: Ac-LLLLRVKR-NH_2. In seeking for modifications to increase the selectivity of this ligand toward PACE4, we replaced one of its P3-Val methyl groups with a basic group capable of forming a salt bridge with D160 of PACE4. The resulting inhibitor is eight times more potent than the P3 Val parent inhibitor and two times more selective over furin, because the equivalent salt bridge with furin E257 is not optimal. Moreover, the β-branched nature of the new P3 residue favors the extended β-sheet conformation usually associated with substrates of proteases. This work provides new insight for better understanding of β-sheet backbone–backbone interactions between serine proteases and their peptidic ligands.

1.3. Introduction

Binding of peptide ligands to their complementary enzyme or receptor is controlled by two important factors from internal and external origins; namely, their conformation and their binding interactions with the target. Thus, in the best scenario, their active conformation corresponds to their intrinsic most stable shape. Moreover, these ligands ideally develop as many noncovalent interactions as possible with the target biomolecule to ensure tighter binding. Here we show that proper substitution of a single key residue of a protease inhibitor can be leveraged to impact both factors in a concerted manner.

β-Strands are ubiquitous secondary structures. They have been identified as important features in antimicrobial peptides and natural ligands for biomolecular hosts like proteolytic enzymes, major histocompatibility complex (MHC) proteins and transferases.[163] It is well known that proteases universally bind to their substrates in extended β-strand conformation.[174] The β-sheet backbone hydrogen bonding pattern (mostly antiparallel) is crucial for peptide-based ligands to bind. In drug design targeting proteases, drug resistance is a serious issue. The active site geometry must be conserved to maintain the catalytic activity, so enhancing the backbone interactions, while stabilizing the active conformation, is a logical way to alleviate the effect of mutations.[175]

Statistic[176] and thermodynamic[177-178] studies clearly established that β-sheets prefer β-branched residues (Val, Ile, and Thr) in their structure rather than other residues. The greater steric clashes between the local backbone and the side chain of β-branched residues, favors β-sheets over all other conformations.[179-180] Moreover, β-sheet hydrogen bonds are shielded from interfering water molecules.[181] Consequently, Val and Ile are privileged residues in peptidic inhibitors of proteolytic enzymes.[182-184]

Side chain to side chain interactions, including those between charged residues,[185-186] cation–π interactions,[187] π–π interactions[188] and covalent bonds like disulfide bonds[189] have been employed to stabilize artificial β-sheet models. Recently, Gellman's group used a series of charged bearing β-branched amino acids making intramolecular salt bridges in their artificial β-sheets. These amino acids proved to be better β-sheet inducers and stabilizers than natural residues.[190] Here, we take advantage of this β-sheet propensity by incorporating such related residues in our peptide protease complexes.

Proprotein convertases (PCs) belong to the family of substilin–kexin serine proteases, which recognize their substrates through pairing with basic residues (R-P3-R/K-R-↓-P1').[86, 164] They proteolytically activate a range of proproteins, including hormones, receptors, growth factors, zymogens, etc. The seven members of proprotein convertases including PC1/3, PC2, PC4, PC5/6, PC7, furin and PACE4 have many resemblances in their active sites. [86, 164] We have shown that PACE4 is a promising target in prostate[117] and ovarian cancer.[191] Optimization of binding selectivity is a major path toward drug candidates to alleviate potential side effects. Additionally, *in vivo* use necessitates the elaboration of stable compounds. Our research group has developed a PACE4 peptide inhibitor with the Ac-LLLLRVKR-NH_2 sequence[166, 170] which named the Multi-Leu (ML) after its four leucine residues. The hydrophobic tetra-Leu tail makes the RVKR tetrapeptide warhead an amphipathic cell penetrating peptide and increases the selectivity toward PACE4 (20-fold). We also reported the P1 Arg modification of ML with 4-amidinobenzylamide (Amba), which resulted in an inhibitor with improved activity and better stability *in vivo*.[167-168]

A P3 modification of a peptidomimetic furin inhibitor (Phac-RVK-Amba, where Phac stands for phenylacetyl) has been investigated by replacing Val with many other natural and modified amino acids.[192] That study suggested to us that β-branched residues[176-178] might be used to stabilize the β-sheet conformation of inhibitors, while concomitantly adding interactions with furin and its homologous PACE4 enzymes, with suit-able β-substituents.

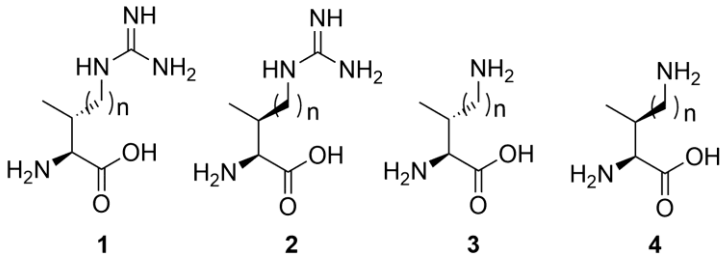

Figure 28. Structure of modified amino acids to be inserted at P3 of ML.

1.4. Results and discussions

According to a homology model of PACE4[87] developed from the crystal structure of furin (1P8J),[74] from all amino acids within the S1-S4 sub-pockets, there is just a single difference between the two enzymes: Asp160 in PACE4 replaces Glu257 of furin in S3. We designed β-branched basic amino acids **1–4** (**Figure 28**) to replace Val at position P3 of ML, to bind Asp160 of PACE4, while stabilizing its β-sheet conformation (**Figure 29**).

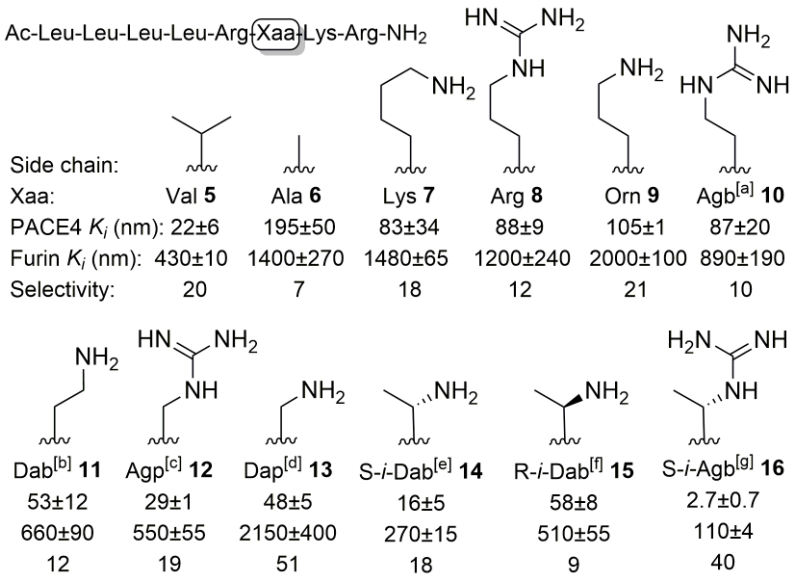

Figure 29. Structure and binding affinities of peptide inhibitors **5–16** for PACE4 and furin and their selectivity profile toward PACE4. All experiments were repeated at least twice, and data are shown as K_i ± SD. [a] 2-amino-4- guanidinobutyryl. [b] 2,3-diaminobutyryl. [c] 2-amino-3-guanidinopropionyl. [d] 2,3-diaminopropionyl. [e] 2*S*,3*S*-diaminobutyryl. [f] 2*S*,3*R*-diaminobutyryl. [g] 2*S*-amino-3*S*-guanidinobutyryl.

The binding affinities and selectivities (toward PACE4) of all the PACE4 inhibitors synthesized in the present work are summarized in **Figure 29**. Initial results from Val (**5**) substitution by Ala (**6**) suggest that β-branching is indeed important. We then endeavored to optimize the side chain length and the basic functional group. A series of ML P3 substituted analogues was prepared from commercial linear basic residues (**7–13**) using solid-phase peptide synthesis (SPPS). Inhibitors **7–10** showed almost the same trend for PACE4 inhibition. Since **12** and **13**, gave the best results, it was then clear that the ideal chain length for the β-branched analogues was 0 (n = 0 in **Figure 28**). We then logically prepared the corresponding inhibitors **14–16** from synthetic β-branched residues **20a** and **20b** (**Scheme 1**).

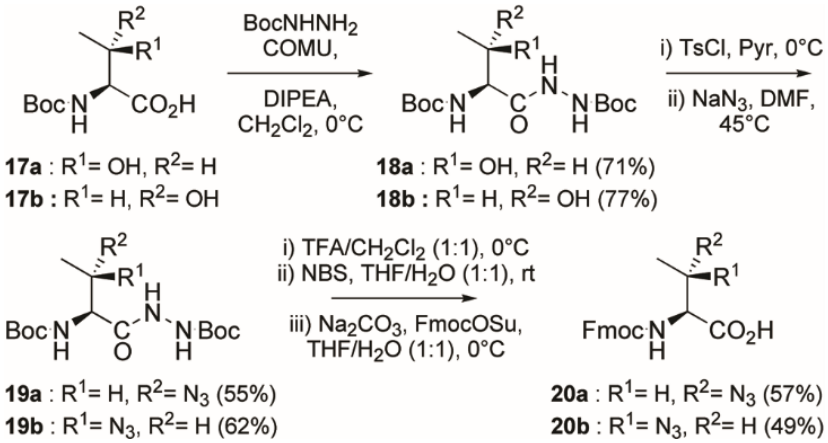

Scheme 1. Synthesis of Fmoc-protected residues **20a** and **20b**.

Thus, Boc-Thr-OH **17a** and Boc-allo-Thr-OH **17b** were protected as the Boc-hydrazides **18a** and **18b**. The β-hydroxy groups were converted into azides **19a** or **19b** through tosylation and subsequent azidation, with inversion of configuration at the β position. The Boc and hydrazide protecting groups were removed with TFA and NBS, respectively. Fmoc groups were installed on the resulting amino acids to yield the protected amino acids **20a** or **20b**, ready for Fmoc-SPPS (**Scheme 2**). After eight cycles of deprotection and coupling with the adequate residues, the terminal amine was deprotected then acetylated. The resin bound peptide azides **21a** and **21b** were reduced to their corresponding amines **22a** and **22b**. The amine **22a** was converted into the guanidine derivative **23**, directly onto the resin. The cleavage and global deprotection of **22a**, **22b** and **23** gave the peptide inhibitors **14**, **15** and **16**, respectively.

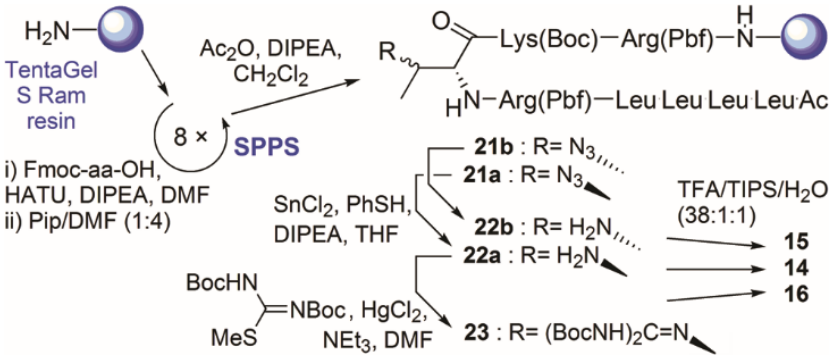

Scheme 2. Synthesis of peptide inhibitors **14–16** with modified residues.

The data reported in **Figure 29** show that, among the new inhibitors with straight chains (**7–13**), **12** is as potent as ML **5**. This suggests that the salt bridge between the guanidinium ion of Agp (2-amino-3-guanidinopropionyl) in **12** and the carboxylate of Asp160 in PACE4 is in fact almost as effective as the β-sheet inducing effect of Val in **5**. The salt bridge is not as strong with a simple ammonium ion as in **13**. Methyl groups were then introduced at the β-position of Dap (2,3-diaminopropionyl) in **13** to transform it into a β-sheet inducer like Val in ML **5**. It appeared that only one isomer, *S*-*i*-Dab (2*S*,3*S*-diaminobutyryl), produced the expected additive effect. The corresponding inhibitor **14** is now more potent than **5**, whereas its stereoisomer **15** is even less active than its parent **13**. The inhibitors **14** and **15** were docked into a model of PACE4 to compare their geometry with **5** (**Figure 30**). To satisfy the salt bridge structural requirements, the methyl group has to orient toward (for 3-S isomer) or away (for 3-R isomer) from the β-sheet hydrogen bond. The orientation of the β-methyl and β-ammonium groups of *S*-*i*-Dab (**14**) is the same as the Val methyl substituents in the crystal structure of furin.[74, 159] We assume that only this orientation is prone to induce the β-sheet conformation of the inhibitor ligand. This is supported by the χ1 value of S-*i*-Dab (-37 °) corresponding precisely to an antiparallel β-sheet.[193] Whereas, in inhibitor **15**, the salt bridge between the ammonium group of *R*-*i*-Dab and D160 forces the residue to adopt a χ1 value (-160°) normally found in parallel β-sheets. This phenomenon is obviously fighting the natural antiparallel mode of binding of inhibitors of PACE4. Consequently, the PACE4-**15** complex is probably less stable than the stereoisomeric complex between PACE4 and **14**.

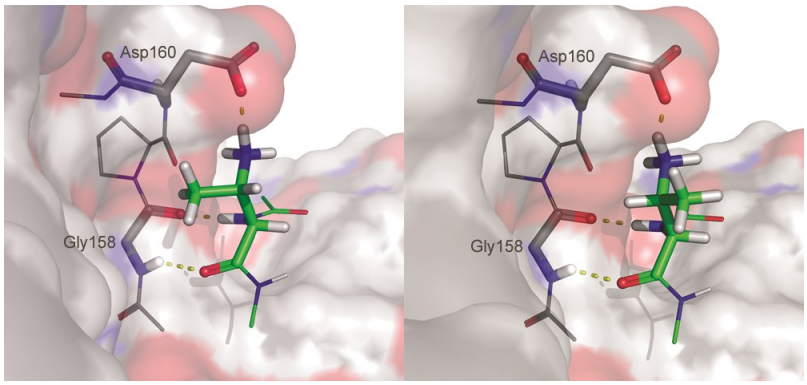

Figure 30. Docking of inhibitors **14** and **15** in PACE4. *S-i*-Dab from **14** (left) and *R-i*-Dab from **15** (right) in the S3 pocket of a PACE4 homology model.

On top of the beneficial β-sheet stabilization in peptide **14**, it is also likely that the isopropyl group orientation could affect the solvation profile of β-sheet hydrogen bonds, by screening them from external water molecules. Such shield effect is absent in inhibitor **15**.

Because inhibitor **14** has the correct stereochemistry for optimal binding, its equivalent guanylated analogue **16** was investigated. Some degree of synergy appears to be at work in its mode of inhibition, because it is eight times more potent for PACE4 than ML **5**, while two times more selective (20-fold vs. 40-fold, respectively).

To gather additional support for our hypothesis that β-branching of P3 residue might affect the conformation of peptide inhibitors; we recorded the CD spectra of inhibitors **5** and **6**. We were expecting to witness different conformational behaviors. Unfortunately, both octapeptides displayed identical random coil spectral patterns. We then turned our attention to molecular dynamics (MD) simulations on a PACE4 homology model in coordination with the two tetrapeptides Ac-RVKR-NH_2 and Ac-RAKR-NH_2 as ligands. Because the P3 side chains in these two model peptides are solvent exposed and have no interactions with the target enzyme, effect of β-branching on conformation could be investigated independently. The Ramachandran plot parameters, Φ and Ψ as descriptors of conformations, were analyzed for the P3 residue during the simulation (**Figure 31a**). The two tetrapeptides adapt different conformations described by the ∠N-H···O hydrogen bond angles (α_1 and α_2) between the P3 residue and Gly158 backbones (**Figures 30** and **31b**). During the MD simulations, the values of these angles for the Val residue remain consistently larger (average α_1 of 149° and α_2 of 159 °) than for the Ala residue (average α_1 of 115° and α_2 of 130°). Because the ideal α_1 and α_2 angles for an antiparallel β-sheet, are

160° ± 10°,[194] the Val residue, in the model tetrapeptide, mostly adopts an antiparallel β-sheet conformation. Whereas the Ala equivalent in P3 is mainly in the poly-Pro II (PPII) helix region, which is often observed in β-turn residues.

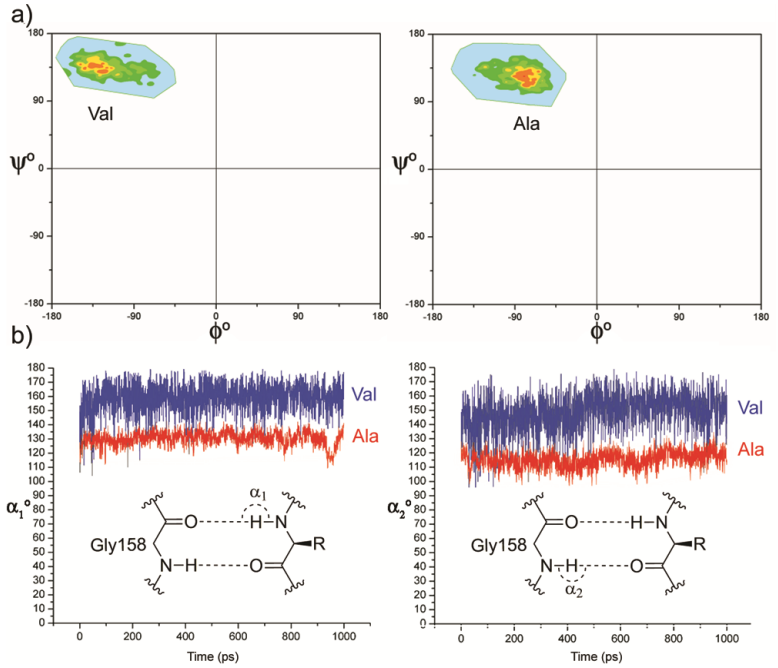

Figure 31.MD simulation (1 ns) of Ac-RVKR-NH2 and Ac-RAKR-NH2 docked in a PACE4 homology model. a) Ramachandran plots for the P3 residues. The F and Y angles for Val correspond to an antiparallel β-sheet, whereas those for Ala correspond to a PPII helix. b) Variations of the hydrogen bond angles a_1 and a_2 (∠N-H···O) between Gly158 of PACE4 and the P3 residues of the inhibitor backbones.

These computational data add credibility to the idea that β-branched residues like Val, *S*-*i*-Dab (as in **14**) and *S*-*i*-Agb (as in **16**) are β-sheet inducers when located at position P3 of PACE4 (as well as furin) inhibitors structurally related to **5**.

1.5. Conclusion

In summary, we introduced a new basic β-branched amino acid (*S*-*i*-Agb in **16**) to the P3 position of the PACE4 inhibitor, ML **5**, leading to the discovery of a peptidic inhibitor with improved potency and selectivity over furin. We propose that this improvement is the result of three additive effects at the same P3 position: 1) additional stabilizing electrostatic interactions with Asp160; 2) stabilizing hydrophobic interaction between the β-methyl substituent (having the correct configuration as in **Figure 30**, left) and the Gly158-Pro159 region of PACE4, and 3) increase in β-sheet propensity resulting from β-branching. To the best of our knowledge, the correlation that might exist between β-sheet propensity of inhibitor

residues and protease inhibition has not been studied. We suggest that β-sheet propensity improvement, coupled with other side chain stabilizing interactions, could be considered as a principle to target other proteases as well.

1.6. Acknowledgements

We acknowledge the Canadian Cancer Society Research Institute (701590 to R.D. and Y.L.D.) and Prostate Cancer Canada (TAG2014-02 to R.D.) for their support. We thank Dr. Manuel E. Than, who offered his PACE4 homology model.

1.7. Supporting information

1.7.1. Chemistry

All solvents and reagents were obtained from commercial suppliers and were used without further purification. All commercial amino acid derivatives and coupling reagents were purchased from Matrix Innovation, Inc. (Montreal, QC, Canada) and ChemImpex International (Wood Dale, IL, USA). TentaGel S RAM resin (loading: 0.22 mmol/g) was purchased from Rapp Polymer (Tübingen, Germany). HPLCs were carried out on an Agilent Technologies 1100 system equipped with a diode array detector (λ = 210, 214, 230, and 254 nm) and an Agilent Eclipse XDB C18 column (5 μm, 4.6 × 250 mm). SELDI-TOF mass spectrometry (ProteinChip, Bio-Rad Laboratories Inc., Hercules, CA, USA) or ESI-TOF mass spectrometry and HRMS (TripleTOF 5600, ABSciex; Foster City, CA, USA) used to confirm the identity of pure products. The ^{1}H and ^{13}C NMR spectra performed on an either Bruker Spectrospin 300 or Bruker Ascend 400 NMR instruments. The following abbreviations were used to describe spin multiplicity: s, singlet; d, doublet; t, triplet; quin, quintet; dd, doublet of doublets; and m, multiplet. The concentrations for $[\alpha]_D^{20}$ are reported in $g.cm^{-1}$.

Peptide Synthesis. All the peptides were synthesized with standard Fmoc-SPPS on Tentagel S-RAM using 3eq amino acids, 3eq of HATU as coupling reagent and 9eq of DIPEA as base for coupling and 20% piperidine/DMF for Fmoc deprotection. N-terminal acetylation of all the inhibitors was done with CH_2Cl_2/acetic anhydride/DIPEA (17:1:1) for 30 min. Peptides were cleaved and deprotected (side chains) with a cocktail of TFA/TIS/H_2O (38:1:1), stirred for 2H at RT, precipitated by cold ether, washed one more time with ether, and lyophilized. The lyophilized peptides were purified on preparative HPLC with a gradient of CH_3CN/H_2O. The fractions were analyzed with a gradient of 10 to 70% of CH_3CN and H_2O

containing 0.1% TFA. The fractions with >95% purity were pooled and used for kinetic studies. All inhibitors were obtained as TFA salts after lyophilization. The retention time and high-resolution mass of all inhibitors is are reported in Table S1.

Table S1. The HPLC retention time and high-resolution mass of peptide inhibitors with Ac-LLLLRXKR-NH_2

Inhibitor	X	Exact Mass		Retention time
		Calculated for	Found	
6	Ala	$[M+2]^{2+}$ 512.3611	512.3614	26.73[a]
7	Lys	$[M+3]^{3+}$ 360.9291	360.9288	16.11[b]
8	Arg	$[M+3]^{3+}$ 370.2645	370.2645	16.28[b]
9	Orn	$[M+3]^{3+}$ 356.2572	356.2570	16.19[b]
10	Agb	$[M+3]^{3+}$ 365.5926	365.5927	16.49[b]
11	Dab	$[M+3]^{3+}$ 351.5853	351.5853	16.23[b]
12	Agp	$[M+3]^{3+}$ 360.9207	360.9228	16.29[b]
13	Dap	$[M+3]^{3+}$ 346.9135	346.9136	25.92[a]
14	*S*-*i*-Dab	$[M+3]^{3+}$ 351.5853	351.5852	25.47[a]
15	*R*-*i*-Dab	$[M+2]^{2+}$ 526.8744	526.8749	25.45[a]
16	*S*-*i*-Agb	$[M+2]^{2+}$ 547.8853	547.8848	26.69[a]

[a] 50 min and [b] 20 min gradient of 10 to 70% of CH_3CN and H_2O containing 0.1% TFA

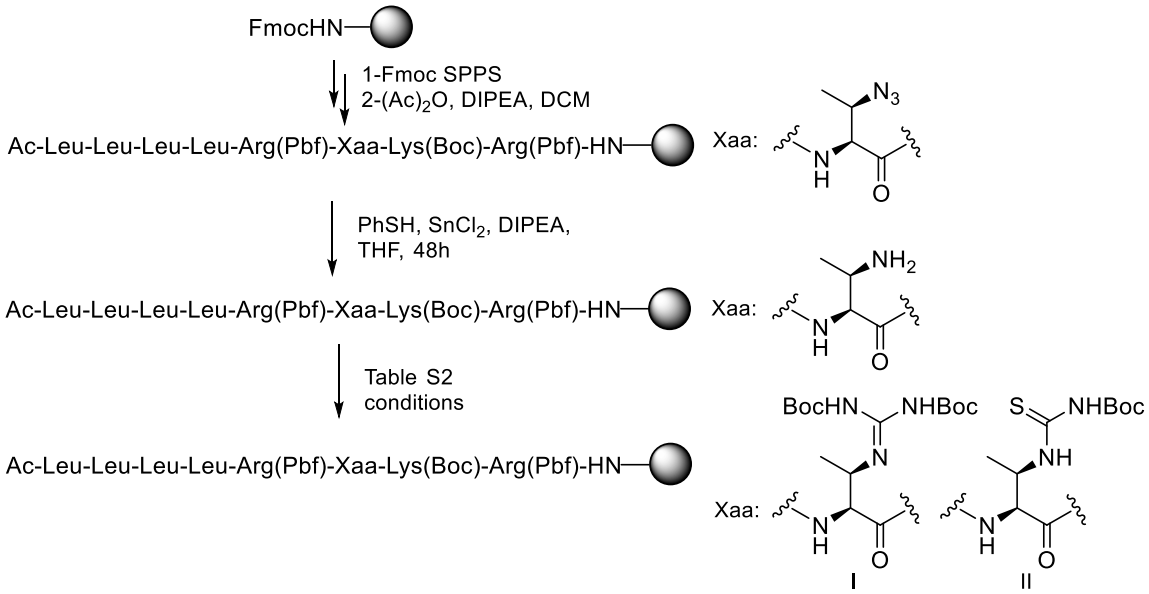

Scheme S1. Synthesis of compounds **14**, **15** and**16**

Reduction of azide group on resin. The resin bound peptide was washed with THF and then a fresh solution of 0.2 M $SnCl_2$, 0.8 M PhSH and 1M of DIEPA in THF (12 mL per g resin) was added[195] and then stirred for 48h. After SELDI-TOF MS indicated the completion of reaction, resin was washed with DMF 3x, MeOH 3x and CH_2Cl_2 3x.

Guanylation on resin. A series of reagents was examined for on resin guanylation (Table S2). The best results were obtained with N,N′-Di-Boc-S-methylisothiourea and $HgCl_2$ reagents. The resin was treated with a solution of 9eq of TEA and 1.5eq of N,N′-Di-Boc-S-methylisothiourea in DMF. It was shaken for 5 min then 3eq $HgCl_2$ were added and shaking was continued for 2h The completion of reaction was monitored with ninhydrin and SELDI-TOF MS then it was washed with 3*DMF, 3*MeOH and 3*CH_2Cl_2.

Table S2. The guanylation conditions

Conditions	Conversion	Product
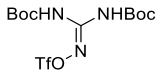 , DMF, 24h[196]	0%	N. R.
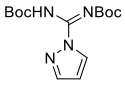 , DMF, 24h[197]	0%	N. R.
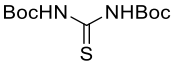 , TEA, $HgCl_2$, 2h	100%	**I** & **II**
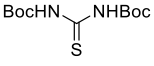 , TEA and after 5min $HgCl_2$,2h[198]	100%	**II**
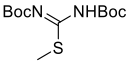 , TEA and after 5min $HgCl_2$,2h	100%	**II**

The overall yields for peptide inhibitors **14**, **15**, **16** were 35%, 32% and 24% respectively. The yields are calculated based on 0.22 g/mol loading of Tentagel S-RAM resin (0.5g).

Synthesis of unnatural amino acids. The Fmoc-Agb(Boc)$_2$-OH and Fmoc-Agp(Boc)$_2$-OH were synthesized from Fmoc-Dab-OH and Fmoc-Dap-OH respectively by a method from literatures and the spectroscopical data are identical with the reported one.[199] The rest of compounds were synthesized as follows.

Boc-Thr-NHNHBoc (18a):

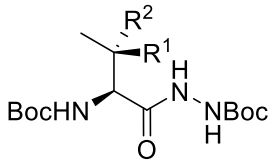

(2S,3R)-**18a** R^1: OH, R^2: H
(2S,3S)-**18b** R^1: H, R^2: OH

To an ice cooled solution of Boc-Thr-OH (18.1 g, 82.6 mmol) and *tert*-butyl carbazate (11.46 g, 86.7 mmol) in dry CH_2Cl_2 (200 mL), 2,6-lutidine (21.8 mL, 165.2 mmol) was added. After 5 min, COMU (37.1 g, 86.7 mmol) was added and the resulting mixture was stirred for 18 h at room temperature. The solvent was evaporated under vacuum and the residue dissolved in EtOAc, washed several times with Sat. $NaHCO_3$ (until the aqueous phase was colorless) then with water, 0.5 N HCl and brine, dried over

$MgSO_4$ and concentrated. The crude product was purified by flash chromatography (CH_2Cl_2/acetone from 90:10 to 70:30) to yield a colorless solid (19.67 g, 71%).

$[\alpha]_D^{20}$= −38.1 (*c*=0.0013 in $CHCl_3$)

^{1}H NMR (400 MHz, $CDCl_3$): δ (ppm): 1.20 (d, *J* = 6.15 Hz, 3H), 1.43 (br. s., 9H), 1.44 (s, 9H), 3.96 (br. s., 1H), 4.21 (d, *J* = 5.98 Hz, 1H), 4.30 (d, *J* = 6.32Hz, 1H), 5.70 (d, *J* = 7.52Hz, 1H), 7.00 (br. s., 1H), 8.64 (br. s., 1H). ^{13}C NMR (100 MHz, $CDCl_3$): δ (ppm): 171.3, 156.2, 155.6, 81.9, 80.4, 77.2, 67.3, 28.2, 28.1, 18.2. HRMS (ESI-TOF): m/z found 334.1969 $[M+H]^+$ (calcd. for $C_{14}H_{28}N_3O_6$, 334.1973).

Boc-*allo*-Thr-NHNHBoc (18b):

White solid. 77% yield

$[\alpha]_D^{20}$= −9.0(*c*=0.0020 in $CHCl_3$)

^{1}H NMR (400 MHz, $CDCl_3$) δ (ppm): 1.31 (d, *J* = 6.32Hz, 3H), 1.44 (s, 9 H), 1.46 (s, 9 H), 3.92 (d, *J* = 5.12Hz, 1H), 4.01 - 4.11 (m, 1H),5.54 (d, *J* = 7.69 Hz, 1H), 6.75 (br. s., 1H), 8.44 (br. s., 1H); ^{13}C NMR (100 MHz, $CDCl_3$) δ (ppm): 171.6, 155.9, 155.7, 82.2, 80.6, 77.2, 69.2, 28.3, 28.1, 19.6; HRMS (ESI-TOF): m/z found 334.1970 $[M+H]^+$ (calcd. for $C_{14}H_{28}N_3O_6$, 334.1973).

***tert*-Butyl 2-((2S,3S)-3-azido-2-((tert-butoxycarbonyl)amino)butanoyl)hydrazine-1-carboxylate 19a:**

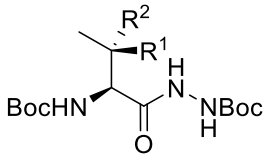

(2S,3S)-**19a** R^1: H, R^2: N_3
(2S,3R)-**19b** R^1: N_3, R^2: H

Tosyl chloride (10.29 g, 54 mmol) was added over 30 min to a solution of alcohol **18a** (13.9 g, 41.6 mmol) in 25 mL pyridine at 0°C. After 24h, stirring pyridine was removed by air and remaining oil was dissolved in EtOAc and washed 5 times with 0.2 N HCl and brine, dried over $MgSO_4$ and concentrated in vacuum to give a white solid, which was dissolved in 150 mL DMF. NaN_3 (8,84 g, 136 mmol) was added and heated for 18 h at 45 °C. After completion of the reaction, water was added and extracted with

Hex/Ether 1:1 three times. The combined organic layers were washed with water and brine, dried over $MgSO_4$ and concentrated. The crude product was purified by flash chromatography (Hex/EtOAc 70:30) to a white solid (8.2 g, 55% two steps).

$[\alpha]_D^{20}$= +15.7 (*c*=0.0017 in $CHCl_3$)

^{1}H NMR (300 MHz, $CDCl_3$) δ (ppm): 1.38 (d, *J* = 6.82 Hz, 3H), 1.45 (br. s., 9H), 1.46 (s, 9H), 3.83 (br. s., 1H), 4.41 (dd, *J* = 8.1, 5.3 Hz, 1H), 5.57 (d, *J* = 8.1 Hz, 1H), 6.82 (br. s., 1H), 8.71 (br. s., 1H). ^{13}C NMR (75 MHz, $CDCl_3$) δ (ppm): 168.9, 155.6, 154.0, 81.9, 80.9, 58.1, 56.0, 28.2, 28.1, 14.9. HRMS (ESI-TOF): m/z found 359.2035 $[M+H]^+$ (calcd. for $C_{14}H_{27}N_6O_5$, 359.2037).

***tert*-Butyl 2-((2S,3R)-3-azido-2-((tert-butoxycarbonyl)amino)butanoyl)hydrazine-1-carboxylate 19b:**

White solid. 62% yield

$[\alpha]_D^{20}$= +11.1 (*c*=0.002 in $CHCl_3$)

^{1}H NMR (400 MHz, $CDCl_3$) δ (ppm): 1.32 (d, *J* = 6.49 Hz, 3H), 1.45 (s, 9H), 1.45 (s, 9H), 4.14 (m, 1H), 4.32 (m, 1H), 5.52 (br. s., 1H), 6.91 (br. s., 1H), 8.71 (br. s., 1H). ^{13}C NMR (100 MHz, $CDCl_3$) δ (ppm): 169.1, 155.9, 155.0, 81.7, 80.7, 58.4, 56.4, 28.1, 28.0, 15.9. HRMS (ESI-TOF): m/z found 359.2032 $[M+H]^+$ (calcd. for $C_{14}H_{27}N_6O_5$, 359.2037).

(2S,3S)-2-((((9H-fluoren-9-yl)methoxy)carbonyl)amino)-3-azidobutanoic acid 20a:

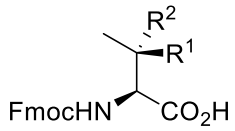

(2S,3S)-**20a** R^1: H, R^2: N_3
(2S,3R)-**20b** R^1: N_3, R^2: H

Azide **19a** (10.5 g, 31.5mmol) was dissolved in 60 mL CH_2Cl_2 at 0°C and 60 mL of TFA was added to this slowly. After 2h the solution was evaporated to dryness and triturated with ether. The residue was dissolved in 150 mL water and cooled to 0°C. Then a solution of (10.68 g, 60 mmol) NBS in 150 mL THF has been added during 30min to this until the solution was remained its yellow color. When UPLC-MS showed complete conversion, THF was removed under reduced pressure. Thereafter reaction mixture

was cooled again in an ice bath and basified slowly with Na_2CO_3 to pH=8 (it turns red because of Br_2) and a solution of Fmoc-OSu (9.6 g, 28.3 mmol) in 80 mL THF was added dropwise. Two third of solvent was removed after 18h stirring at room temperature and then pH was adjusted to 3 with conc. HCl and extracted with CH_2Cl_2 three times, dried over $MgSO_4$ and concentrated in vacuum. The residue was purified by flash chromatography (CH_2Cl_2/MeOH/AcOH 98:1:1) to a colorless solid (6.57 g, 57%, three steps).

$[\alpha]_D^{20}$=+41.1 (*c*=0.00085 in $CHCl_3$)

^{1}H NMR (300 MHz, CD_3OD) δ (ppm): 1.32 (d, *J* = 6.82 Hz, 3H), 3.92 (quin, *J* = 6.22 Hz, 1H), 4.20 - 4.29 (m, 1H), 4.33-4.45 (overlapped m, 3H), 7.28 - 7.35 (m, 2H), 7.36 -7.43 (m, 2H), 7.68 (d, *J* = 7.26 Hz, 2H), 7.80 (d, *J* = 7.48 Hz, 2H). ^{13}C NMR (75 MHz, CD_3OD) δ (ppm): 172.7, 158.7, 145.3, 142.7, 128.9, 128.3, 126.4, 121.0, 68.3, 59.3, 59.2, 48.5, 15.4. HRMS (ESI-TOF): m/z found 367.1393 $[M+H]^+$ (calcd. for $C_{19}H_{19}N_4O_4$, 367.1401).

(2S,3R)-2-((((9H-Fluoren-9-yl)methoxy)carbonyl)amino)-3-azidobutanoic acid 20b:

White solid. 49% yield

$[\alpha]_D^{20}$=+8.2 (*c*=0.0011 in $CHCl_3$)

^{1}H NMR (400 MHz, CD_3OD) δ (ppm): 1.31 (d, *J* = 6.30 Hz, 5H), 4.17 - 4.23 (m, 1H), 4.24 - 4.30 (m, 1H), 4.33 (d, *J* = 3.07 Hz, 1H), 4.41 (m, 2H), 7.29 - 7.36 (m, 2H), 7.38 - 7.44 (m, 2H), 7.71 (t, *J* = 7.43 Hz, 2H), 7.82 (d, *J* = 7.52 Hz, 2H). ^{13}C NMR (75 MHz, $CDCl_3$) δ (ppm): 172.5, 156.8, 143.4, 141.3, 127.7, 127.1, 125.0, 120.0, 67.5, 58.1, 57.7, 47.0, 14.1. HRMS (ESI-TOF): m/z found 367.1394 $[M+H]^+$ (calcd. for $C_{19}H_{19}N_4O_4$, 367.1401).

1.7.2. Biology

For the enzyme kinetics, the human enzymes furin, and PACE4 expressed in Drosophila Schneider 2 cells and purified as previously described.[80] Enzyme inhibition assays carried out in 100 mM Hepes pH 7.5, 1 mM $CaCl_2$, 1 mM β- mercaptoethanol, and 1.8 mg/mL BSA for furin, while assaying for PACE4 were performed in 20 mM Bis-Tis pH 6.5, 1 mM $CaCl_2$, and 1.8 mg/mL BSA. All assays were performed with the 100 μM of substrate pyroGlu-Arg-ValLys-Arg-methyl-coumaryl-7-amide (Bachem, Switzerland) at 37 °C for 60 min, and real-time fluorescence measurement accomplished using a Gemini EM 96-well

spectrofluorometer (Molecular Devices, Sunnyvale, CA, USA) ($\lambda_{EX.}$, 370 nm; $\lambda_{EM.}$, 460 nm; Cut Off, 435 nm). Inhibitors (as TFA salts) were added to the wells based on a decreasing concentration. Kinetics assays were analyzed using SoftMaxPro5, and K_i values were determined from IC_{50} using Cheng and Prusoff's equation[200] and for those inhibitors who have concentrations equal or less than enzyme in the experiment, the K_i were calculated according to the Morrison equation for kinetics of reversible tight-binding inhibitors.[201]

1.7.3. MD Simulation

The protein-ligand complexes which prepared with Schrodinger package Protein Preparation Wizard,[202] were stated in a sphere of SPC water molecules of radius 100 Å, about 70 000 atoms. We used Gromacs 4.6.6[203-208] for MD simulations of system. For the ligands and proteins the Amber GS force field[209]was used. The first MD simulations step was heating the solvent to 300 K over a period of 20 ps and cooling to 100 K over a period of 5 ps, keeping the solute fixed. Then over 25 ps the system was gradually heated to 300 K. The simulation was endured for 1050 ps (total time) under constant temperature (body temperature, 310 K) and pressure (NPT), applying periodic boundary conditions. Every 10-time steps energy data, every 0.5 ps solute coordinates, and every 5 ps solvent coordinates were stored. An equilibrated state with respect to the total potential energy and temperature in the system was reached after 100 ps. The distance, angles and ramachandran parameters were calculated using gmx distance, angle and rama commands, respectively.

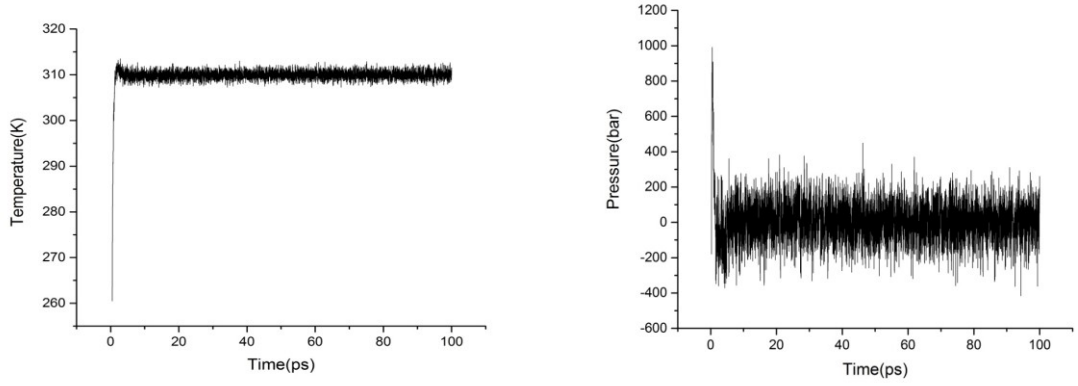

Figure S1: Equilibration of temperature in system and pressure (NPT) during 100 ps

CHAPTER 2 : IMPROVING THE SELECTIVITY OF PACE4 INHIBITORS THROUGH MODIFICATIONS OF THE P1 RESIDUE

The current chapter is published ns as a full article in the *J. Med. Chem.*, **2018**, *61* (24), pp 11250–11260 (DOI**:** 10.1021/acs.jmedchem.8b01381) with the following title, authors and affiliations.

Improving the Selectivity of PACE4 Inhibitors through Modifications of the P1 Residue

Vahid Dianati,† Pauline Navals, † Frédéric Couture,‡ Roxane Desjardins,‡ Anthony Dame,‡ Anna Kwiatkowska,‡ Robert Day‡ and Yves L. Dory†**

† Institut de Pharmacologie de Sherbrooke, IPS, Département de Chimie, Faculté des Sciences, Université de Sherbrooke, 3001 12e Avenue Nord, Sherbrooke, Québec J1H 5N4 (Canada)

E-mail: Yves.Dory@usherbrooke.ca

‡ Institut de Pharmacologie de Sherbrooke, Département de Chirurgie/Urologie, Université de Sherbrooke, 3001 12e Avenue Nord, Sherbrooke, Québec, J1H 5N4 (Canada)

E-mail: Robert.Day@USherbrooke.ca

2.1. Author contributions

This work was done in the Institut de Pharmacologie de Sherbrooke of Université de Sherbrooke under supervision of Pr. Robert Day and Pr. Yves L. Dory. The original research article by Vahid Dianati, Pauline Navals, Frédéric Couture, Roxane Desjardins, Anthony Dame, Anna Kwiatkowska, Robert Day, and Yves L. Dory was published in Journal of Medicinal Chemistry. Vahid Dianati, Robert Day and Yves L. Dory designed the compounds. Vahid Dianati synthesized all the peptides except compound **8** and its Arg mimetic which was synthesized by Pauline Navals. Roxane Desjardins purified the recombinant enzymes for kinetic assays. The kinetic assays and cellular assays were performed by Frédéric Couture, Roxane Desjardins, Anna Kwiatkowska and Anthony Dame. Vahid Dianati, Robert Day and Yves L. Dory analyzed the data. Vahid Dianati wrote the manuscript with notes from Pauline Navals, Frédéric Couture and Anna Kwiatkowska, and revisions from Robert Day and Yves L. Dory.

2.2. Abstract

Paired basic amino acid cleaving enzyme 4 (PACE4), a serine endoprotease of the proprotein convertases family, has been recognized as a promising target for prostate cancer. We first reported a selective and potent peptide-based inhibitor for PACE4, named the multi-leu peptide (Ac-LLLLRVKR-NH_2 sequence), which was then modified into a more potent and stable compound named C23 with the structure; Ac-DLeu-LLLRVK-Amba (Amba: 4-amidinobenzylamide). Despite improvements in both *in vitro* and *in vivo* profiles of C23, its selectivity for PACE4 was significantly reduced. We examined other Arg-mimetics instead of Amba to regain the lost selectivity. Our results indicated that the replacement of Amba with 5-(aminomethyl)picolinimidamide significantly increased the affinity for PACE4 and restored selectivity. Our results also provide a better insight on how structural differences between S1 pockets of PACE4 and furin could be employed in the rational design of selective inhibitors.

2.3. Introduction

There is substantial evidence that proprotein convertases (PCs) are broadly involved in the malignancy of tumors and angiogenesis.[210] This family of serine endoproteases consists of seven members namely PC1/3, PC2, furin, PACE4, PC4, PC5/6 and PC7, which process their substrates at the consensus motif of R-X-R/K-R-↓-X, X being any amino acid residue.[86] The role of PCs in malignancies is through the activation proteolysis of oncogenic precursor proteins. Among these substrates, growth factors and their receptors (e.g, transforming growth factor-β and insulin-like growth factor-1 receptor family members) are crucial for cell growth. Other PC substrates, such as proteases from ADAM (a disintegrin and metalloproteinase) and Matrix-metalloprotease families, as well as adhesion molecules (e.g. E-cadherin) are crucial for cell adhesion and metastasis.[106] Additionally, the list of substrates includes other regulatory proteins, along with bacterial and viral toxins.[211]

The cellular overexpression of PCs provides a clue for their role in tumorigenesis, as observed in many malignant cell types.[94] This is the case for PACE4 which is overexpressed in prostate cancer (PCa) and related cell lines.[108, 111-112, 114, 117] mRNA silencing studies demonstrated that inhibition of PACE4 had effects on tumorigenesis and neovascularization PCa cell line and animal models.[170] More recently, pro-growth differentiation factor-15 (pro-GDF-15) was identified as a PACE4 specific substrate in PCa involved in the proliferative phenotype. A PACE4 isoform, known as PACE4-altCT is overexpressed in PCa cell lines has been found to be responsible for sustained tumor progression.[91] It is clear that PACE4

inhibition could open a new therapeutic strategy for PCa either as mono or co-therapy, thus justifying our increased efforts to develop clinically relevant PACE4 inhibitors.

In a previous study, we showed that the lipophilic tail composed of four leucine residues attached to the N-terminus of the RVKR tetrapeptide, was critical to increase the selectivity of PACE4 inhibitors. Thus, our octapeptide, named Multi-Leu peptide (compound **1**), inhibits PACE4 and furin with K_i = 22 and 430 nM, respectively (**Figure 32**).[166] The replacement of P1-Arg with 4-amidinobenzylamide (Amba) and P8-Leu with its D isomer resulted in our current lead, named C23 (compound **2**; **Figure 32**), with improved PACE4 affinity (K_i = 4.9 nM). Whereas the Multi-Leu peptide **1** was rapidly metabolized when tested *in vivo*, C23 was much more stable and consequently displayed prominent pharmacological efficiency (IC_{50} = 25 and 45 µM for DU145 and LNCaP PCa cells, respectively) with rapid uptake by xenografted tumors, and a human plasma half-life of 1.7 h.[168, 170] However, Amba develops stronger interactions with furin S1 pocket compared Arg C-terminal residue in compound **1** resulting in a significant reduction in selectivity (only 2-fold) for PACE4 over furin. The furin preference for P1-Amba is even more visible with the tetrapeptide Ac-RVK-Amba. This simple ligand is twice as selective toward furin, emphasizing on the undeniable role and necessity of the four leucine-tail for PACE4 selectivity.[157]

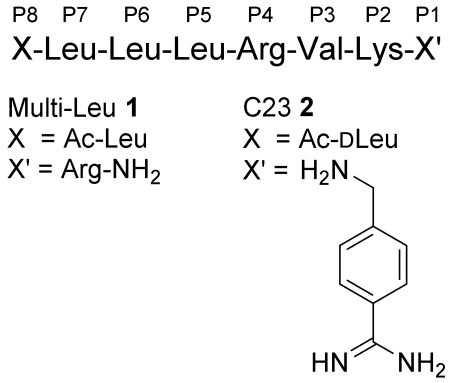

Figure 32. Structure of control PACE4 inhibitors

In another study, we successfully improved the selectivity of the multi-Leu peptide by introducing β-branched basic residues in the P3 position. This led to a 40-fold selective inhibitor.[212] However, further studies determined that this type of compound, harboring four consecutive basic residues, was devoid of PCa cells antiproliferative activity, suggesting a lack of cell penetration to reach the PACE4-altCT intracellular target. Trials to improve the selectivity of C23 by manipulating its P5-P8 portion met with limited success (3-fold selectivity in favor of PACE4). All these data reveal that the Amba residue

constitutes a barrier for achieving more selective compounds.[171] This work relates our efforts to find alternative residues that could successfully replace Amba at the P1 position.

Homology models of PACE4 suggest that the S1 pocket, which accommodates the P1 residue of the inhibitors, is constructed from two remote regions (primary structure): the first one described as a β-sheet then loop motif runs from S305 to G319 and the second one, a loop−helix−loop, encompasses residues S345 to I364. These two parts of the cleft are clamped together by means of several interactions including a Ca^{2+} cation involved in salt bridges with D310, D353, D358, and E381 (**Figure 33**).[87] The guanidinium ion of the P1 residue (Ac-RVKR-NH_2) is strongly held inside the S1 pocket by means of ionic forces with aspartates 310 and 358, as well as ion−dipole interactions with the carbonyl groups of P308 and A344. These interactions are identical within all PCs.[87] However, despite the high degree of homology in and around the S1 pocket, differences exist, as observed in the matching sequences ^{300}**HDSCN** and ^{352}**GDYCS** of furin and PACE4, respectively (see **Figure 33**). One hypothesis is that these disparities, that concern three residues only, alter the shape of the S1 pocket in furin and PACE4 and can be held responsible of the observed selectivity differences between compounds **1** and **2**.

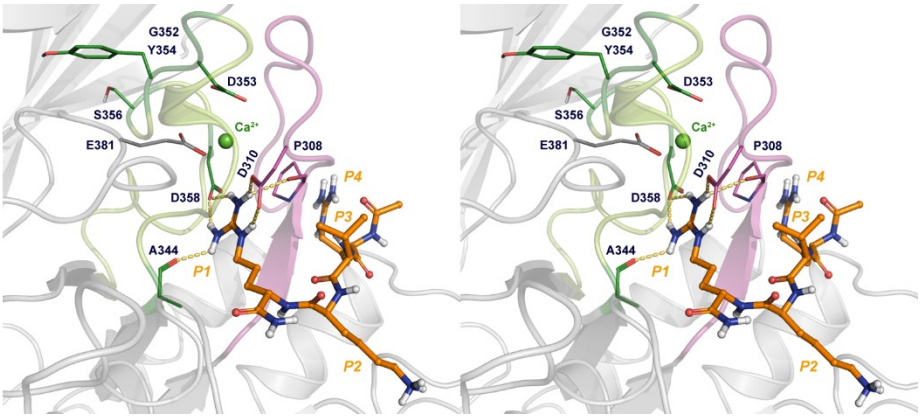

Figure 33. The stereo representation of PACE4 P1–P4 active site with the Ac-RVKR-NH_2 (orange) inhibitor. The Ca^{2+} cation (green sphere), located deep inside the S1 subsite, is essential for its stability.

Generally, refining the selectivity is more laborious than enhancing the potency,[213] and given the high degree of homology between furin and PACE4, discrimination between these two enzymes is challenging. Although C23 is highly potent to block tumor progression of xenograft PCa animal models, inhibition of the most ubiquitous member of the PC family, furin, could potentially lead to unforeseen side effects and drawbacks. In the present study, new residues are rationally designed, then introduced in the P1 position, based on available structural data and structure activity relationship (SAR) studies conducted on both PACE4 and furin. The main goal of our investigations is to determine the structural

factors (P1 position) that might discriminate between PACE4 and furin, in order to create potent and selective PACE4 inhibitors.

2.4. Results and discussions

2.4.1. Design and binding affinities

Two groups of mimetics were designed (and biologically tested: PACE4 and furin K_i, DU145 and LNCaP cell lines IC_{50}) for the P1 residue of PACE4 inhibitors (**Figure 34**): (a) an aliphatic series in which inhibitors **3**−**6** possess a guanidine group like Arg itself; and (b) an aromatic series whose members **7**−**13** bear an amidine function like Amba. Compound **3** is an epimer of **1** at position P8. Both compounds have similar K_i values, but **3** is more selective (PACE4 K_i = 24 nM, 32 times selective for PACE4). The D residue at position P8 imparts metabolic stability and this is likely the reason why **3** is endowed with an improved ability to inhibit PCa cells proliferation. Accordingly, all newly synthesized inhibitors discussed in this work have a DLeu residue at position P8, like compounds **2** and **3**.[167] The first two derivatives **4** and **5** were rigidified analogs of **3**, from which the terminal amide had been removed (agmatine). The alkene **4** proved to be much better than the alkyne **5**.[168] The improved affinity of **4** (K_i = 13 nM**)**, compared to compound **3**, however was associated with substantial reduction of selectivity (3-fold for PACE4). Conversion of the C-terminus amide to an alcohol moiety in **6** resulted in a poor and non-selective inhibitor of PACE4. These observations are, however, consistent with the poor inhibition of peptide alcohols reported for other serine proteases.[214-215]

Together with the Amba derivative **2**, the compounds **7** and **8** were used to carry out a preliminary SAR study of the aromatic amidine. Contrary to the Arg analogs **3**−**6**, the side chain of Amba is more rigid and it is also bulkier.[87, 159] It is anticipated that the amidine group will be held in the S1 pocket by the enzyme residues interfering with the equivalent guanidine of Arg (**Figure 33** and **36**). As can be observed, P308 and A344 carbonyls, and D310 and D358 carboxylates bind tightly to the two external NH_2 parts of the guanidinium ion. Additionally, D310 develops an extra interaction with the arginine delta-NH, so any designed mimics ideally need an equivalent hydrogen bond donor. Obviously, this latter interaction cannot exist in an amidinium ion.

First, the analogues **7** and **8** were designed to assess the width and length of the S1 pocket. Further extension of Amba with one methylene unit, producing inhibitor **7**, not only did not offer any improvement in selectivity, but also reduced the binding affinity (PACE4 K_i = 17 nM). The tetra-

fluorinated Amba derivative **8** has very little affinity toward PACE4 and furin. There are two possible explanations for this negative result: either the S1 pocket is too narrow to accommodate the four fluorine atoms or the positive charge is absent because the calculated pK_a of the tetrafluoro-benzamidine is as low as 6.9.[216]

According to plans, O and NH substituents were introduced at the ortho position of the amidine, inside a fused 5-membred ring as in **9** and **10** respectively, then as free phenol **11** and aniline **12**. Finally, the pyridine **13** was designed as a more direct mimetic of **2**, because it could fill up the same space in the S1 pocket. The inhibitor candidates **9–13** were synthesized then tested biologically. The bicyclic systems **9** and **10** proved essentially inactive; whereas, the K_i values of the corresponding open systems, **11** and **12**, are in the same range as those of Multi-Leu **1** and its diastereomer **3**, albeit with lower selectivities. Compound **13** is indeed a strong and selective inhibitor (K_i = 2.6 nM, PACE4). The P1 residue of compound **10** has been recently used in P1 of furin inhibitors with no success.[161]

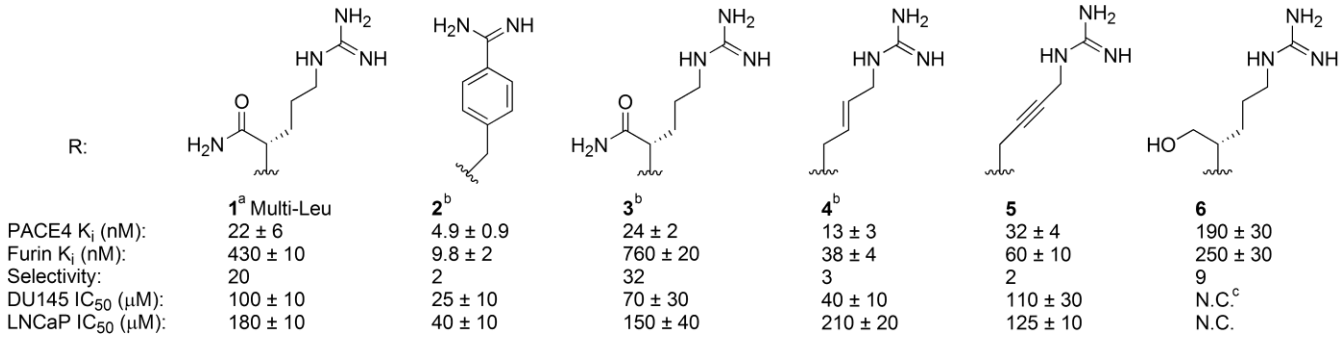

R:	**1**[a] Multi-Leu	**2**[b]	**3**[b]	**4**[b]	**5**	**6**
PACE4 K_i (nM):	22 ± 6	4.9 ± 0.9	24 ± 2	13 ± 3	32 ± 4	190 ± 30
Furin K_i (nM):	430 ± 10	9.8 ± 2	760 ± 20	38 ± 4	60 ± 10	250 ± 30
Selectivity:	20	2	32	3	2	9
DU145 IC_{50} (μM):	100 ± 10	25 ± 10	70 ± 30	40 ± 10	110 ± 30	N.C.[c]
LNCaP IC_{50} (μM):	180 ± 10	40 ± 10	150 ± 40	210 ± 20	125 ± 10	N.C.

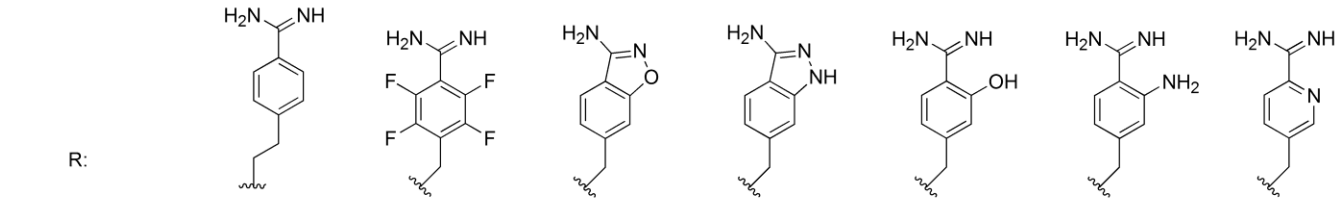

R:	**7**	**8**	**9**	**10**	**11**	**12**	**13**
PACE4 K_i (nM):	17 ± 3	240 ± 20	500 ± 130	700 ± 50	53 ± 7	14 ± 4	2.6 ± 0.1
Furin K_i (nM):	41 ± 3	600 ± 100	614 ± 2	825 ± 10	240 ± 20	60 ± 10	21.5 ± 0.9
Selectivity:	2	2	1	1	5	4	8
DU145 IC_{50} (μM):	80 ± 10	69 ± 7	N.D.[d]	N.D.	50 ± 10	61 ± 7	130 ± 20
LNCaP IC_{50} (μM):	80 ± 6	230 ± 50	N.D.	N.D.	113 ± 1	58 ± 7	140 ± 10

Figure 34. Structure of P1 arginine mimetics used for PACE4 inhibitors with general structure of Ac-DLeu-Leu-Leu-Leu-Arg-Val-Lys-NHR apart from **1**. [a] with Leu at position P8 instead of DLeu. The inhibition of PACE4 and furin are represented as K_i ± standard deviation, and antiproliferative activity on PCa cell lines as IC_{50} ± SEM. Data adapted from Ref.[166] ([b]Data adapted from Ref.[168]; [c]Not calculable,

indicates that the curve did not converged to 50% with doses up to 150 μm; [d]Not determined, because of solubility/precipitation problems.

In order to provide a rational for the various K_i values, that are linked to the mode of binding of the P1 side chains, density functional theory (DFT) calculations were run (**Figure 35**). These calculations were intended to disclose the minimum energy conformations of Amba derivatives and other relevant properties. The pK_a figures of the amidinium ions and ortho functional groups were also estimated. It was first confirmed that the rigid Amba (side chain in **Figure 35b**) is indeed a good mimic of Arg (**Figure 35a**). For these two P1 residues, the distances between the Cα and the central cation C atoms are 6.24 Å and 5.78 Å for Arg and Amba respectively (**Figure 36**). Amba, being slightly shorter, can fit in the S1 cavity without much distortion. This does not hold true for the longer Amba analog **7**, as demonstrated by its lower affinity (17 nM). In terms of charges, both guanidine and amidine are also similar since they exist as guanidinium and amidinium cations at physiological pH. By incorporating these functional groups in rings through addition of O and NH atoms, the resulting bicyclic systems (**Figure 35c**,**d**) are fully aromatic. Consequently, their N atoms are no longer basic (pK_a: 1.0-3.5) and do become positively charged at physiological pH. As for compound **8** (mostly neutral at pH 7.4), which suffered the same drawback, the affinities of analogs **9** and **10** are drastically diminished. Upon breaking the N-O and the N-N bonds, the amidine moiety becomes strongly basic (**Figure 35e,f**) and the corresponding peptidomimetics **11** and **12** recover some inhibitory activity, the aniline **12** being much stronger than the phenol **11** (**Figure 34**). Calculations show that at physiological pH (7.4), the phenolate anion is the predominant species. Since a negative charge in that region of the inhibitor may lead to unfavorable interactions with the carboxylate of D310 (**Figures 36**), this may easily account for the lower affinity of inhibitor **11** for both furin and PACE4. In addition, the introduction of the aniline and phenol groups increases steric hindrance in the deep S1 subsite and may explain why both **11** and **12** are less potent than **2**.

Despite its additional NH_2 group, the aniline (**Figure 35f**) is geometrically very close to its parent amidine devoid of substituents (**Figure 35b**). For both cases, the amidinium plane is rotated relative to the aromatic ring by ~ 35°. Surprisingly, this torsion angle is smaller in the case of the aniline, because of its ortho position that induces the formation of an intramolecular hydrogen bond N−H···N. However, for obvious steric reasons, the aniline-substituted amidine is prevented from reaching a fully flat geometry, contrarily to the simpler amidine that can, at a cost of 2.8 kcal/mol according to DFT calculations. The

K_i values (PACE4) for the corresponding inhibitors **2** and **12** are 4.9 and 14 nM, respectively (**Figure 34**).

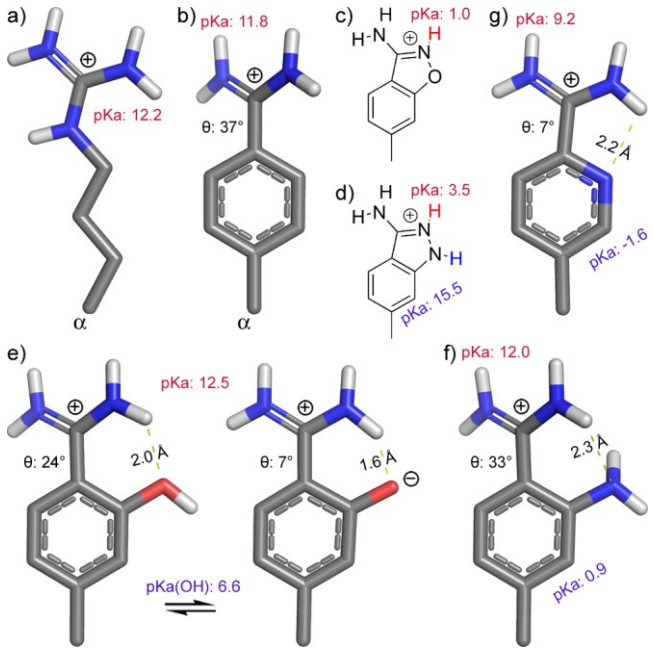

Figure 35. Energy-minimized (DFT) side chain conformers of arginine (a) and arginine mimetics (b,e−g) and estimated pKa values of relevant functional groups. Torsion angles between amidine and aromatic planes are shown (θ).

The best compound of the whole series is the pyridine **13**, in terms of affinity for PACE4 (2.6 nM) as well as selectivity (8 for compound **13** compared to only 2 for compound **2**). This overall beneficial effect does not arise from a better electronic complementarity with D310, because the pyridine nucleus is so electron-deficient that it is not basic at all (pK_a: -1.6, **Figure 35g**) and remains neutral at all pHs. Nevertheless, the lone pair of the pyridine is ideally positioned in yet another intramolecular hydrogen bond N···H−N with the neighboring amidinium partner. As a result, the terminal side chain of **13** is very flat indeed, its torsion angle θ is as small as 7°, a significant gain of 30° by comparison with isosteric peptide mimic **2** (see **Figure 35b** and **35g**). Induced-fit docking models (**Figure 36**) suggest that the pyridine N atom makes no additional interaction with PACE4, in which case its sole purpose is to freeze the amidinium side chain in its flat conformation. From all these results, it can be inferred that a planar conformation of the P1 residue might fit better in PACE4 S1 pocket compared to furin.

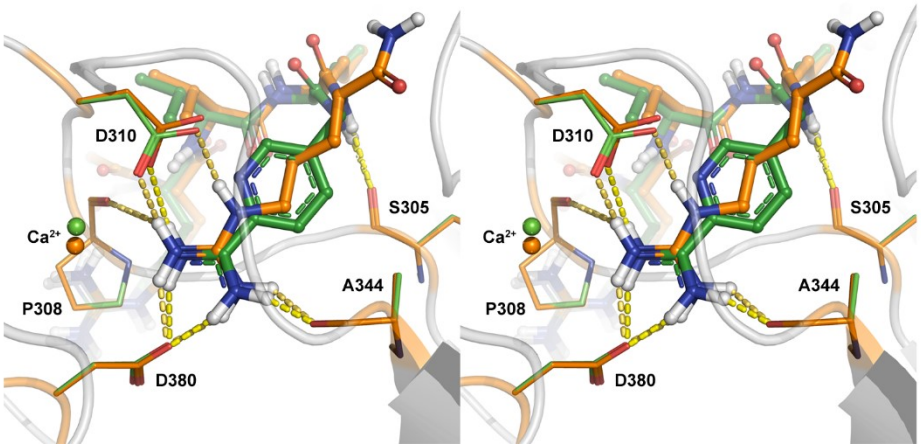

Figure 36. Superimposed induced fit docking pose of Ac-RVKX corresponding to the P5−P1 region of compounds 1 (orange) and 13 (green) in the PACE4 homology model active site. [87] Enzyme's side chain C atoms colored the same as corresponding ligand for clarity. H, N and O atoms are in white, blue and red color, respectively. The H bonds represented as yellow dashes.

2.4.2. Cell-based assays

In order to evaluate the cell antiproliferative activity, all the inhibitors were tested against PCa cell lines (DU145 and LNCaP) using an MTT proliferation assay **(Figure 34)**. In terms of cell-based efficacy, neither compounds **4** nor **5** showed significant advantage over compound **3** despite their differences in PACE4 affinity and selectivity. However, the poor affinity of inhibitor **6** for PACE4 entirely translated into antiproliferative activity, and no effect was observed on both cell lines for this inhibitor in concentrations below 150 μM further depicting the relationship between the anti-proliferative response and PACE4 inhibition.

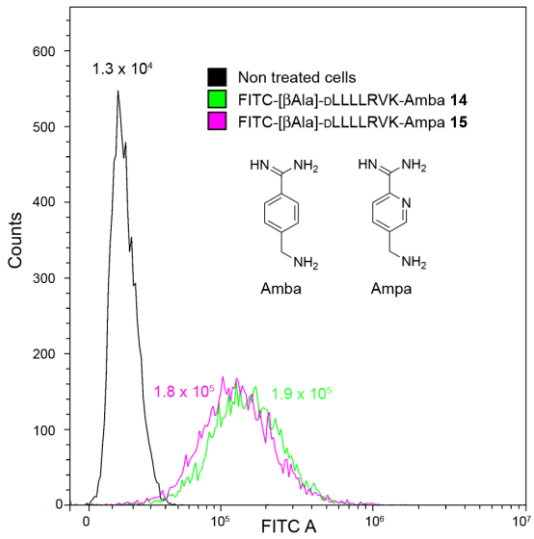

Figure 37. Cell permeability comparison of FITC-labeled analogues of compounds **2** and **13**.

Inhibitors **9** and **10**, precipitated during the assay and, thus, their IC_{50} values were not measurable. Analogues **7**, **8**, **11** and **12** which are less potent PACE4 inhibitors compared to the parent compound **2**, displayed inferior antiproliferative activity (**Figure 34**). Conversely, inhibitor **13** (IC_{50} = 130 and 140 μM for DU145 and LNCaP cells, respectively) displayed lower antiproliferative activity than control compound **2** (IC_{50} = 25 and 45 μM for DU145 and LNCaP cells, respectively). Knowing the requirements of PACE4 inhibition to reach the intracellular PACE4 for efficient antiproliferative activity, the cell permeability of **13** was tested using a N-terminally FITC labelled version (compound **15**).[91, 166, 173] However, the results depicted no considerable difference in the permeability compared to control FITC-labeled analogue **14** corresponding to inhibitor **2** (**Figure 37**).

Overall, compound **13** with the best affinity for PACE4 and reasonable selectivity among the P1 modified inhibitors provided reasonable antiproliferative activity in PCa cell lines. The Ampa could be an appropriate P1 residue for further development of more selective PACE4 inhibitors.

2.4.3. Chemistry

All the peptides **5** and **7**−**13** were synthesized using a combination of solid and solution phase peptide synthesis as reported earlier for compound **2**.[168] Briefly, the fully protected P8−P2 peptide was synthesized with conventional Fmoc-tBu strategy on a 2-chlorotrytylchloride resin. After coupling of the last amino acid and removal of the Fmoc protective group, the peptide was acetylated and then cleaved from the resin under mild acidic conditions. The P1 residue amines were then coupled with the protected peptide in solution. The fragment coupling procedure used to connect the heptapeptide to arginine mimetic synthons may obviously lead to some degree of epimerization at the P2 position, the lysine residue. However, the final products were proven to be pure by ^{1}H NMR spectroscopy after reverse-phase (RP) preparative high-performance liquid chromatography (HPLC). Compound **6** was prepared in a different manner using a literature's method for the synthesis of C-terminal alcohol peptides.[217] In the final step, the side chains of all the peptides, were deprotected using TFA cocktails. The FITC-labeling of compound **15** was carried out as previously reported for compound **14**.[168]

The alkyne **18**, P1 residue of compound **5**, was obtained from two consecutive Mitsunobu reactions on 2-butyne-1,4-diol **16** and a final phthalimide deprotection (**Scheme 3**). For the P1 residues of **9** and **10**, compound **19** was converted to a dinitrile **20**. The regioselective formation of 5-membered ring, was

followed by reduction of remaining nitrile moiety to yield compounds **21** and **22**. The inhibitor **11** was then prepared by catalytic hydrogenation of inhibitor **9**.

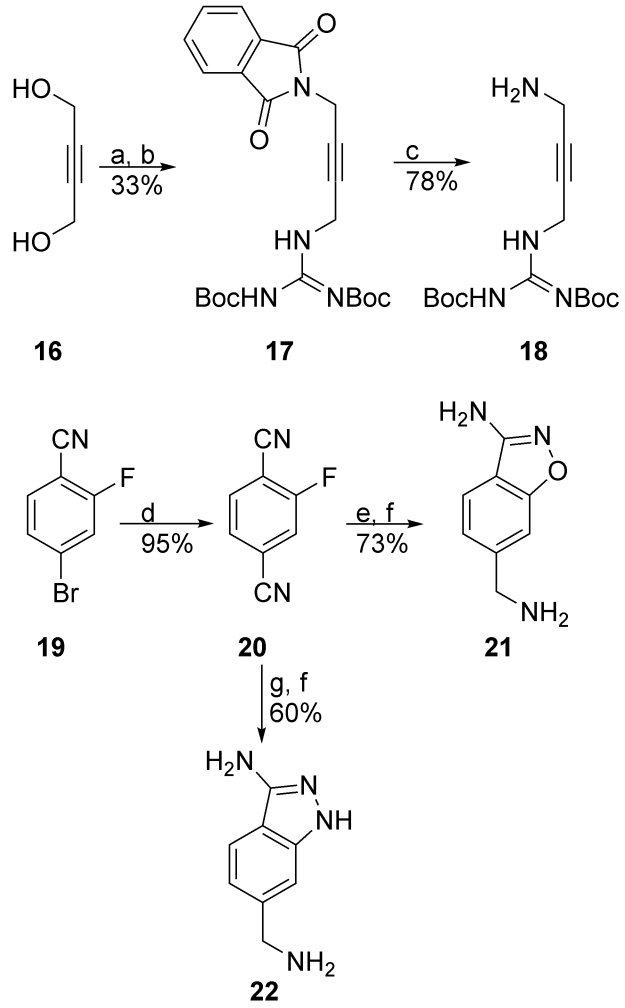

Scheme 3. Synthesis of P1 arginine mimetics for inhibitors **5**, **9** and **10**. Reagents and conditions: (a) phthalimide, DIAD, PPh_3, THF, 0 ºC to rt, 16 h; (b) *N,N'*-Di-Boc-guanidine, DIAD, PPh_3, THF, 0 ºC to rt, 16 h; (c) $N_2H_4.H_2O$, $CHCl_3$/MeOH, 4 h; (d) $Pd(PPh_3)_4$, $Zn(CN)_2$, DMF, 80 ºC, 6 h; (e) AcNHOH, K_2CO_3, DMF, 12 h; (f) BH_3-THF 1 M in THF, 0 ºC to rt, 6 h; (g) $N_2H_4.H_2O$, *n*-BuOH, reflux, 16 h.

The synthetic pathways of four other P1 residues are outlined in **Scheme 4**. Compound **25** was obtained by condensation of 4-formylbenzonitrile **23** with nitromethane prior to consecutive reduction of the double bond and nitro group and then Boc protection of the resulting amine giving compound **25**. The nitrile group of this compound was then converted to an amidine and the Boc protection was removed to afford compound **26**.[218] Nitromethane was also employed in a S_NAr2 reaction to prepare **28** from pentafluoro-benzonitrile **27**. The nitro product **28** was transformed to the Arg mimetic **29** by conversion

of nitrile to amidine. The final step of the conversion to **29** included a catalytic reduction which the nitromethyl moiety was reduced to the aminomethyl as well. The benzylic alcohol **31** was prepared by oxidation of the methyl substituent in the starting material **30**. The alcohol **31** was transformed to the corresponding tosylate, and then azide, which was finally converted to the Boc-protected amine **32** via a Staudinger reaction. The nitrile of **32** was transformed into an amidine as before (**25** to **26**), during which process the nitro group was also reduced to an aniline (step f in **Scheme 4**). Cleavage of the Boc group yielded the amine **33**. The bromide in **34** was replaced by a nitrile, then its ester was reduced to the benzylic alcohol **35**. Mitsunobu reaction on **35**, using phthalimide as nucleophile, followed by hydrazine opening of the resulting phthalimide led to the corresponding amine, that was immediately protected as its *t*-butyl carbamate **36**. From there, the same three-step procedure used to prepare **26** from **25**, and **29** from **28**, was applied to **36** to obtain the amine **37**.

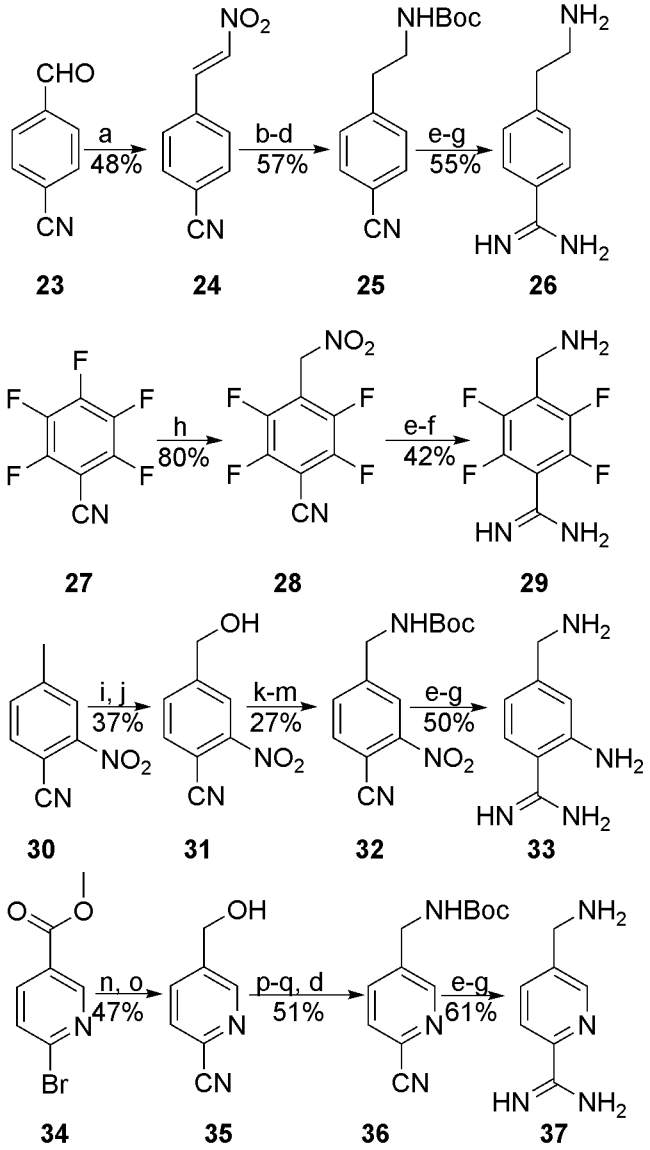

Scheme 4. Synthesis of P1 arginine mimetics for inhibitors **7**, **8**, **12** and **13**. Reagents and conditions: (a) $MeNO_2$, NaOH, MeOH/H_2O, <10-15 ºC, 15 min then 5 M HCl; (b) Bu_3SnH, CH_2Cl_2, rt, 16 h; (c) Zn, HCl(aq), 65 ºC, 1h; (d) $(Boc)_2O$, K_2CO_3, THF/H_2O, 16 h; (e) $NH_2OH.HCl$, DIPEA, MeOH, 60 ºC, 16 h; (f) Ac_2O, DIPEA, THF then 10% Pd/C, AcOH/MeOH, 35 atm H_2, 12 h; (g) Conc. HCl(aq), MeOH, 0 ºC to rt, 1 h; (h) $MeNO_2$, TMG, -35 ºC, 5 min; (i) H_5IO_6, CrO_3, MeCN, 3 h; (j) *i*-BuOCOCl, NMM, THF, 0 ºC, 2 min then $NaBH_4$ in MeOH, 30 min; (k) TsCl, Et_3N, DMAP, MeCN, 1 h; (l) NaN_3, NaI, DMF, 1 h; (m) PPh_3, H_2O, THF, 16 h then K_2CO_3, $(Boc)_2O$, 16 h; (n) $Pd(PPh_3)_4$, $Zn(CN)_2$, DMF, 100 ºC, 16 h; (o) $NaBH_4$, LiCl, MeOH, 2 h; (p) phthalimide, DIAD, PPh_3, THF, 0 ºC to rt, 16 h; (q) $N_2H_4.H_2O$, $CHCl_3$/MeOH, 3 h;

2.5. Conclusion

In conclusion, we developed new inhibitors for PACE4 through SAR studies of the P1 residue. Our results emphasize structural differences in the S1 pocket that can be used to discriminate between furin and PACE4. This could open a novel avenue for achieving higher selectivity. Inhibitor **13** is the most potent and selective inhibitor in the series and displayed K_i = 2.6 nM which is 2-fold more potent and 4-fold more selective than C23 (compound **2**). Although the P1-Ampa in **13** introduces the same stabilizing Van der Waals contacts as Amba in **2**, the former is held rigidly (intramolecular H bond) in a flat conformation, suggesting that its gain in affinity for PACE4 might precisely results from this rigidifying process. Despite similarities in structures and cell permeabilities, surprisingly, compound **13** exhibited lower efficiency in PCa cell antiproliferative assay compared to **2**. Further studies may provide the knowledge to explain this impairment, however, this significant improvement at the P1 position can now be used in combination with other modifications at other positions.

2.6. Experimental

2.6.1. Chemistry

All chemical reagents and solvents were obtained from commercial resources and used without further purification. Fmoc-protected amino acids and coupling reagents, were purchased from ChemPep (Miami, FL, USA) or Chem-Impex International (Wood Dale, IL, USA), and 2-chlorotrityl-chloride resin from Rapp Polymer (Tübingen, Germany). Other reagents were purchased from Sigma Aldrich (St. Louis, MO, USA). Manual Fmoc/tBu strategy was utilized for peptide synthesis. Analytical reverse phase HPLC was performed on an Agilent Technologies 1100 system equipped with a diode array detector (λ = 210, 214, 230, and 254 nm). Preparative HPLC were accomplished on a Waters preparative HPLC machine [Autosampler 2707, Quaternary gradient module 2535, UV detector 2489 (λ = 214 and 230 nm), fraction collector WFCIII] equipped with an ACE5 C18 column (250 × 21.2 mm, 5 µm spherical particle size). Analytical HPLC was carried out using C18 columns, either Agilent Eclipse XDB (5 mm, 4.6 µm, 250 mm) or a Phenomenex Jupiter (5 mm, 4.6 µm, 250 mm). A gradient of H_2O/MeCN containing 0.1% TFA was used as eluent for both analytical and preparative HPLC. The identity of the pure products was confirmed using an ESI-HRMS system (TripleTOF 5600, ABSciex; Foster City, CA, USA). For synthesis check a Water H Class Acquity UPLC coupled with an SQ Detector 2 and a PDA eλ detector paired with an Acquity UPLC CSH C18 column (1.7 µm×2.1 mm×50 mm) was used with a linear gradient from 5 to 95% of MeCN containing 0.1% formic acid in 0.1% aqueous formic acid was used for 1.3 min and a

flow rate of 0.8 mL/min. NMR experiment were carried out on either AV300 Bruker (300 MHz for ^{1}H and 75 MHz for ^{13}C), Avance III hd 400 Bruker (400 MHz for ^{1}H , 377 MHz for ^{19}F and 100 MHz for ^{13}C) or Agilent Varian (600 MHz for ^{1}H). Complete decoupling of protons was applied in ^{13}C NMR experiments. The new compounds were additionally characterized with IR spectroscopy (Alpha-Platinum ATR Bruker, diamond crystal). The purity of biologically tested compounds **5**−**13** and **15** were confirmed to be more than 95% using RP analytical HPLC and ^{1}H NMR (**13**). The compounds were characterized by HRMS.

Peptide synthesis general procedures. Compounds **5** and **7**−**10**, **12** and **13** were provided as follows: Fmoc-Lys(Boc)-OH (1.2 equiv) was attached to a 2-chlorotrityl chloride resin in the presence of *N,N*-diisopropylethylamine (DIPEA) (4 equiv) in dimethylformamide (DMF) for 3 h. The resin was washed using a sequence of DCM (3×), a cycle of MeOH/DCM (3×) and DCM (5×). The peptide chain was elongated by standard Fmoc-SPPS. The Fmoc group was removed with 20% piperidine in DMF. The Fmoc-protected amino acids were coupled using 5 equiv of protected amino acids, 5 equiv of HATU, and 15 equiv of DIPEA in DMF for 45 min. The last residue was acetylated by a solution of Ac_2O/DIPEA/DCM (5:10:85) for 30 min. Each protected peptide was released from the resin with a solution of 20% hexafluoro-2-propanol (HFIP) in DCM. The solvents were evaporated in vacuo, and the residue was lyophilized in *tert*-BuOH/H_2O (50:50). DIPEA (7.5 equiv) was added to an ice-cooled solution (0 °C) of protected peptide, arginine mimetic (2.5 equiv), benzotriazol-1-yl-oxytripyrrolidino-phosphonium hexafluorophosphatehexafluorophosphate (2.7 equiv), and 6-chloro-1-hydroxybenzotriazole (7.5 equiv) in DMF, and the reaction was stirred overnight at room temperature. The solvent was removed with an air stream to afford the crude protected peptide. The final deprotection of side chains was achieved by a solution of H_2O/TIPS/TFA (2.5:2.5:95) for 2 h. Purification with RP preparative HPLC (gradients of H_2O/MeCN containing 0.1% TFA) resulted in pure peptides as their TFA salts after lyophilization.

Compound 6. Fmoc-Arg(Pbf)-ol (0.63 g, 0.99 mmol)[219] was added to a 2% solution of DBU in DMF (7.0 mL) and agitated with 2-chlorotrytylchloride resin (0.3 g, 0.33 mmol) for 7 h. Fmoc-Lys(Boc)-OH (0.93 g, 1.98 mmol) was coupled to the free alcohol using DIPEA (0.15 mL, 0.99 mmol) and DMAP (0.01 g, 0.11 mmol). Then, the peptide was synthesized via deprotection/coupling cycles on the resin as previously mentioned in the general procedure for peptide synthesis. After final acetylation, the protected peptide was obtained by treating the resin with a 25% solution of HFIP in DCM (5.0 mL). Solvents were

removed, and the O−N acyl migration was performed by stirring a solution of the resulting crude product in 20% piperidine in DMF (4.0 mL) for 1 h. Global deprotection was carried out as mentioned in the general procedure for peptide synthesis. The crude peptide was purified by preparative HPLC as described in the general procedure.

Compound 11. The peptide inhibitor **9** (0.05 g, 0.05 mmol) was dissolved in MeOH/H_2O (50:50, 4.0 mL). 10% Pd/C (50 mg) was added and the slurry was stirred under H_2 (1 atm) for 16 h. After the completion of reaction (monitored by UPLC-MS), the reaction mixture was filtered through a pad of diatomaceous earth. The pad was washed with distilled water and the filtrate evaporated to dryness with a stream of air. The residue was purified by reversed phase preparative HPLC as described in general procedure.

Compound 13. ^{1}H NMR (600 MHz, D2O): δ (ppm) 8.64 (d, J = 1.8 Hz, 1H), 8.01 (d, J = 7.9 Hz, 1H), 7.94 (dd, J = 7.9, 1.8 Hz, 1H), 4.55 (AB d, J = 15.6 Hz, 1H), 4.49 (AB d, J = 15.6 Hz, 1H), 4.32−4.16 (m, 6H), 4.04 (d, J = 7.9 Hz, 1H), 3.14 (m, 2H), 2.96 (quin, J = 6.1 Hz, 2H), 2.01 (m, 1H), 1.97 (s, 3H), 1.86−1.70 (m, 4H), 1.70−1.49 (m, 16H), 1.45 (m, 1H), 1.37 (m, 1H), 0.92−0.80 (m, 30H).

***N*-(4-Phthalimido-but-2-ynyl)-*N′*,*N″*-1,3-bis(*tert*-butyloxycarbonyl)guanidine (17).**

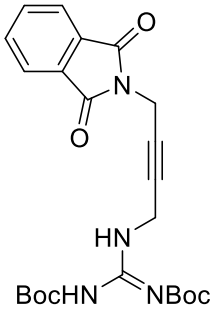

4-*N*-Phthalimido-but-2-yn-1-ol was obtained as a colorless solid in 52% yield using a reported procedure with all obtained spectra agreed with the literature.[220] ^{1}H NMR (400 MHz, $CDCl_3$) δ (ppm): 7.88 (dd, *J* = 5.4, 3.0 Hz, 2H), 7.75 (dd, *J* = 5.4, 3.0 Hz, 2H), 4.49 (s, 2H), 4.25 (br. s., 2H). ^{13}C NMR (100 MHz, $CDCl_3$) δ (ppm): 169.1, 134.2, 131.9, 123.5, 81.4, 79.2, 51.0, 27.2. HRMS–ESI (*m/z*): $[M + H]^+$ calcd for $C_{12}H_{10}NO_3$ 216.0665; found, 216.0653. The achieved product (0.66 g, 3.1 mmol) was added to a solution of PPh_3 (0.78 g, 3.1 mmol), and 1,3-bis(*tert*-butoxycarbonyl)guanidine in dry THF (5.0 mL). DIAD (0.5 mL, 3.1 mmol) was added to ice-cooled above solution in a dropwise manner. The reaction stirred for 16 h at room temperature under inert atmosphere. The colorless title product was isolated by column

chromatography with EtOAc/hexanes as eluent (0.87 g, 63%). ^{1}H NMR (400 MHz, $CDCl_3$) δ (ppm): 9.36 (br. s., 1H), 9.14 (br. s., 1H), 7.88 (dd, *J* = 5.4, 3.0 Hz, 2H), 7.74 (dd, *J* = 5.4, 3.0 Hz, 2H), 4.74 (s, 2H), 4.44 (s, 2H), 1.48 (s, 9H), 1.47 (s, 9H). ^{13}C NMR (100 MHz, $CDCl_3$) δ (ppm): 167.0, 163.4,159.7, 154.2, 134.1, 132.0, 123.4, 84.5, 79.3, 79.0, 75.6, 34.4, 28.2, 27.8, 27.2. IR (neat) ν (cm^{-1}): 3381, 3279, 3246, 3029, 2978, 2941, 2358 (weak), 1728, 1686, 1604. HRMS–ESI (*m/z*): $[M + H]^+$ calcd. for $C_{23}H_{29}N_4O_6$ 457.2082; found 457.2068.

_N_-(4-Amino-but-2-ynyl)-_N'_,_N''_-1,3-bis(*tert*-butyloxycarbonyl)guanidine (18).

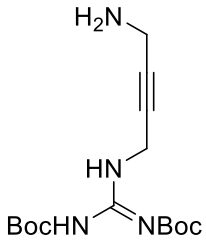

Compound **17** (0.71 g, 1.6 mmol) was dissolved in MeOH (12.0 mL) and $CHCl_3$ (9.5 mL), then hydrazine monohydrate 64-65% (1.0 mL) was added to the solution and stirred for 4 h. The white solid byproduct was filtered off. The filtrate was evaporated and diluted with more $CHCl_3$ and then washed with 1 M sodium hydroxide. The organic phase was dried with magnesium sulfate, filtered and concentrated to give the desired product as a brownish yellow solid (0.41 g, 78%). ^{1}H NMR (400 MHz, $CDCl_3$) δ (ppm): 9.36 (br. s., 1H), 9.14 (br. s., 1H), 4.73 (s, 2H), 3.39 (s, 2H), 1.52 (s, 9H), 1.47 (s, 9H). ^{13}C NMR (100 MHz, $CDCl_3$) δ (ppm): 163.4, 159.7, 154.3, 84.26, 79.3, 78.9, 34.6, 31.5, 28.2, 27.9. IR (neat) ν (cm^{-1}): 3380, 2977, 2933, 2370 (weak), 1717, 1610. HRMS–ESI (*m/z*): $[M + H]^+$ calcd. for $C_{15}H_{27}N_4O_4$ 327.2027; found 327.2048.

2-Fluoroterephthalonitrile (20).

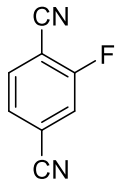

The yellow slurry of 4-bromo-2-flouro-benzonitrile **19** (1.00 g, 5.0 mmol), $Pd(PPh_3)_4$ (0.29 g, 0.25 mmol, 0.05 equiv) and $Zn(CN)_2$ (0.35 g, 3.0 mmol, 0.6 equiv) in deoxygenated dry DMF (6.5 mL) was heated at 80 ºC for 6 h. The resulting solution was diluted with EtOAc and washed twice with 2 M ammonium hydroxide and brine. A yellow solid was obtained after flash chromatography with 15-20% EtOAc in hexanes (0.70 g, 95% yield). The spectroscopic data are in accordance with literatures.[221] ^{1}H NMR (400

MHz, $CDCl_3$) δ (ppm): 7.62 (dd, *J* = 1.4, 0.6 Hz, 1H), 7.60 (dd, *J* = 1.4, 0.6 Hz, 1H), 7.56 (dd, *J* = 1.4, 0.6 Hz, 1H). ^{13}C NMR (100 MHz, $CDCl_3$) δ (ppm): 162.9 (d, *J* = 260.0 Hz) 134.5, 128.5, 120.2 (d, *J* = 23.0 Hz) 118.4 (d, *J* = 10.0 Hz) 115.8 (d, *J* = 3.0 Hz) 112.1, 106.37 (d, *J* = 15.0 Hz). HRMS–ESI (*m/z*): $[M + H]^+$ calcd. for $C_8H_4FN_2$ 147.0353; found 147.0351.

6-(Aminomethyl)benzo[*d*]isoxazol-3-amine (21).

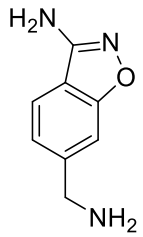

Acetyl-hydroxamic acid (0.68 g, 9.0 mmol) was dissolved in DMF (12.0 mL). K_2CO_3 (2.21 g, 16.0 mmol) was added, followed by a few drops of H_2O. The mixture was stirred at room temperature for 30 min, then compound **20** (0.58 g, 4.0 mmol) was added. The stirring was continued for 12 h, and then diluted with EtOAc and H_2O. The phases were separated, and aqueous phase extracted twice with EtOAc. The combined organic phases were dried over $MgSO_4$, filtered and evaporated under vacuum to give a colorless solid which was dissolved in dry THF (5.0 mL). A 1 M solution of BH_3-THF in THF (12.0 mL, 12.0 mmol) was added dropwise to the ice-cooled above solution. The stirring was continued for 6 h. Then, 6 M HCl (15.0 mL) solution was added to the resulting white slurry and stirred for 2 h. The obtained solution was evaporated to dryness and purified by reverse phase HPLC to give the product as a colorless solid (0.48 g, 73% for two steps) ^1H NMR (300 MHz, D_2O) δ (ppm): 7.67 (d, *J* = 8.1 Hz, 1H), 7.42 (s, 1H), 7.26 (d, *J* = 8.1 Hz, 1H), 4.23 (s, 2H). ^{13}C NMR (75 MHz, D_2O) δ (ppm): 162.2, 159.0, 135.8, 123.5, 122.2, 116.3, 110.1, 42.9. HRMS–ESI (*m/z*): $[M + H]^+$ calcd. for $C_8H_{10}N_3O$ 164.08184; found 164.0819.

6-(Aminomethyl)-1H-indazol-3-amine (22).

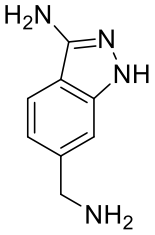

A mixture of bis-nitril **20** (0.60 g, 4.1 mmol) and hydrazine hydrate (0.6 mL, 12.3 mmol) in *n*-butanol (16.0 mL) was heated at reflux under inert atmosphere for 16 h. After completion of the reaction, the mixture was dried under vacuum and purified by flash chromatography (66−100% EtOAc in hexane as

eluent) to yield brown crystalline needles (0.60 g, 93%). ^{1}H NMR (400 MHz, $CDCl_3$): δ (ppm) 11.96 (br s, 1H) 7.88 (dd, J = 8.3, 1.0 Hz, 1H) 7.78 (t, J = 1.0 Hz, 1H) 7.21 (dd, J = 8.3, 1.0 Hz, 1H) 5.63 (s, 2H). ^{13}C NMR (100 MHz, $CDCl_3$): δ (ppm) 149.6, 139.7, 121.9, 119.8, 119.3, 115.7, 114.8, 108.1. This compound was treated with BH_3−THF, as was mentioned for compound 21's synthesis, to get 22 as a brownish solid (0.58 g, 60%). ^{1}H NMR (300 MHz, D_2O): δ (ppm) 4.27 (s, 2H), 7.22 (d, J = 8.4 Hz, 1H), 7.47 (s, 1H), 7.81 (d, J = 8.4 Hz, 1H). ^{13}C NMR (75 MHz, D_2O): δ (ppm) 145.8, 142.5, 137.0, 122.3, 122.2, 112.1, 111.6, 43.0. HRMS-ESI (m/ z): $[M + H]^+$ calcd. for $C_8H_{11}N_4$, 163.0978; found, 163.0966.

(*E*)-4-(2-Nitrovinyl)benzonitrile (24).

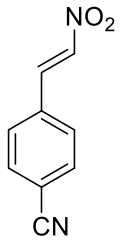

A solution of NaOH (0.84 g, 21.0 mmol) in ice-cold water (40.0 mL) was added dropwise to a solution of 4-formylbenzonitrile **23** (2.60 g, 20.0 mmol) and nitromethane (1.1 mL, 20.0 mmol) in MeOH (40.0 mL). The reaction temperature was kept below 10−15 °C during the addition of the NaOH solution. After stirring for 15 min, the whole reaction mixture was transferred to a separating funnel and slowly added to 5 M HCl (100.0 mL). A yellow solid was obtained almost instantly; it was filtered, washed with cold water, dried, and recrystallized from hot EtOH to furnish the pure product **24** as yellow needles (1.66 g, 48%). The spectroscopic data are in accordance with literatures.[222] ^{1}H NMR (400 MHz, $CDCl_3$): δ (ppm) 8.00 (d, J = 13.7 Hz, 1H), 7.77 (d, J = 8.4 Hz, 2H), 7.67 (d, J = 8.4 Hz, 2H), 7.62 (d, J = 13.7 Hz, 1H). ^{13}C NMR (100 MHz, $CDCl_3$): δ (ppm) 139.5, 136.5, 134.4, 133.0, 129.4, 117.8, 115.3.

***tert*-Butyl (4-cyanophenethyl)carbamate (25).**

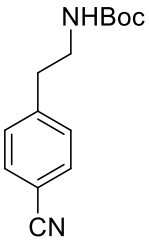

n-Bu_3SnH (2.4 mL, 8.9 mmol) was added to a solution of **24** (1.29 g, 7.4 mmol) in dry DCM (19.0 mL) under inert atmosphere, and the reaction mixture was stirred for 16 h. The solvent was evaporated under

reduced pressure, and the residue was partitioned between MeCN (100.0 mL) and hexane (30.0 mL). The MeCN phase was washed two times with hexane to remove the remained tin by-products and concentrated under reduced pressure. The residue was dissolved in MeOH (110.0 mL) and 2 M HCl (110.0 mL). Zinc powder (6.00 g, 90.0 mmol) was added slowly to the solution. After stirring for 1 h at 65 °C, the reaction mixture was cooled and basified to pH = 8 using sodium carbonate. The solid was filtered off, and the filtrate was concentrated to half of its volume. $(Boc)_2O$ (1.62 g, 7.4 mmol) in THF (50.0 mL) was added to the above solution and stirred for 16 h. THF was evaporated, and the resulting aqueous phase was extracted three times with EtOAc. The combined organic phases were washed with brine, dried over magnesium sulfate, filtered, and evaporated to dryness. The residue was purified by flash chromatography (20% EtOAc in hexane as eluent) to furnish the title compound as a colorless crystalline solid (1.13 g, 57% yield for three steps). The spectroscopic data are in accordance with literatures.[223] ^{1}H NMR (300 MHz, $CDCl_3$): δ (ppm) 7.59 (d, J = 8.0 Hz, 2H), 7.30 (d, J = 8.0 Hz, 2H), 4.60 (br s, 1H), 3.38 (q, J = 6.5 Hz, 2H), 2.86 (t, J = 6.5 Hz, 2H), 1.42 (s, 9H). ^{13}C NMR (75 MHz, $CDCl_3$): δ (ppm) 155.7, 144.7, 132.3, 129.6, 118.8, 110.3, 79.5, 41.3, 36.4, 28.3. HRMS-ESI(m/z): calcd. for $C_{14}H_{19}N_2O_2$ $[M + H]^+$, 247.1441; found, 247.1415.

4-(2-Aminoethyl)benzimidamide (26).

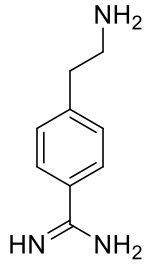

To a solution of carbamte **25** (0.27 g, 1.07 mmol) in MeOH (20.0 mL) were added hydroxylammonium chloride (0.11 g, 1.60 mmol) and DIPEA (0.28 mL, 1.60 mmol), and the reaction was stirred at 60 °C for 16 h. Then, the solvent was evaporated, and the residue was dissolved in EtOAc, washed with water and brine, and dried over $MgSO_4$. The solvent was removed, and the residue was dissolved in THF (10.0 mL). DIPEA (0.28 mL, 1.60 mmol) and acetic anhydride (0.15 mL, 1.60 mmol) were added to the solution. The amidoxime intermediate was acetylated within 30 min as monitored by TLC. The excess of acetic anhydride was quenched by addition of H_2O (0.50 mL). Stirring was continued for 30 min. Then, the solvent was evaporated, and the residue was dissolved in MeOH/AcOH (50:50), and 10% Pd/C (0.05 g) was added. The hydrogenation was conducted under 35 psi pressure of H_2 in a Parr hydrogenator reactor for 12 h. Upon completion of the reaction (HPLC-MS), the mixture was filtered through a pad of

diatomaceous earth and purified by preparative HPLC (gradient of 0−30% MeCN in water) to yield a colorless solid which was dissolved in MeOH (3.0 mL). Concentrated HCl (1.0 mL) was added slowly at 0 °C. After stirring for 1 h, the volatiles were removed using an air stream overnight. The residue was triturated using MeOH/Et_2O to furnish 26 as a white solid (55% for three steps). ^{1}H NMR (400 MHz, DMSO-d_6): δ (ppm) 9.34 (s, 2H), 8.40 (br. s, 2H), 7.87 (d, J = 8.4 Hz, 2H), 7.51 (d, J = 8.4 Hz, 2H), 3.00−3.09 (m, 4H). ^{13}C NMR (100 MHz, DMSO-d_6): δ (ppm) 165.3, 144.0, 129.3, 128.4, 126.1, 39.2, 32.7. HRMS (ESI) calcd. for $C_9H_{14}N_3$ m/z $[M + H]^+$, 164.1182; found, 164.1181.

2,3,5,6-Tetrafluoro-4-(nitromethyl)benzonitrile (28).

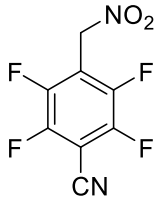

Nitromethane (2.8 mL, 51.30 mmol) was placed in a flask that was flushed with nitrogen for about 10 min then treated with 1,1,3,3-tetramethylguanidine (0.5 mL, 4.27 mmol), was stirred for 20 min, cooled to -35°C and treated slowly with pentafluorobenzonitrile (0.5 mL, 4.30 mmol). The reaction was stirred for 5 min and quickly quenched with a 1 M aq. solution of HCl saturated with NaCl (10.0 mL). The solution was then extracted with EtOAc three times. The combined organic layers were washed with 0.1 M HCl then dried with magnesium sulfate, filtered and volatiles were removed in vacuum to give the desired product, a yellowish powder (0.80 g, 80%). The spectroscopic data are in accordance with literatures.[224] ^{1}H NMR (400 MHz, $CDCl_3$) δ (ppm): 5.69 (s, 2H). ^{13}C NMR (100 MHz, $CDCl_3$) δ (ppm): 147.2 (m), 145.5 (m), 114.5 (t, *J* = 16.9 Hz), 106.6 (t, *J* = 3.7 Hz), 96.9 (t, *J* = 2.9 Hz), 65.5. ^{19}F NMR (377 MHz, $CDCl_3$) δ ppm: -137.2 (m, 2F), -130.5(m, 2F). HRMS (ESI) calcd. for $C_8H_3N_2O_2F_4$ m/z $[M+H]^+$ 235.0125; found 235.0143.

4-(Aminomethyl)-2,3,5,6-tetrafluorobenzimidamide (29).

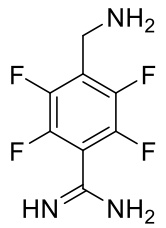

Compound **28** (0.60 g, 2.56 mmol) and hydroxylamine hydrochloride (0.27 g, 3.85 mmol) were added to a solution of DIPEA (0.7 mL, 3.85 mmol) in MeOH (40.0 mL), which was stirred gently overnight at

room temperature. The mixture was extracted with ethyl acetate, and the organic layer was washed three times with saturated aqueous $NaHCO_3$ followed by brine, then dried with magnesium sulfate, filtered, and evaporated in vacuo. The obtained crude product (0.25 g, 0.95 mmol) and acetic anhydride (0.3 mL, 2.8 mmol) were added to a solution of acetic acid (5.0 mL), and the mixture was stirred for 1 h. Water (0.5 mL) was then added to the solution that was stirred for 1 h before addition of 10% Pd/C (0.08 g). After 48 h of stirring under hydrogen (balloon), the palladium was removed by filtration on diatomaceous earth, and the solvents were evaporated in vacuo. The product was purified by flash chromatography with 15% MeOH in DCM as eluent to furnish the title compound as a yellowish-brown oil (0.09 g, 15%). ^{1}H NMR (400 MHz, D_2O): δ (ppm) 5.69 (s, 2H). ^{13}C NMR (100 MHz, D_2O): δ (ppm) 156.8 (m), 144.6 (m), 142.7 (m) 122.2 (m), 113.1 (m), 32.7 (s). ^{19}F NMR (377 MHz, D_2O): δ (ppm) −141.0 (br. m, 2F), −139.8 (br. m, 2F). IR (neat) ν (cm^{-1}): 3566−2323 (br.), 1736, 1647, 1474. HRMS (ESI) calcd. for $C_8H_8N_3F_4$ m/z [M + H]$^{+}$, 222.0649; found, 222.0661.

4-(Hydroxymethyl)-2-nitrobenzonitrile (31).

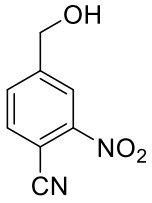

To a solution of H_5IO_6 (17.00 g, 75.0 mmol) in MeCN (300.0 mL) was stirred vigorously and treated CrO_3 (0.30 g, 3.0 mmol). Upon the addition of 4-methyl-2-nitro-benzonitrile **30** (4.90 g, 30.0 mmol) to the above solution, a white precipitate formed immediately. After 3 h of stirring, the liquid was decanted from the precipitate and evaporated. The obtained product (2.70 g, 13.9 mmol) was dissolved in dry THF. The solution was cooled to 0 °C, and treated sequentially with isobutyl chloroformate (1.8 mL, 13.9 mmol) and NMM (1.5 mL, 13.9 mmol). After 2 min, a solution of $NaBH_4$ (1.60 g, 41.7 mmol) in water (2.0 mL) was added to the above solution in one portion. The reaction mixture was stirred until the gas evolution ceased (30 min) then it was quenched with a saturated NH_4Cl aqueous solution. The volatiles were removed under vacuum, and the residue was extracted three times with EtOAc. Combined organic phases were dried over $MgSO_4$, filtered and the solvent was removed in vaccuo. Column chromatography (40 to 50% EtOAc in hexanes) furnished a white solid as product (2.0 g, 37% for two steps). The spectroscopic data are in accordance with literatures.[225] ^{1}H NMR (400 MHz, DMSO-d_6) δ (ppm): 8.32 (s, 1H), 8.13 (d, J = 7.8 Hz, 1H), 7.89 (d, J = 7.8 Hz, 1H), 5.75 (br. s, 1H), 4.70 (d, J = 4.9 Hz, 2H). ^{13}C

NMR (100 MHz, DMSO-d_6) δ (ppm): 150.5, 148.2, 135.6, 131.9, 122.6, 115.7, 104.7, 61.41. HRMS–ESI (*m/z*): $[M + H]^+$ calcd. for $C_8H_7N_2O_3$ 179.0451; found 179.0444.

***tert*-Butyl (4-cyano-3-nitrobenzyl)carbamate (32).**

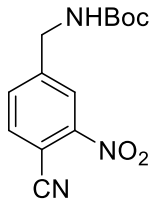

DMAP (0.06 g, 0.5 mmol) and triethylamine (1.7 mL, 12.0 mmol) were added to an ice-cooled solution of tosyl chloride (1.05 g, 5.5 mmol) and 31 (0.85 g, 4.8 mmol) in MeCN (10.0 mL). The reaction mixture was stirred for 1 h prior to evaporation of solvent. The residue was taken into EtOAc and washed with 0.5 M HCl and brine. The organic phase was then dried over $MgSO_4$, filtered, and evaporated to dryness. The resulting solid was dissolved in DMF (10.0 mL). NaN_3 (0.94 g, 14.4 mmol) and NaI (0.36 g, 2.4 mmol) were added to the reaction mixture, which was stirred at room temperature for 1 h. The reaction was quenched by addition of water, and the product was extracted with Et_2O (3×). The combined organic phases were dried over $MgSO_4$ and evaporated to dryness. The residue was purified by column chromatography, using 20% EtOAc in hexane as eluent, to give a pale yellow oil (0.58 g, 60% for two steps). ^{1}H NMR (400 MHz, $CDCl_3$): δ (ppm) 8.31 (s, 1H), 7.95 (d, J = 8.0 Hz, 1H), 7.79 (d, J = 8.0 Hz, 1H), 4.65 (s, 2H). ^{13}C NMR (100 MHz, $CDCl_3$): δ (ppm) 142.9, 135.9, 132.9, 124.4, 114.6, 107.5, 53.1. HRMS-ESI (m/z): $[M + H]^+$ calcd for $C_8H_7N_5O_2$, 204.0516; found, 204.0513. The obtained 4-(azidomethyl)-2-nitrobenzonitrile (0.58 g, 2.9 mmol) was dissolved in a mixture of THF (10.0 mL) and H_2O (4.0 mL), and PPh_3 (0.76 g, 2.9 mmol) was added slowly to the solution. The mixture was stirred for 16 h and its volume was reduced to one-third of the original by evaporation. 2 M HCl was added to the residual aqueous solution, which was washed with EtOAc. The pH of the combined aqueous phases was adjusted to 8−9 by addition of solid K_2CO_3. A solution of $(Boc)_2O$ (0.62 g, 2.9 mmol) in THF (10.0 mL) was added to the above solution that was stirred for a further 16 h. THF was evaporated from the reaction mixture, and the resulting aqueous phase was extracted with EtOAc (three times). The organic extract was dried ($MgSO_4$), the volatiles were removed, and the residue was purified by column chromatography with 30% EtOAc in hexanes. Evaporation of the collected fractions gave a yellow oil which was solidified at ambient temperature (0.36 g, 45%) was achieved. ^{1}H NMR (400 MHz, $CDCl_3$) δ (ppm): 8.25 (s, 1H), 7.88 (d, *J* = 7.9 Hz, 1H), 7.74 (d, *J* = 7.9 Hz, 1H), 4.48 (d, *J* = 6.1 Hz, 2H), 1.47 (s, 10H). ^{13}C NMR (100

MHz, $CDCl_3$) δ (ppm): 155.8, 148.8, 146.9, 135.7, 132.5, 123.8, 114.9, 106.6, 80.7, 43.7, 28.3. IR (neat) ν (cm^{-1}): 3370, 3083, 2978, 2232, 1682, 1516, 1341, 1281. HRMS–ESI (*m/z*): $[M + H]^+$ calcd. for $C_{13}H_{16}N_3O_4$ 278.1135; found 278.1119.

2-Amino-4-(aminomethyl)benzimidamide (33).

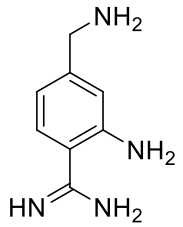

This compound was prepared from **32** as a yellow solid with the same procedure that was used to get compound **26** from **25** (0.18 g, 50% yield for three steps). ^1H NMR (400 MHz, D_2O) δ (ppm): 7.39 (d, *J* = 8.0 Hz, 1H), 6.92 (d, *J* = 1.0 Hz, 1H), 6.87 (dd, *J* = 8.0, 1.0 Hz, 1H), 4.10 (s, 2H). ^{13}C NMR (100 MHz, D_2O) δ (ppm): 165.7, 145.3, 138.4, 130.1, 118.2, 117.4, 114.4, 42.5. IR (neat) ν (cm^{-1}): 3403-2602 (br.), 1738, 1637. HRMS–ESI (*m/z*): $[M + H]^+$ calcd. for $C_8H_{13}N_4$ 165.1135; found 165.1126.

5-(Hydroxymethyl)picolinonitrile (35).

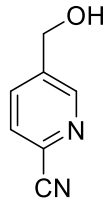

The cyanation of methyl 6-bromonicotinate **34** (1.30 g, 6.0 mmol) was accomplished as noted in the preparation of **20** except the reaction mixture was heated at 100 ºC for 16 h. The residue was purified by column chromatography (15% EtOAc in hexane) to give the intermediate cyanoester as a colorless solid (0.70 g, 64%).^1H NMR (400 MHz, $CDCl_3$) δ (ppm): 9.30 (d, *J* = 1.0 Hz, 1H), 8.45 (dd, *J* = 8.0, 1.0 Hz, 1H), 7.81 (dd, *J* = 8.0, 1.0 Hz, 1H), 4.02 (s, 3H). ^{13}C NMR (100 MHz, $CDCl_3$) δ (ppm): 164.1, 151.8, 138.1, 137.0, 128.5, 128.1, 116.5, 53.1. HRMS–ESI (*m/z*): $[M + H]^+$ calcd. for $C_8H_7N_2O_2$ 163.0502; found 163.0489. The obtained solid (0.62 g, 3.8 mmol) was dissolved in MeOH (2.5 mL) prior to addition of LiCl (0.32 g, 7.7 mmol). Then, $NaBH_4$ (0.29 g, 7.7 mmol) was slowly added, and the reaction mixture was stirred for 2 h. The volatiles were removed by evaporation. The residue was treated with sat. aqueous NH_4Cl and extracted three times using EtOAc. The combined organic phases were dried over $MgSO_4$ and the solvent was removed in vacuum. The residue was purified by column chromatography (50% EtOAc in hexane) to furnish the title compound as a white solid (0.34 g, 73%). The spectroscopic data are in

accordance with literatures.[226] ^{1}H NMR (400 MHz, $CDCl_3$) δ (ppm): 8.71 (s, 1H), 7.89 (d, *J* = 7.9 Hz, 1H), 7.71 (d, *J* = 7.9 Hz, 1H), 4.86 (d, *J* = 5.2 Hz, 2H), 2.22 (t, *J* = 5.2 Hz, 1H). ^{13}C NMR (100 MHz, $CDCl_3$) δ (ppm): 149.5, 140.2, 135.0, 132.7, 128.3, 117.2, 61.9. HRMS–ESI (*m/z*): $[M + H]^+$ calcd. for $C_7H_7N_2O$ 135.0553; found 135.0538.

***tert*-Butyl((6-cyanopyridin-3-yl)methyl)carbamate (36).**

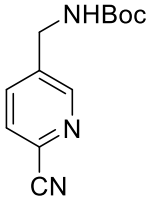

5(Hydroxymethyl)picolinonitrile 35 (0.34 g, 2.5 mmol), PPh_3 (1.00 g, 3.8 mmol), and phthalimide (0.56 g, 3.8 mmol) were dissolved in dry THF (5.0 mL) under inert conditions and cooled to 0 °C in an ice bath. DIAD (0.75 mL, 3.8 mmol) was added by small portions over 30 min. The reaction mixture was stirred for 16 h at ambient temperature after which the solvent was removed in vacuo. The crude product was purified by column chromatography. ^{1}H NMR (400 MHz, $CDCl_3$): δ (ppm) 8.81 (d, J = 2.0 Hz, 1H), 7.92 (dd, J = 8.0, 2.0 Hz, 1H), 7.89 (dd, J = 5.5, 3.0 Hz, 2H), 7.77 (dd, J = 5.5, 3.0 Hz, 2H), 7.67 (d, J = 8.0 Hz, 1H), 4.93 (s, 2H). ^{13}C NMR (100 MHz, $CDCl_3$): δ (ppm) 168.1, 151.9, 137.7, 136.2, 135.0, 133.8, 132.2, 128.5, 124.3, 117.4, 39.2. The phthalimide-protecting group was removed using the same procedure described for the preparation of **18** from **17**. The obtained solid was dissolved in H_2O (60.0 mL), and the pH was adjusted to 8−9 using K_2CO_3. A solution of $(Boc)_2O$ (0.83 g, 3.8 mmol) in THF (30.0 mL) was added to the mixture that was stirred for 18 h. After reducing to one-third of the original volume by evaporation of the volatiles, the mixture was extracted three times with EtOAc. The volatiles were evaporated, and the residue purified by column chromatography using 30% EtOAc in hexane to yield the title compound as a white solid. (0.30 g, 51% for three steps). ^{1}H NMR (400 MHz, $CDCl_3$) δ (ppm): 8.65 (d, *J* = 1.4 Hz, 1H), 7.78 (dd, *J* = 7.9, 1.4 Hz, 1H), 7.68 (d, *J* = 7.9 Hz, 1H), 5.07 (br. s., 1H), 4.40 (d, *J* = 5.8 Hz, 2H), 1.46 (s, 9H). ^{13}C NMR (100 MHz, $CDCl_3$) δ (ppm): 155.8, 150.2, 138.9, 135.8, 132.6, 128.3, 117.1, 80.5, 41.9, 28.3. IR (neat) ν (cm^{-1}): 3380, 2997, 2981, 2970, 2931, 2240, 1738, 1679, 1513. HRMS–ESI (*m/z*): $[M + H]^+$ calcd. for $C_{12}H_{16}N_3O_2$ 234.1237; found 234.1217.

5-(Aminomethyl)picolinimidamide (37).

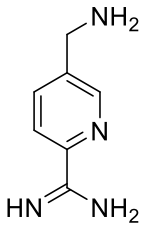

This compound was prepared using the same procedure as described for the preparation of amine **26** as a yellow solid (0.12 g, 61% for three steps). ^{1}H NMR (300 MHz, D_2O) δ (ppm): 4.39 (s, 2H), 8.14 (d, *J* = 8.1 Hz, 1H), 8.20 (dd, *J* = 8.1, 1.0 Hz, 1H), 8.83 (d, *J* = 1.0 Hz, 1H). ^{13}C NMR (75 MHz, D_2O) δ (ppm): 162.3, 150.3, 144.3, 139.2, 133.8, 123.4, 40.1. IR (neat) ν (cm^{-1}): 3587-2629 (br.), 1672, 1650. HRMS–ESI (*m/z*): calcd. for $C_7H_{11}N_4$ $[M+H]^+$ 151.0987; found 151.0951.

2.6.2. Molecular modeling

DFT calculations. High-level DFT calculations (M06-2X/6.31Gdp)[227-229] were performed in water as solvent using GAMESS software (version R1, May 1st, 2013).[230]

Docking studies. Calculations were performed with the Molecular Operating Environment (MOE),[231] using a homology model of PACE4 developed based on the furin crystal structure (PDB code; 1P8J).[74, 87] The Ac-RVKR-NH_2 was modified with the "builder" tool to the desired ligand and then minimized using the OPLS-AA force field. The general docking protocol of MOE (receptor: receptor + solvent; site: ligand atoms; ligand: ligand atoms) was used for docking, and the Triangle Matcher routine (timeout: 300 s; returned poses: 1000) was employed as the placement method and the acquired poses were scored with the "London dG" algorithm (30 retained poses). The different poses were refined with the induced fit protocol (refinement > induced fit; cutoff: 15 Å; side chains: free; termination criterion: gradient 0.01; iterations: 500; pharmacophore restraint: force constant 100; radius offset: 0.4) and rescored with the "GBVI/WSA dG" algorithm (5 retained poses). The docking score and the presence of vital interactions were used to select the best poses.

2.6.3. Biology

Enzyme kinetics. As reported earlier,[212] the PACE4 and furin inhibitory constants of compounds **5-13** were calculated using Cheng and Prusoff's equation[123] and the SoftMaxPro5 program, except for compound **13**'s PACE4 affinity which was calculated by Morrison's equation[232] and Prism 6.0 (GraphPad Software). All measurements were performed on a Gemini EM 96-well spectrofluorometer (Molecular

Devices Sunnyvale, CA, USA) (λ_{ex} = 370 nm; λ_{em} = 460 nm; cutoff, 435 nm). The recombinant human furin ([E_0] = 0.54 nM, K_m = 5.040 μM) and recombinant human PACE4 ([E_0] = 20.18 nM, K_m = 4.035 μM) were prepared and purified as described before.[80] The competitive substrate was pyroGlu-Arg-Thr-Lys-Arg-AMC peptide (Bachem, Switzerland) for both furin and PACE4 with a concentration of 100 μM per well.

Cell proliferation assay. Cell lines were purchased from the American Type Culture Collection (ATCC) and maintained in RPMI-1640 and supplemented with 5% fetal bovine serum (FBS) for DU145 and 10% FBS for LNCaP. The antiproliferative activity of compounds **5-13** was evaluated as reported earlier.[167] The IC_{50} values were calculated using Prism 6.0 (GraphPad Software).

Cell permeability. The DU145 cells were plated (200000 cells per 100 mm petri dish) and incubated for 48 h at 37 ºC. After addition of a 1 μM solution of FITC-labeled analogs and further incubation for 1 h at 37 ºC, cells were collected by treatment with 0.05% trypsin and subsequently was inactivated with FBS-containing media. Cell pellets were washed with PBS, centrifuged and resuspended in 200 μL of fresh PBS prior to addition of propidium iodide (final concentration of 10 μg/mL) just before fluorescence acquisition. In another set of tubes, trypan blue (final concentration of 0.04%) was used to quench the non-penetrated fluorophore. Fluorescence analysis (at least 10000 events) was performed in a CytoFLEX 15 flow cytometer (Beckman Coulter, Brea, CA, USA) with the following diode lasers: 488 nm and 638 nm, 50 mW each. The resulting fluorescence was divided into four channels and detected through band pass filters (Forward scatter area, side scattered area and side scattered width signals) to discriminate the live gates from exclude debris and cell clumps. Dead cells (PI-positive) were omitted with gating in the red channel.

2.7. Acknowledgements

We acknowledge the Canadian Cancer Society Research Institute (701590 to R.D. and Y.L.D.) and Prostate Cancer Canada (TAG2014-02 to R.D.) for their support. F.C. holds a Banting and Charles Best Canada Graduate Scholarships (grant#315690) from CIHR and Graduate Studentship from Prostate Cancer Canada (Grant #GS-2015-07). We thank Compute/Calcul Canada for providing computational facilities and time. We also thank Hugo Gagnon and Jean-Philippe Couture (PhenoSwitch Biosciences Inc.) for HRMS analysis.

2.8. Supporting information

Analytical data of peptide inhibitors and the FITC-labeled analogue is presented in the **Table S1**.

Table S1. The analytical data for all peptide inhibitors and the FITC-labeled analogue.

Compound	Exact Mass		HPLC retention time
	Calculated for	Found	
5	$[M+2]^{2+}$ 502.8582	502.8687	29.77[a]
6	$[M+2]^{2+}$ 519.8791	519.8777	8.47[b]
7	$[M+2]^{2+}$ 521.3684	521.3770	29.36[a]
8	$[M+3]^{3+}$ 367.2302	367.2260	12.95[b]
9	$[M+2]^{2+}$ 521.3502	521.3488	11.49[b]
10	$[M+2]^{2+}$ 520.8582	520.8664	10.57[b]
11	$[M+2]^{2+}$ 523.3659	523.3609	28.67[a]
12	$[M+2]^{2+}$ 514.8582	514.8667	28.50[a]
13	$[M+2]^{2+}$ 521.8660	521.8744	28.41[a]
15	$[M+3]^{3+}$ 482.9287	482.9315	31.75[a]

[a]50 min and [b]16 min gradient of 10 to 70% of CH_3CN and H_2O containing 0.1% TFA

CHAPTER 3 : INCREASING C-TERMINAL HYDROPHOBICITY IMPROVES THE CELL PERMEABILITY AND ANTIPROLIFERATIVE ACTIVITY OF PACE4 INHIBITORS AGAINST PROSTATE CANCER CELL LINES

The current chapter is published as a full article in *J. Med. Chem.*, **2018**, *61* (18), pp 8457–8467 (DOI: 10.1021/acs.jmedchem.8b01144) with the following title, authors and affiliations;

Increasing C-Terminal Hydrophobicity Improves the Cell Permeability and Antiproliferative Activity of PACE4 Inhibitors against Prostate Cancer Cell Lines

Vahid Dianati,† Anna Kwiatkowska,‡ Frédéric Couture,‡ Roxane Desjardins,‡ Yves L. Dory† and Robert Day‡**

† Institut de Pharmacologie de Sherbrooke, IPS, Département de Chimie, Faculté des Sciences, Université de Sherbrooke, 3001 12e Avenue Nord, Sherbrooke, Québec J1H 5N4 (Canada)

E-mail: Yves.Dory@usherbrooke.ca

‡ Institut de Pharmacologie de Sherbrooke, Département de Chirurgie/Urologie, Université de Sherbrooke, 3001 12e Avenue Nord, Sherbrooke, Québec, J1H 5N4 (Canada)

E-mail: Robert.Day@USherbrooke.ca

3.1. Author contributions

This work was done in the Institut de Pharmacologie de Sherbrooke of Université de Sherbrooke under supervision of Pr. Robert Day and Pr. Yves L. Dory. The original research article by Vahid Dianati, Pauline Navals, Frédéric Couture, Roxane Desjardins, Anthony Dame, Anna Kwiatkowska, Robert Day, and Yves L. Dory is accepted for publishing in Journal of Medicinal Chemistry. Vahid Dianati, Robert Day and Yves L. Dory designed the compounds. Vahid Dianati synthesized all the peptides and intermediate molecules. The kinetic assays were done by Vahid Dianati (compounds **3-21**), Anna Kwiatkowska (compounds **28** and **29**) and Roxane Desjardins (compounds **28-33**). Antiproliferative cellular assays were performed by Vahid Dianati (compound **3-21**), Anna Kwiatkowska (compounds **3-21**), Frédéric Couture (compounds **28-32**) and Roxane Desjardins (compound **33**). Roxane Desjardins

performed the cell toxicity and cell permeability studies as well. Vahid Dianati, Robert Day and Yves L. Dory analyzed the data. Vahid Dianati wrote the manuscript with revisions from Frédéric Couture, Anna Kwiatkowska, Robert Day and Yves L. Dory.

3.2. Abstract

The serine protease, PACE4, is a proprotein convertase which plays a substantial role in malignancy of prostate cancer. Our initial selective PACE4 inhibitor (Ac-LLLLRVKR-NH_2) has evolved to the current lead compound C23 (Ac-dLeu-LLLRVK-Amba), which is active both in-vitro and in-vivo. By screening natural residues, except Cys, in C-terminal P1' position, it was established that increasing hydrophobicity was improving cell permeability, which was directly translated into PCa cells antiproliferative activity. This cell antiproliferation enhancement seems independent from effect of P1' residue on PACE4 affinity. Replacement of P1-Amba of C23 by Acpa ((*S*)-2-amino-3-(4-carbamimidoylphenyl)propanoic acid) followed by addition of tryptamine in P1' resulted in compound **32** exhibiting superior PCa cells antiproliferative activity over the reference compound C23 (3-fold). This study sheds light on key factors that improve cell penetrating property and antiproliferative activity of PACE4 inhibitors.

3.3. Introduction

PACE4 is an enzyme in the family of proprotein convertases (PCs) that activates secretory protein precursors through peptide bond cleavage at paired basic amino acids (i.e., consensus cleavage site R-X-R/K-R↓). PACE4 transits within the secretory pathway and is secreted.[210, 233] Our studies were the first to demonstrate the role of PACE4 in prostate cancer (PCa).[114] We showed an overexpression of PACE4 in PCa tissues obtained from patients who underwent radical prostatectomy for clinically localized tumor, while no other PC showed any significant changes. Using mouse PCa xenograft models, we also showed that only PACE4 inhibition blocks PCa progression, and not the inhibition of other PCs.[117] Recently, we discovered that PCa cells utilize an alternative splicing mechanism to generate a cancer-specific C-terminally modified PACE4 isoform (named PACE4-altCT), which is retained in the cell.[91] RNA interference silencing studies targeting PACE4-altCT demonstrate that this isoform is responsible for PACE4-associated cancer progression. PACE4 is also overexpressed and involved in other malignancy including non-small cell lung carcinoma, ovarian, and breast cancer.[108, 111-112, 114, 117] The sum of our data provides the proof of concept and the justification to proceed with a development plan for PACE4 inhibitors for a novel cancer therapy.

In this regard, we developed a specific PACE4 inhibitor named the Multi-Leu peptide (ML-peptide).[166-167] In enzyme kinetic assays, the ML-peptide (sequence: Ac-LLLLRVKR-NH_2) **1** is potent (K_i = 22 ± 6 nM) and selective for PACE4 (e.g., 20-fold over furin). In cell-based assays, the compound **1** blocks the proliferation of PCa cell lines (LNCaP, DU145 and 22Rv1) and induces G_0/G_1 cell cycle arrest. We also discovered that the target of the compound **1** is intracellular since a cell impermeable analog (i.e., PEG8-ML-peptide) has no effect on cell proliferation.[166] We believe compound **1** exerts its anti-proliferative effects by reaching PACE4-altCT (i.e., cell retained PACE4 isoform). While potent in cell-based assays, the compound **1** displays poor stability *in vivo*, so we developed a stable version named C23 (compound **2**; **Figure 38**).[170] Among the modifications in compound **2**, the replacement of the P1 Arg by 4-amidinobenzylamide (Amba) gives this PACE4 inhibitor with higher potency than the compound **1** and antiproliferative activity against PCa cell lines and improved stability and pharmacokinetic profile.[167-169] The additional change of P8-Leu to its d-isomer, raised the plasma stability up to 1.7 hours with almost no loss of potency and anti-proliferative activity.[168,234] In LNCaP xenografted mice, compound **2** (2 mg/kg/day iv) diminished tumor volumes by 60% over 18 days with a 47% reduction in plasma PSA levels, as well as a significant decrease in cells progressing through the cell cycle, increased apoptosis and impaired neovascularization.[170]

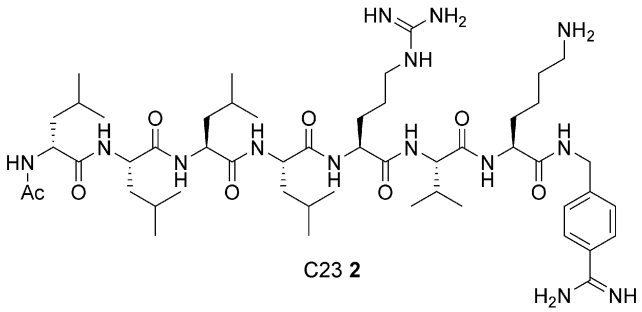

C23 **2**

Figure 38. Structure of lead compound **2** (C23).

While compound **2** represents a significant improvement for PACE4 inhibition *in vivo*, further refinements may be needed. Indeed, a systematic scan of positions P5 to P8 of compound **2** revealed that these four residues have to be hydrophobic. It was even shown that charged residues at those positions reduce antiproliferative activity on PCa cell lines. This may be due to the disruption of the amphipathic nature of the inhibitor, which affects its cell penetrating properties.[171] Parallel studies on the compound **1** indicated that introduction of a β-branched basic residue, (2*S*)-amino-(3*S*)-guanidinobutyryl (*S*-*i*-Agb), in the P3 position led to a compound with unprecedented high potency and selectivity towards PACE4.[212]

However, further antiproliferative PCa cells analysis of this compound and related analogs showed very poor activity.

The analysis of PC homology models based on furin crystal structure suggests that the S1 to S4 pockets are strongly conserved among PCs.[87] However, these models also highlight noticeable differences in the P' region of PC catalytic pockets. Despite few reports, no comprehensive investigation has been done on the significance of the P' region of the catalytic site for PACE4 inhibitors.[80, 138] Accordingly, a screening was conducted with natural residues at the P1' position of the compound **1**. The impact of these modifications was evaluated on the inhibition of PACE4 and PCa cell lines antiproliferative activity of new compounds. Additional molecules were further designed based on the obtained results to evaluate any potential gain in terms of PACE4 inhibition and cellular activity.

3.4. Results and discussion

3.4.1. Screening of DNA-encoded residues in P1'

So far, the most potent PACE4 inhibitors including our lead compound **2** have been armed with Amba at their P1 C-terminal. For synthetic feasibility reasons in the investigation of the P1' position, Amba was replaced by Arg-NH_2. The 20 natural amino acids, except Cys, have been incorporated in the P1' position of compound **1**. The inhibitory constants (K_i) of each peptide have been determined for PACE4 and furin using a fluorometric assay to compare the binding affinities. The efficacy of compounds was further assessed ex vivo using DU145 and LNCaP PCa cell lines using an MTT cell proliferation assay.

The PACE4 and furin affinities (**Table 3**) of the new compounds **3−21**, compared to the control compounds **1** and **2**, reveal that P1'-Lys (**10**) and P1'-Arg (**16**) are the least-favored residues for the S1' pocket of both enzyme which is in accordance with what has been observed for affinity of PC's substrates.[87] However, only compounds **10** and **16** remain as selective as compound **1** (17 and 16 times more selective toward PACE4, respectively). As illustrated in **Figure 40**, other P1'-modified peptides, except Pro (**14**) and Leu (**11**), inhibit PACE4 in the range of compound **1** (20-64 nM). Compounds **6**, **20** and **21** with aromatic residues (Phe, Trp and Tyr) in P1' are among the best PACE4 inhibitors in this series, with compound **6** displaying a K_i value as low as 20 ± 2 nM for PACE4. In general, most of the inhibitors were showing enhanced affinity for furin and diminished inhibition of PACE4, in comparison to compound **1**. As a result, no gain in selectivity was ever observed with the introduction of residues in position P1'. The PACE4 inhibition profile of compounds **3−21** suggests that no natural residue could introduce a favorable interaction with PACE4 in the S1' pocket.

Table 3. Inhibition profiles and cellular antiproliferative activities of compounds **3−21** with general structure of Ac-Leu-Leu-Leu-Leu-Arg-Val-Lys-Xaa-NH_2 compared to control compounds **1** and **2**.

Entry	Structure	K_i (nM) ± SEM[a]		Selectivity for PACE4	IC_{50} (μM) ± SEM[a]	
		PACE4	Furin		DU145	LNCaP
1	Ac-Leu-Leu-Leu-Leu-Arg-Val-Lys-Arg-NH_2[b]	22 ± 6	430 ± 10	20	100 ± 10	180 ± 60
2	Ac-**dLeu-**Leu-Leu-Leu-Arg-Val-Lys-**Amba**[b]	4.9 ± 0.9	9.8 ± 2	2	25 ± 10	45 ± 10
3	Ac-Leu-Leu-Leu-Leu-Arg-Val-Lys-Arg-**Ala**-NH_2	37 ± 5	210±10	6	160 ± 10	N.D.[c]
4	Ac-Leu-Leu-Leu-Leu-Arg-Val-Lys-Arg-**Asp**-NH_2	30 ± 2	74 ± 8	2	230 ± 20	N.D.
5	Ac-Leu-Leu-Leu-Leu-Arg-Val-Lys-Arg-**Glu**-NH_2	58 ± 4	260 ± 30	4	N.C.[d]	N.D.
6	Ac-Leu-Leu-Leu-Leu-Arg-Val-Lys-Arg-**Phe**-NH_2	20 ± 2	74 ± 9	4	70 ± 8	170 ± 40
7	Ac-Leu-Leu-Leu-Leu-Arg-Val-Lys-Arg-**Gly**-NH_2	44 ± 5	500 ± 30	11	N.C.	N.D.
8	Ac-Leu-Leu-Leu-Leu-Arg-Val-Lys-Arg-**His**-NH_2	33 ± 7	140 ± 10	4	N.C.	N.D.
9	Ac-Leu-Leu-Leu-Leu-Arg-Val-Lys-Arg-**Ile**-NH_2	64 ± 4	290 ± 10	5	72 ± 8	N.C.
10	Ac-Leu-Leu-Leu-Leu-Arg-Val-Lys-Arg-**Lys**-NH_2	150 ± 20	2600 ± 100	17	130 ± 10	N.D.
11	Ac-Leu-Leu-Leu-Leu-Arg-Val-Lys-Arg-**Leu**-NH_2	170 ± 30	990 ± 30	6	90 ± 10	N.D.
12	Ac-Leu-Leu-Leu-Leu-Arg-Val-Lys-Arg-**Met**-NH_2	32 ± 2	170 ± 10	5	130 ± 20	N.D.
13	Ac-Leu-Leu-Leu-Leu-Arg-Val-Lys-Arg-**Asn**-NH_2	28 ± 3	130 ± 20	5	N.C.	N.D.
14	Ac-Leu-Leu-Leu-Leu-Arg-Val-Lys-Arg-**Pro**-NH_2	250 ± 10	990 ± 30	4	210 ± 30	N.D.
15	Ac-Leu-Leu-Leu-Leu-Arg-Val-Lys-Arg-**Gln**-NH_2	43 ± 3	190 ± 10	5	210 ± 20	N.D.
16	Ac-Leu-Leu-Leu-Leu-Arg-Val-Lys-Arg-**Arg**-NH_2	160 ± 5	2500 ± 400	16	71 ± 7	N.C.
17	Ac-Leu-Leu-Leu-Leu-Arg-Val-Lys-Arg-**Ser**-NH_2	64 ± 2	330 ± 20	5	240 ± 50	N.D.
18	Ac-Leu-Leu-Leu-Leu-Arg-Val-Lys-Arg-**Thr**-NH_2	22 ± 2	100 ± 10	5	170 ± 10	N.D.
19	Ac-Leu-Leu-Leu-Leu-Arg-Val-Lys-Arg-**Val**-NH_2	38 ± 4	200 ± 10	5	170 ± 10	N.D.
20	Ac-Leu-Leu-Leu-Leu-Arg-Val-Lys-Arg-**Trp**-NH_2	29 ± 1	110 ± 10	4	25 ± 2	31 ± 3
21	Ac-Leu-Leu-Leu-Leu-Arg-Val-Lys-Arg-**Tyr**-NH_2	29 ± 1	64 ± 5	2	100 ± 20	N.D.

[a]K_i and IC_{50} values are based on at least two independent experiments. Errors reported as SEM for K_i and IC_{50}. For more details of inhibitor concentrations used in the MTT antiproliferative assay see experimental section. [b]Data were adapted from references.[166, 168] [c]N.D.: Not determined. [d]N.C.: Not calculable as the curves did not converge to 50% with doses up to 300 μM.

MTT cell proliferation was then investigated to assess the cell activity of inhibitors on PCa cell lines (**Table 3**). The compounds **3−21** were first monitored on DU145 cells. Thereafter, the most active compounds were also examined on LNCaP cells. Clearly, the introduction of hydrophobic residues in P1' position enhances the antiproliferative activity of peptides. For instance, compounds with P1' residues

Phe (**6**), Ile (**9**), Leu (**11**) and Trp (**20**) led to the IC_{50} values of 70 ± 8, 72 ± 8, 90 ± 10 and 24 ± 2 μM, for DU145 PCa cells, respectively. As exceptions for polar residues, we were at first very surprised by the P1'-Lys (**10**) and P1'-Arg (**16**) peptides with their respective antiproliferative IC_{50} values of 130 ± 20 and 71 ± 7 μM while they are very weak PACE4 inhibitors. Based on these results, it was then uncovered that positive charge and hydrophobicity in P1' residue are the main factors for enhancing the antiproliferative activity.

3.4.2. SAR studies based on the screening.

Following the encouraging data collected for peptides **6**, **16** and **20** (**Table 3**), the next logical move was to combine the basic nature of Arg and the aromatic nature of Phe at position P1'. This is how the new residues 4-aminophenylalanine (Apa) **22**, 4-guanidinophenylalanine (Gpa) **23** and 4-(2-aminoethyl)benzimidamide (Aeba) **24** were designed (**Figure 39-a**). Hence, the corresponding compounds **28−30** were synthesized on solid support, then tested (**Figure 39-b**). Only compound **29** inhibited PACE4 with an improved K_i of 11 ± 2 nM but once again, this increased affinity didn't translate to antiproliferative activity. The reduced polarity in Aeba **24** with no C-terminal $-CONH_2$ group, contributed to the antiproliferative properties of compound **30** (41 ± 9 and 67 ± 7 μM for DU145 and LNCaP cells, respectively) which is no better than lead compound **2**.

a)

Entry	Structure	K_i (nM) ± SEM		Selectivity for PACE4	IC_{50} (μM) ± SEM	
		PACE4	Furin		DU145	LNCaP
28	Ac-Leu-Leu-Leu-Leu-Arg-Val-Lys-Arg-**Apa**-NH_2	32 ± 4	130 ± 10	4	139 ± 4	170 ± 10
29	Ac-Leu-Leu-Leu-Leu-Arg-Val-Lys-Arg-**Gpa**-NH_2	11 ± 2	140 ± 10	13	83 ± 2	92 ± 2
30	Ac-**D**Leu-Leu-Leu-Leu-Arg-Val-Lys-Arg-**Aeba**	68 ± 1	700 ± 100	10	41 ± 9	67 ± 7
31	Ac-**D**Leu-Leu-Leu-Leu-Arg-Val-Lys-Arg-**Tryp**	70 ± 10	280 ± 2	4	14 ± 2	18 ± 5
32	Ac-**D**Leu-Leu-Leu-Leu-Arg-Val-Lys-Arg-**Acpa-Tryp**	41 ± 5	80 ± 10	2	7.5 ± 0.8	13 ± 1
33	Ac-**D**Leu-Leu-Leu-Leu-Arg-Val-Lys-Arg-**Aca-Tryp**	248 ± 6	3000 ± 500	12	40 ± 20	70 ± 20

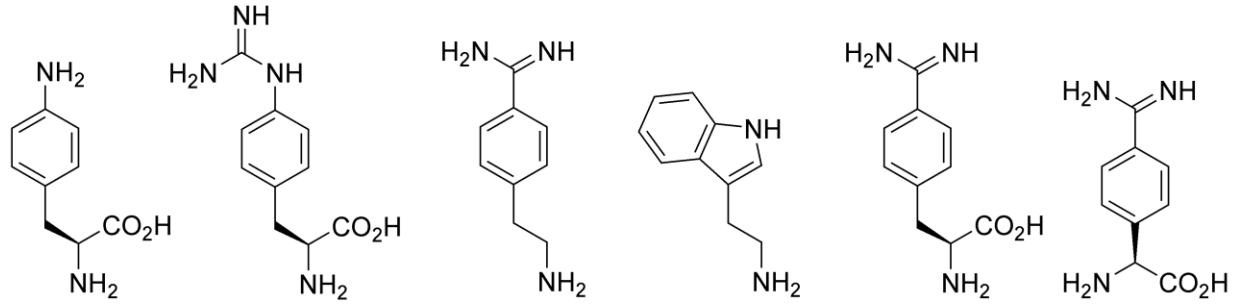

Apa **22** Gpa **23** Aeba **24** Tryp **25** Acpa **26** Aca **27**

b)

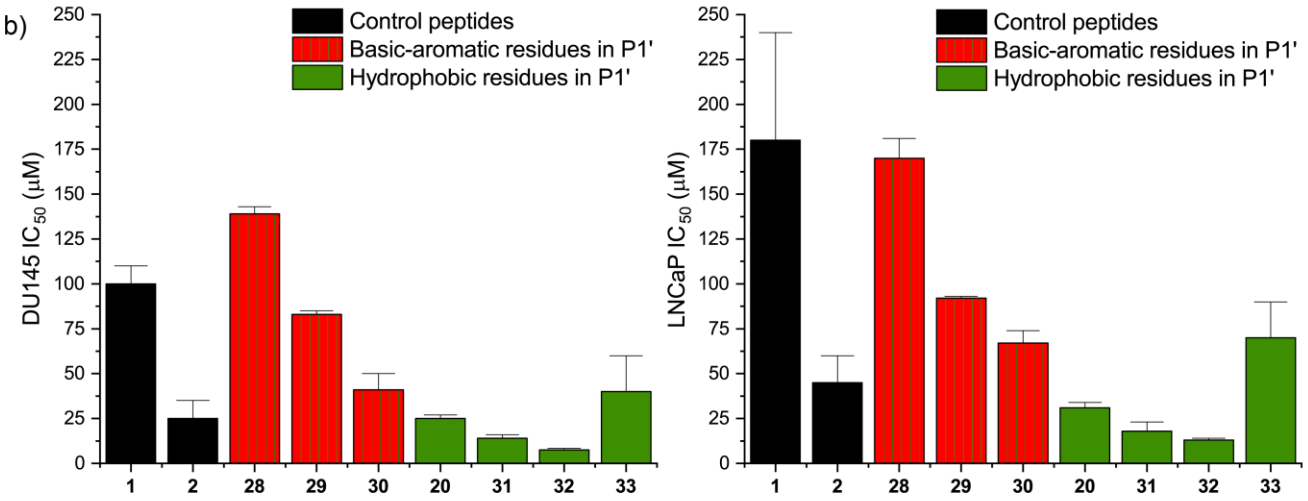

Figure 39. a) The PACE4 affinity and antiproliferative activity of compounds **28–33**. K_i and IC_{50} values are means of at least two independent experiments. Errors reported as SEM for K_i and IC_{50}. For more details on the concentration of inhibitors in the MTT antiproliferative assay see experimental section. b) The IC_{50} values of selected compounds for DU145 and LNCaP PCa cell lines.

Since the decarboxylated compound **30** (residue **24** at P1') showed better IC_{50} values than compounds **28** and **29**, P1'-Trp in compound **20** was replaced with tryptamine (Tryp) **25** increasing the C-terminal hydrophobicity. As expected, compound **31** showed promising IC_{50} values (14 ± 2 μM for DU145 and 18 ± 5 μM for LNCaP cells). To further increase the cell efficacy, compound **31** was modified in P1 position by substituting Arg with (*S*)-2-amino-3-(4-carbamimidoylphenyl)propanoic acid (Acpa) **26** and

(*S*)-2-amino-3-(4-carbamimidoylphenyl)acetic acid (Aca) **27** which have the 4-amidinophenyl side chain similar to Amba in compound **2**. Those modifications led to the compounds **32** (PACE4 K_i of 41 ± 7 nM) and **33** (PACE4 K_i of 248 ± 6 nM). The PACE4 affinity comparison of these compounds with compound **31** indicates a 2-fold preference for Acpa (**32**) over Arg (**31**) in P1 position while Aca (**33**) is 6 times disfavored. The diminished PACE4 affinity of compound **33** is most likely due to the steric hindrance around the opening of P1 pocket. Overall, there seems to be no correlation between affinity and antiproliferative activity linked to the nature of the P1' residues (**Figure 40-a**). On the other hand, observations indicate that such a correlation may exist at the P1 position, since PACE4 affinity is well translated into PCa cell antiproliferative activity in both compounds **32** and **33**. Compound **32**, displaying unprecedented IC_{50} values (7.5 ± 0.8 and 13 ± 1 µM for DU145 and LNCaP cells, respectively) for PCa cell lines, is a good candidate for further *in vivo* studies (**Figure 39-b**).

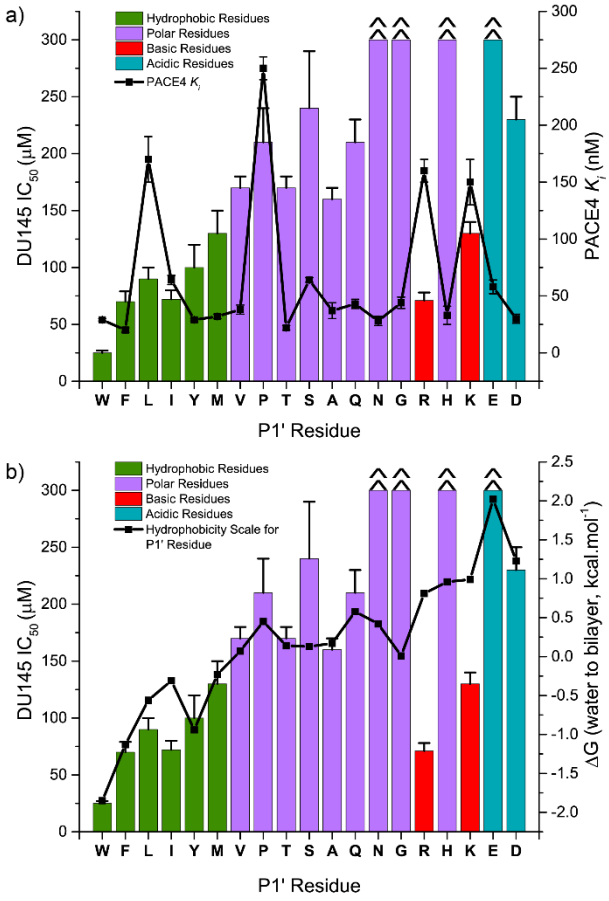

Figure 40. a) Linear relation of IC_{50} values for MTT antiproliferative assay on DU145 PCa cell line with Wimley-White bilayer scale for hydrophobicity of P1' residues and b) weak correlation to PACE4 affinity of compounds **3**−**21**.

3.4.3. Cell permeability studies.

The relationship between K_i and IC_{50} is clearly not linear. It is obvious that PACE4 affinity of inhibitors translates poorly into antiproliferative activity with introduction of the P1' residue (**Figure 40-a**). On the other hand, there is a linear relation between hydrophobicity of P1' residues and antiproliferative activity of compounds (**Figure 40-b**). The IC_{50} values are in respectable agreement with Wimley-White bilayer scale for hydrophobicity of amino acids.[235] In this scale, the $\Delta G_{(water\ to\ bilayer)}$, is calculated for the partitioning of peptides Ac-WL-X-LL-OH (X: natural amino acid) between water and a POPC lipid bilayer.[236] The $\Delta G_{(water\ to\ bilayer)}$ value of each amino acid can be used to evaluate its contribution to membrane penetration.

We, thus, suggest that the preeminent cytostatic activity of compounds with a hydrophobic P1'-residue originated from enhancement in penetration of such peptides through cell membrane. Thus, the compounds **35**−**38** which were FITC-labeled in their N-terminal. After an hour of incubation of the labeled compounds with DU145 cells, the emitted fluorescence from cells was analyzed using fluorescence-activated cell sorting (FACS) and compared to compound **34** as control. The signal of membrane absorbed peptides was eliminated by treatment of cells with trypan blue prior to analysis. The depicted results in **Figure 41** revealed that the higher permeability achieved with increased P1' hydrophobicity. In comparison to control compound **34**, uptake of compounds **37** and **38** enhanced by 2 and 3.5-fold, respectively, which totally correlate with IC_{50} values for compounds **20** and **31**. The better penetration of compounds with Arg (**35**) and Lys (**36**) in P1' position, compared to control, also suggests that lower PACE4 affinity of compounds **16** and **10** were compensated by their amended cell penetration.

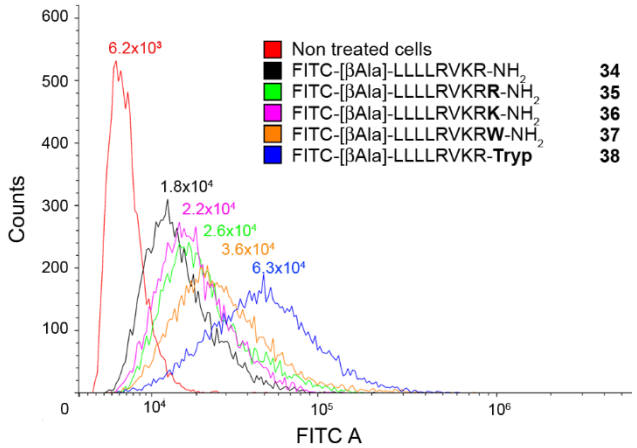

Figure 41. Quantitative cell penetration assessment of FITC-labeled compounds **35**−**38** compared to control compound **34**.

The direct relation between cell penetration and antiproliferative activity has been constantly observed for compound **1** and its derivatives.[167-168] The cell permeability is required to reach the intracellular PACE4-altCT isoform which is responsible for PACE4-associated cell growth of prostate malignant cells.[91] This is consistent with our previous observations with N-terminal PEGylated derivatives of compound **1** displayed no cell permeability and thus no antiproliferative activity.[166] The amphipathic nature of peptide inhibitors with the charged warhead and four hydrophobic residues in N-terminal has been considered crucial for cell derivatives of compound **2**.[171] Arg residues play the key role in cell permeability of poly-arginine cell penetrating peptides (CPPs), including compound **1** derivatives, through bidentate electrostatic and hydrogen bonds with negatively charged groups of membrane.[237] Hydrophobic residues, when present in a CPP, increase the interactions with lipid bilayer and thus increasing translocation of peptides through membrane.[238] Among hydrophobic residues, inclusion of Trp within basic peptides is a molecular determinant for enhancement of cell uptake efficiency.[239-242] For instance, more abundancy of Trp residues in amphiphilic helical CPPs increased their uptake in A549 cell lines.[243] The exclusive role of tryptophan in cell penetration of polyarginine peptides is ascribed to the interaction with sulfated glycosaminoglycans possibly through hydrophobic and π–anion interactions in addition to its important hydrophobic interactions with lipid bilayer.[244-245]

3.4.4. DU145 cell toxicity studies

The toxicity of compounds **10**, **16**, **20**, **31** and **32** on DU145 cells was evaluated to ascertain the fact that observed fluorescence in the permeability assay is related to pure cell penetration of peptides and not to cell lysis. Hence, DU145 cells treated with peptides for 1.5 h and the number of live cells was assessed by addition of PI (propidium iodide) followed by FACS measurement of fluorescence. The compounds **10** and **16**, displayed no toxicity to doses up to 100 μM. The results for compounds **20**, **31**, and **32** revealed that toxicity for these compounds occurred at concentrations above 10 μM which is more than 10-fold higher than the tested concentration for FITC-labeled peptides (1μM) in permeability assays (**Figure S1**). For compound **32**, a few more concentrations were tested to obtain a dose-response curve for cellular toxicity (DU145 IC_{50} (PI) = 28 ± 2 μM; **Figure 43**). In comparison, this compound inhibited metabolic activity of DU145 cells in 4-fold lower doses (DU145 IC_{50} (MTT) = 7.5 ± 0.8 μM). The fact that 4-fold more concentration of compound **32** is necessary for DU145 cytotoxicity, suggests that this compound is likely mediating its effects through mechanisms other than killing the cells in one-digit μM concentrations.

3.4.5. Plasma stability studies

Despite rapid tumor uptake of PACE4-inhibitor, which permits *in vivo* efficacy, the half-lives of all-natural residue peptide inhibitors of PACE4 in human plasma is quite short.[170] Accordingly, increasing the peptide stability in biological matrices is essential. Half-life ($t_{1/2}$) of compound **31** with dLeu in P8 and Tryp in P1' (0.8 h) was less than half of compound **2** (1.7 h). Statistically, addition of a residue in P1' increased the number of breakable amide bonds thus making the modified peptides more prone to the plasma proteases than their 8-mer counterparts. It is well known that replacement of natural residues with the unnatural one, is a way that could potentially increase the stability of peptides.[246] As a result, modification of P1-Arg in **31** with Acpa in **32** increased the plasma half-life up to 2.0 h (**Figure 42**).

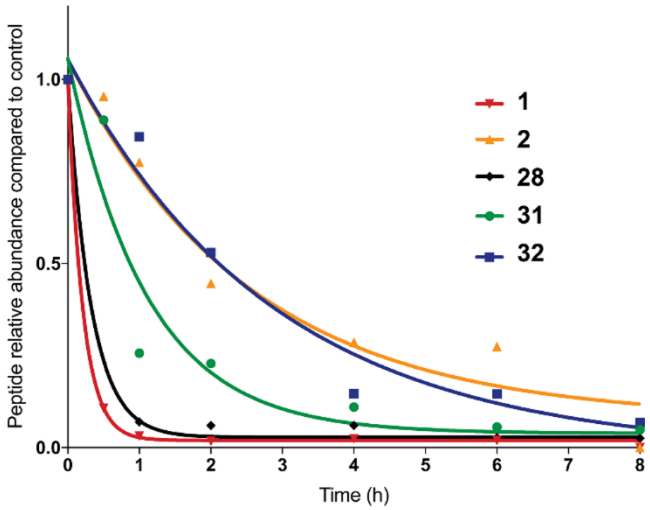

Figure 42. Stability of compounds **28**, **31** and **32** in human plasma comparing to lead compounds **1** and **2**.

3.4.6. Acute toxicity studies

To assess the safety profile of compound **32**, the acute toxicity of this compound was studied on healthy mice. The experiment included a single intravenous or intraperitoneal administration dose of compound **32** into healthy mice (CD1 mice as standard for toxicological and safety evaluations) at various doses to find the toxicity threshold (maximum tolerated dose, MTD). The results indicated that this compound has an MTD of at least 5 mg/kg for intravenous administration (**Figure 43-b**).

In a previous study, we showed that a 2 mg/kg/day dose of compound **2** is sufficient for therapeutic activity in a LNCaP xenografted model of prostate cancer[170] while it displayed safe profile in acute

toxicity studies (MTDs of 10 mg/kg in healthy mice).[168] The *in vivo* therapeutic activity for compound **32** is yet to be evaluated in LNCaP xenografted models.

a)

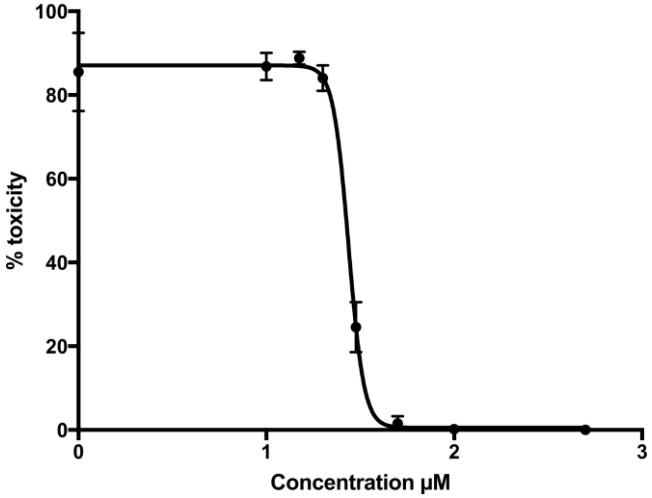

b)

Compound	IC_{50} (PI)	MTD (i.v.)
32	28 ± 2 µM	>5 mg/kg

Figure 43. The toxicity profile of compound **32**. a) The dose-response curve for DU145 cellular toxicity was performed using PI as a staining reagent. The errors are reported as SEM. For more details on concentration of inhibitors in this assay see experimental section. b) Table showing IC_{50}(PI) and MTD values of compound **32** in healthy CD1 mice. Data are representative of at least two independent experiments.

3.4.7. Synthesis

Compounds **3**−**21**, **28** and **29** with amino acid residues in P1' were prepared with conventional 9-fluorenylmethyloxycarbonyl (Fmoc)-based solid phase peptide synthesis (SPPS) on TentaGel® S RAM resin (**Scheme S1**). The decarboxylated analogues **30**, **31**, **32** and **33** were synthesized using a combination of solid and solution phase peptide synthesis (**Schemes 5** and **6**). At first crude protected peptide were obtained from Fmoc-SPPS on 2-chlorotrityl chloride resin, and then the free C-terminal was coupled with the corresponding amines in solution. The global deprotection with a TFA cocktail (composed of TFA/TIPS/H_2O 95:5:5) yielded the desired peptides.

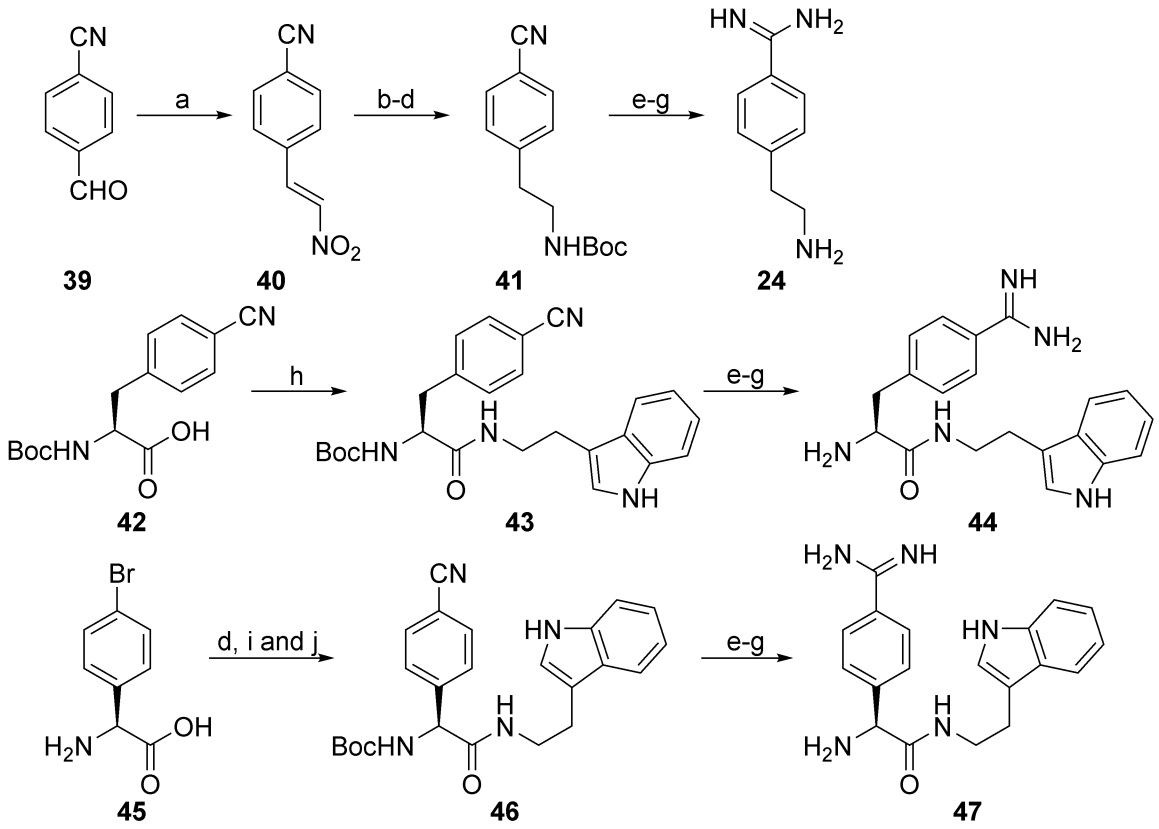

Scheme 5. Synthesis of P1 residue of compound **30**, and P1-P1' adduct of compounds **32** and **33**. Reagents and conditions: (a) CH_3NO_2, NaOH, MeOH/H_2O, <10-15 ºC, 15 min then 5 M HCl; (b) Bu_3SnH, DCM, rt, 16 h; (c) Zn, HCl(aq), 65 ºC, 1 h; (d) $(Boc)_2O$, K_2CO_3, THF/H_2O, 16 h; (e) NH_2OH.HCl, DIPEA, MeOH, 60 ºC, 16 h; (f) Ac_2O, DIPEA, THF then 5% Pd/C, AcOH/MeOH 35 atm H_2, 16 h; (g) Conc. HCl(aq), MeOH, 0 ºC to rt, 1 h; (h) tryptamine hydrochloride, EDCI, 6-Cl-HOBt, DIPEA, DCM, 0 ºC to rt, 16 h; (i) *i*-BuOCOCl, DIPEA, tryptamine hydrochloride, THF, −20 ºC, 2 h; (j) $Pd(PPh_3)_4$, $Zn(CN)_2$, DMF, 100 ºC, 16 h.

For obtaining Aeba **24**, aldehyde **39** condensed with nitromethane to give (*E*)-4-(2-nitrovinyl)benzonitrile **40** (**Scheme 5**). The double bond and nitro moiety were reduced using tributyltin hydride and Zn/HCl, respectively. The resulting amine was protected with *t*-butyl carbamate (Boc) group for more convenient purification in the following steps. Transformation of nitrile **41** to amidine in compound **24** was performed as previously reported for Amba.[167] Boc-Phe(4-CN)-OH **42** was coupled with tryptamine **25** using EDCI coupling reagent. Compound **45**'s amino group was protected with Boc and then coupled with tryptamine **25** at low temperature using acyl chloride strategy. An additional cyanation step was necessary to obtain compound **46**. The conversion of nitrile groups in compounds **43** and **46** to the corresponding amidines in **44** and **47** was performed with a similar procedure as was used for AEBA **24**.

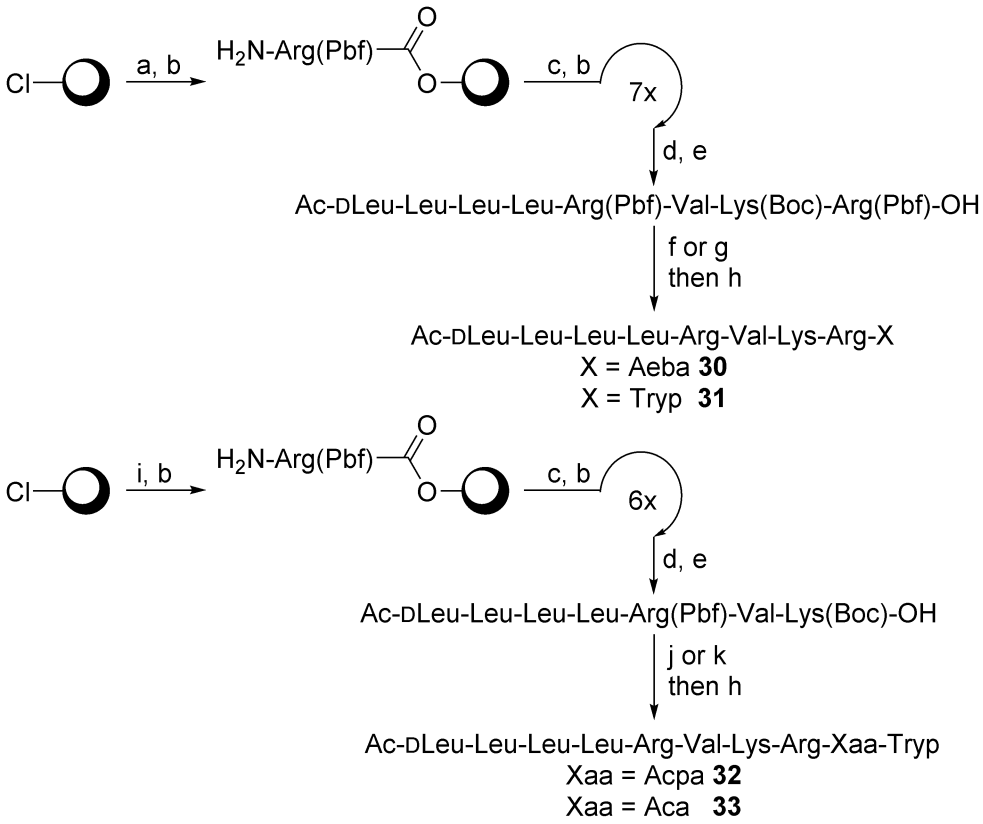

Scheme 6. Synthesis of compounds **30**−**33**. Reagents and conditions: (a) Fmoc-Arg(Pbf)-OH, DIPEA, DMF/DCM (1:1); (b) Pip/DMF (1:4); (c) Fmoc-aa-OH, HATU, DIPEA, DMF; (d) Ac-dLeu-OH, HATU, DIPEA, DMF; (e) HFIP/DCM (1:4); (f) PyBOP, 6-Cl-HOBt, DIPEA, DMF, **24**, 0 °C to rt, 16 h; (g) PyBOP, 6-Cl-HOBt, DIPEA, DMF, tryptamine hydrochloride, 0 °C to rt, 16 h; (h) TFA/TIPS/H_2O (38:1:1); (i) Fmoc-Lys(Boc)-OH, DIPEA, DMF/DCM (1:1); (j) PyBOP, 6-Cl-HOBt, DIPEA, DMF, **44**, 0 °C to rt, 16 h; (k) PyBOP, 6-Cl-HOBt, DIPEA, DMF, **47**, 0 °C to rt, 16 h.

3.5. Conclusion

In conclusion, we developed PACE4 inhibitors by SAR studies in P1 and P1' using ML-peptide **1** as template. By performing a systematic screening of natural amino acids in P1' position of peptide **1**, compound **20** (Trp in P1') was identified as having improved antiproliferative effect on PCa cell lines. Further modification of this Trp residue to Tryp (**31**) increased the hydrophobicity in the C-terminal region of the resulting peptide. Despite its diminished affinity for recombinant PACE4, Trp to Tryp replacement improved plasma stability and cell efficacy. In an attempt to further increase the *in vitro* cell activity of compound **31**, P1-Arg was replaced with an Acpa residue. This change contributed to the plasma stability and antiproliferative effect of compound **32** which possesses the best cell efficacy of peptide **1** derivatives reported to date. The enhancement of antiproliferative activity with the

incorporation of Trp or Tryp in the C-terminal region was found to be related to the improved cell penetration properties of such inhibitors. The cell permeability is the main obstacle in the development of multi-basic inhibitors of PACE4 as well as similar targets such as furin and some other flaviviral proteases.[247-249] The present study constitutes a significant step forward to address such cell penetration issues.

3.6. Experimental

3.6.1. Chemistry

General Experimental Methods. All chemical reagents and solvents were obtained from commercial resources and used without further purification. Fmoc-protected amino acids and Boc-protected amino acid **42** and coupling reagents, were purchased from ChemPep (Miami, FL, USA) or Chem-Impex International (Wood Dale, IL, USA). Tryptamine and most of other reagents were bought from Sigma Aldrich (St. Louis, MO, USA). TentaGel® S RAM resin and 2-chlorotrityl-chloride resin were received from Rapp Polymer (Tübingen, Germany). Peptide synthesis (Fmoc/*t*Bu strategy) was accomplished either manually or automatically on a Pioneer peptide synthesizer (Applied Biosystems). The purification and purity check of peptide inhibitors were performed using reverse phase high-performance liquid chromatography (RP-HPLC) on an Agilent Technologies 1100 system (analytical and semi-prep) equipped with a diode array detector (λ = 210, 214, 230, and 254 nm). Preparative HPLC were done using either a Varian ProStar preparative system equipped with a UV-Vis detector (λ = 214 nm) or a Waters preparative HPLC system (Autosampler 2707, Quaternary gradient module 2535, UV detector 2489 (λ = 214 and 230 nm), fraction collector WFCIII) equipped with an ACE5 C18 column (250 × 21.2 mm, 5 µm spherical particle size). A gradient of 0.1% TFA in water and acetonitrile was used as eluent. Analytical HPLC was carried out using C18 columns, either Agilent Eclipse XDB (5 mm, 4.6 µm, 250 mm) or a Phenomenex Jupiter (5 mm, 4.6 µm, 250 mm). ESI-HRMS (TripleTOF 5600, ABSciex; Foster City, CA, USA) was used to confirm the identity of the pure products. Water H Class Acquity UPLC coupled with an SQ Detector 2 and a PDA eλ detector paired with an Acquity UPLC CSH C18 column (1.7 µm×2.1 mm×50 mm) was also used for synthesis check and plasma stability assessment (linear gradient from 5 to 95% of ACN containing 0.1% formic acid in 0.1% aqueous formic acid was used for 1.3 min, flow rate 0.8 mL/min). NMR experiment were performed on either AV300 Bruker (300 MHz for ^{1}H and 75 MHz for ^{13}C) or an Avance III hd 400 Bruker (400 MHz for ^{1}H and 100 MHz for ^{13}C). ^{13}C NMR

experiments were done with complete decoupling of protons. Infrared (IR) spectra were recorded using Alpha-Platinum ATR Bruker, diamond crystal.

Peptide Synthesis. A sequence of washes including DMF 3×, a cycle of MeOH/DCM 3× and DCM 3× was applied, after every reaction on resin except stated otherwise. TentaGel® S RAM resin was used for the synthesis of compounds **3**−**21**, **28** and **29**. The chain length growth was performed by standard Fmoc-SPPS. Fmoc group was removed with 20% piperidine in DMF. Fmoc protected amino acids were coupled using 5 equiv of protected amino acids, 5 equiv of HATU and 15 equiv of DIPEA in DMF. The cleavage from resin and side chain deprotection was carried out in one step with a cocktail of TFA/TIPS/H_2O 95:2.5:2.5 for 2 h. The crude peptides were triturated with Et_2O after evaporation of 50% of cleaving cocktail, centrifuged and the supernatant was discarded. For compounds **30**−**33** the peptide cores were synthesized on 2-chlorotrtiyl chloride resin as following. 1.2 equiv of first amino acid was loaded on resin in the presence of 4 equiv DIPEA in DMF for 3 h. The unreacted groups were capped with a mixture of DCM/MeOH/DIPEA 85:10:5, and the resin was washed by a sequence of DCM 3×, a cycle of MeOH/DCM 3× and DCM 5×. The protected peptides were cleaved from resin with 20% hexafluoro-2-propanol in DCM. The solvent was evaporated in vacuo and the residue was dissolved in a mixture of *t*-BuOH/H_2O (1:1) and lyophilized. A mixture of protected peptide, 2.5 equiv of corresponding P1' or P1-P1' amine, 2.2 equiv of PyBOP, 7.5 equiv of 6-Cl-HOBt was dissolved in DMF and cooled in an ice bath, then 7.5 equiv of DIPEA was added to the solution and the reaction was stirred overnight. Solvent was removed with an air stream and the crude protected peptide was deprotected with the same TFA cocktail as compounds **3**−**21**. FITC-labeled peptides were prepared as reported elsewhere.[167] The crude of compounds **3**−**21**, **28**−**33** and **35**−**38** were purified using preparative HPLC. Analytical HPLC was used for confirmation of purity (>95%) of fractions. These compounds were characterized by high-resolution mass spectroscopy (HRMS). The HPLC chromatograms and HRMS details of these compounds are provided in supplementary material.

4-(2-Aminoethyl)benzimidamide (Aeba, 24).

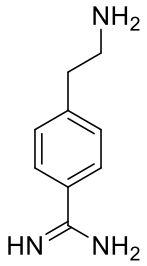

Aeba **24** was prepared as previously reported in chapter 2.

***tert*-Butyl (*S*)-(1-((2-(1H-indol-2-yl)ethyl)amino)-3-(4-cyanophenyl)-1-oxopropan-2-yl)-carbamate (43).**

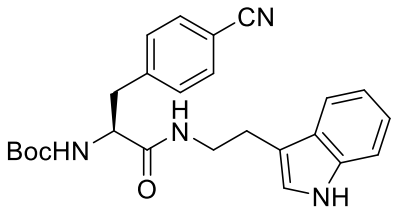

To a suspension of Boc-Phe(4-CN)-OH **42** (1.45 g, 5.00 mmol), tryptamine hydrochloride (0.98 g, 5.00 mmol) and 6-Cl-HOBt (0.93 g, 5.50 mmol) in DCM (15 mL) DIPEA (2.61 mL, 15.00 mmol) was added maintaining the temperature between 0-5 ºC. Once a clear solution was obtained, EDCI (1.05 g, 5.50 mmol) was added at the same temperature. The resulting solution was stirred for 16 h at room temperature. The volatiles were evaporated, and the residue was taken into EtOAc and washed with 10% citric acid, saturated $NaHCO_3$ and brine, dried over $MgSO_4$ and evaporated to a residue that was triturated with DCM and hexanes to obtain the title compound as a white solid (1.96 g, 90% yield). ^{1}H NMR (400 MHz, DMSO-*d*6) δ (ppm) 10.81 (br. s., 1H), 8.05 (br. s., 1H), 7.72 (d, *J* = 7.7 Hz, 2H), 7.54 (d, *J* = 7.8 Hz, 1H), 7.42 (d, *J* = 7.7 Hz, 2H), 7.34 (d, *J* = 7.8 Hz, 1H), 7.15 (s, 1H), 7.07 (t, *J* = 7.8 Hz, 1H), 6.91 - 7.02 (overlapped, 2H), 4.18 (m, 1H), 3.35 (m, 2H), 3.00 (dd, *J* = 13.0, 3.1 Hz, 1H), 2.80 (overlapped, 3H), 1.28 (s, 9H). ^{13}C NMR (100 MHz, DMSO-*d*6) δ (ppm) 171.0, 155.2, 144.5, 136.3, 131.9, 130.4 (overlapped 2C), 127.2, 122.7, 121.0, 119.1, 118.3, 111.7, 111.4, 109.1, 78.1, 55.3, 41.2, 37.9, 28.1, 25.1. IR (neat) ν (cm^{-1}) 1651, 1682, 2228, 2918, 2956, 3327, 3348, 3407, 3412. HRMS (ESI) calculated for $C_{25}H_{29}N_4O_3$ m/z $[M+H]^+$ 433.2234 found 433.2306. Mp; 174-176 ºC.

(*S*)-*N*-(2-(1H-indol-2-yl)ethyl)-2-amino-3-(4-cyanophenyl)propanamide (44).

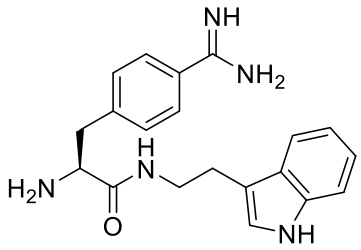

The amidine **44** was prepared from **43** (0.4 g, 9.2 mmol) using the previously reported protocol for the preparation of amidine **24**. ^{1}H NMR (400 MHz, D_2O) δ (ppm) 7.68 (d, *J* = 8.5 Hz, 2H), 7.56 (d, *J* = 7.9 Hz, 1H), 7.42 (d, *J* = 8.5 Hz, 2H), 7.33 (d, *J* = 7.9 Hz, 1H), 7.08 - 7.12 (m, 1H), 7.06 (s, 1H), 6.97-7.03

(m, 1H), 4.30 (dd, *J* = 9.0, 5.6 Hz, 1H), 3.42 - 3.57 (m, 2H), 3.13 (dd, *J* = 13.5, 5.6 Hz, 1H), 2.92 (t, *J* = 7.0 Hz, 2H), 2.86 (dd, *J* = 13.5, 9.0 Hz, 1H). ^{13}C NMR (100 MHz, D_2O) δ (ppm) 168.3, 157.6, 146.3, 138.3, 131.6, 129.0, 127.9, 123.6, 122.5, 119.8, 119.4, 116.9, 113.2, 112.4, 57.2, 41.4, 39.4, 26.3. IR (neat) ν (cm^{-1}) 1666, 1678, 2905, 2943, 2989, 3296, 3393, 3413 HRMS (ESI) calculated for $C_{20}H_{23}N_5O$ m/z $[M+H]^+$ 350.1975 found 350.1995. Mp; decomposed at >300 ºC.

***tert*-Butyl (*S*)-(2-((2-(1H-indol-3-yl)ethyl)amino)-1-(4-cyanophenyl)-2-oxoethyl)carbamate (46).**

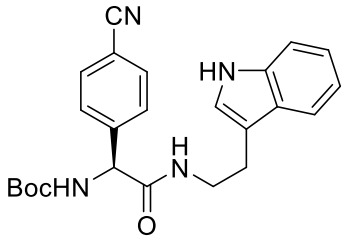

4-bromo-phenylglycine **45** (0.92 g, 4.00 mmol) and K_2CO_3 (0.55 g, 4.00 mmol) were dissolved in H_2O (50 mL), treated with $(Boc)_2O$ (1.05 g, 4.80 mmol) in THF (25 mL), stirred overnight, and the mixture was evaporated under reduced pressure. The resulting aqueous phase was neutralized with solid citric acid and extracted with EtOAc (3x). The combined organic phases were washed with brine, dried over magnesium sulfate and evaporated to dryness to give Boc-Phg(4-Br)-OH in quantitative yield. This white solid (1.38 g, 4.00 mmol) and *i*-butyl chloroformate (0.52 mL, 4.00 mmol) were dissolved in THF (20 mL), cooled to -20 ºC prior and treated with precooled (-20 ºC) DIPEA (0.70 mL, 4.00 mmol, precooled to -20 ºC). The suspension was agitated for 10 min before the addition of a mixture of tryptamine hydrochloride (0.94 g, 4.80 mmol) and DIPEA (0.84 mL, 4.8 mmol) in THF (5 mL). After stirring for 24 h at -20 ºC, the volatiles were removed, and the residue was partitioned between EtOAc and water. The phases were separated, and the organic phase was washed with saturated $NaHCO_3$, water, 10% citric acid and brine solutions. The volatiles were evaporated in vacuum and the residue was purified by column chromatography to yield Boc-Phg(4-Br)-Tryp as a white solid (1.13 g, 60 %) ^{1}H NMR (400 MHz, $CDCl_3$) δ (ppm) 8.19 (br. s, 1H), 7.49 (d, *J* = 8.00 Hz, 1H), 7.38 (d, *J* = 8.0 Hz, 2H), 7.35 (d, *J* = 8.0 Hz, 1H), 7.20 (t, *J* = 8.0 Hz, 1H), 7.06-7.15 (overlapped, 3H), 6.68 (d, *J* = 2.2 Hz, 1H), 5.93 (overlapped, 2H), 5.02 (br. s, 1H), 3.58 (dt, *J* = 13.0, 6.5 Hz, 1H), 3.49 (dt, *J* = 13.0, 6.5 Hz, 1H), 2.80 - 2.96 (m, 2H), 1.40 (s, 9H). ^{13}C NMR (100 MHz, $CDCl_3$) δ (ppm) 169.4, 155.1, 137.7, 136.3, 131.9, 128.7 (overlapped 2C), 127.0, 122.2, 122.1, 119.4, 118.4, 112.1, 111.3, 80.2, 57.9, 39.9, 28.2, 24.9. HRMS (ESI) calculated for $C_{23}H_{27}BrN_3O_3$ m/z $[M+H]^+$ 472.1230 found 472.1217. The obtained solid plus $Zn(CN)_2$ (0.16 g, 1.40 mmol) and $Pd(PPh_3)_4$ (0.13 g, 0.11 mmol) were suspended in deoxygenated dry DMF (3 mL) under inert

condition. The yellow slurry was heated to 100 ºC for 16 h, then taken into EtOAc and washed three times with 20% NH_4OH, dried over $MgSO_4$, and purified by column chromatography to yield the title compound as a white solid (0.39 g, 40%) ^{1}H NMR (400 MHz, $CDCl_3$) δ (ppm) 8.07 (br. s, 1H), 7.46 - 7.57 (overlapped, 3H), 7.38 (d, *J* = 8.0 Hz, 1H), 7.31 (d, *J* = 8.0 Hz, 2H), 7.23 (t, *J* = 8.0 Hz, 1H), 7.12 (t, *J* = 8.0 Hz, 1 H), 6.79 (d, *J* = 2.0 Hz, 1H), 5.94 (br. s, 1H), 5.76 (br. s, 1H), 5.05 (br. s, 1H), 3.57-3.67 (m, 2H), 2.84 - 2.98 (m, 2H), 1.40 (br. s., 9H). ^{13}C NMR (100 MHz, $CDCl_3$) δ (ppm) 168.5, 164.8, 143.8, 136.3, 132.6, 127.7, 127.0, 122.4, 122.0, 119.7, 118.4, 118.4, 112.1, 112.0, 111.4, 80.5, 60.4, 40.1, 28.2, 24.8. IR (neat) ν (cm^{-1}) 1659, 1699, 2235, 2939, 2983, 3234, 3290, 3421. HRMS (ESI) calculated for $C_{24}H_{27}N_4O_3$ m/z $[M+H]^+$ 419.2077 found 419.2137. Mp; 98-101 ºC.

(*S*)-*N*-(2-(1H-Indol-3-yl)ethyl)-2-amino-2-(4-carbamimidoylphenyl)acetamide 47.

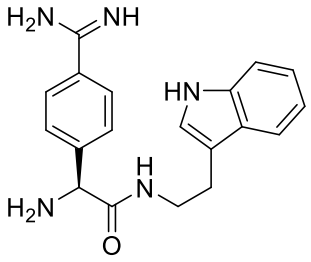

The amidine **47** was synthesized from **46** (0.3 g, 7.2 mmol) using the protocol previously described for the preparation of **24**. ^{1}H NMR (400 MHz, D_2O) δ (ppm) 7.54 (d, *J* = 8.54 Hz, 2H), 7.44 (d, *J* = 7.86 Hz, 1H), 7.39 (d, *J* = 8.20 Hz, 1H), 7.26 - 7.33 (m, 2H), 7.16 (t, *J* = 7.2 Hz, 1H), 7.02 (t, *J* = 7.2 Hz, 1H), 6.89 (s, 1H), 5.00 (s, 1H), 3.89 (ddd, *J* = 13.6, 8.7, 5.1 Hz, 1H), 3.39 (dt, *J* = 13.6, 5.1 Hz, 1H), 2.94 (dt, *J* = 13.6, 5.1 Hz, 1H), 2.83 (ddd, *J* = 13.6, 8.7, 5.1 Hz, 1H). ^{13}C NMR (100 MHz, D_2O) δ (ppm) 165.6, 162.8,137.5, 135.9, 128.5, 128.1, 126.9, 123.1, 121.6,118.9, 118.2, 114.9, 111.5, 111.0, 55.8, 39.5, 23.5. IR (neat) ν (cm^{-1}) 1622, 1682, 2914, 2970, 3010, 3265, 3292. HRMS (ESI) calculated for $C_{19}H_{22}N_5O$ m/z $[M+H]^+$ 336.1819 found 336.1872. Mp; decomposed at >300 ºC.

3.6.2. Enzyme kinetics

The fluorometric K_i measurements of PC enzymes was performed using a Gemini EM 96-well spectrofluorometer (Molecular Devices; Sunnyvale, CA, USA) ($\lambda_{EX.}$, 370 nm; $\lambda_{EM.}$, 460 nm; Cut Off, 435 nm). Both PACE4 and furin are human recombinant proteins produced from S2 insect cells and purified as described earlier.[80] All the experiments were done in duplicate or triplicate. Furin inhibition measurements were performed in 100 mM of HEPES buffer (pH = 7.5), 1 mM $CaCl_2$, 1 mM β-

mercaptoethanol, and 1.8 g/L BSA, while PACE4 inhibition assays were done in a 20 mM Bis-Tris buffer (pH = 6.5), 1 mM $CaCl_2$, and 1.8 g/L BSA. The competitive substrate was pyroGlu-Arg-Thr-Lys-Arg-AMC peptide (Bachem, Switzerland) for both furin and PACE4 with the concentration of 100 μM in each well. Inhibitors were added at various concentrations in the range of 0-10 μM. Enzyme (final concentration 100 μL) was added in each well, and the real-time fluorescence was measured during 1 h of experiments. The K_i values were calculated using the Cheng and Prusoff's equation and the SoftMaxPro5 program.[36]

3.6.3. Cell proliferation

MTT antiproliferative assays were performed on DU145 and LNCaP PCa cell lines as reported earlier.[166] The 96 well plates were seeded with an approximate density of 1500 cells for DU145 or 2500 cells for LNCaP. The media was changed after 24 h and the cells were subsequently treated with different concentrations of peptide inhibitor (peptides **3**−**19**, **21** and **28** were used at a concentration range of 300, 200, 100, 50, 25, 10 and 1 μM; peptides **20** and **29**−**33** were employed at a concentration range of 150, 100, 75, 50, 25, 10 and 1 μM). After incubation continued for 72 h, the MTT reagent was added (with final concentration per well of 1 g/L). Incubation was continued for 4 h, when the media was removed, and the cells were treated with 0.10 mL of 2-propanol/HCl (24:1 N) to solubilize the formazan produced in the mitochondria. Cell metabolic activity assessed relative to vehicle treated cells (Sterile bi-distilled water 0.1% DMSO). The maintenance of cells and all the assay steps were performed in RPMI 1640 5% FBS for DU145 and 10% FBS for LNCaP cells. The IC_{50} values were calculated using Prism 6.0 (GraphPad software).

3.6.4. Cell permeability

The DU145 cells were plated at a density of 200000 cells per 100 mm petri dish and incubated for 48 h at 37 ºC. Cells were treated with 1 μM of FITC analogs for 1 h at 37 ºC prior to collection using 0.05% trypsin and subsequent inactivation using FBS-containing media. Cell pellets were washed one more time with PBS and were resuspended in 200 μL of fresh PBS after centrifugation. PI was added at a final concentration of 10 μg/mL just before doing the acquisition. In another set of tubes, fluorophore was quenched using trypan blue at a final concentration of 0.04%. Cells were analyzed (at least 10000 events) by CytoFLEX 15 flow cytometer (Beckman Coulter, Brea, CA, USA) with the following diode lasers: 488 nm and 638 nm, 50 mW each. The emitted fluorescence was split into four channels and detected through band pass filters (forward scatter area, side scattered area and side scattered width signals) to

establish the live gates and exclude debris and cell clumps. Dead cells (PI-positive) were excluded by the gating in the red channel.

3.6.5. Cell toxicity

200 000 cellules were plated in a 6-well plate and treated respectively with 1, 10, 50 and 100 μM concentrations of compounds **10**, **16**, **20** and **31** in serum free media for 1.5 h (for compound **32** the concentrations were 1, 10, 15, 20, 30, 50, 100 μM). Cells were collected using trypsin prior to washing and then resuspension in PBS. PI at a final concentration of 10 μg/mL was added just prior to acquisition of fluorescence by a CytoFLEX 15 flow cytometer as described above. The IC_{50}(PI) value for compound **32** was calculated using Prism 6.0 (GraphPad software).

3.6.6. Plasma stability

Peptide samples for determination of $t_{1/2}$ half-lives were prepared as follows. The total concentration of 50 μM peptide in human serum (from male AB plasma; Sigma Aldrich) was incubated at 37 ºC. At each indicated timepoint and just following peptide addition, 25 μL of plasma were precipitated with 100 μL of MeOH containing 20 μM Fmoc-Leu-OH as internal standard. Samples, were centrifuged at 12000 ×g for 10 min at room temperature to remove precipitated proteins and clear supernatants were filtered on 0.2 μM PVDF centrifugal filters (Canadian Life Science) prior to analysis. Quantitative analysis was performed based on the peptide/standard ratio of integrated area under the curve in the total ion chromatogram and reported from 0 h incubation. The one-phase decay curve-fit of GraphPad Prism was used to determine $t_{1/2}$ values.

3.6.7. *In vivo* acute toxicity

All experimental procedures were performed as reported earlier in accordance with regulations of the Canadian Council on Animal Care.[168]

3.7. Acknowledgments

We acknowledge the Canadian Cancer Society Research Institute (701590 to R.D. and Y.L.D.) and Prostate Cancer Canada (TAG2014-02 to R.D.) for their support. F.C. holds a Banting and Charles Best Canada Graduate Scholarships (grant#315690) from CIHR and Graduate Studentship from Prostate Cancer Canada (Grant #GS-2015-07). We also thank Hugo Gagnon and Jean-Philippe Couture (PhenoSwitch Biosciences Inc.) for HRMS analysis and Sandra Gagnon for acute toxicity analysis.

3.8. Supporting information

3.8.1. The synthesis of compounds **3-21**, **28** and **29**

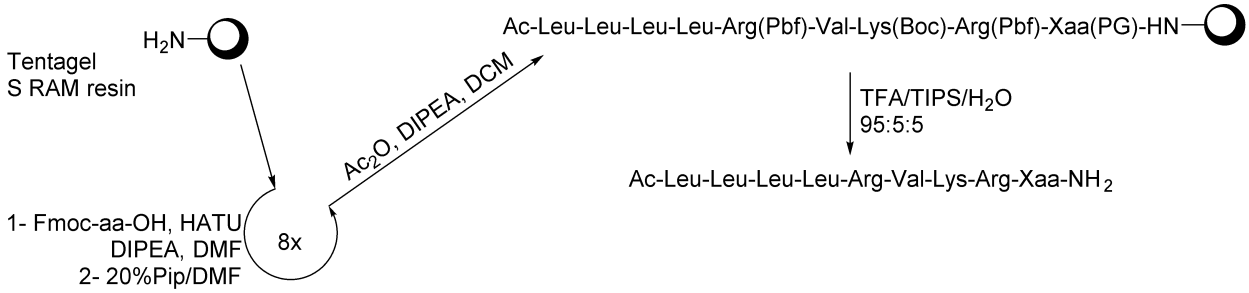

Scheme S1. Synthesis of compound **3-21**, **28** and **29** using conventional Fmoc-solid phase peptide synthesis (Xaa: Apa, Gpa and natural amino acids except Cys)

3.8.2. Details of enzyme kinetic assays

Both PACE4 and furin are human recombinant enzymes and were produced from S2 insect cells and purified by a method described earlier.[80]

Table S1. Substrate concentration and enzymes properties used in assays.

Enzyme	[E_0] (nM)	[Substrate] (µM)	Km (µM)
Furin	20.18	100	5.04
PACE4	0.545	100	4.035

3.8.3. Cell toxicity experiments

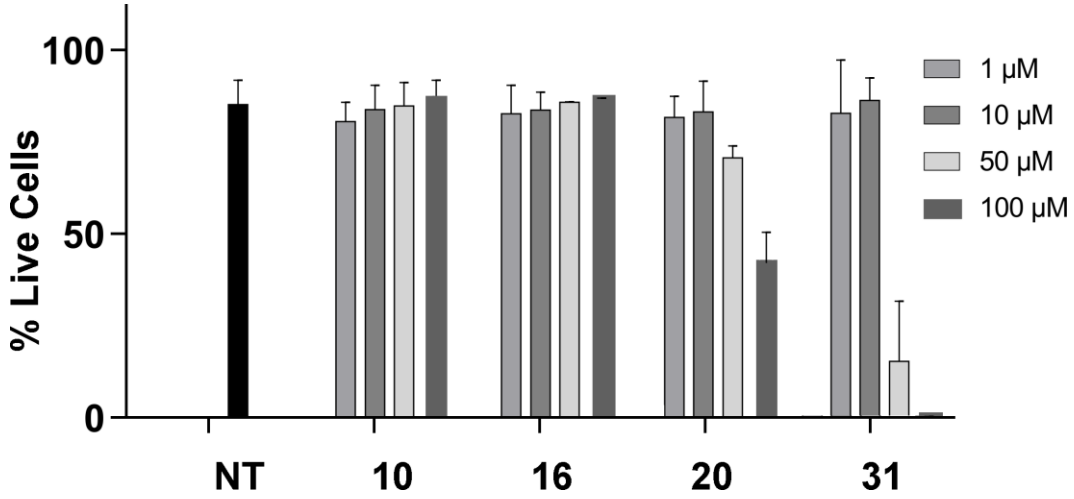

Figure S1. DU145 cell toxicity of selected peptides.

3.8.4. Analytical data of peptide inhibitors and their FITC-labeled analogues.

Table S2. The analytical data for all peptide inhibitors and FITC-labeled analogues.

Compound	Structure	Exact Mass		HPLC rt
		Calculated for	Found	
3	Ac-Leu-Leu-Leu-Leu-Arg-Val-Lys-Arg-Ala-NH_2	$[M+2]^{2+}$ 561.8953	561.8923	29.78[a]
4	Ac-Leu-Leu-Leu-Leu-Arg-Val-Lys-Arg-Asp-NH_2	$[M+2]^{2+}$ 583.89.02	583.8775	29.61[a]
5	Ac-Leu-Leu-Leu-Leu-Arg-Val-Lys-Arg-Glu-NH_2	$[M+2]^{2+}$ 590.8981	590.8262	29.66[a]
6	Ac-Leu-Leu-Leu-Leu-Arg-Val-Lys-Arg-Phe-NH_2	$[M+2]^{2+}$ 599.9110	599.9123	32.23[a]
7	Ac-Leu-Leu-Leu-Leu-Arg-Val-Lys-Arg-Gly-NH_2	$[M+2]^{2+}$ 554.8875	554.8856	29.58[a]
8	Ac-Leu-Leu-Leu-Leu-Arg-Val-Lys-Arg-His-NH_2	$[M+2]^{2+}$ 594.9062	594.9053	28.66[a]
9	Ac-Leu-Leu-Leu-Leu-Arg-Val-Lys-Arg-Ile-NH_2	$[M+2]^{2+}$ 582.9188	582.9190	31.66[a]
10	Ac-Leu-Leu-Leu-Leu-Arg-Val-Lys-Arg-Lys-NH_2	$[M+2]^{2+}$ 590.4242	590.4243	28.54[a]
11	Ac-Leu-Leu-Leu-Leu-Arg-Val-Lys-Arg-Leu-NH_2	$[M+2]^{2+}$ 582.9188	582.9162	22.47[b]
12	Ac-Leu-Leu-Leu-Leu-Arg-Val-Lys-Arg-Met-NH_2	$[M+2]^{2+}$ 591.8970	591.8972	31.47[a]
13	Ac-Leu-Leu-Leu-Leu-Arg-Val-Lys-Arg-Asn-NH_2	$[M+2]^{2+}$ 583.3982	583.3988	29.37[a]
14	Ac-Leu-Leu-Leu-Leu-Arg-Val-Lys-Arg-Pro-NH_2	$[M+2]^{2+}$ 574.9031	574.9015	21.66[b]
15	Ac-Leu-Leu-Leu-Leu-Arg-Val-Lys-Arg-Gln-NH_2	$[M+2]^{2+}$ 590.4061	590.4063	29.33[a]
16	Ac-Leu-Leu-Leu-Leu-Arg-Val-Lys-Arg-Arg-NH_2	$[M+3]^{3+}$ 403.2873	403.2831	28.82[a]
17	Ac-Leu-Leu-Leu-Leu-Arg-Val-Lys-Arg-Ser-NH_2	$[M+2]^{2+}$ 569.8928	569.8940	21.29[b]
18	Ac-Leu-Leu-Leu-Leu-Arg-Val-Lys-Arg-Thr-NH_2	$[M+2]^{2+}$ 576.9006	576.9011	29.74[a]
19	Ac-Leu-Leu-Leu-Leu-Arg-Val-Lys-Arg-Val-NH_2	$[M+2]^{2+}$ 575.9110	575.9110	22.05[b]
20	Ac-Leu-Leu-Leu-Leu-Arg-Val-Lys-Arg-Trp-NH_2	$[M+2]^{2+}$ 619.4164	619.4143	32.88[a]
21	Ac-Leu-Leu-Leu-Leu-Arg-Val-Lys-Arg-Tyr-NH_2	$[M+2]^{2+}$ 607.9084	607.9086	30.85[a]
28	Ac-Leu-Leu-Leu-Leu-Arg-Val-Lys-Arg-Apa-NH_2	$[M+2]^{2+}$ 607.4239	607.4164	29.20[a]
29	Ac-Leu-Leu-Leu-Leu-Arg-Val-Lys-Arg-Gpa-NH_2	$[M+2]^{2+}$ 628.4273	628.4314	26.74[a]
30	Ac-DLeu-Leu-Leu-Leu-Arg-Val-Lys-Arg-Aeba	$[M+2]^{2+}$ 599.4190	599.4163	27.64[a]
31	Ac-DLeu-Leu-Leu-Leu-Arg-Val-Lys-Arg-Tryp	$[M+3]^{3+}$ 348.9183	348.9135	32.43[a]
32	Ac-DLeu-Leu-Leu-Leu-Arg-Val-Lys-Acpa-Tryp	$[M+2]^{2+}$ 614.4080	614.4150	19.46[c]
33	Ac-DLeu-Leu-Leu-Leu-Arg-Val-Lys-Aca-Tryp	$[M+2]^{2+}$ 607.4002	607.4071	31.68[a]
35	FITC-βAla-Leu-Leu-Leu-Leu-Arg-Val-Lys-Arg-Arg-NH_2	$[M+3]^{3+}$ 542.6414	542.6483	18.34[c]
36	FITC-βAla-Leu-Leu-Leu-Leu-Arg-Val-Lys-Arg-Lys-NH_2	$[M+3]^{3+}$ 533.3060	533.3094	18.22[c]
37	FITC-βAla-Leu-Leu-Leu-Leu-Arg-Val-Lys-Arg-Trp-NH_2	$[M+3]^{3+}$ 552.6341	552.6426	19.72[c]
38	FITC-βAla-DLeu-Leu-Leu-Leu-Arg-Val-Lys-Arg-Tryp	$[M+3]^{3+}$ 543.6305	543.6361	34.82[a]

[a] 50 min, [b] 25 min and [c] 20 min gradient of 10 to 70% of CH_3CN and H_2O containing 0.1% TFA

CHAPTER 4: GENERAL DISCUSSION AND PERSPECTIVE

4.1. General discussions

PACE4, a proprotein convertase, has been recognized as a validated target in prostate cancer. The inhibition of PACE4 using substrate-like inhibitors (peptides and peptidomimetics) has shown effective *in vitro* antiproliferative effects on PCa cell lines (both LNCaP and DU145 cells). Such inhibitors also reduced the growth of xenografted prostate tumors in mice. In light of their promising activity *in vitro* and *in vivo*, lead compounds ML peptide (Ac-LLLLRVKR-NH_2) and C23 (Ac-DLeu-LLLRVK-Amba) merit further development. The primary objective of the current dissertation was to increase the selectivity and affinity of these inhibitors towards PACE4 over furin. In this regard, three approaches were applied to enhance the selectivity of PACE4 inhibitors using structure activity relationship studies on ML and C23 compounds. These approaches included modifications in the P3, P1 and P1' positions of the lead compounds.

Benefiting from a structural difference of the S3 sub-pocket between PACE4 and furin, the inhibitor P3 Val of ML has been modified to target PACE4 Asp160 vs furin Glu256. The other main interaction in S3 is the β-sheet-like hydrogen bonding of P3 Val with Gly158 of PACE4. This is a general attribute of proteases substrates to form a β-sheet with the active site residues. The β-branched amino acids like Val and Ile are known to enhance this interaction in β-sheets. The β-sheet-like interaction in S3 is vital to optimizing the inhibitor's conformation in the active site and drives all P1 to P4 residues into their respective sub-pockets. In order to sum up both mentioned interactions in S3, some β-branched basic amino acids were designed and synthesized.

With the objective of optimizing the length of the side chain, different basic amino acids were examined. These residues were introduced at the P3 position of the ML peptide and the PACE4 and furin inhibitions of the resulting compounds were measured. The inhibitors with P3-Dap ((*S*)-2,3-diaminopropionyl) and P3-Apg ((*S*)-2-amino-3-guanidinopropionyl) residues were found to be the most potent compounds in the series. The corresponding methyl β-branched analogues were synthesized based on them. With *S*-*i*-Abg ((*S*)3-guanidino- (*S*)-2-aminobutyric acid) at the P3 position, the selectivity was improved compared to ML (40-fold vs 20-fold), while the potency was enhanced by 7-folds (PACE4 K_i = 2.7 vs 22 nM). The hydrogen bonds between Ala or Val backbones of the ligand and Gly158 of PACE4 in the S3 subsite were analyzed using molecular dynamic simulations of Ac-RXKR-NH_2 (X = Val and Ala).

Computational analysis indicated, the β-sheet-like hydrogen bonds were tighter for β-branched Val compared to Ala. Moreover, the geometry of the tetrapeptide Ac-RVKR-NH_2 matched closely that of an antiparallel β-sheet. Such was not the case for Ac-RAKR-NH_2.

The introduction of a basic β-branched residue (*S*-*i*-Abg) instead of Val at the P3 position of ML resulted in better selectivity and increased potency. In addition, it was shown that β-branching at the P3 position is important for the formation of the necessary β-sheet conformation of peptide substrates and inhibitors in the active site.

Despite the superior profile of C23 over ML in terms of PACE4 affinity and cellular antiproliferative activity, C23 is not as selective as ML (2 times selective vs 20 times for PACE4 over furin). Considering that the most important difference between the two inhibitors was the replacement of Arg in P1 by Amba, the structural impact of this modification was further explored. Therefore, P1-modified inhibitors were designed based on the lead compound C23 (PACE4 K_i = 4.9 nM) to increase the PACE4 selectivity and potency. Two sets of aliphatic residues based on Arg and aromatic residues derived from Amba were investigated at this position. Although the aliphatic modifications were not successful in improving the potency nor selectivity, replacement of Amba with 5-(aminomethyl)picolinimidamide (Ampa) as a P1 residue increased the PACE4 selectivity and binding affinity by 8-fold and 2-fold, respectively (K_i = 2.6 nM). DFT calculations and molecular docking suggested that the flatter geometry of Ampa comparing to Amba may be a responsible factor for the observed improvement in potency and selectivity for PACE4. This flat geometry is the result of an intramolecular hydrogen bonding between the pyridine N (acting as the acceptor) and the suitable amidinium NH (acting as the donor) in Ampa. However, despite improvements in PACE4 affinity and selectivity, the Ac-DLeu-Leu-Leu-Leu-Arg-Val-Lys-Ampa peptide displayed moderate antiproliferative activity. The cell permeability was not the reason for this phenomenon because penetration into the DU145 cells was observed using the Ampa analog in amounts similar to that of C23. Further studies are necessary to provide better insight into this issue.

In another study aimed at exploring the P1' position to optimize the selectivity profile of the ML-derived PACE4 inhibitors, a biased library of peptides with the general sequence Ac-LLLLRVKRX-NH_2 (X is a natural amino acid apart for Cys) was synthesized and their inhibitory potency was examined. Although the resulting analogues showed no improvement for PACE4 affinity and selectivity, their antiproliferative activity against prostate cancer cell lines illustrated that hydrophobic residues like tryptophan increased the antiproliferative effect in a dose-dependent manner. Replacement of tryptophan with the even more

hydrophobic tryptamine (Tryp) in the P1' position further improved the antiproliferative activity. To duplicate the C23 P1 features in a new inhibitor, P1-Arg was modified to Acpa (2-amino-3-(4-carbamimidoylphenyl)propanoic acid). The resulting inhibitor with the structure Ac-DLeu-Leu-Leu-Leu-Arg-Val-Lys-Acpa-Tryp displayed a 3-fold improvement in the IC_{50} values for PCa cells compared to C23 (7.5 ± 0.8 and 13 ± 1 μM for DU145 and LNCaP cells, respectively). The observed cellular potency was the consequence of improved cell permeability of the P1'-modified inhibitors (evaluated using N-terminally FITC-labeled compounds). Additionally, this inhibitor was slightly more stable than C23 with $t_{1/2}$ of 2 h vs 1.74 h. By comparing the PI cell toxicity and MTT metabolic activity in DU145 cells, antiproliferative activity was shown to be due to the factors other than cell death in low micromolar concentrations of the inhibitor.

In summary, the SAR exploration of the P1 and P3 positions of the ML and C23 compounds resulted in more selective and potent inhibitors, and additional modifications in the P1' position led to inhibitors that are more permeable to PCa cells and with enhanced antiproliferative activity.

4.2. Future studies

Diminished cellular activity was found to be the main issue for the inhibitors Ac-LLLLR-[*S*-*i*-Agb]-KR-NH_2 and Ac-DLeu-LLLRVK-Ampa despite their improved PACE4 affinity and selectivity. One of the possible reasons behind the reduced cellular activity of P3-modified inhibitors could be the increased number of positively charged residues. Hence, some compounds may be investigated to solve this problem. One of the charges could be removed by replacing the least important P2-Lys residue of the P4–P1 warhead by a hydrophobic residue (e.g. Trp). The expected loss of affinity might be compensated by the concurrent introduction of an *S*-*i*-Abg residue in P3 (**Figure 44**). The resulting inhibitor could then benefit from increased cell permeability by having an additional Trp residue as discussed in section 3.4.4.

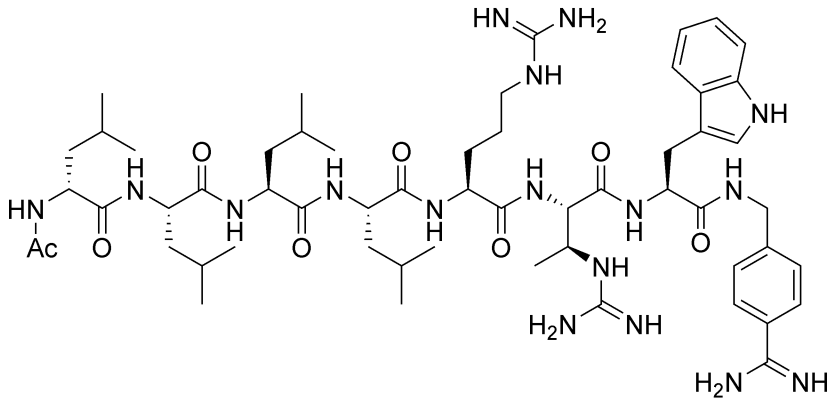

Figure 44. Reducing the total charge by replacing P2-Lys with Trp

Another strategy is to use the most potent cellular antiproliferative compound Ac-DLeu-Leu-Leu-Leu-Arg-Val-Lys-Acpa-Tryp as the basis for the design of PACE4 inhibitors with improved affinity and selectivity. In this regard, replacing concomitantly P3-Val with *S*-*i*-Abg and P2-Lys with Trp could be helpful to find the right combination of modifications (**Figure 45**, top molecule).

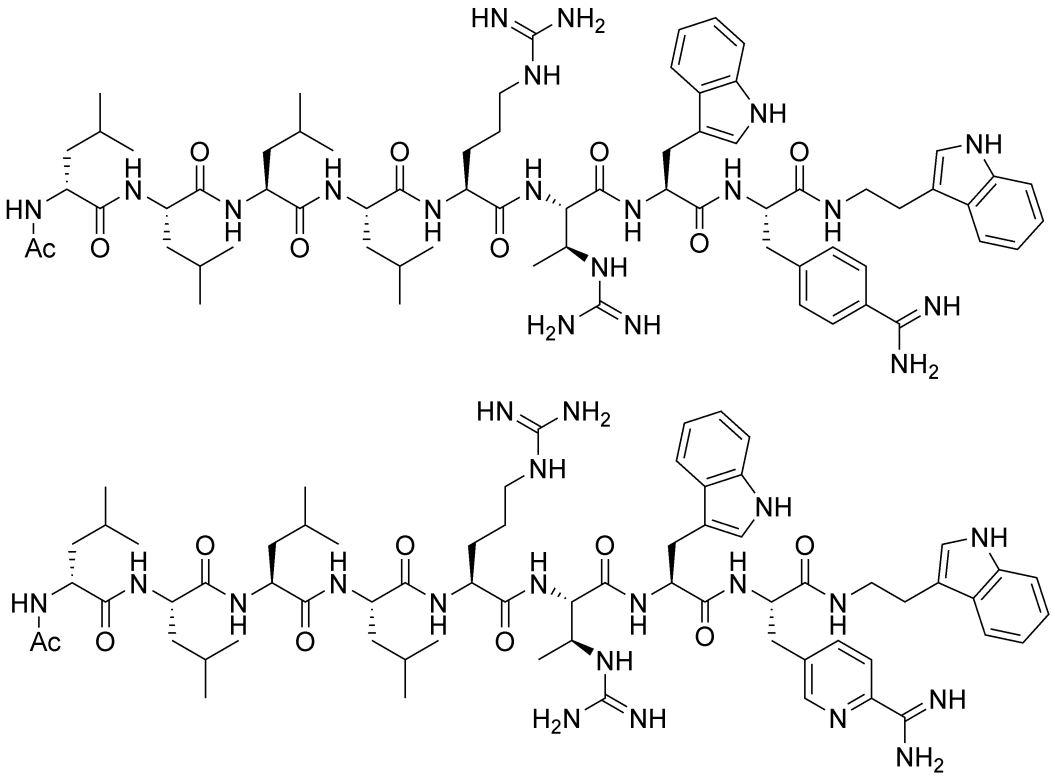

Figure 45. Combining modifications at P1' and P3 of lead inhibitor **32** (Chapter 3).

The final design strategy is to combine the best P1 modifications discussed in chapter 2 and 3 in a new unusual amino acid. This modified P1 residue should have a picolinimidamide side chain similar to Ampa (**Figure 45**, bottom molecule).

The synthesis pathway for the new unusual amino acid is outlined in **Scheme 7**, it begins with a Horner-Wadsworth-Emmons type reaction followed by the reduction of the double bond and cyanation of the resulting amino acid as described in the literature.[250-251] The conversion of the pyridine N to its N-oxide during the synthesis was shown to be necessary for increasing the enantioselectivity of the hydrogenation.[241]

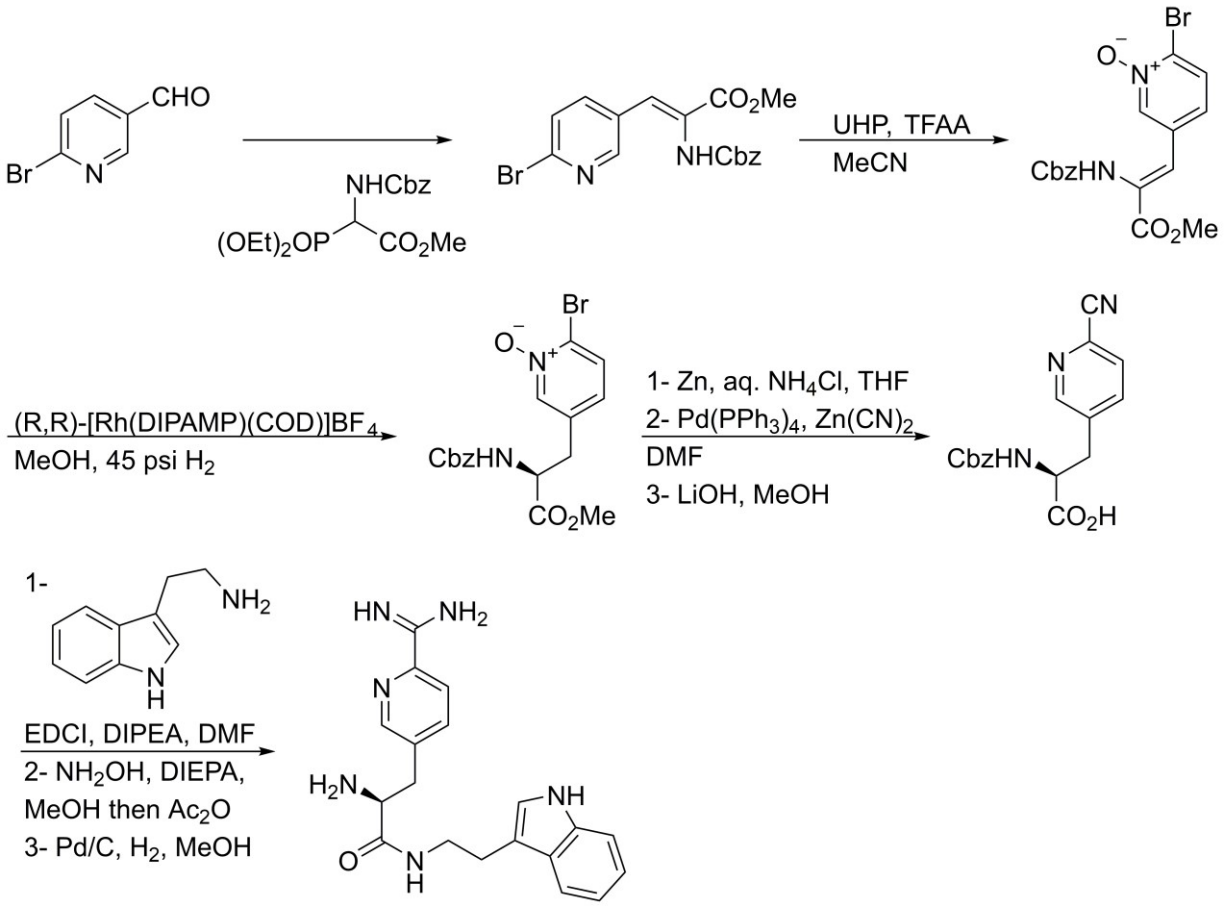

Scheme 7. The proposed synthesis for the novel P1-P1' dipeptide. UHP: Urea-hydrogen peroxide adduct.

CONCLUSION

In the first chapter, a new basic β-branched amino acid (*S*-*i*-Agb) was used in the P3 position of ML, which led to the discovery of a PACE4 inhibitor with enhanced potency and selectivity for PACE4. The inclusion of this residue in the P3 position introduced additional stabilizing electrostatic interactions with Asp160. As a β-branched residue, *S*-*i*-Agb increased the β-sheet propensity of the peptide inhibitor. To the best of our knowledge, the correlation between β-sheet propensity of inhibitor residues and protease inhibition had not been studied before. This β-sheet propensity improvement coupled with other side chain stabilizing interactions could be used as a principle for targeting other proteases as well.

In the second chapter, PACE4 inhibitors were modified at their P1 position and their SAR was studied. The results indicated structural differences in the S1 pocket that could be used to discriminate between furin and PACE4 and open new frontiers for achieving higher selectivity. The most potent and selective inhibitor in the series displayed a K_i value of 2.6 nM for PACE4 (2-fold more potent and 4-fold more selective than C23). Using Ampa as the P1 residue was associated with the same stabilizing van der Waals contacts as Amba in C23. It was found that Ampa is held rigidly (intramolecular hydrogen bond) in a flat conformation. It was suggested that the gain in affinity for PACE4 could arise from this rigidifying process. Surprisingly, the compound with P1-Ampa displayed lower efficiency in PCa cell antiproliferative assays compared to C23. Further studies may provide the knowledge necessary to explain this impairment. However, this significant improvement at the P1 position can now be used in combination with other modifications at other positions.

In the third chapter, SAR studies were performed on P1 and P1' of the ML peptide to yield potent PACE4 inhibitors. By screening natural amino acids in the P1' position of ML, it was discovered that Trp improved the antiproliferative effect on PCa cell lines. Further modification of this Trp residue to Tryp enhanced the hydrophobicity in the C-terminal region of the resulting peptide. This Trp-to-Tryp replacement also improved plasma stability and cell efficacy although the affinity of the resulting inhibitor to recombinant PACE4 had been reduced. Since P1-Amba in C23 had resulted in better PACE4 affinity and cellular activity, a new related unnatural residue, Acpa (4-amidinophenyl as side chain), was designed and synthesized to replace P1-Arg in the former inhibitor (with Tryp). This additional change contributed to improve the plasma stability and the antiproliferative effect of the resulting compound. The antiproliferative activity enhancement introduced by C-terminal Trp or Tryp was related to the

improved cell permeability of these inhibitors. This study sets a good example for addressing the impact of cell penetration on the cell efficacy and overall activity of PACE4 inhibitors.

In conclusion, rational design of PACE4 inhibitors by modifications in P3 (chapter 1) and P1 (chapters 2 and 3) resulted in more selective and potent compounds. Although the cellular activity of both P3 and P1-modified inhibitors was less than that in the parent compounds ML and C23, we believe that the combination of these modifications with others could lead to an improvement in cellular antiproliferative activity. Although the original objective of selectivity improvement was not achieved in chapter 3, increased cell permeability led to enhanced antiproliferative activity by using hydrophobic residues in the P1' position.

APPENDIX I

Table of the copyright reference numbers for figures adapted from literatures in the chapter of introduction

Graphic content	Reference number (Copyright clearance center)	Date of receiving the permission
Figure 4	4432470429691	Jun 15, 2011
Figure 10	4396660786195	Jul 26, 2018
Figure 11	4396660786195	Jul 26, 2018
Figure 12	4397170444644	Jul 27, 2018
Figure 13	4398970264683	Jul 30, 2018
Figure 15	4404271138682	Aug 8, 2018
Figure 20	2234402	Sep 19, 2018
Figure 21	2234402	Sep 19, 2018
Figure 26	4517340916645	Jan 27, 2019

APPENDIX II

All the HPLC chromatograms of inhibitors and NMR spectra for small molecule intermediates synthesized in chapter 1 is presented in this appendix.

HPLC chromatograms:

Inhibitor **11**:

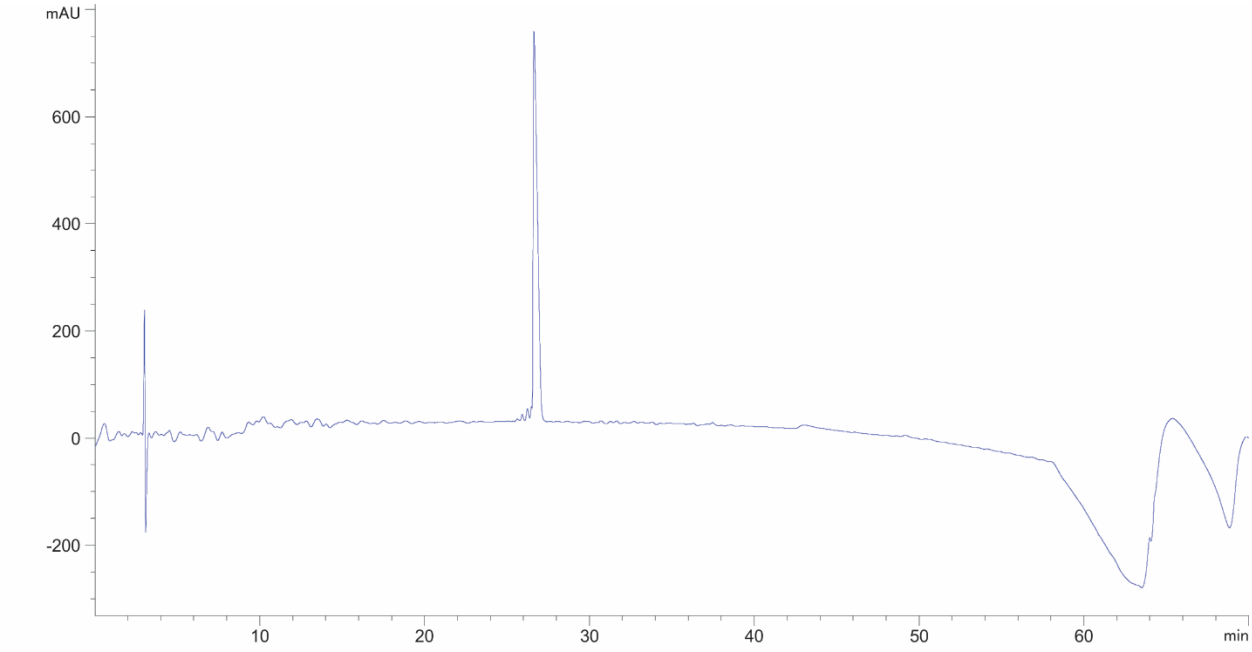

Inhibitor **12**:

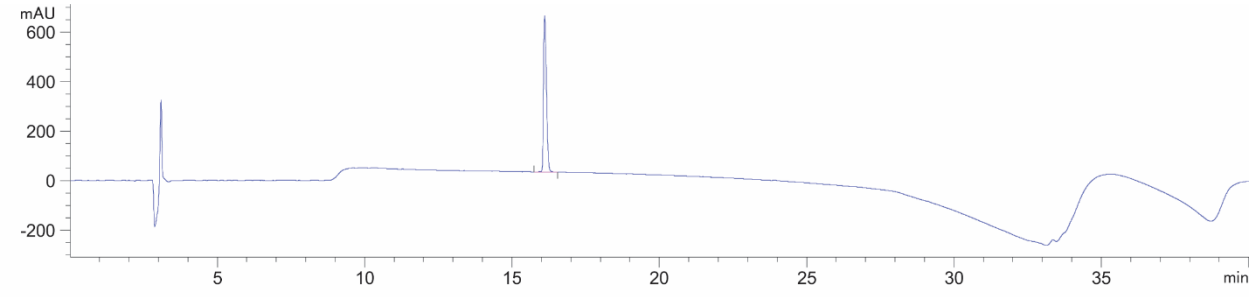

Inhibitor **13**:

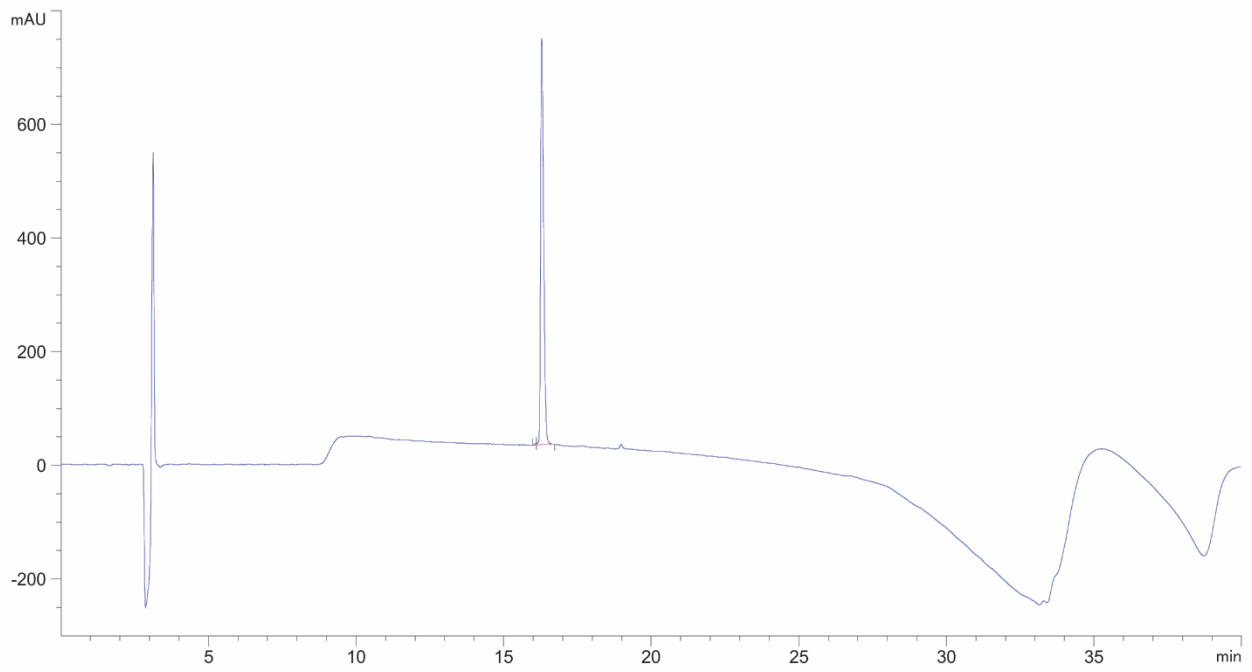

Inhibitor **14**:

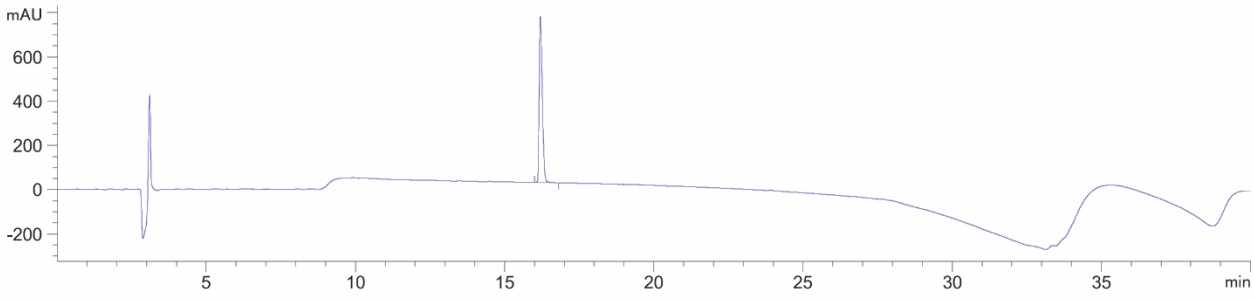

Inhibitor **15**:

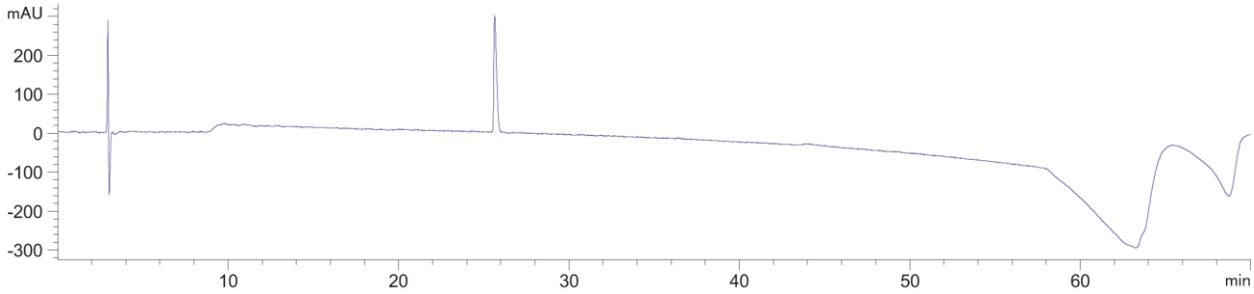

Inhibitor **16**:

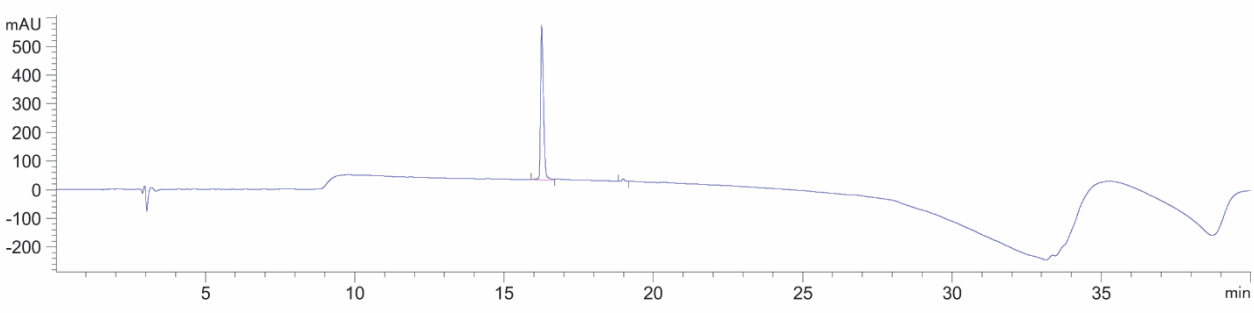

Inhibitor **17**:

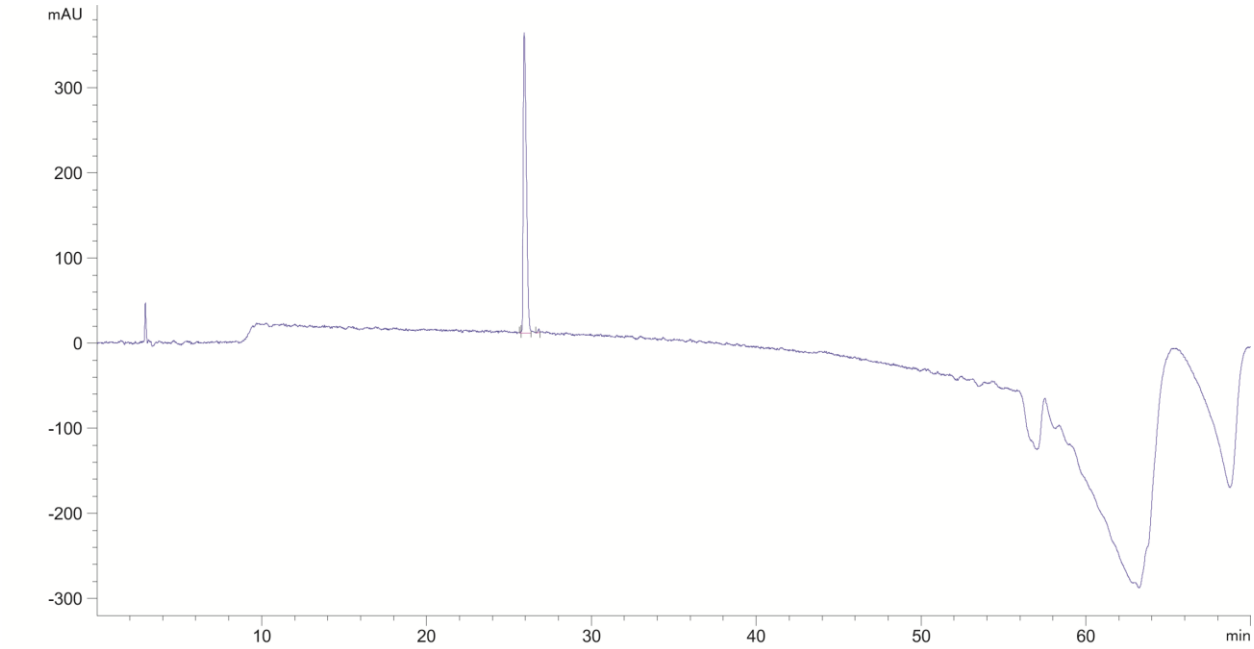

Inhibitor **18**:

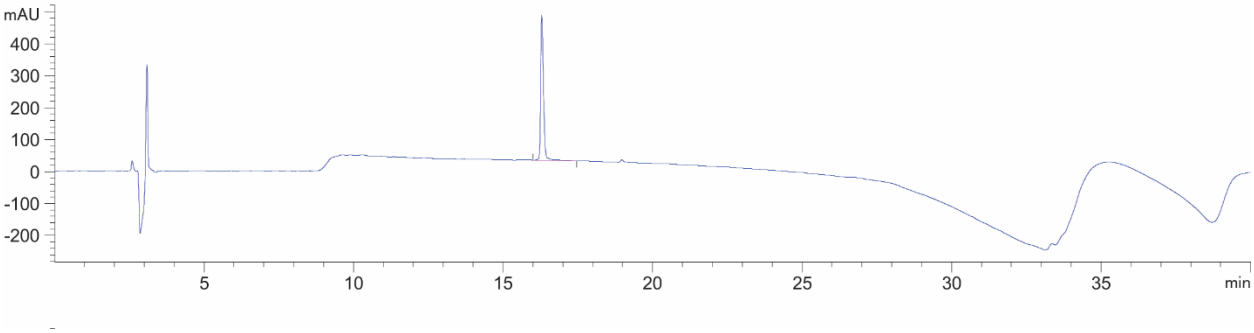

Inhibitor **19**:

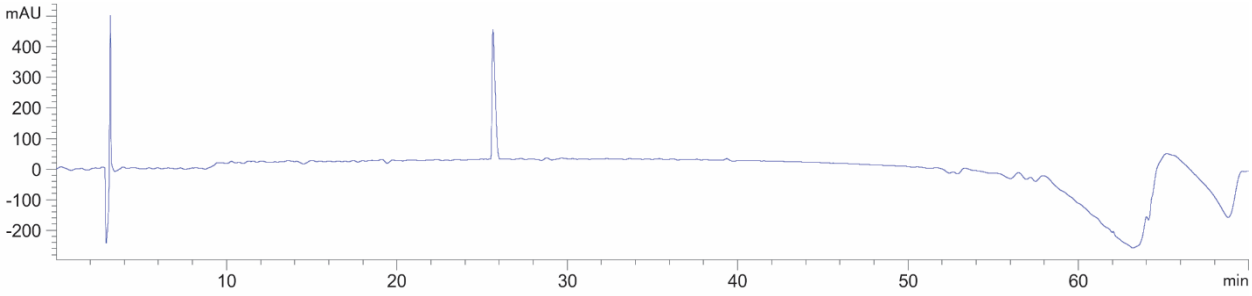

Inhibitor **20**:

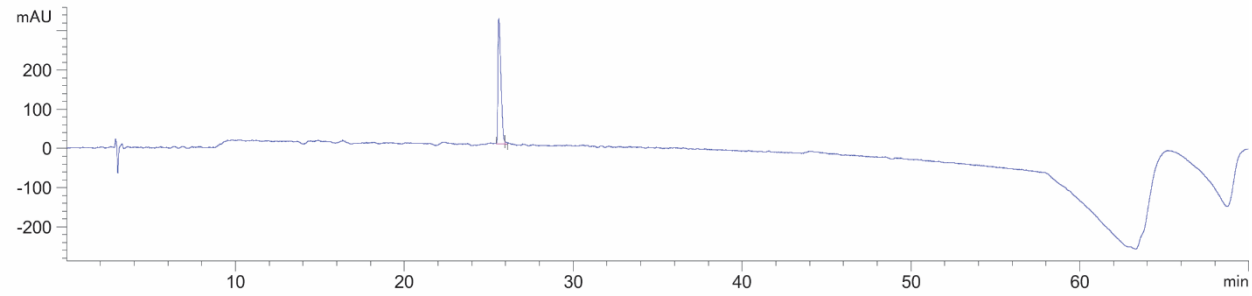

Inhibitor **21**:

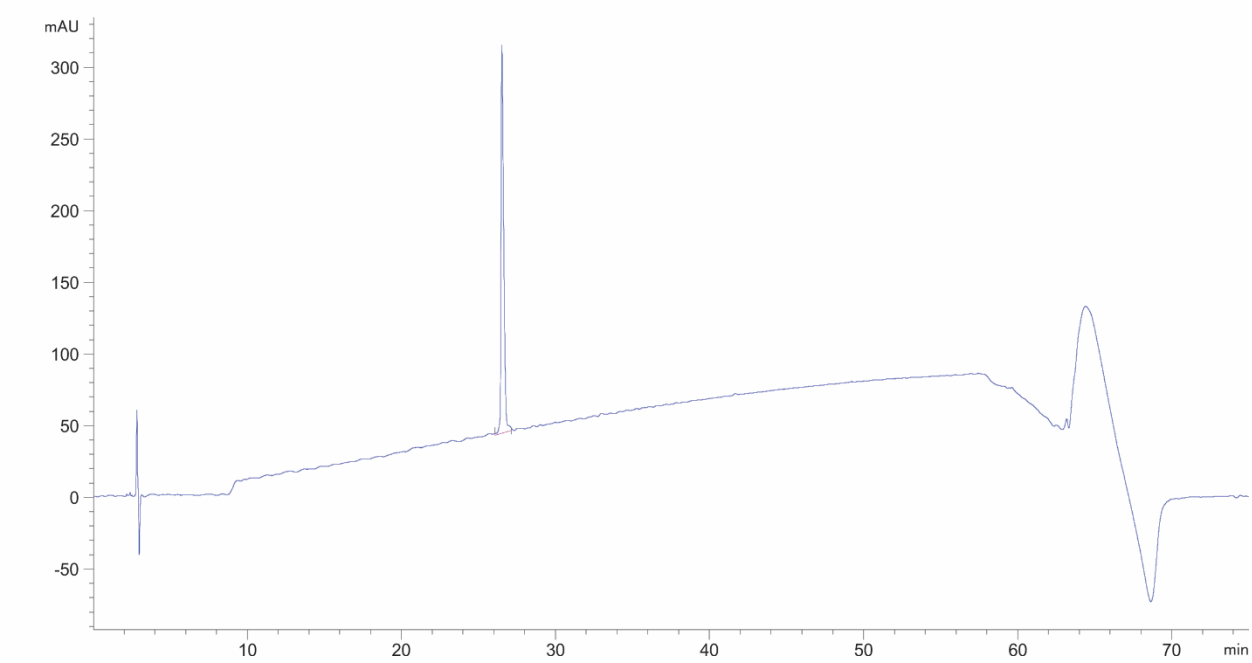

^{1}H NMR and ^{13}C NMR spectra:

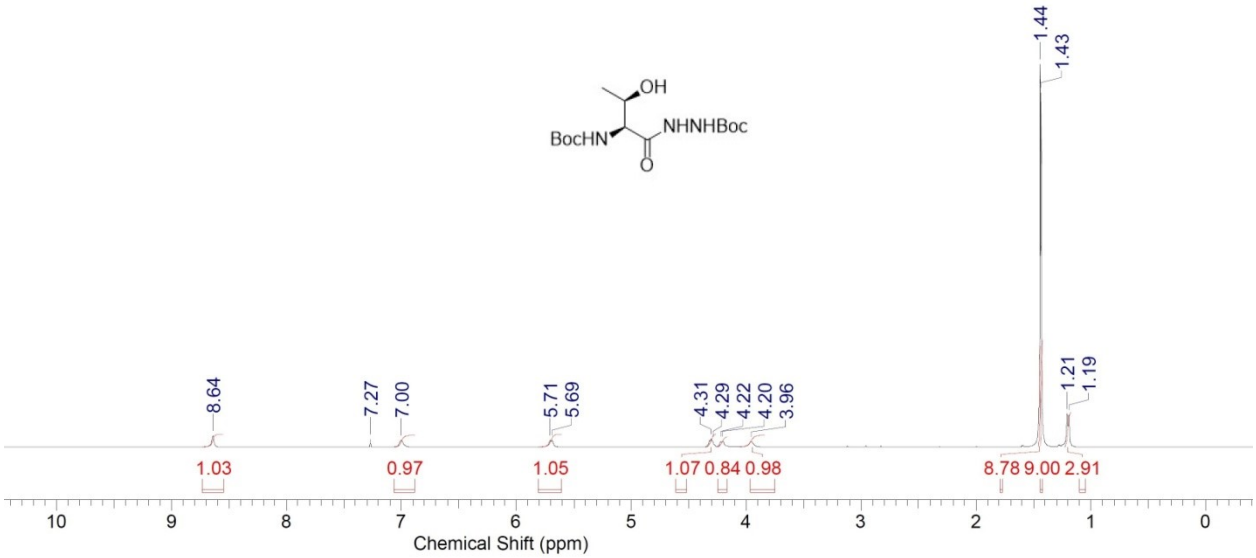

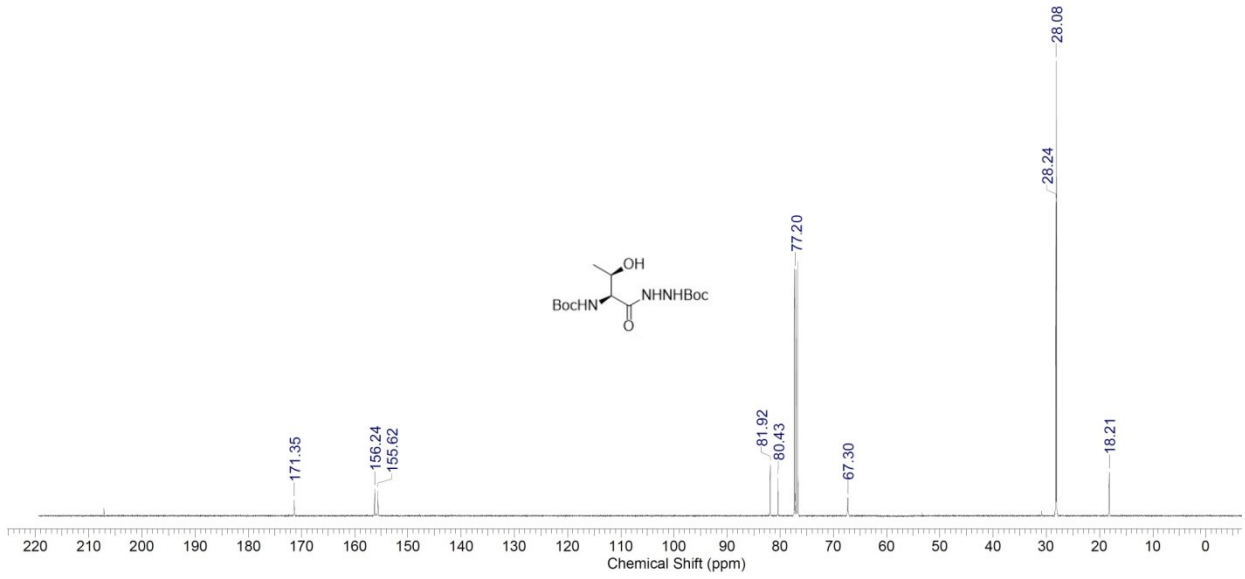

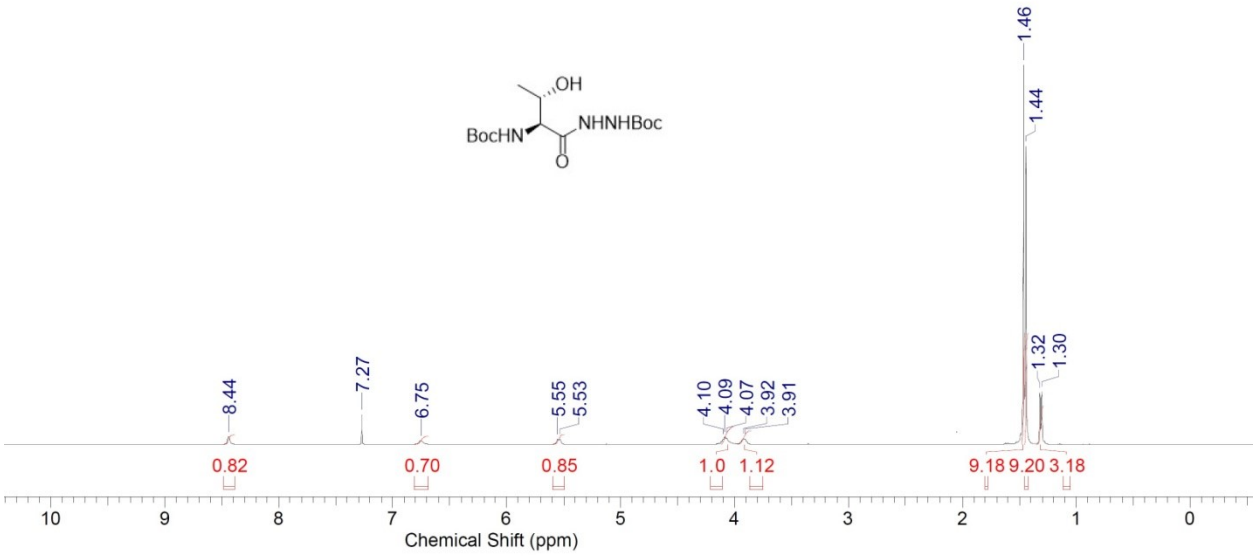
OH
BocHN
NHNHBoc
O
1.46
1.44
1.32
1.30
8.44
7.27
6.75
5.55
5.53
4.10
4.09
4.07
3.92
3.91
0.82
0.70
0.85
1.0
1.12
9.18
9.20
3.18
10
9
8
7
6
5
4
3
2
1
0
Chemical Shift (ppm)

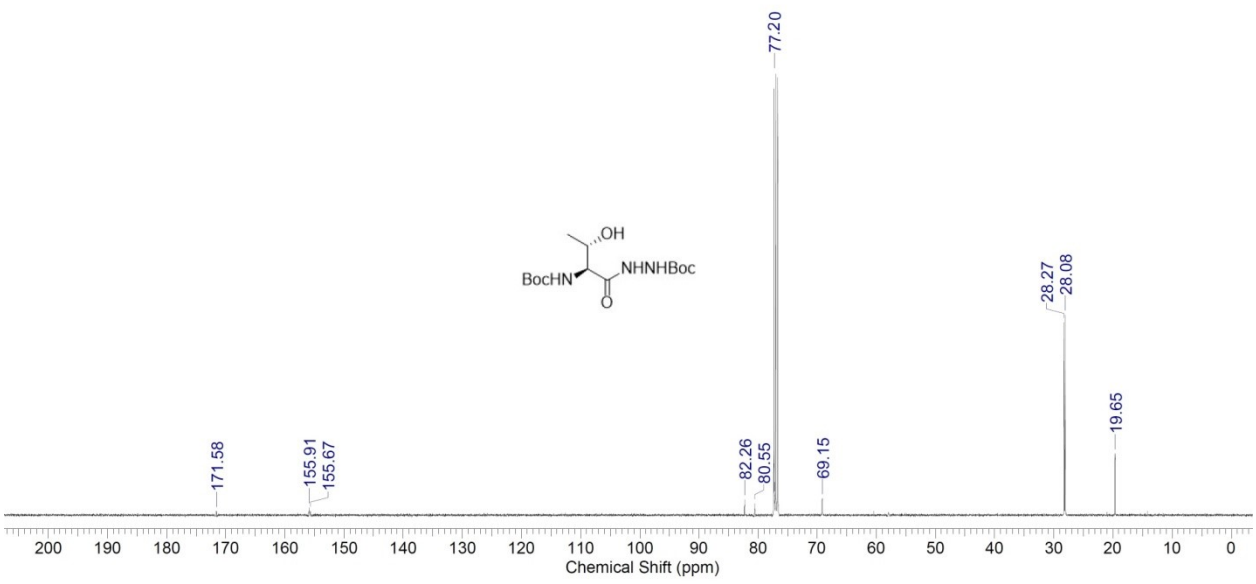
OH
BocHN
NHNHBoc
O
77.20
28.27
28.08
19.65
171.58
155.91
155.67
82.26
80.55
69.15
200
190
180
170
160
150
140
130
120
110
100
90
80
70
60
50
40
30
20
10
0
Chemical Shift (ppm)

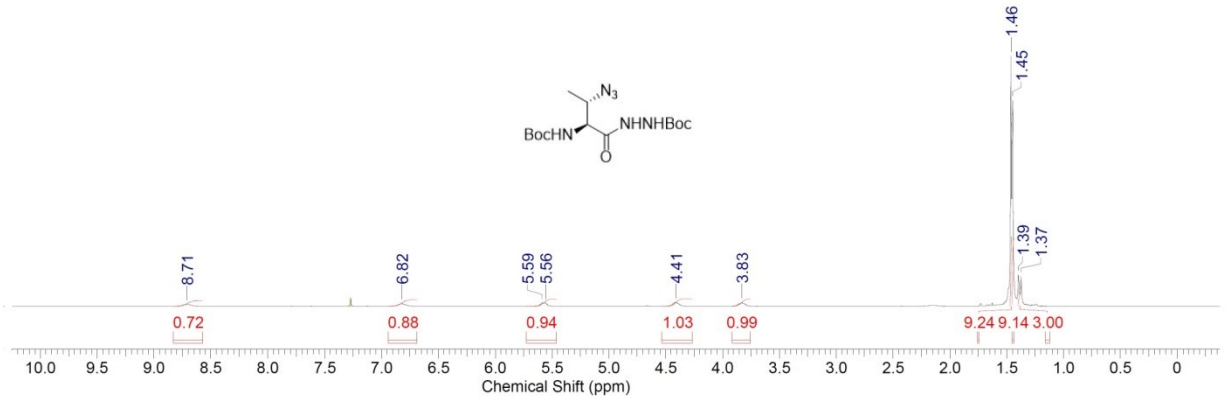
1.46
1.45
N3
BocHN
NHNHBoc
O
8.71
6.82
5.59
5.56
4.41
3.83
1.39
1.37
0.72
0.88
0.94
1.03
0.99
9.24
9.14
3.00
Chemical Shift (ppm)

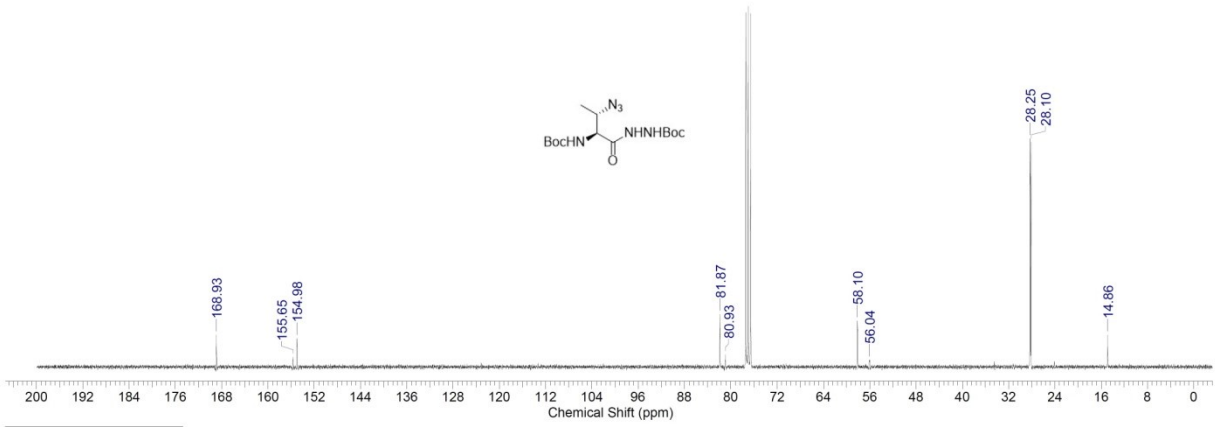
N3
BocHN
NHNHBoc
O
28.25
28.10
168.93
155.65
154.98
81.87
80.93
58.10
56.04
14.86
Chemical Shift (ppm)

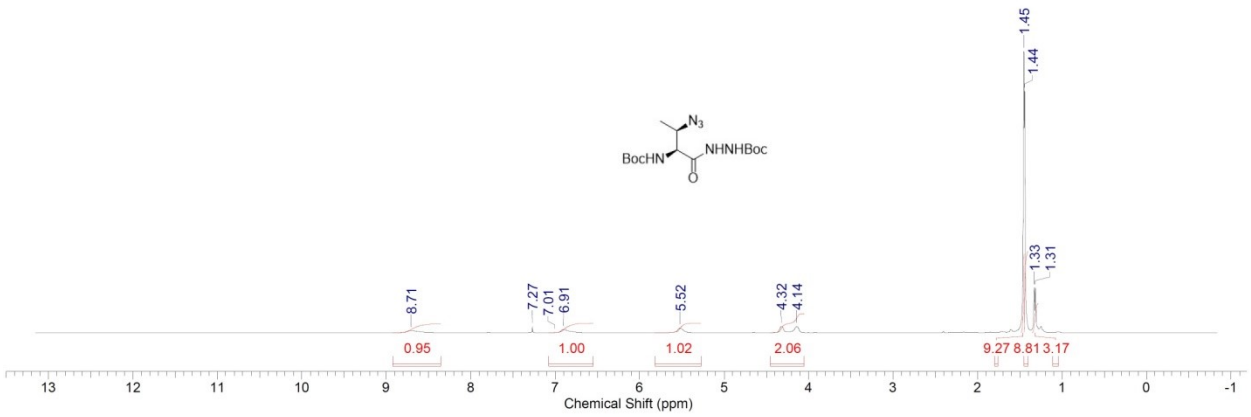
1.45
1.44
N3
BocHN
NHNHBoc
O
1.33
1.31
8.71
7.27
7.01
6.91
5.52
4.32
4.14
0.95
1.00
1.02
2.06
9.27
8.81
3.17
13 12 11 10 9 8 7 6 5 4 3 2 1 0 -1
Chemical Shift (ppm)

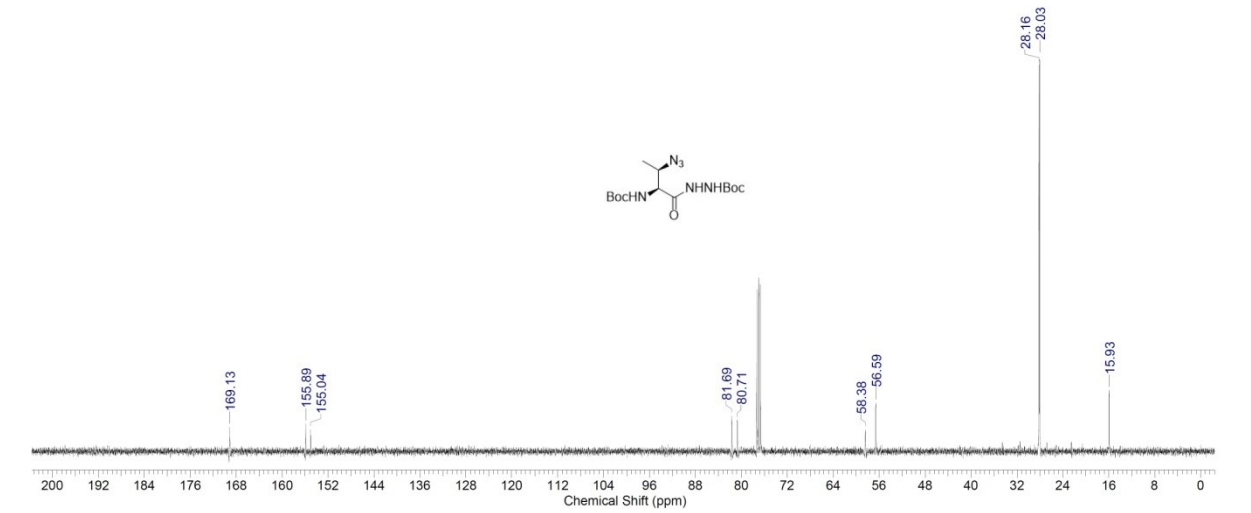
28.16
28.03
N3
BocHN
NHNHBoc
O
169.13
155.89
155.04
81.69
80.71
58.38
56.59
15.93
200 192 184 176 168 160 152 144 136 128 120 112 104 96 88 80 72 64 56 48 40 32 24 16 8 0
Chemical Shift (ppm)

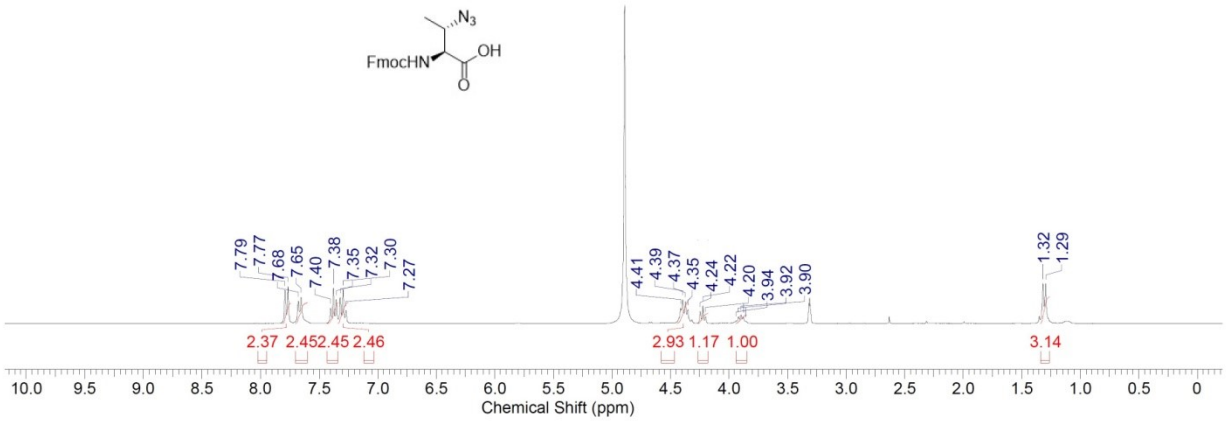
FmocHN
N3
OH
O
7.79
7.77
7.68
7.65
7.40
7.38
7.35
7.32
7.30
7.27
4.41
4.39
4.37
4.35
4.24
4.22
4.20
3.94
3.92
3.90
1.32
1.29
2.37 2.45 2.45 2.46
2.93 1.17 1.00
3.14
Chemical Shift (ppm)

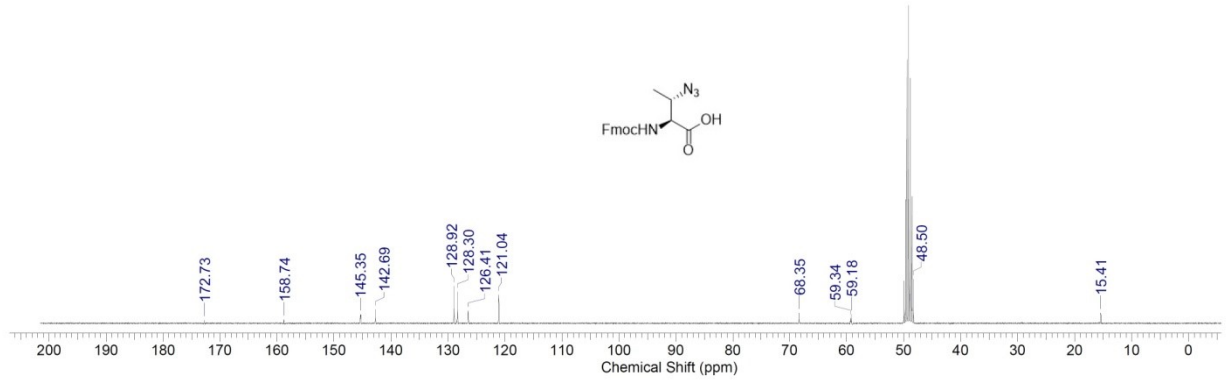
FmocHN
N3
OH
O
172.73
158.74
145.35
142.69
128.92
128.30
126.41
121.04
68.35
59.34
59.18
48.50
15.41
Chemical Shift (ppm)

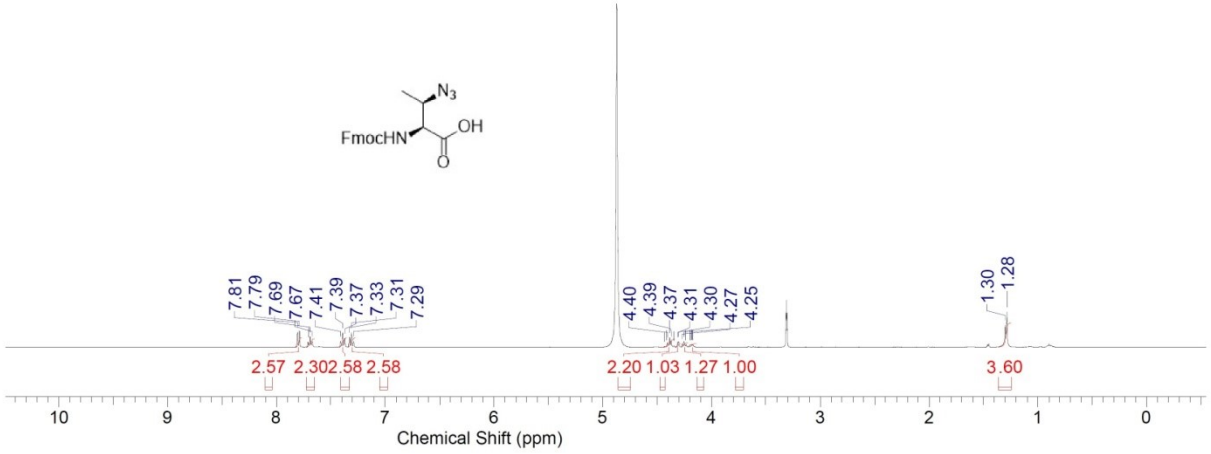
N3
FmocHN
OH
O
7.81
7.79
7.69
7.67
7.41
7.39
7.37
7.33
7.31
7.29
4.40
4.39
4.37
4.31
4.30
4.27
4.25
1.30
1.28
2.57 2.30 2.58 2.58
2.20 1.03 1.27 1.00
3.60
Chemical Shift (ppm)

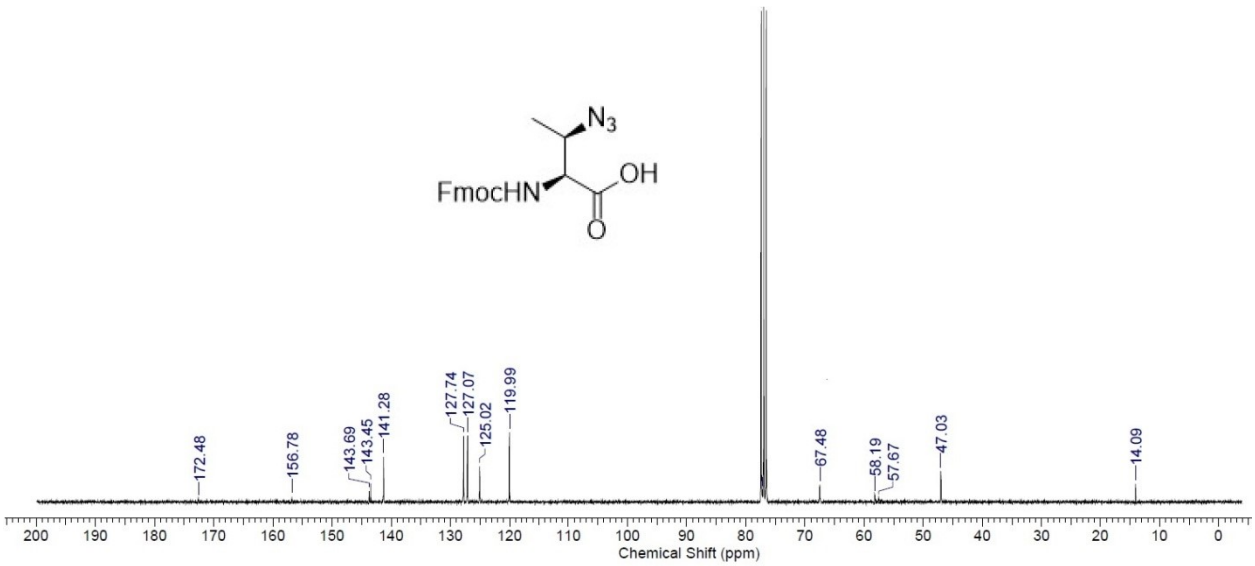
N3
FmocHN
OH
O
172.48
156.78
143.69
143.45
141.28
127.74
127.07
125.02
119.99
67.48
58.19
57.67
47.03
14.09
Chemical Shift (ppm)

APPENDIX III

All the HPLC chromatograms of peptides and NMR spectra for small molecule intermediates synthesized in chapter 2 is presented in this appendix.

HPLC chromatograms:

Compound **5**:

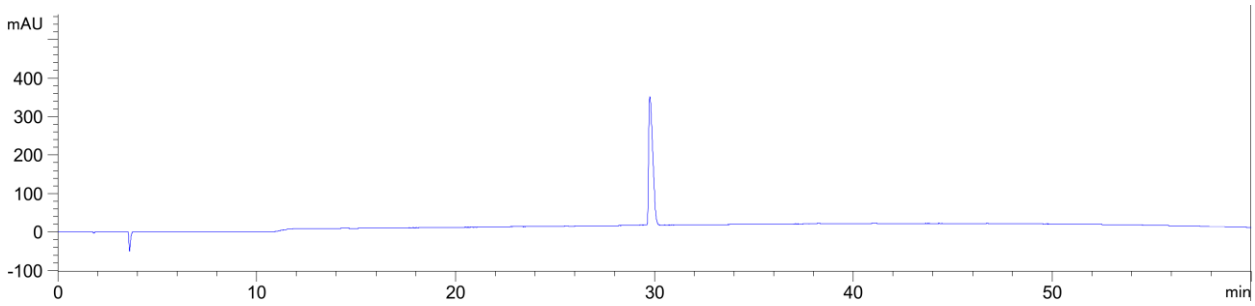

Compound **6**:

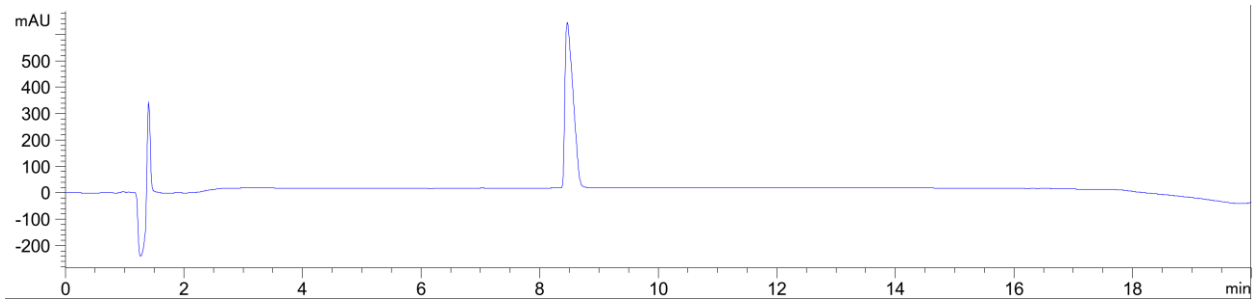

Compound **7**:

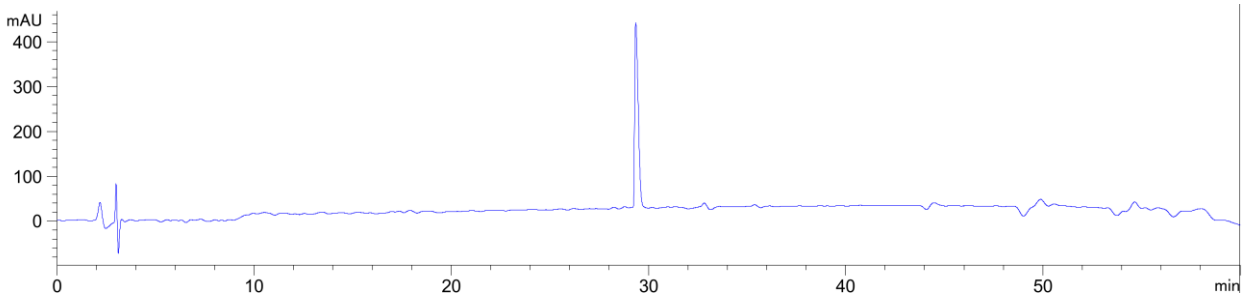

Compound **8**:

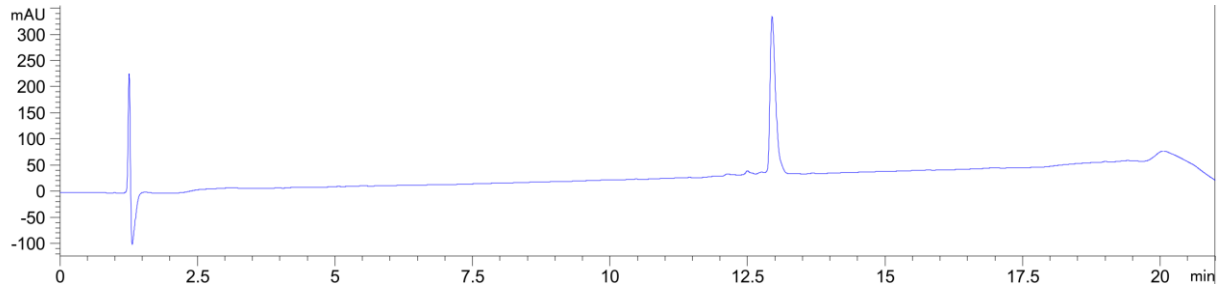

Compound **9**:

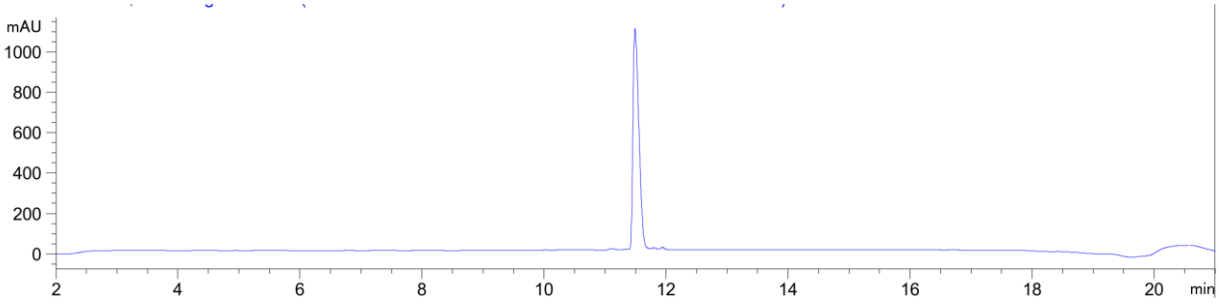

Compound **10**:

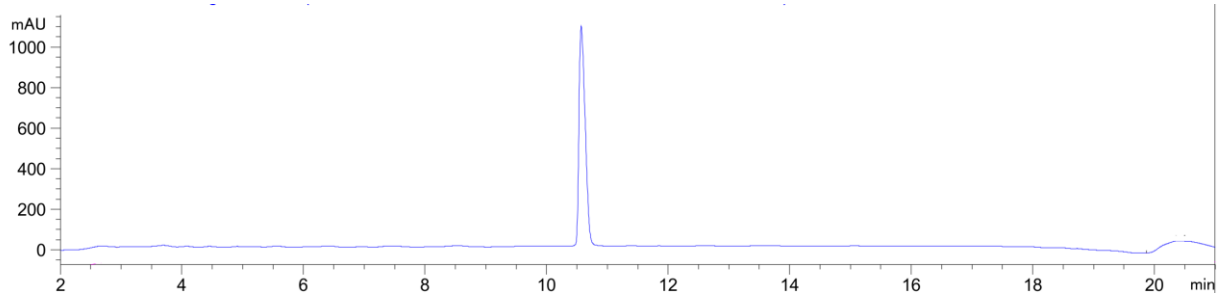

Compound **11**:

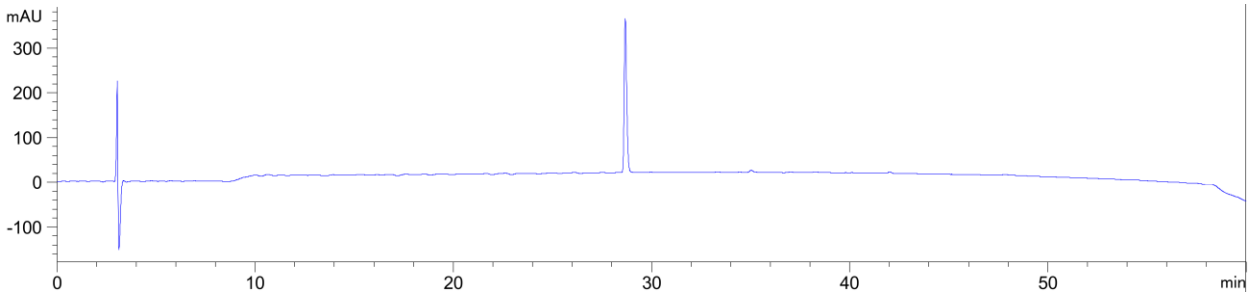

Compound **12**:

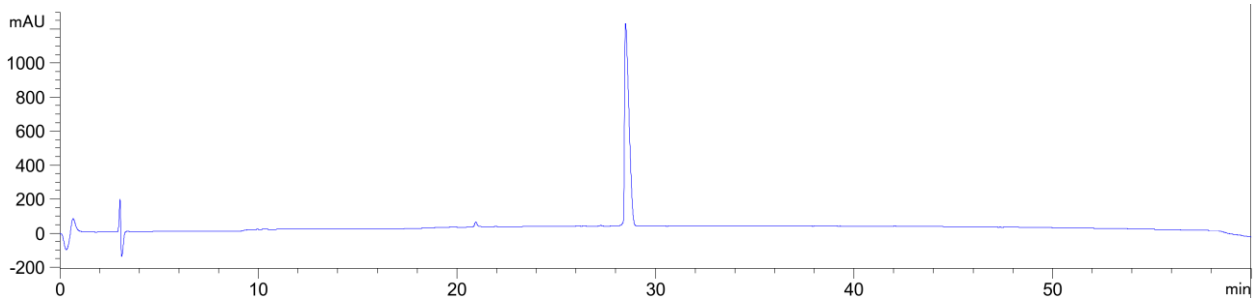

Compound **13**:

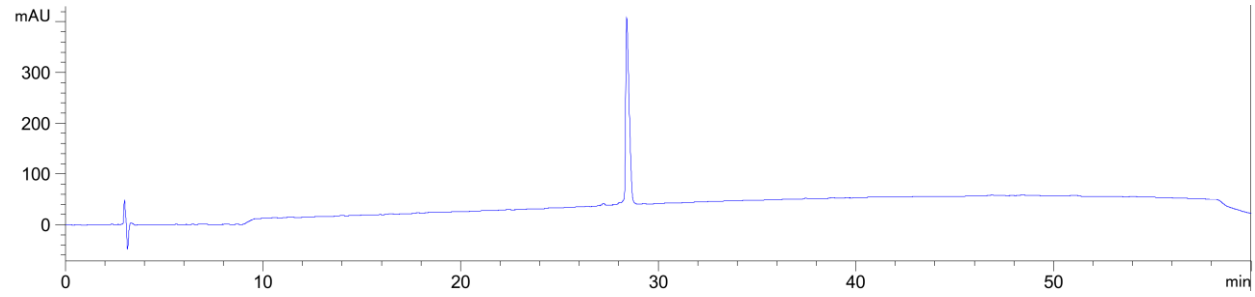

Compound **15**:

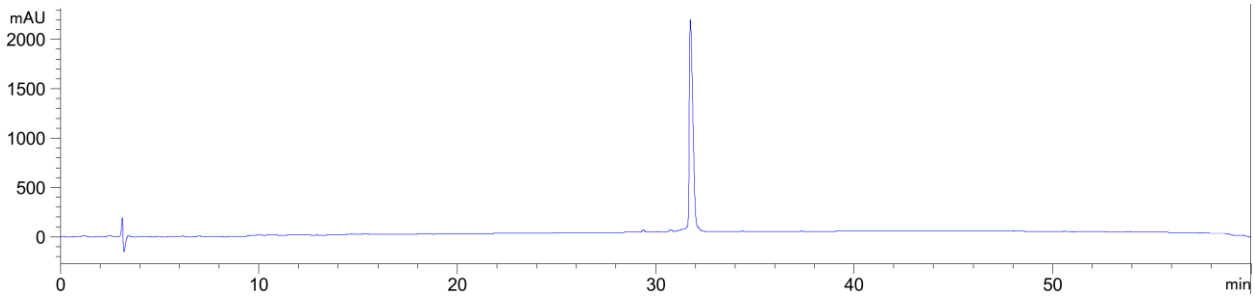

^{1}H NMR and ^{13}C NMR and ^{19}F NMR spectra:

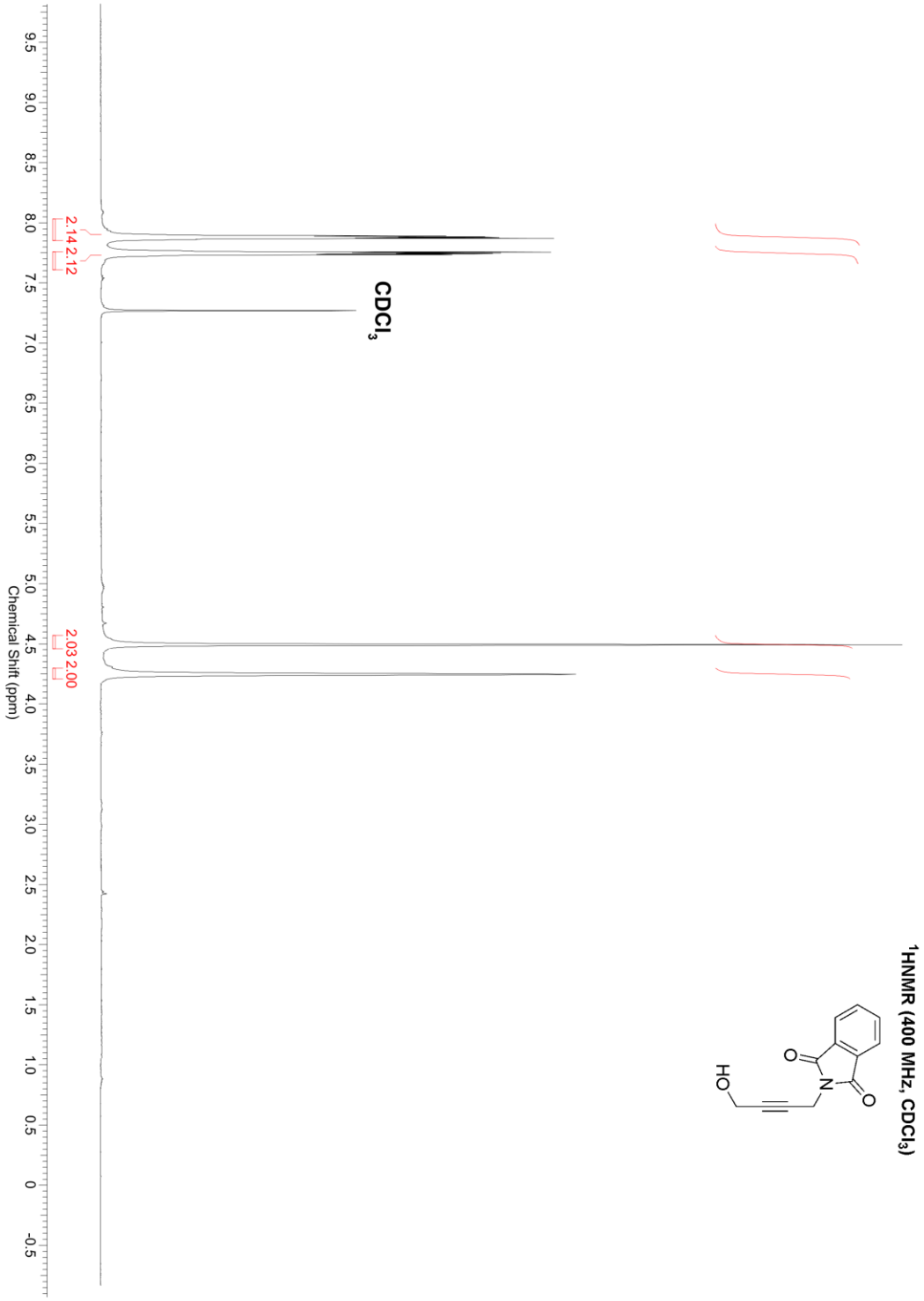

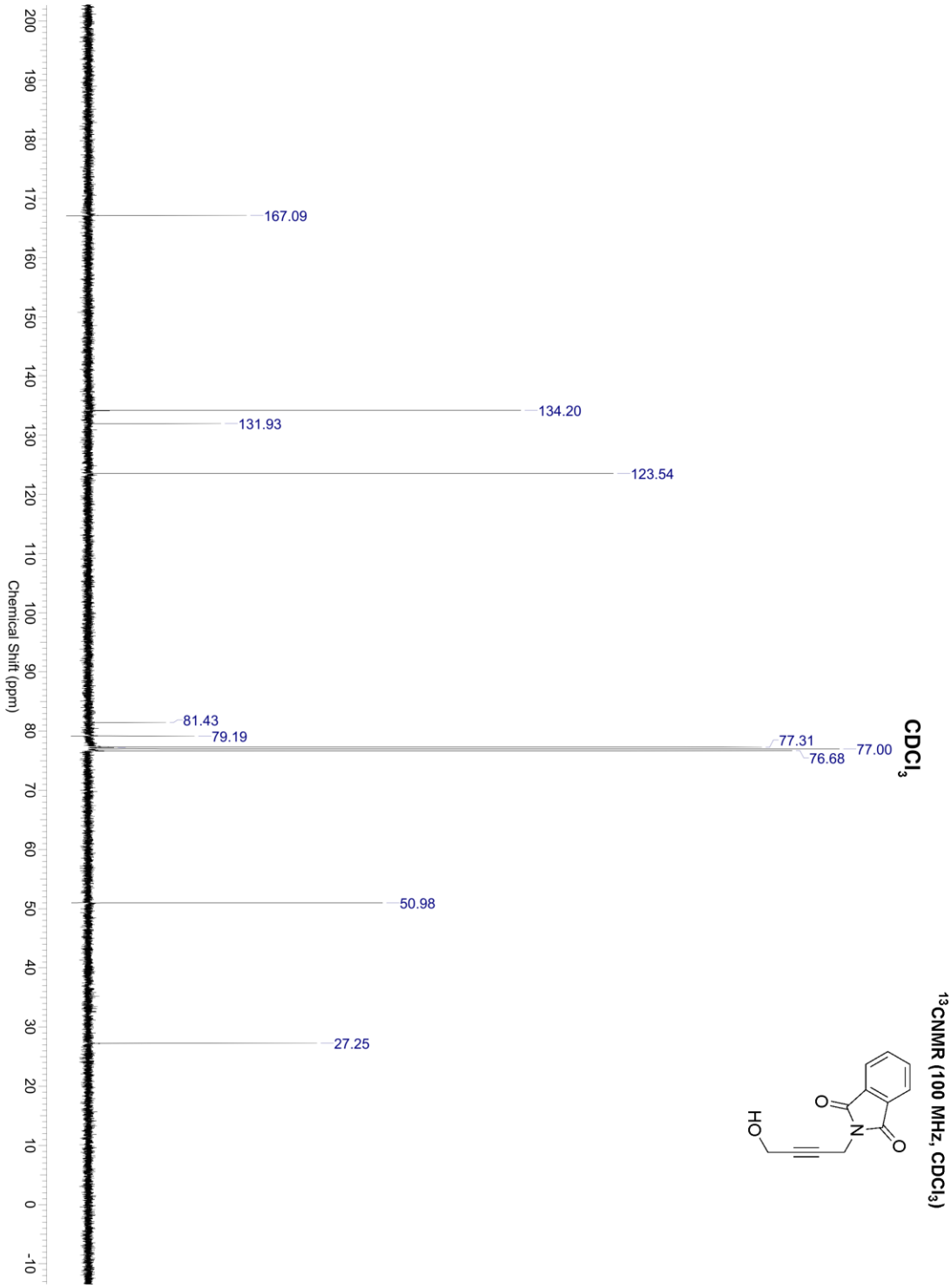

^{13}CNMR (100 MHz, $CDCl_3$)

^{1}HNMR (400 MHz, $CDCl_3$)

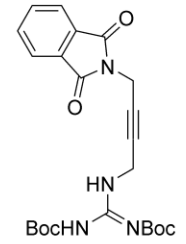

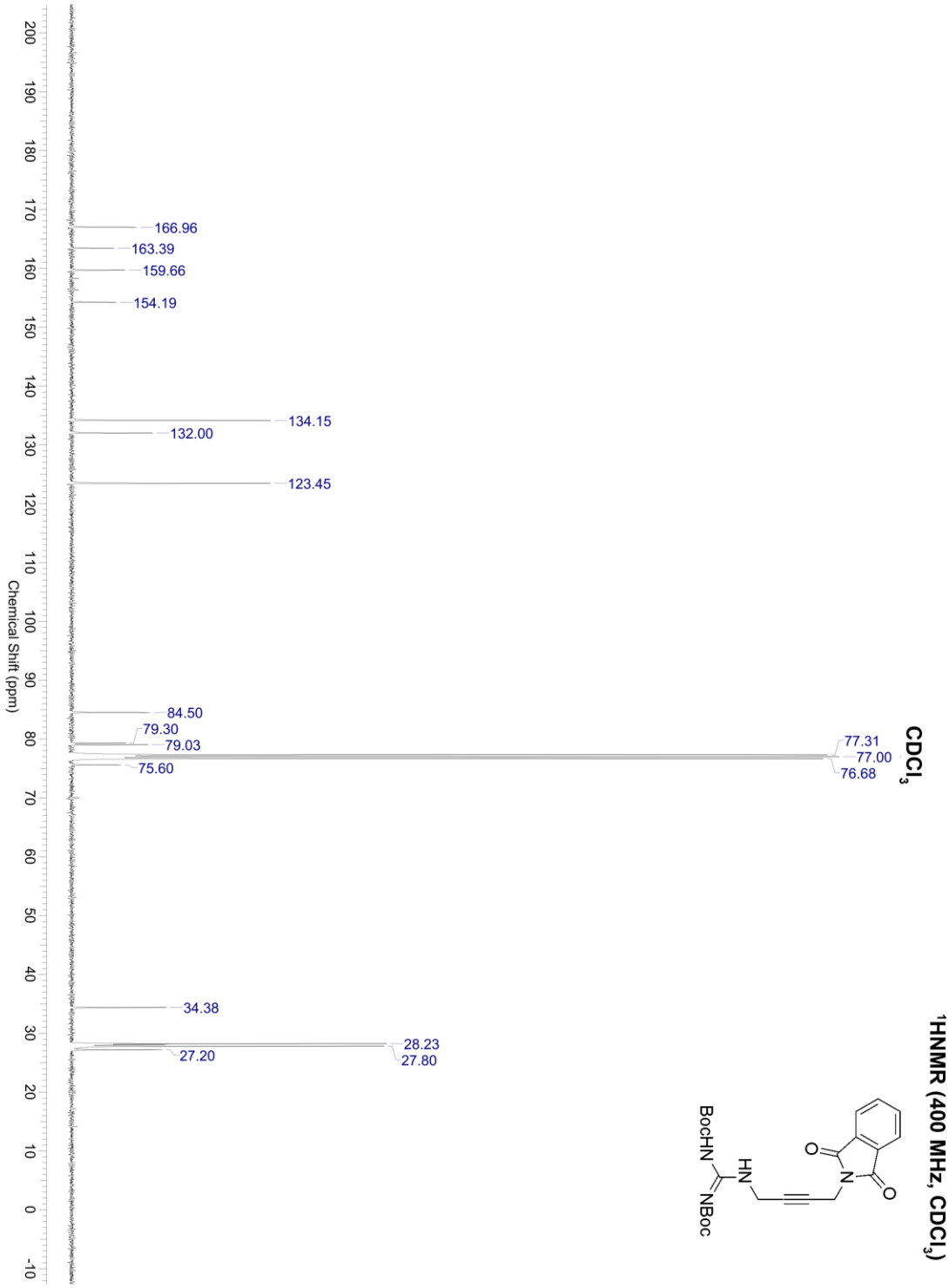

^{1}HNMR (400 MHz, $CDCl_3$)

^{1}HNMR (400 MHz, $CDCl_3$)

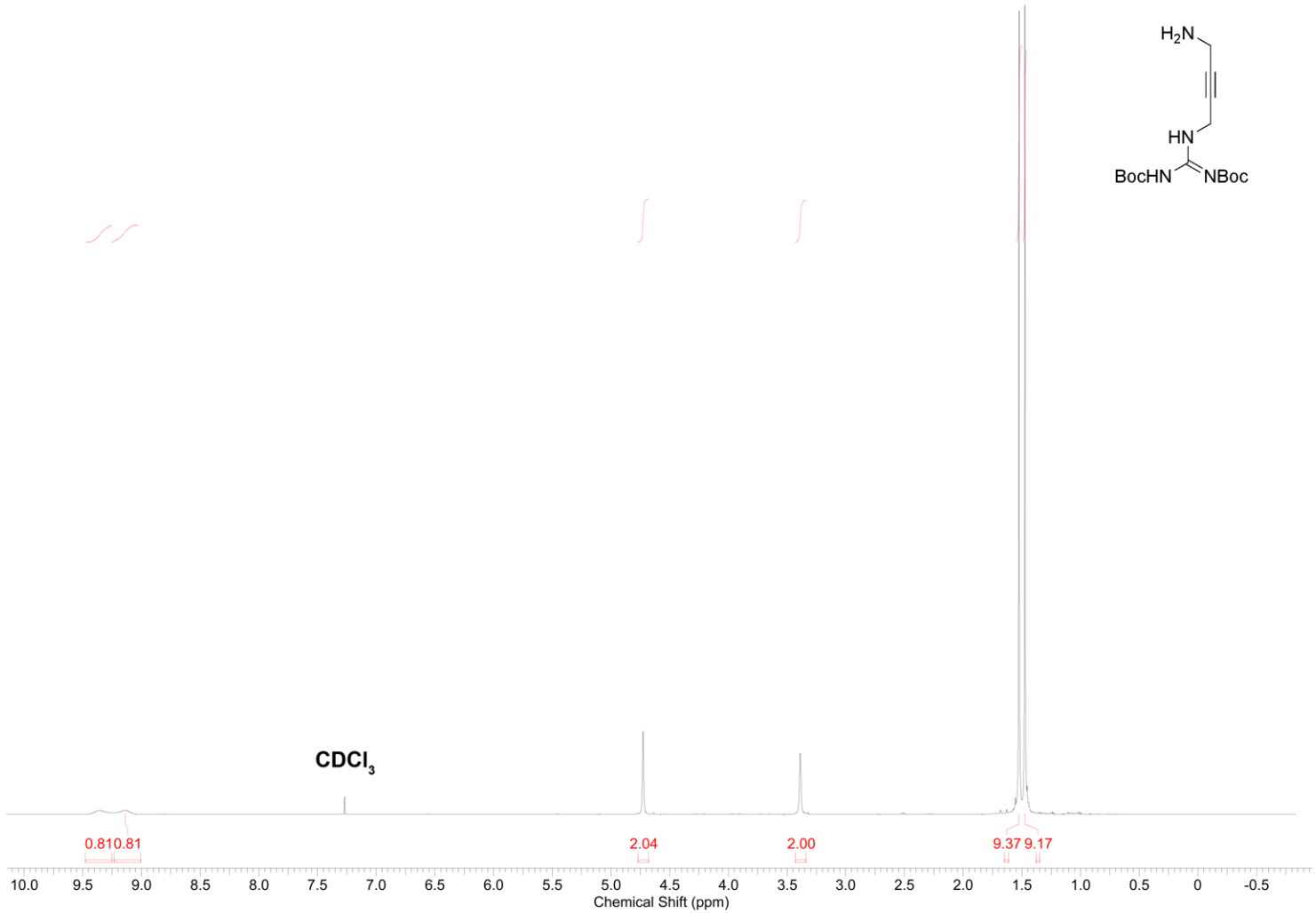

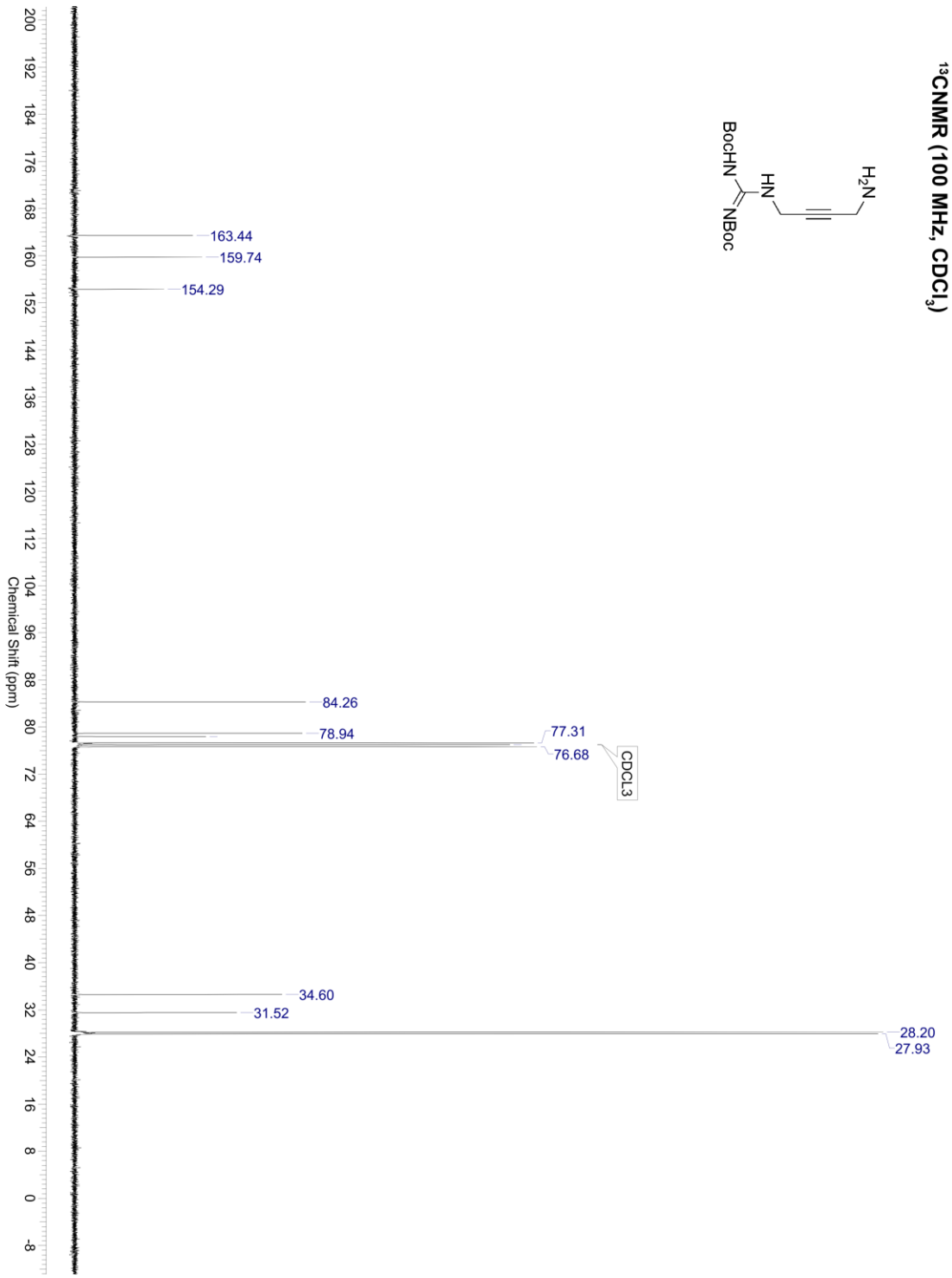
^{13}CNMR (100 MHz, $CDCl_3$)
BocHN
NBoc
HN
H_2N
163.44
159.74
154.29
84.26
78.94
77.31
76.68
CDCL3
34.60
31.52
28.20
27.93
Chemical Shift (ppm)
200
192
184
176
168
160
152
144
136
128
120
112
104
96
88
80
72
64
56
48
40
32
24
16
8
0
-8

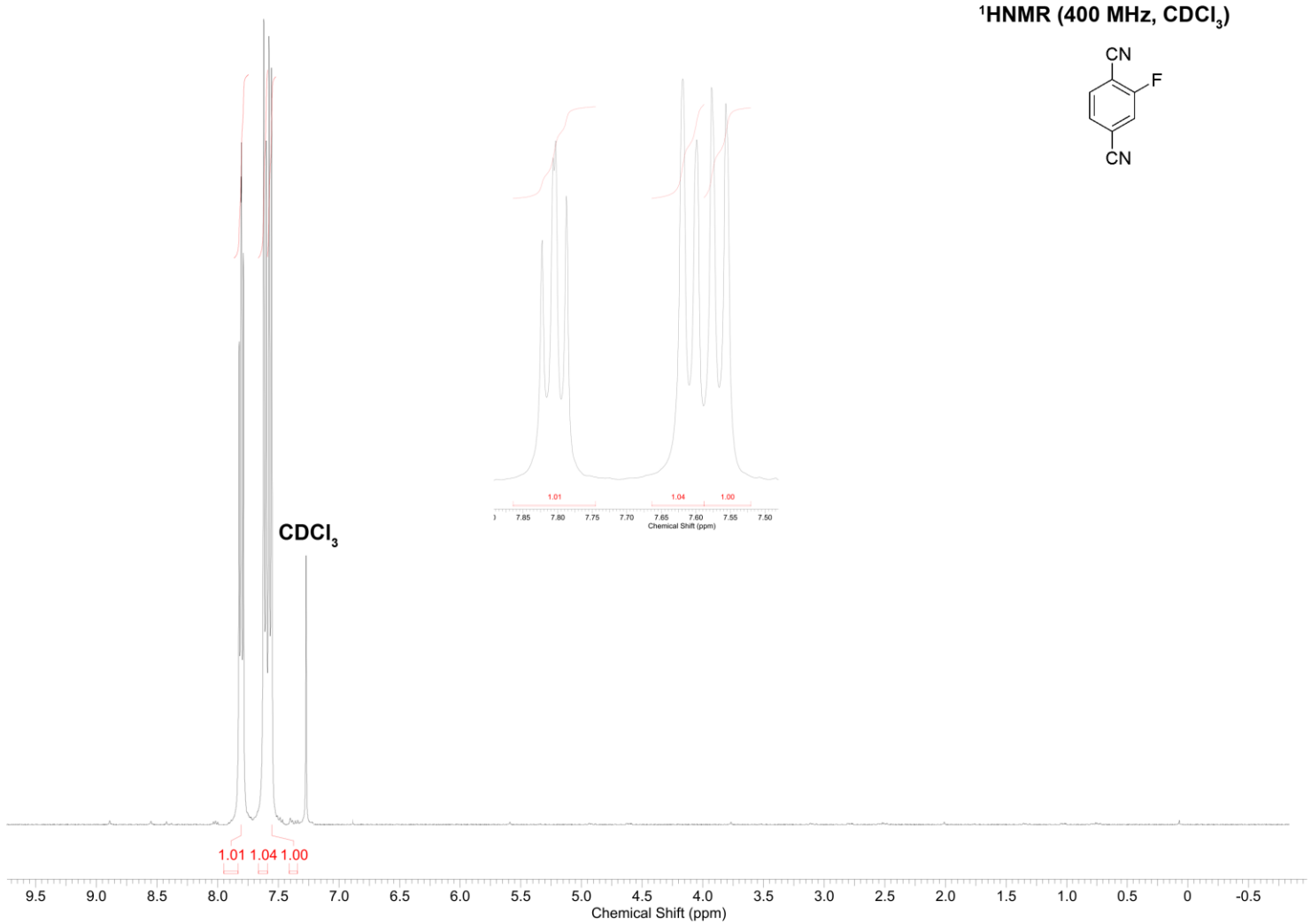
^{1}HNMR (400 MHz, $CDCl_3$)
CN
F
CN
$CDCl_3$
1.01 1.04 1.00
9.5 9.0 8.5 8.0 7.5 7.0 6.5 6.0 5.5 5.0 4.5 4.0 3.5 3.0 2.5 2.0 1.5 1.0 0.5 0 -0.5
Chemical Shift (ppm)
1.01 1.04 1.00
7.85 7.80 7.75 7.70 7.65 7.60 7.55 7.50
Chemical Shift (ppm)

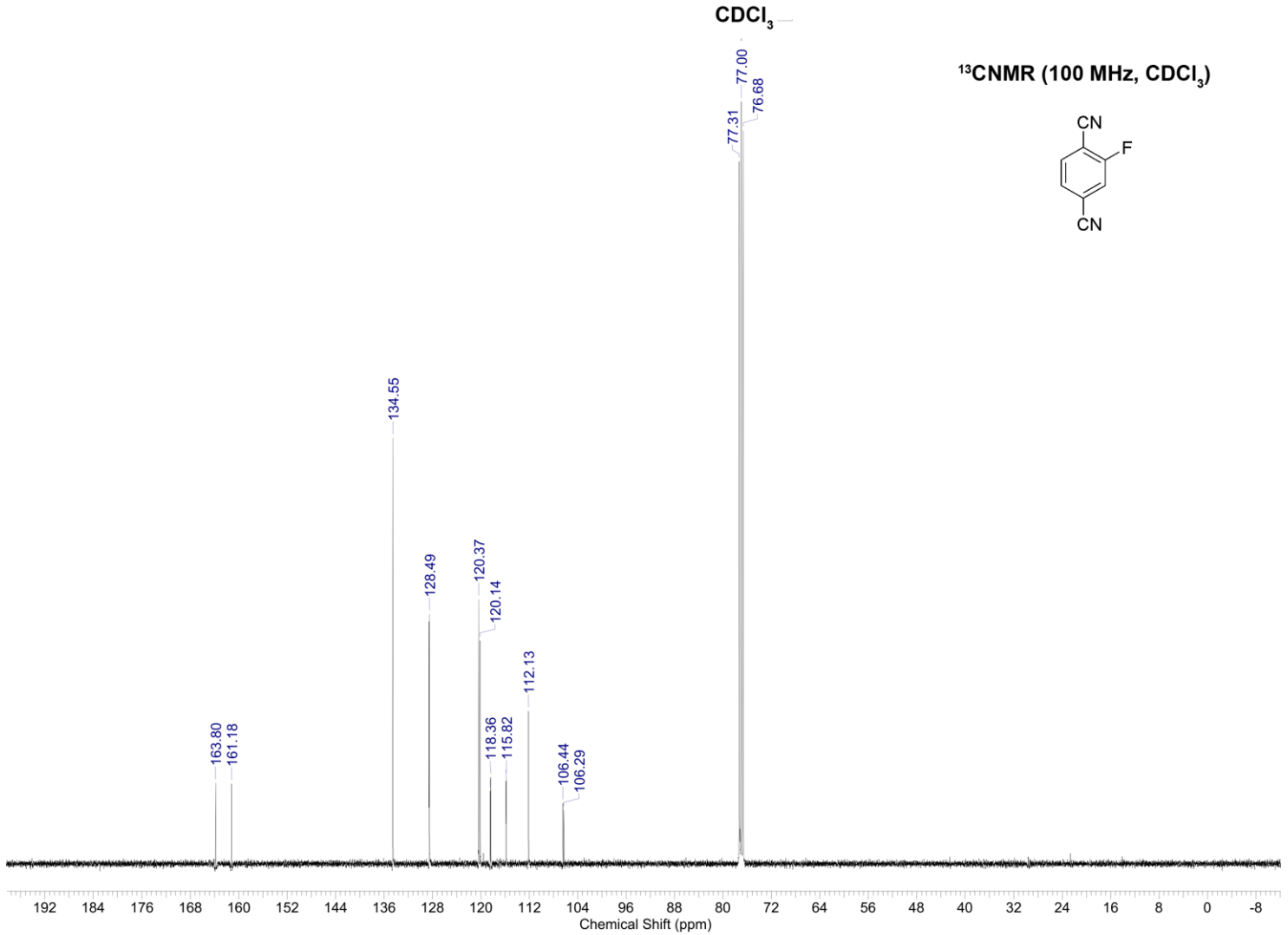

^{13}CNMR (100 MHz, $CDCl_3$)

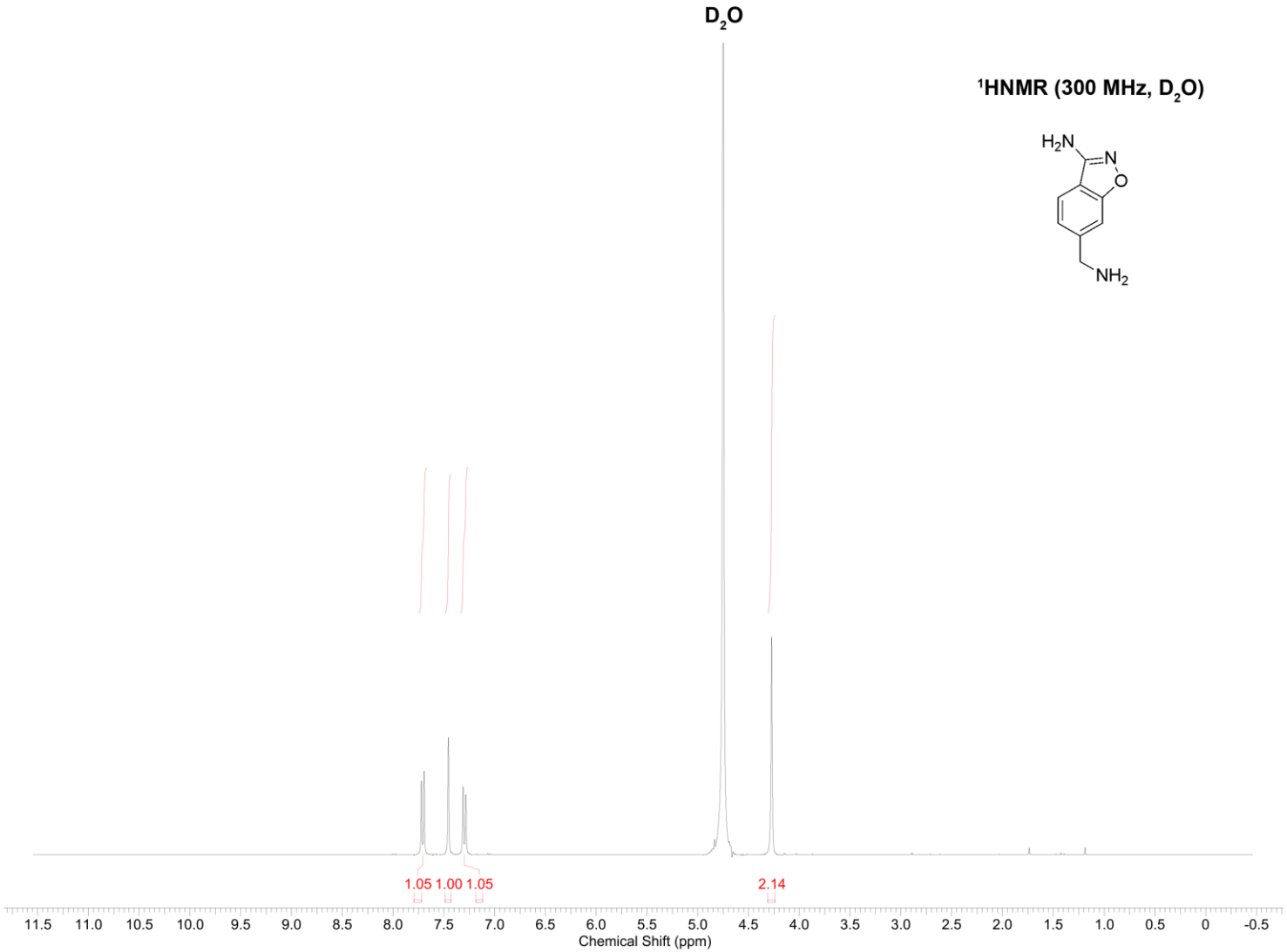
D2O
1HNMR (300 MHz, D2O)
H2N
N
O
NH2
1.05 1.00 1.05
2.14
11.5 11.0 10.5 10.0 9.5 9.0 8.5 8.0 7.5 7.0 6.5 6.0 5.5 5.0 4.5 4.0 3.5 3.0 2.5 2.0 1.5 1.0 0.5 0 -0.5
Chemical Shift (ppm)

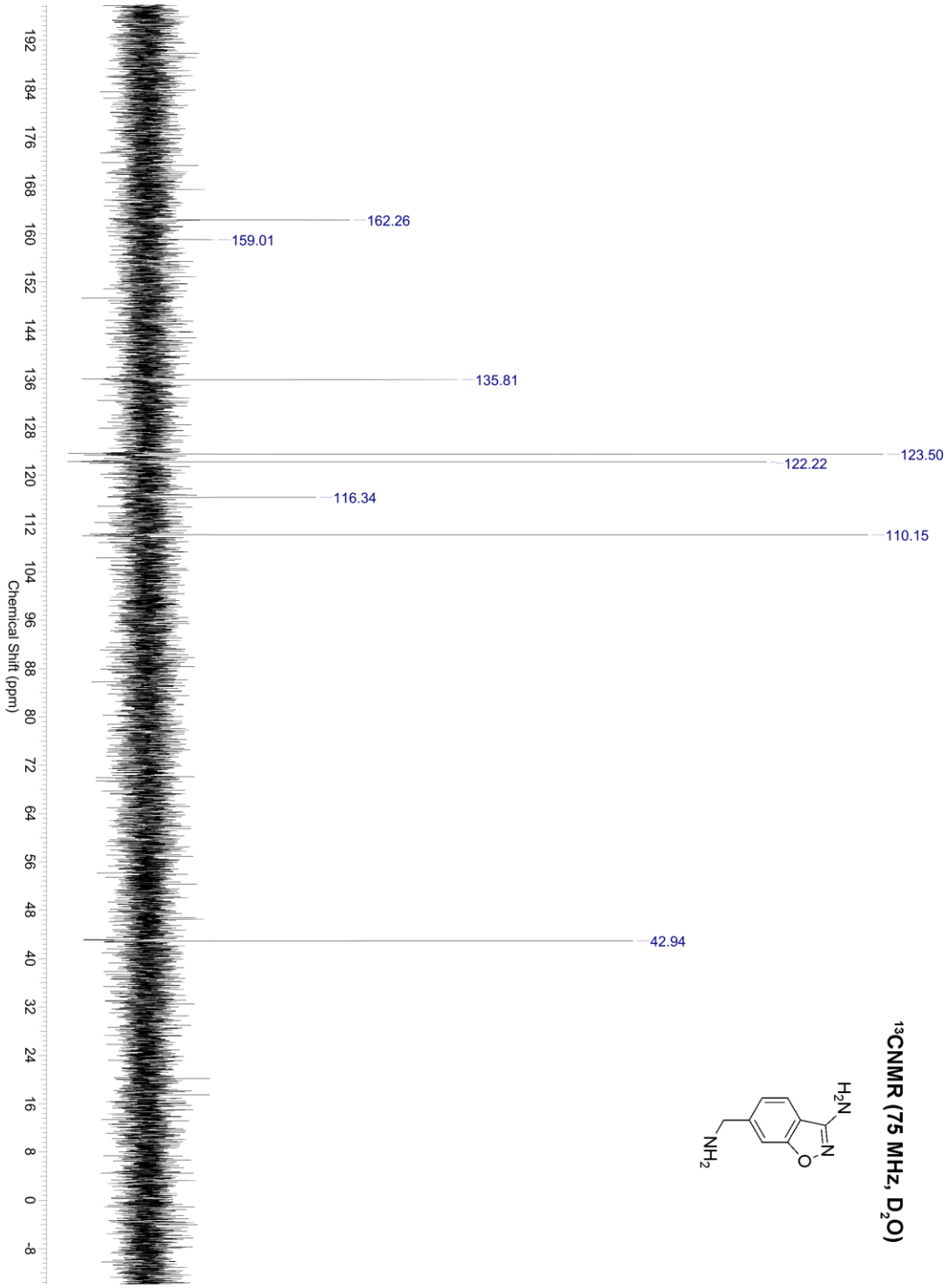

^{13}CNMR (75 MHz, D_2O)

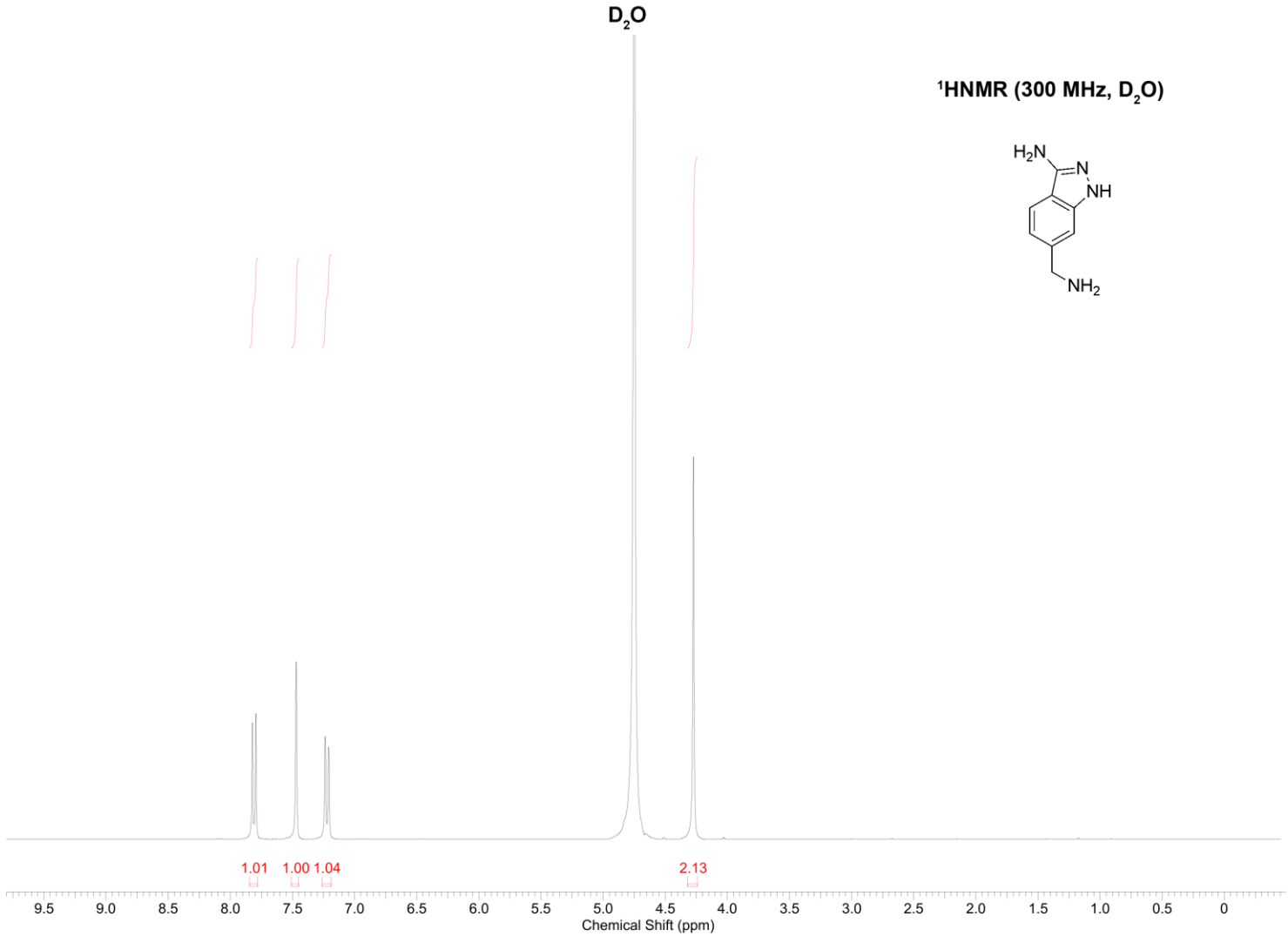
D2O
1HNMR (300 MHz, D2O)
H2N
N
NH
NH2
1.01
1.00
1.04
2.13
9.5
9.0
8.5
8.0
7.5
7.0
6.5
6.0
5.5
5.0
4.5
4.0
3.5
3.0
2.5
2.0
1.5
1.0
0.5
0
Chemical Shift (ppm)

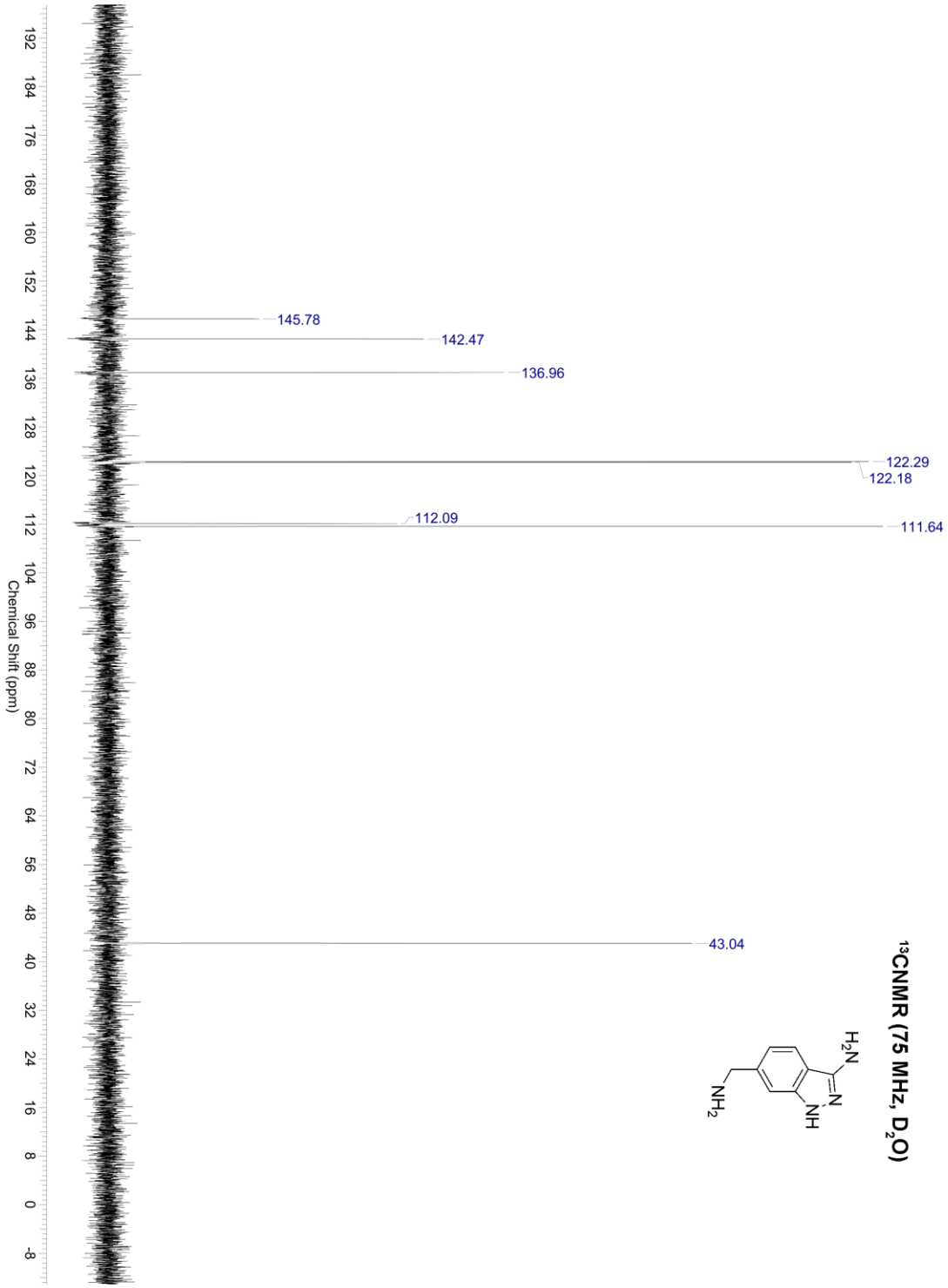
145.78
142.47
136.96
122.29
122.18
112.09
111.64
43.04
Chemical Shift (ppm)
192 184 176 168 160 152 144 136 128 120 112 104 96 88 80 72 64 56 48 40 32 24 16 8 0 -8
^{13}CNMR (75 MHz, D_2O)
H_2N
N
NH
NH_2

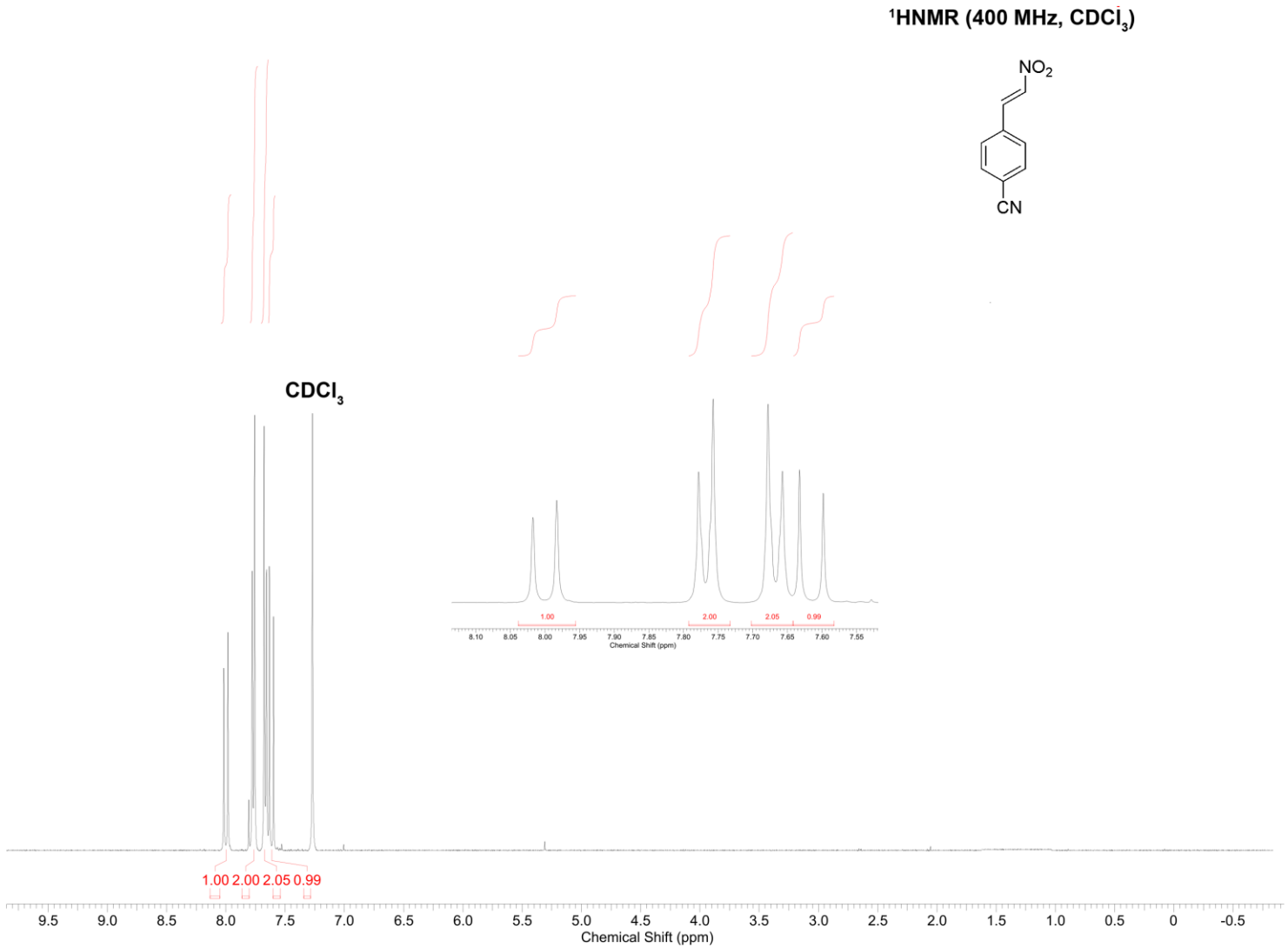
^{1}HNMR (400 MHz, $CDCl_3$)
NO_2
CN
$CDCl_3$
1.00 2.00 2.05 0.99
Chemical Shift (ppm)

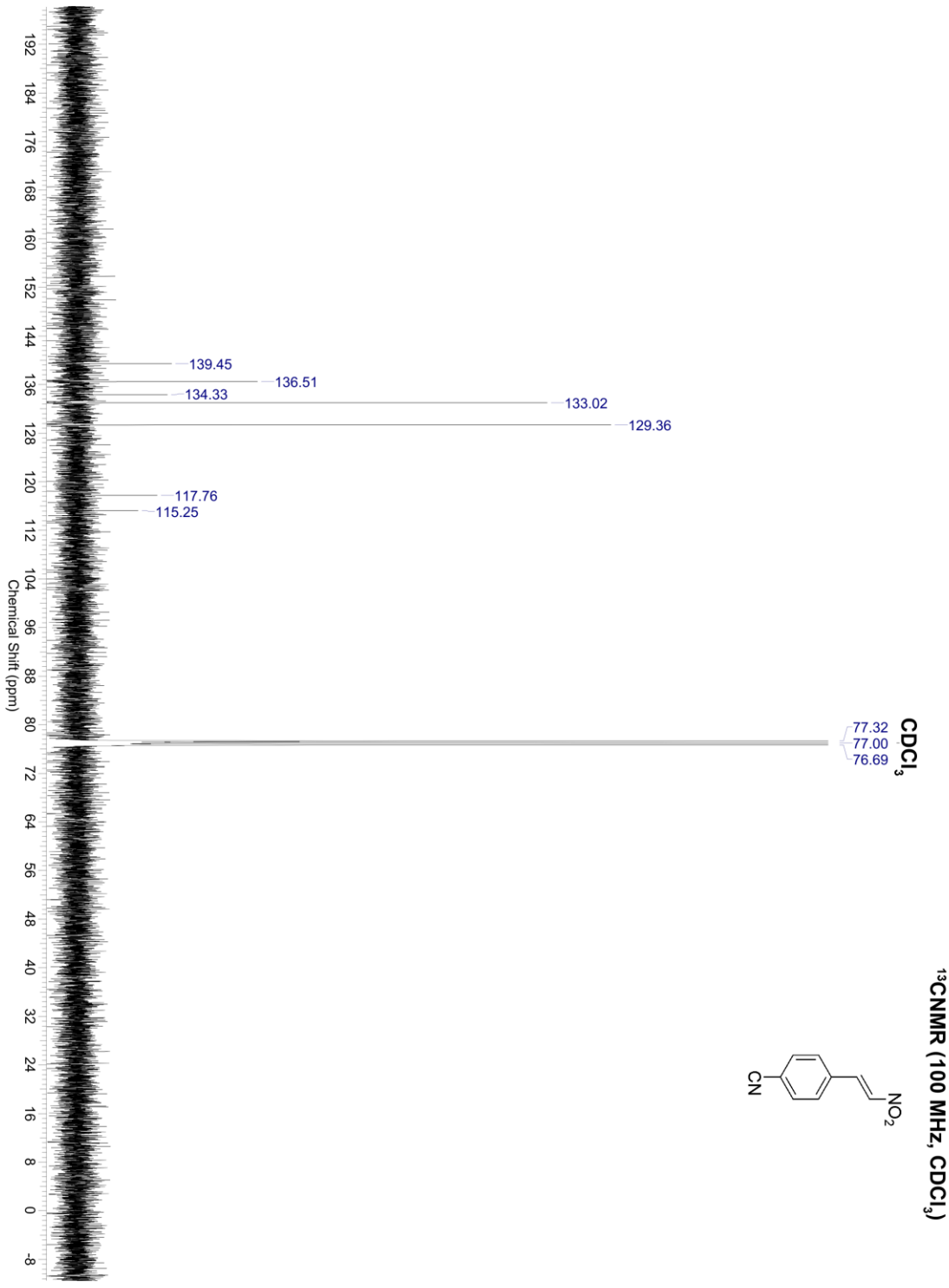

^{13}CNMR (100 MHz, $CDCl_3$)

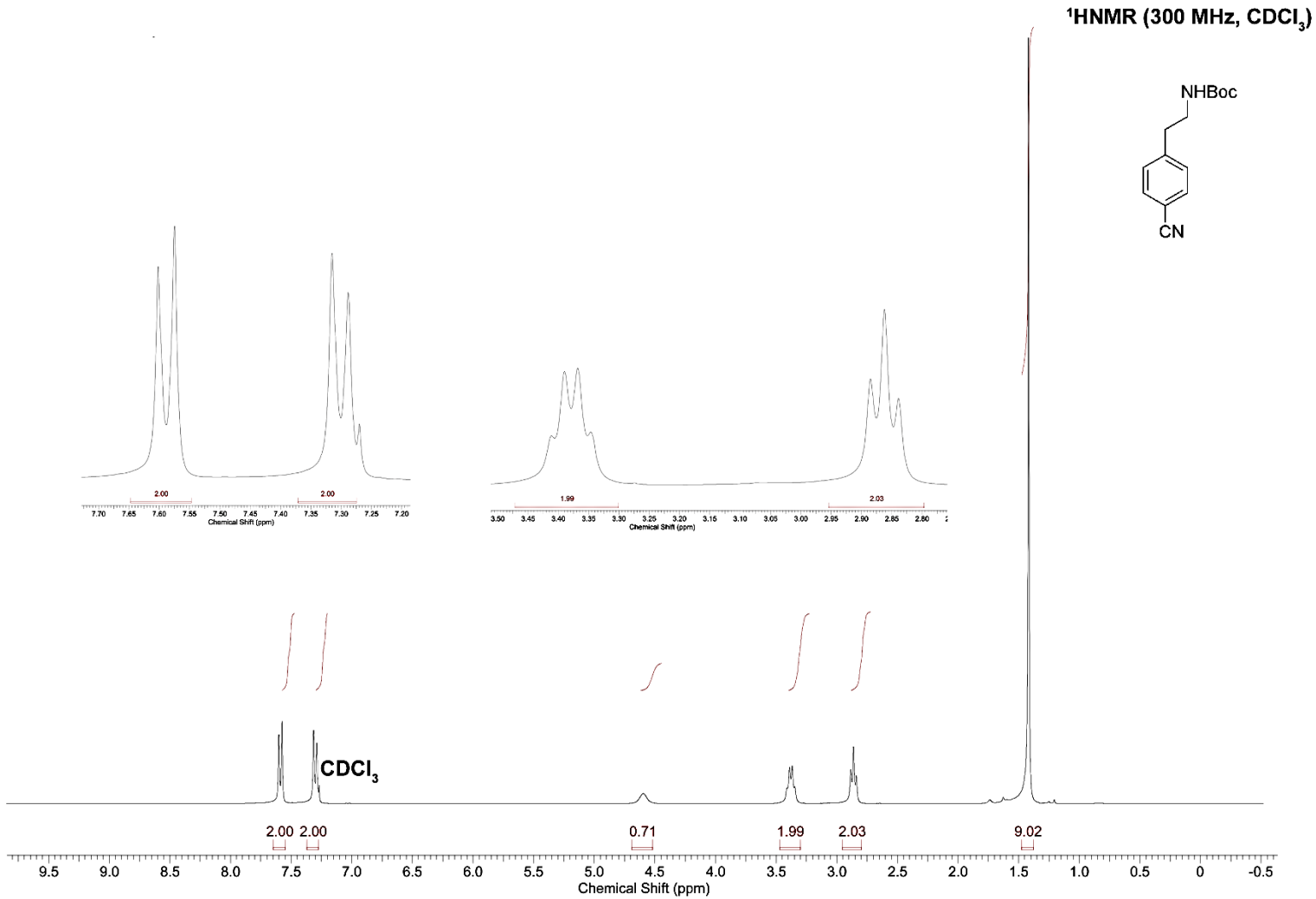
¹HNMR (300 MHz, CDCl3)
NHBoc
CN
CDCl3
2.00 2.00
0.71
1.99
2.03
9.02
Chemical Shift (ppm)

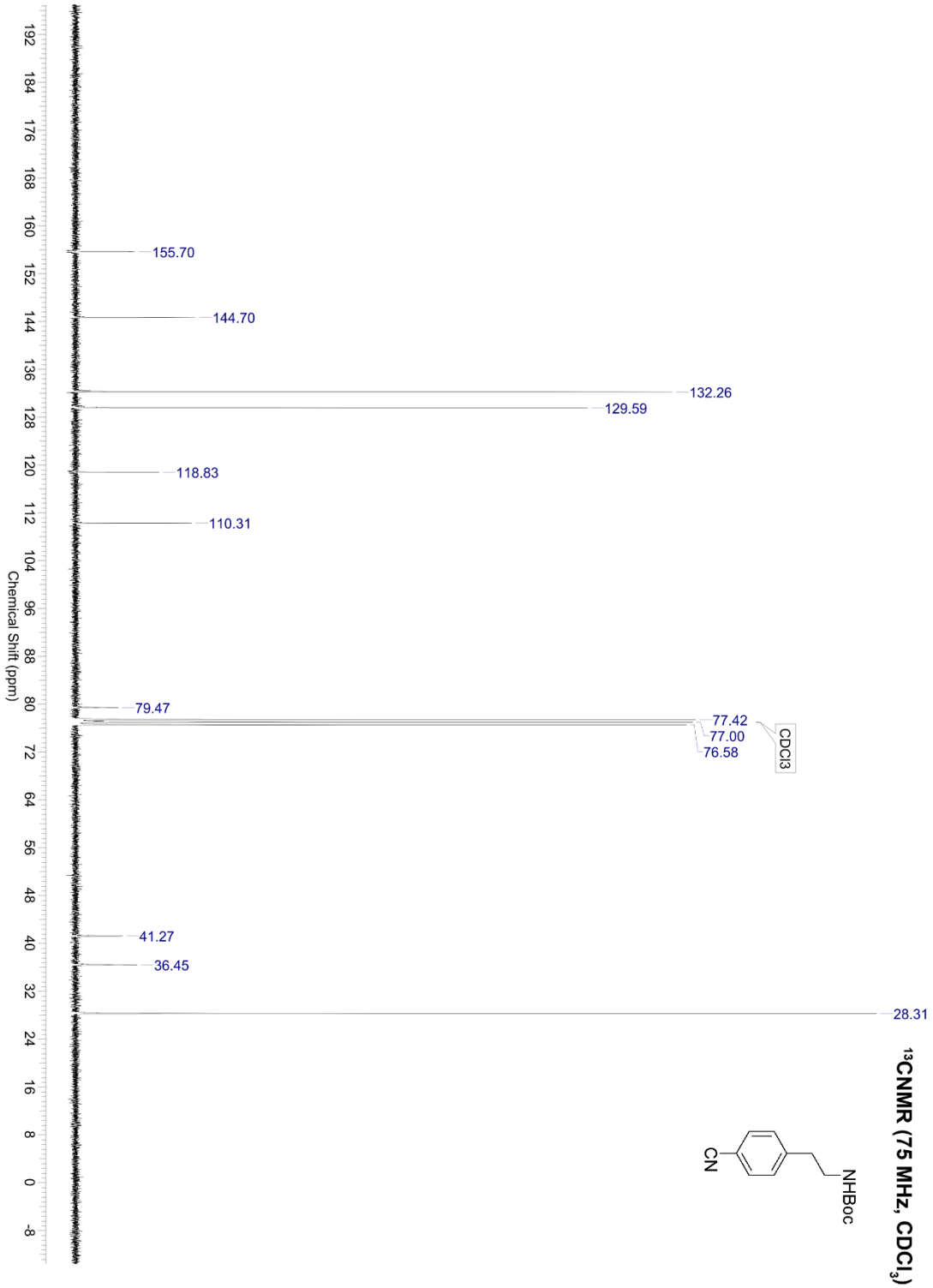
155.70
144.70
132.26
129.59
118.83
110.31
79.47
77.42
77.00
76.58
CDCl3
41.27
36.45
28.31
Chemical Shift (ppm)
192
184
176
168
160
152
144
136
128
120
112
104
96
88
80
72
64
56
48
40
32
24
16
8
0
-8
CN
NHBoc
13CNMR (75 MHz, CDCl3)

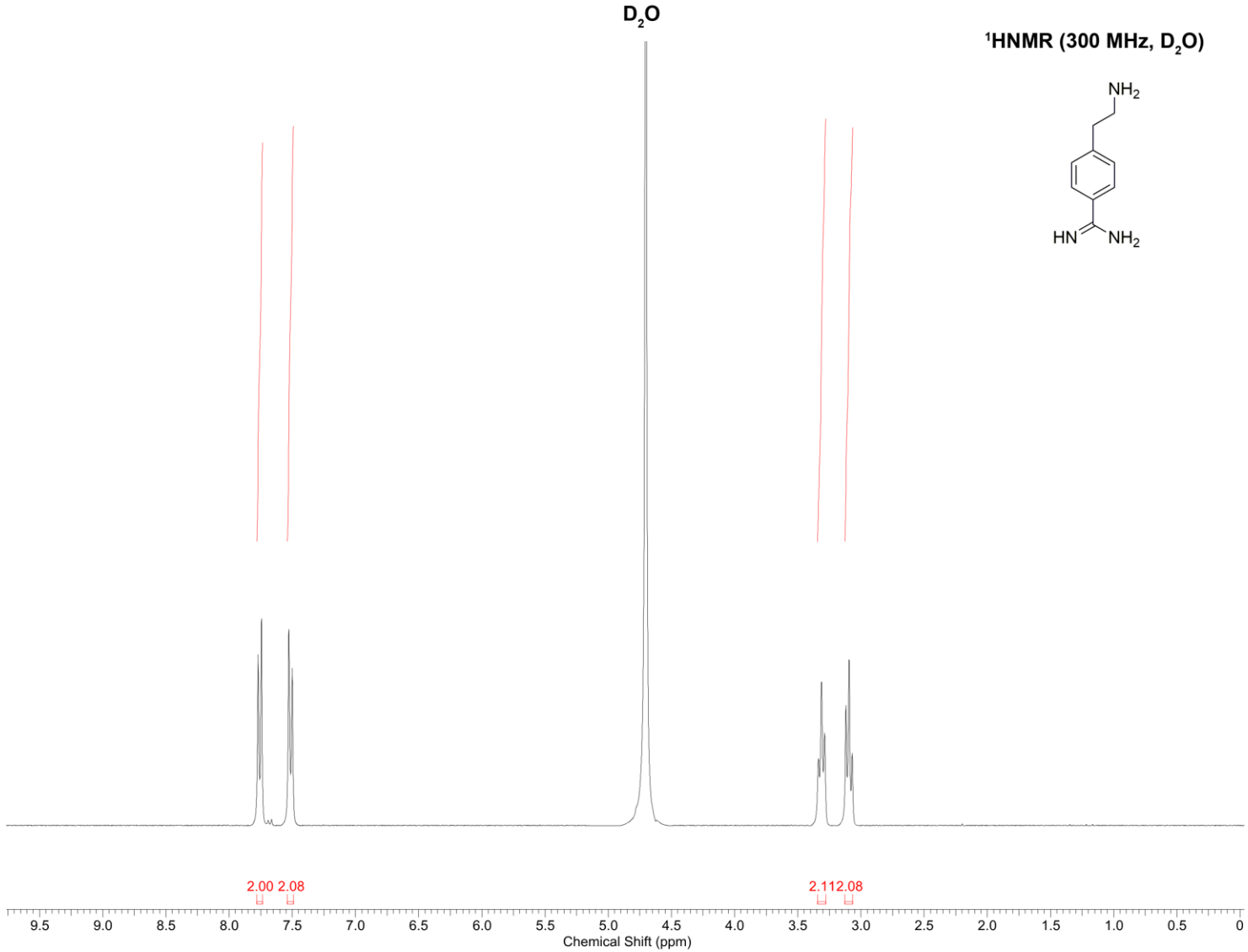
D2O
1HNMR (300 MHz, D2O)
NH2
HN
NH2
2.00 2.08
2.11 2.08
9.5 9.0 8.5 8.0 7.5 7.0 6.5 6.0 5.5 5.0 4.5 4.0 3.5 3.0 2.5 2.0 1.5 1.0 0.5 0
Chemical Shift (ppm)

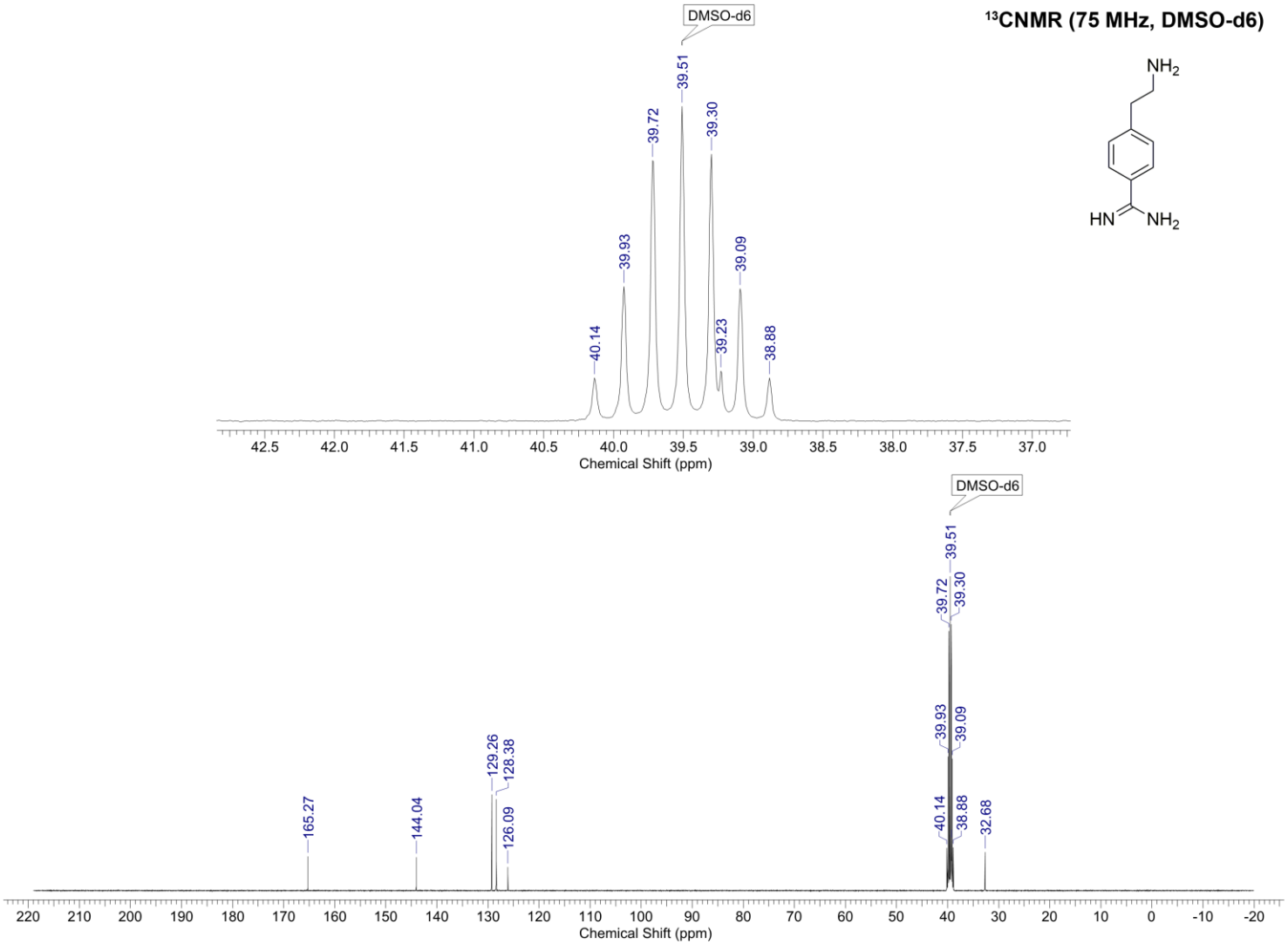
13CNMR (75 MHz, DMSO-d6)
NH2
HN
NH2
DMSO-d6
39.51
39.72
39.30
39.93
39.09
39.23
40.14
38.88
42.5 42.0 41.5 41.0 40.5 40.0 39.5 39.0 38.5 38.0 37.5 37.0
Chemical Shift (ppm)
DMSO-d6
39.51
39.72
39.30
39.93
39.09
129.26
128.38
165.27
144.04
126.09
40.14
38.88
32.68
220 210 200 190 180 170 160 150 140 130 120 110 100 90 80 70 60 50 40 30 20 10 0 -10 -20
Chemical Shift (ppm)

^{1}HNMR (400 MHz, $CDCl_3$)

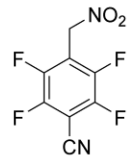

^{19}FNMR (377 MHz, $CDCl_3$)

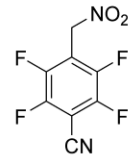

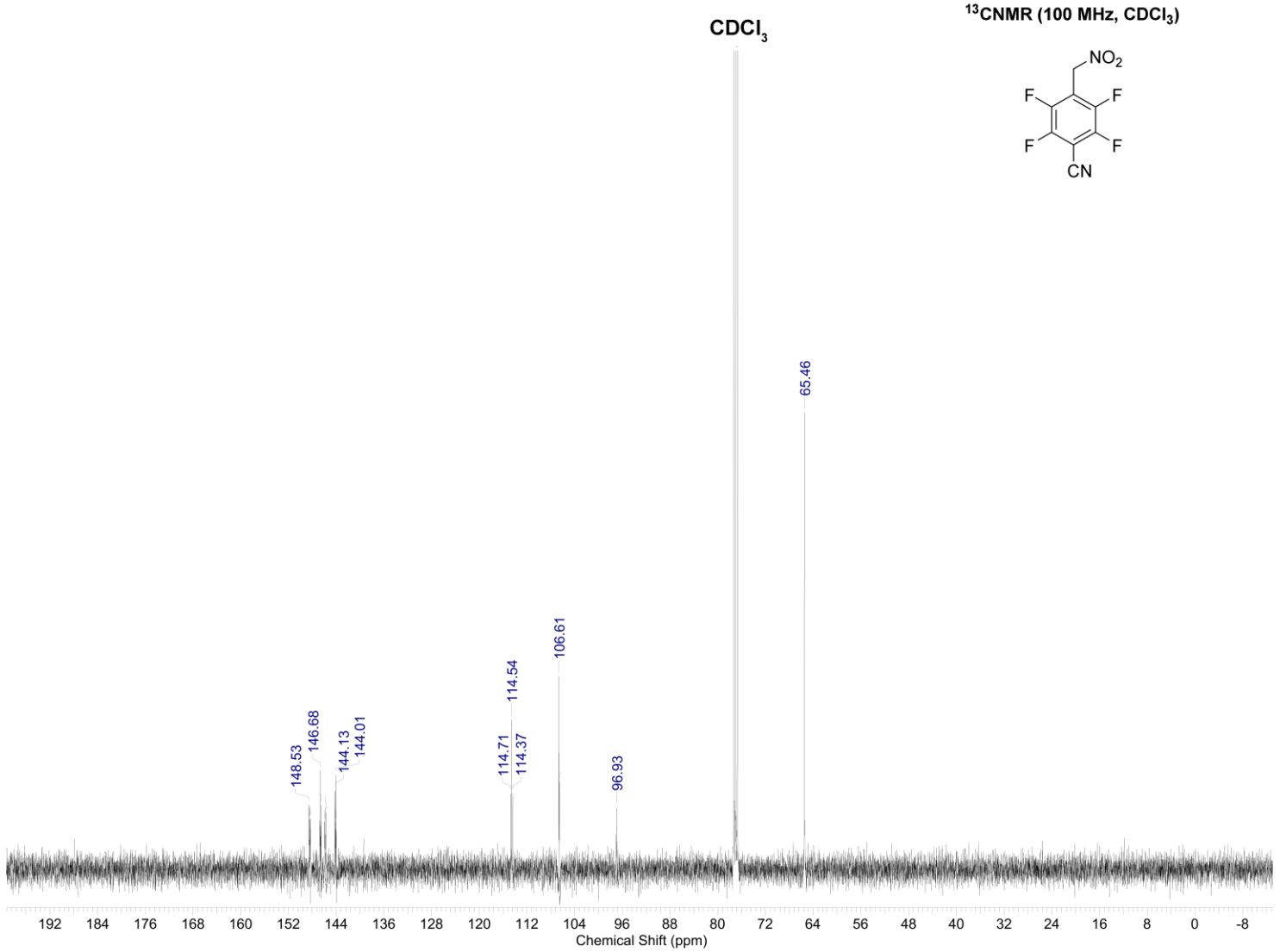
^{13}CNMR (100 MHz, $CDCl_3$)
$CDCl_3$
NO_2
F
F
F
F
CN
65.46
106.61
114.54
114.71
114.37
96.93
148.53
146.68
144.13
144.01
192 184 176 168 160 152 144 136 128 120 112 104 96 88 80 72 64 56 48 40 32 24 16 8 0 -8
Chemical Shift (ppm)

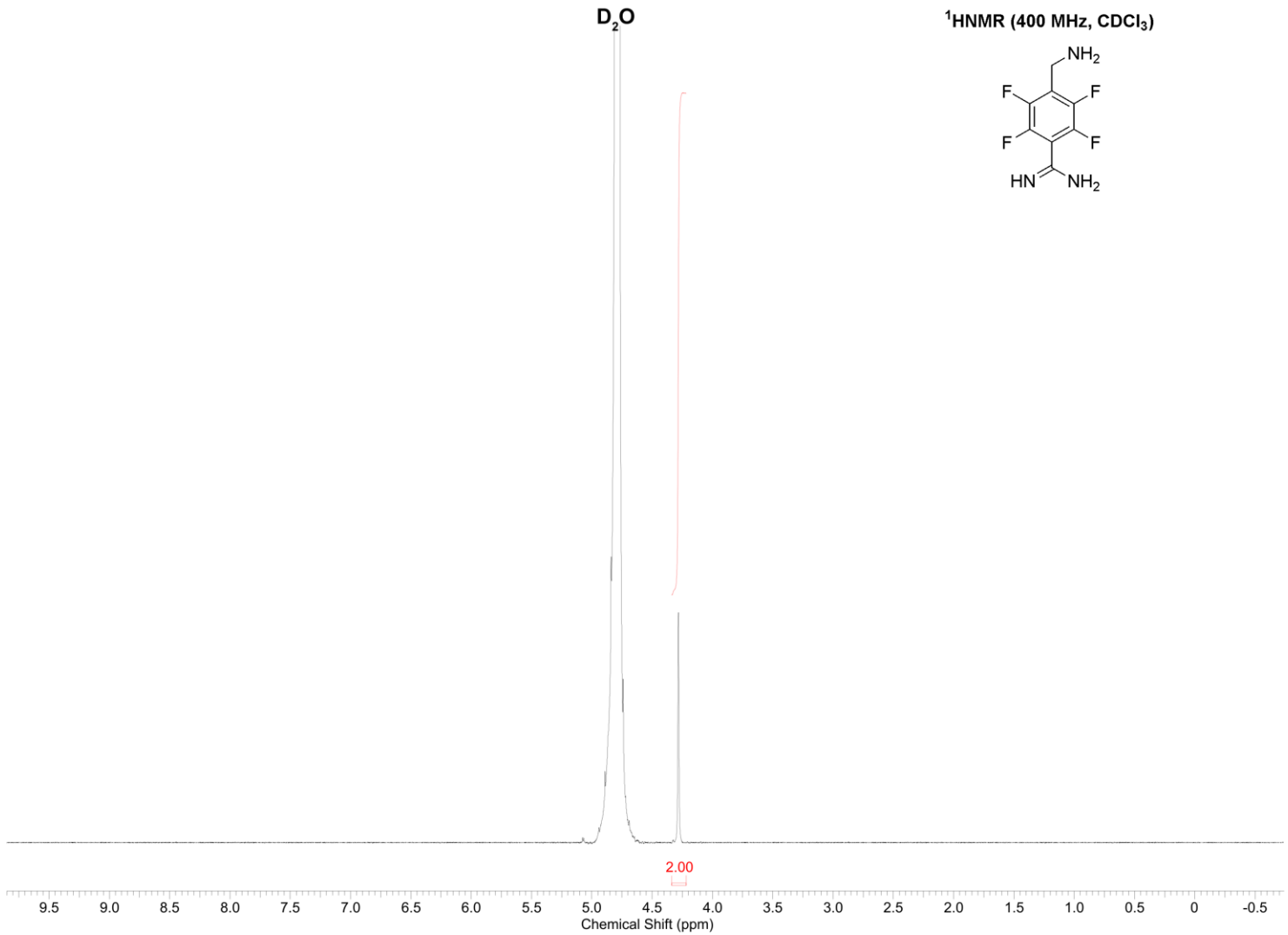
D2O
1HNMR (400 MHz, CDCl3)
NH2
F
F
F
F
HN
NH2
2.00
9.5
9.0
8.5
8.0
7.5
7.0
6.5
6.0
5.5
5.0
4.5
4.0
3.5
3.0
2.5
2.0
1.5
1.0
0.5
0
-0.5
Chemical Shift (ppm)

^{19}FNMR (377 MHz, $CDCl_3$)

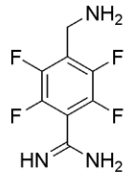

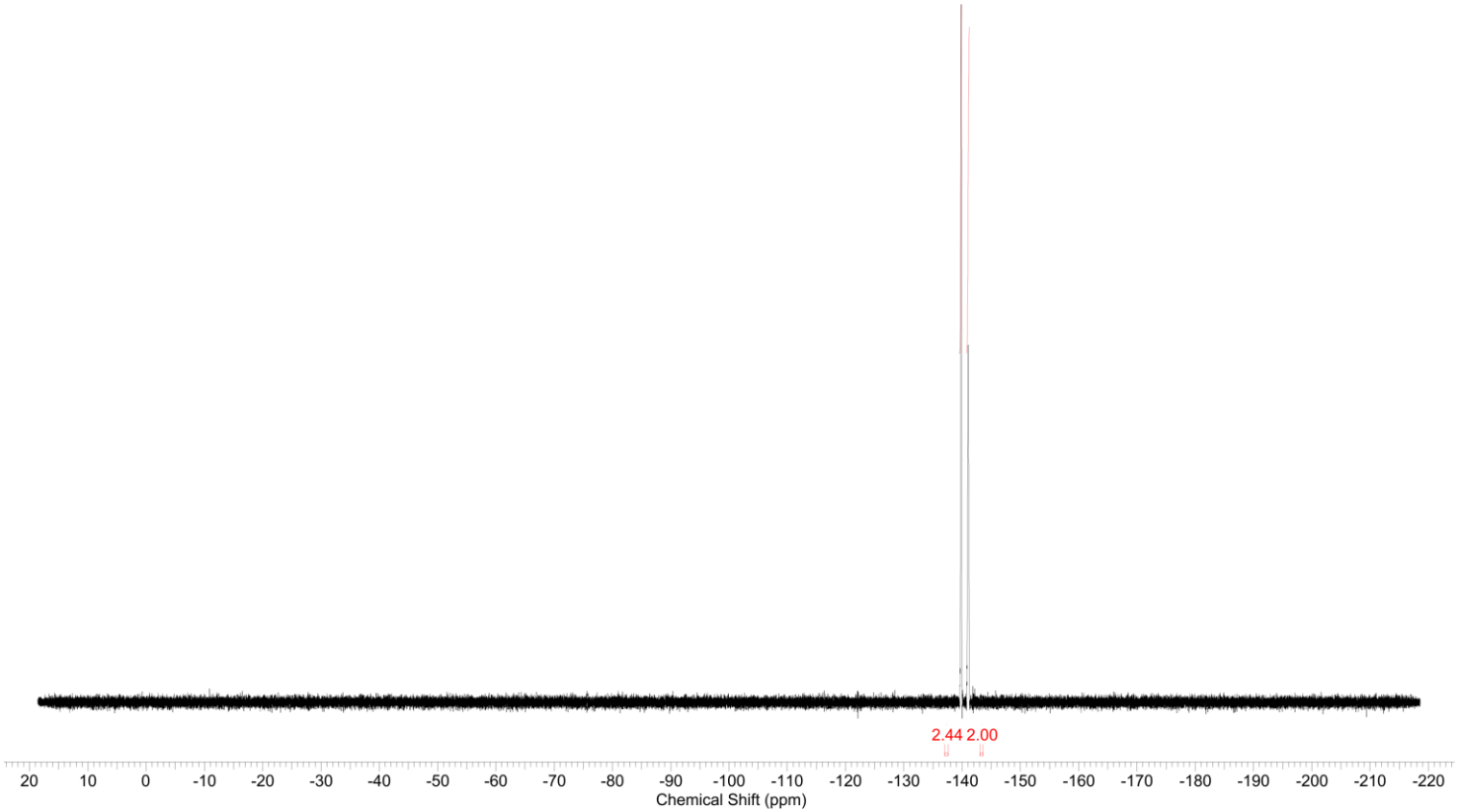

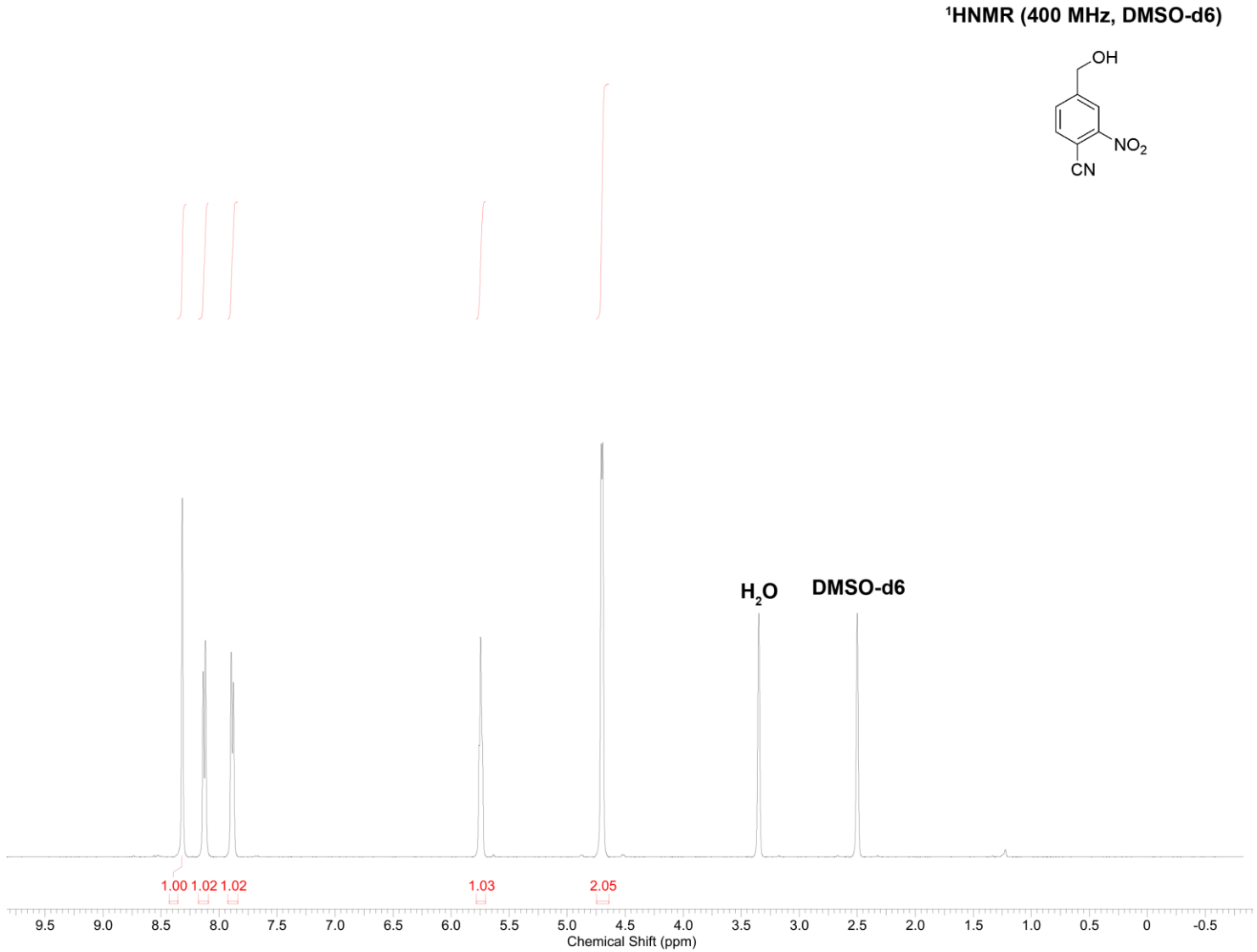
¹HNMR (400 MHz, DMSO-d6)
OH
NO2
CN
H2O
DMSO-d6
1.00 1.02 1.02
1.03
2.05
9.5 9.0 8.5 8.0 7.5 7.0 6.5 6.0 5.5 5.0 4.5 4.0 3.5 3.0 2.5 2.0 1.5 1.0 0.5 0 -0.5
Chemical Shift (ppm)

^{13}CNMR (100 MHz, DMSO-d6)

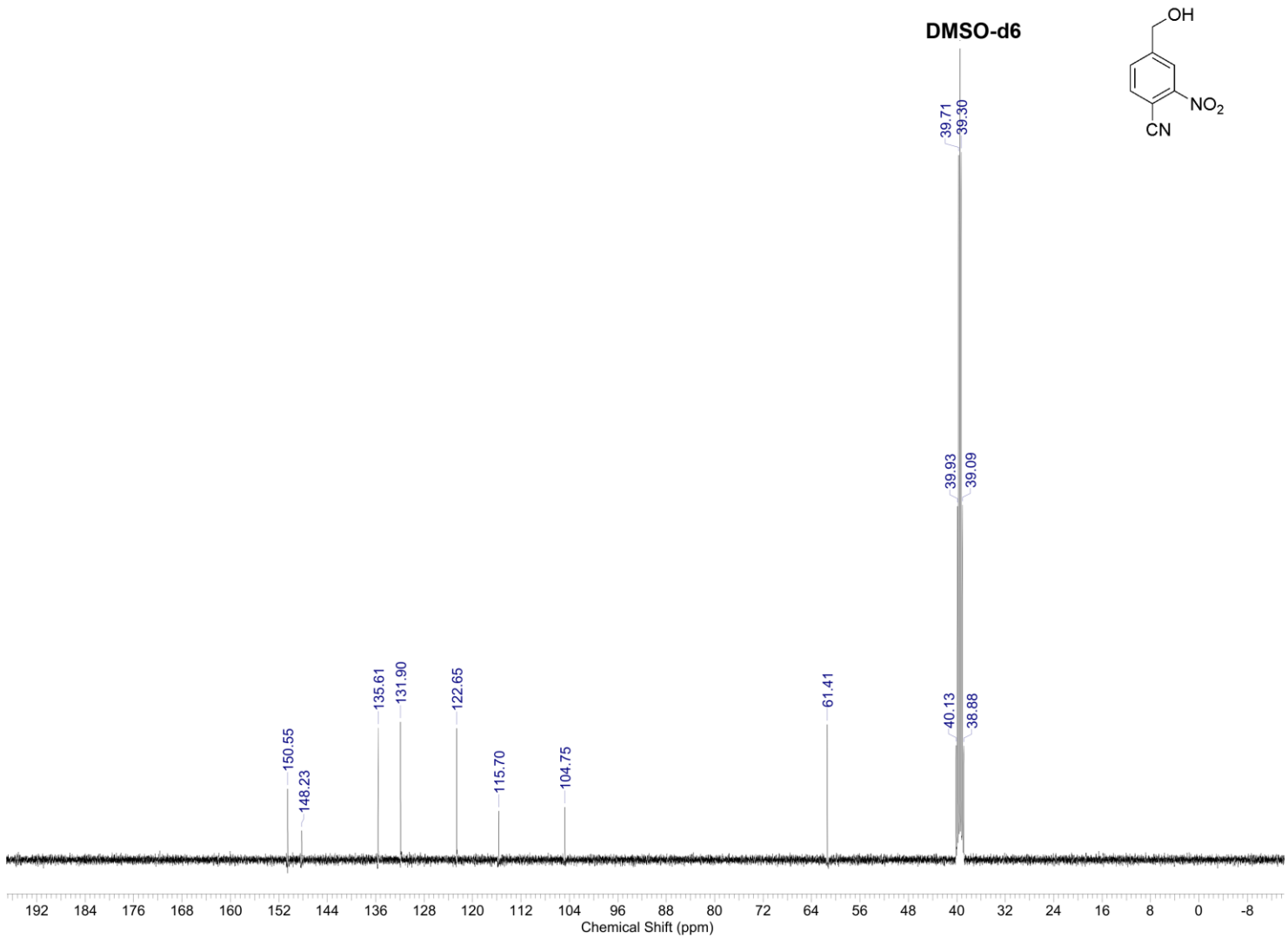

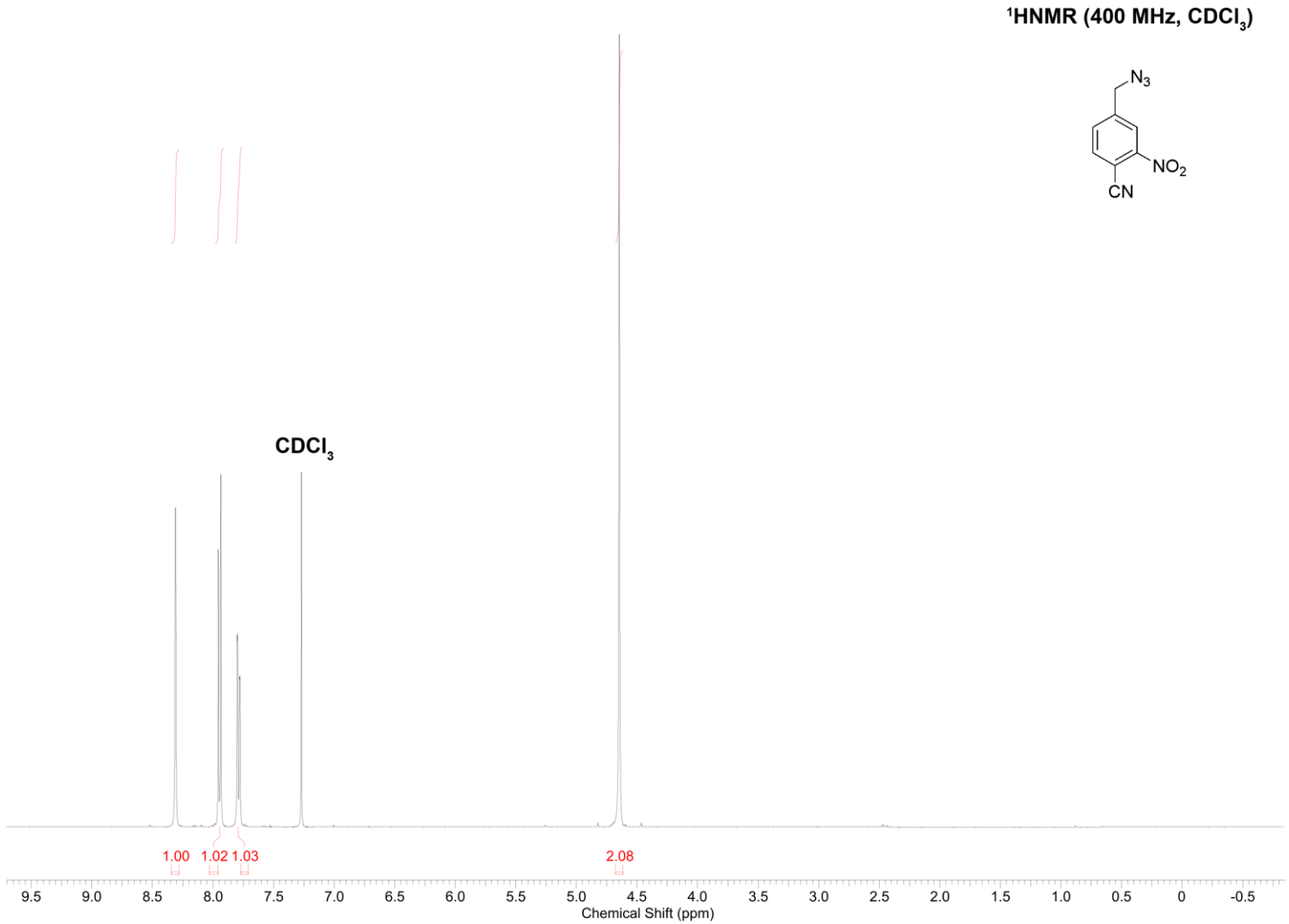
^{1}HNMR (400 MHz, $CDCl_3$)
N_3
NO_2
CN
$CDCl_3$
1.00
1.02
1.03
2.08
9.5 9.0 8.5 8.0 7.5 7.0 6.5 6.0 5.5 5.0 4.5 4.0 3.5 3.0 2.5 2.0 1.5 1.0 0.5 0 -0.5
Chemical Shift (ppm)

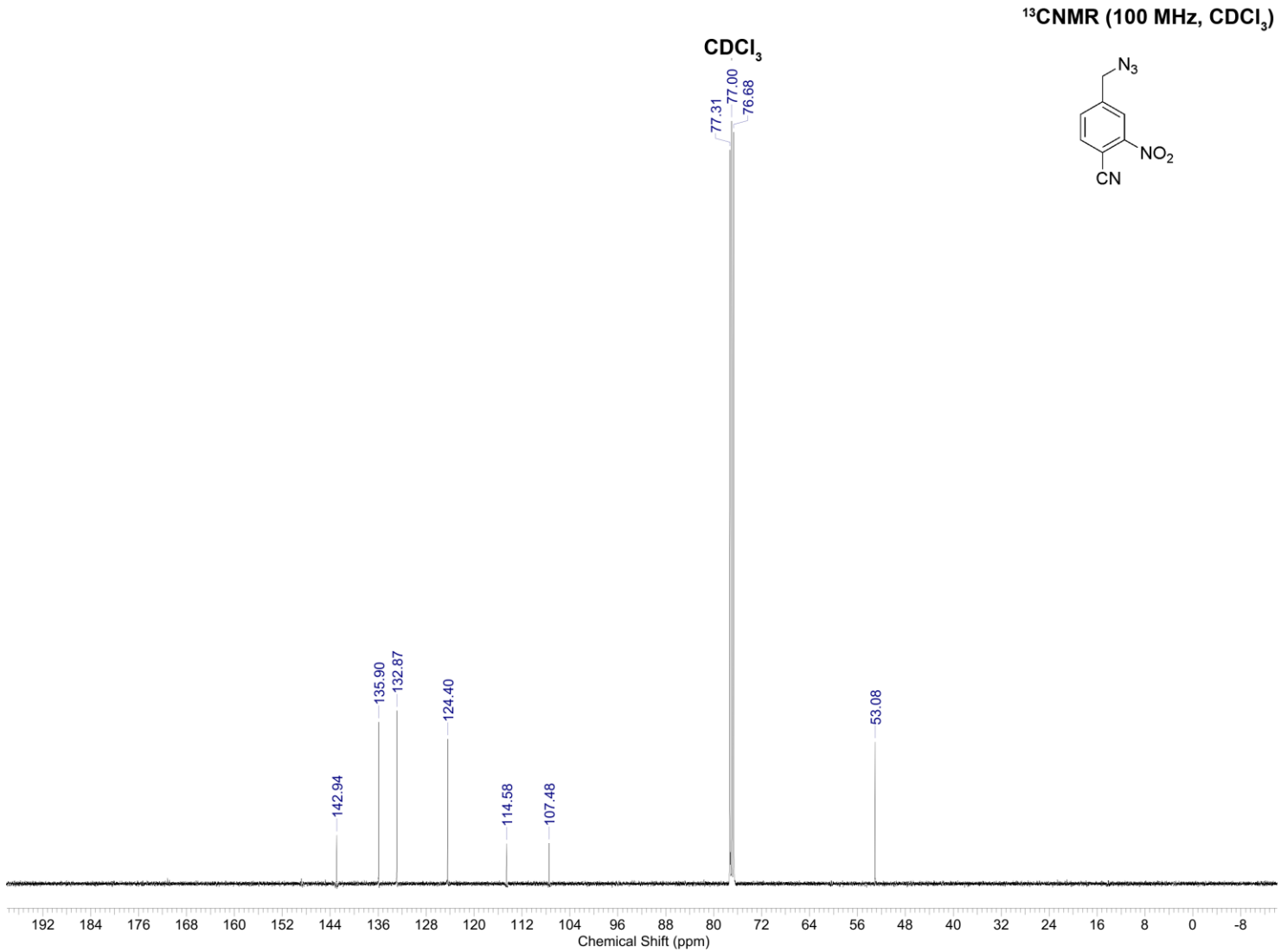
^{13}CNMR (100 MHz, $CDCl_3$)
$CDCl_3$
77.31
77.00
76.68
142.94
135.90
132.87
124.40
114.58
107.48
53.08
N_3
NO_2
CN
192 184 176 168 160 152 144 136 128 120 112 104 96 88 80 72 64 56 48 40 32 24 16 8 0 -8
Chemical Shift (ppm)

^{1}HNMR (400 MHz, $CDCl_3$)

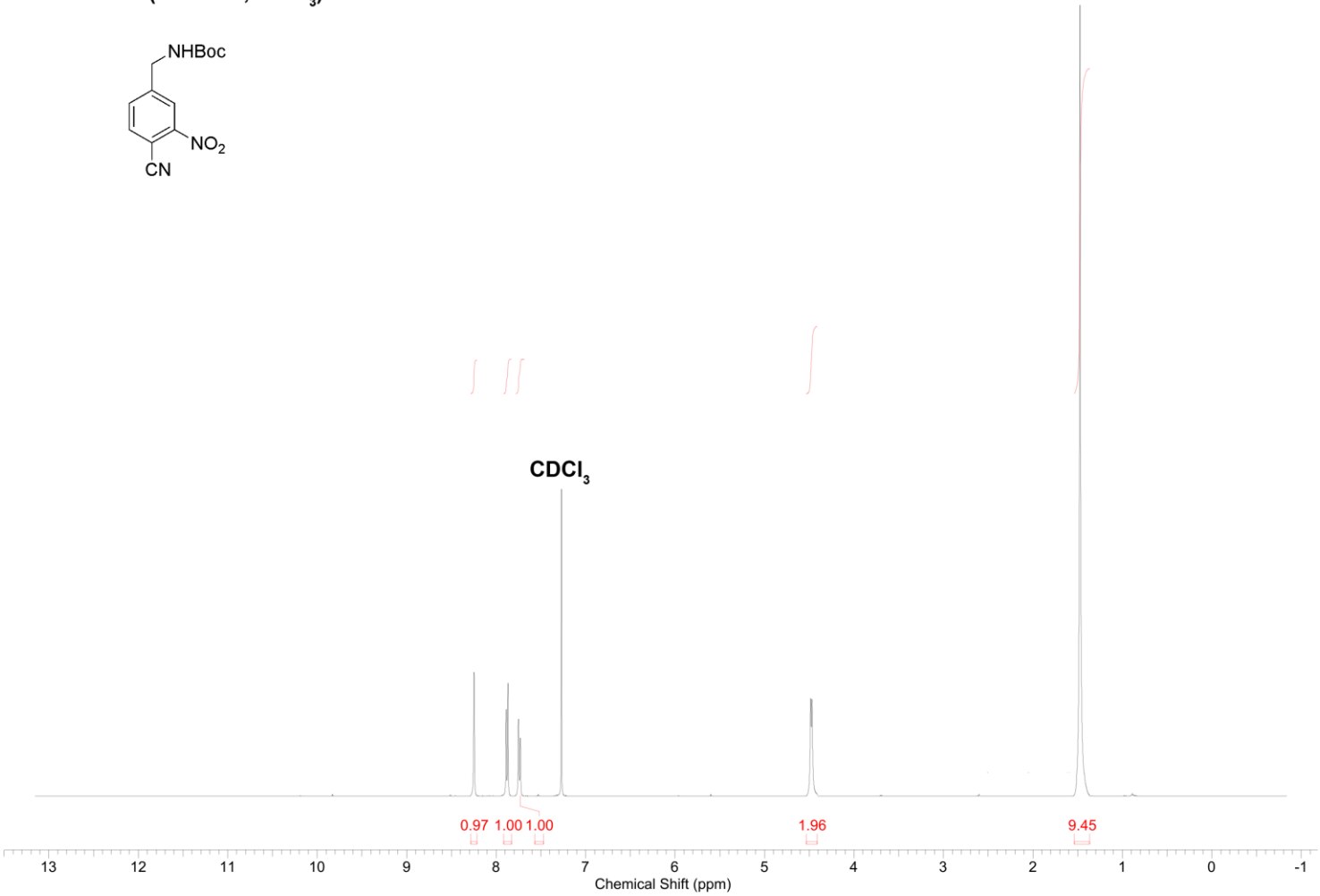

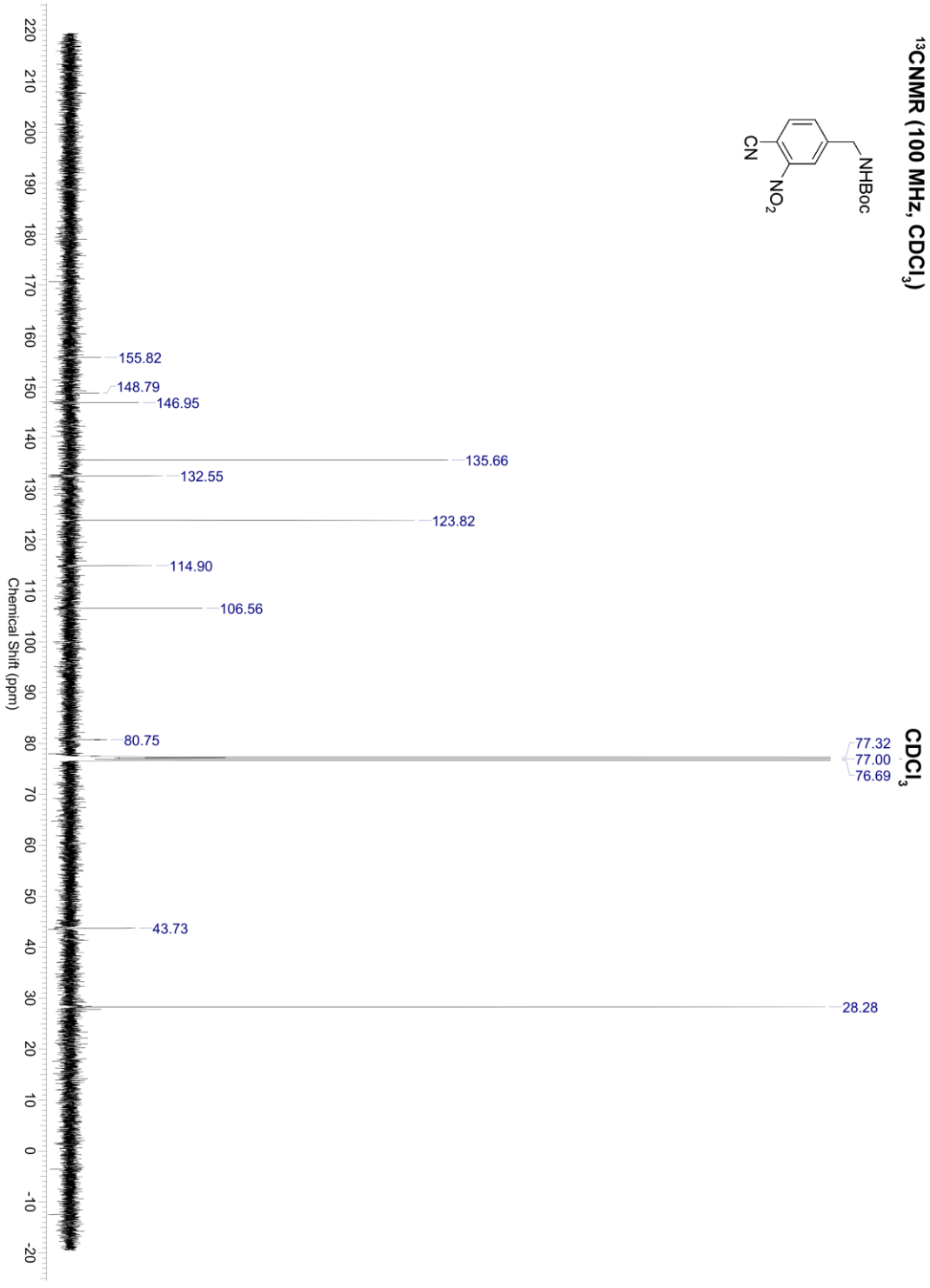
^{13}CNMR (100 MHz, $CDCl_3$)
CN
NO_2
NHBoc
155.82
148.79
146.95
135.66
132.55
123.82
114.90
106.56
80.75
77.32
77.00
76.69
$CDCl_3$
43.73
28.28
Chemical Shift (ppm)

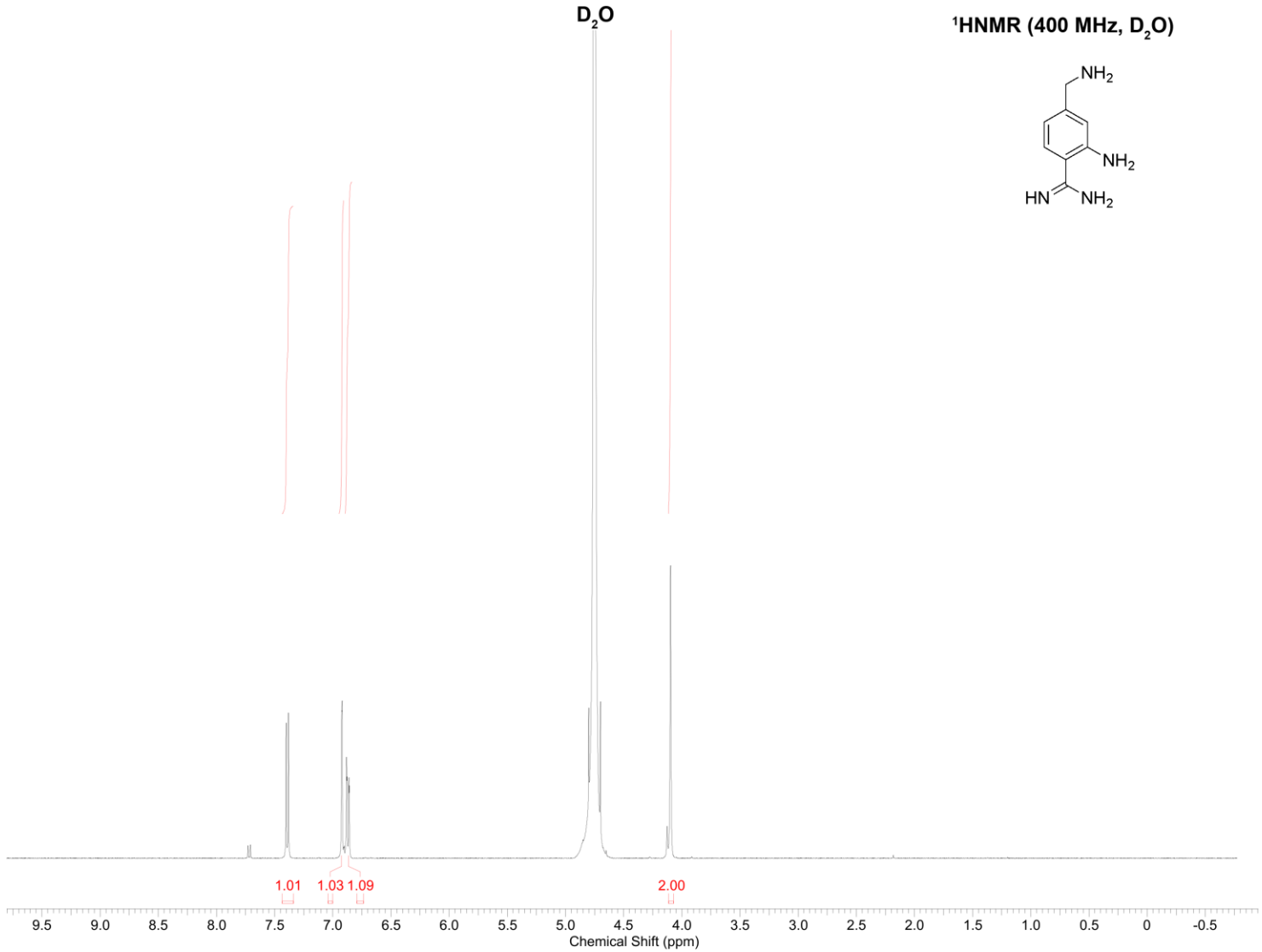
D2O
1HNMR (400 MHz, D2O)
NH2
NH2
HN
NH2
1.01
1.03
1.09
2.00
9.5
9.0
8.5
8.0
7.5
7.0
6.5
6.0
5.5
5.0
4.5
4.0
3.5
3.0
2.5
2.0
1.5
1.0
0.5
0
-0.5
Chemical Shift (ppm)

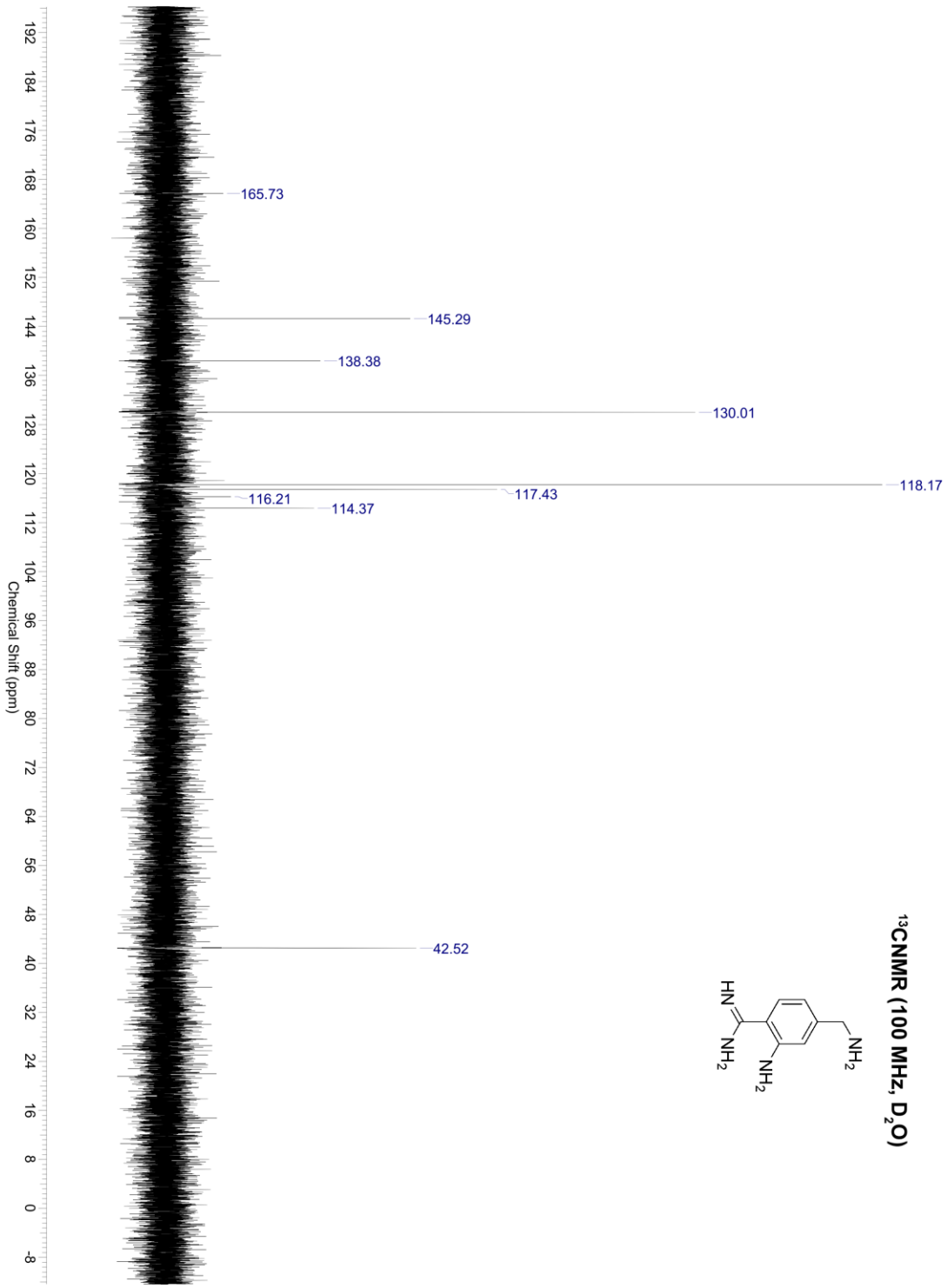

^{13}CNMR (100 MHz, D_2O)

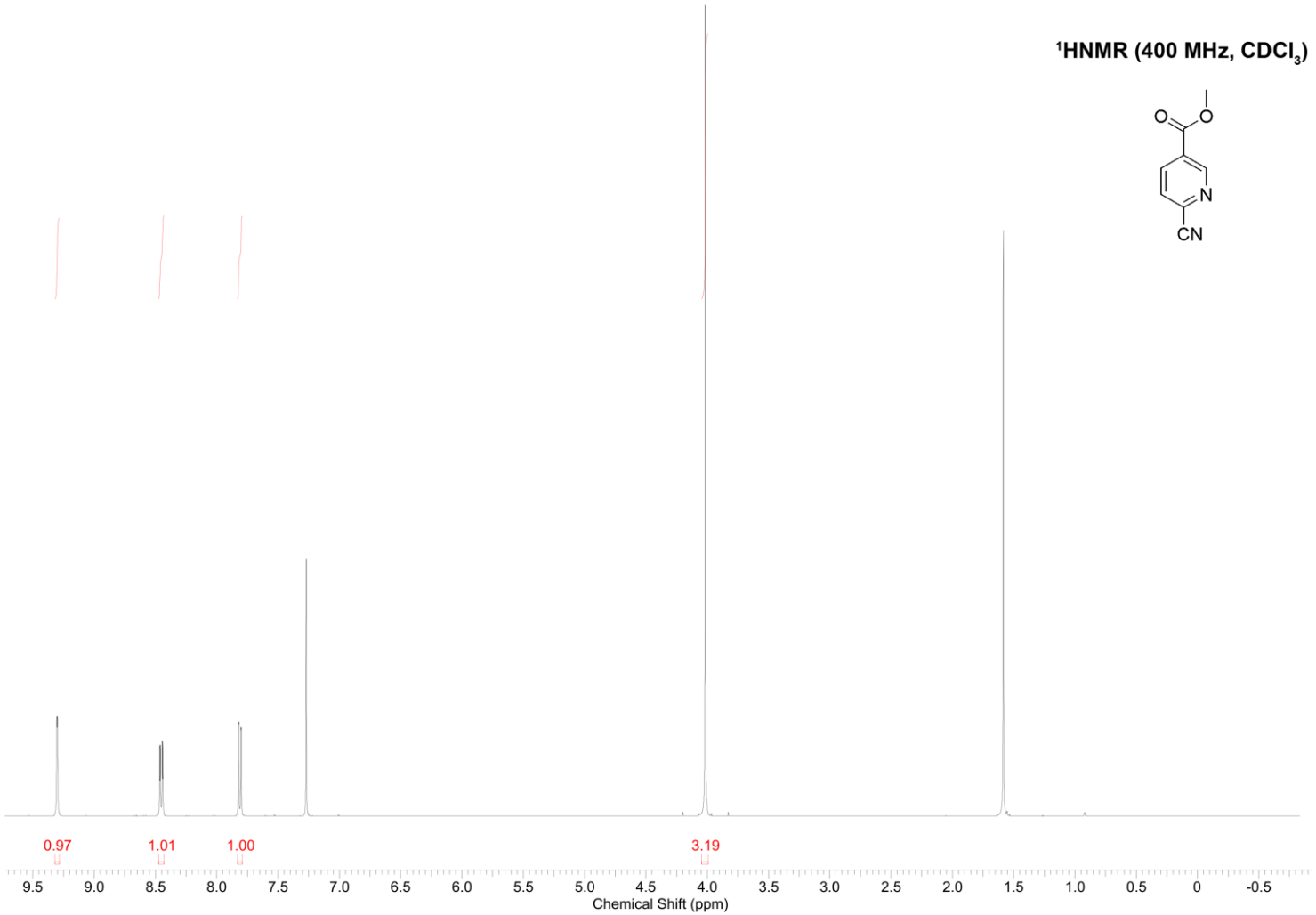
^{1}HNMR (400 MHz, $CDCl_3$)
O
O
N
CN
0.97
1.01
1.00
3.19
9.5 9.0 8.5 8.0 7.5 7.0 6.5 6.0 5.5 5.0 4.5 4.0 3.5 3.0 2.5 2.0 1.5 1.0 0.5 0 -0.5
Chemical Shift (ppm)

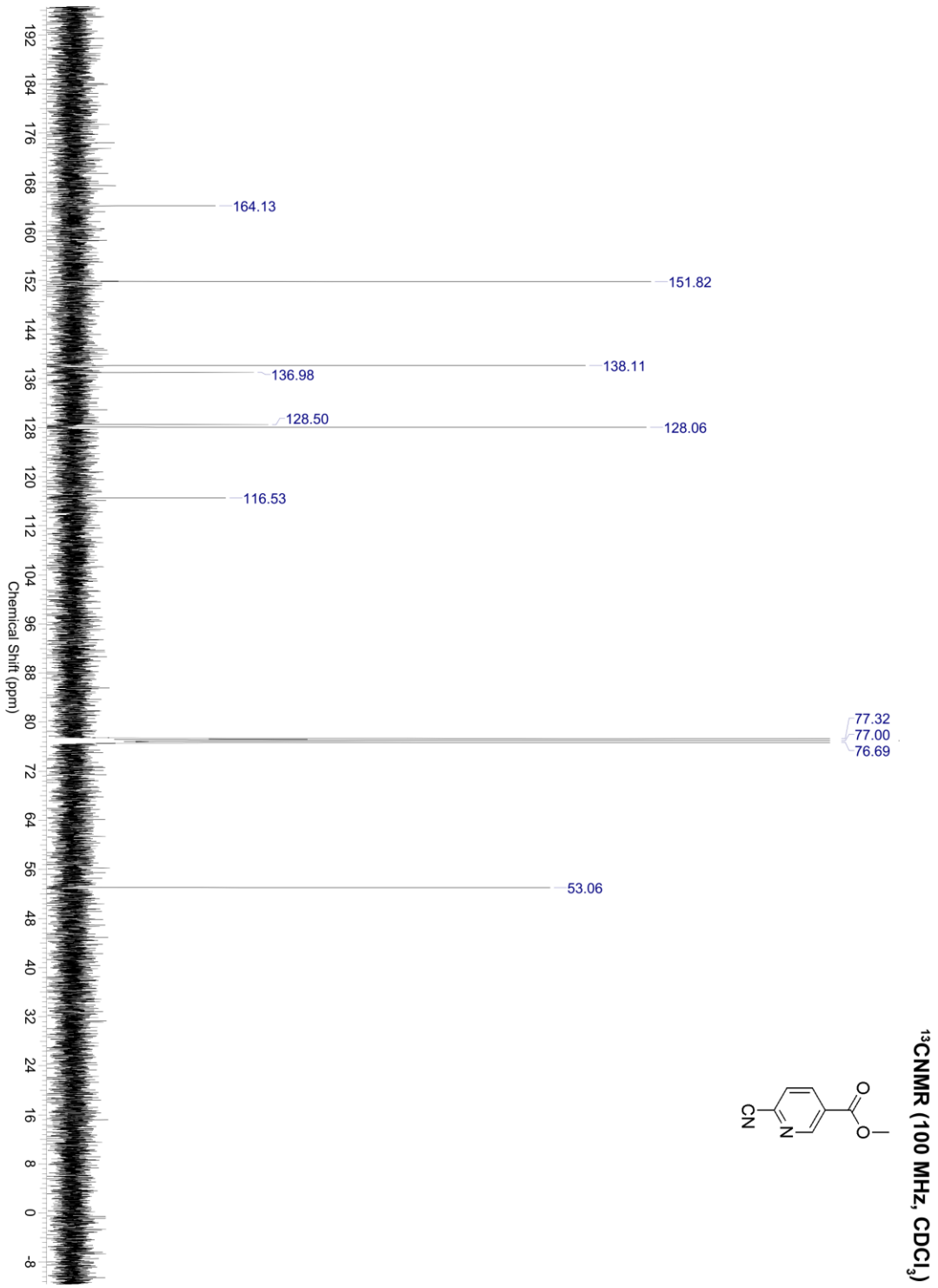

^{13}CNMR (100 MHz, $CDCl_3$)

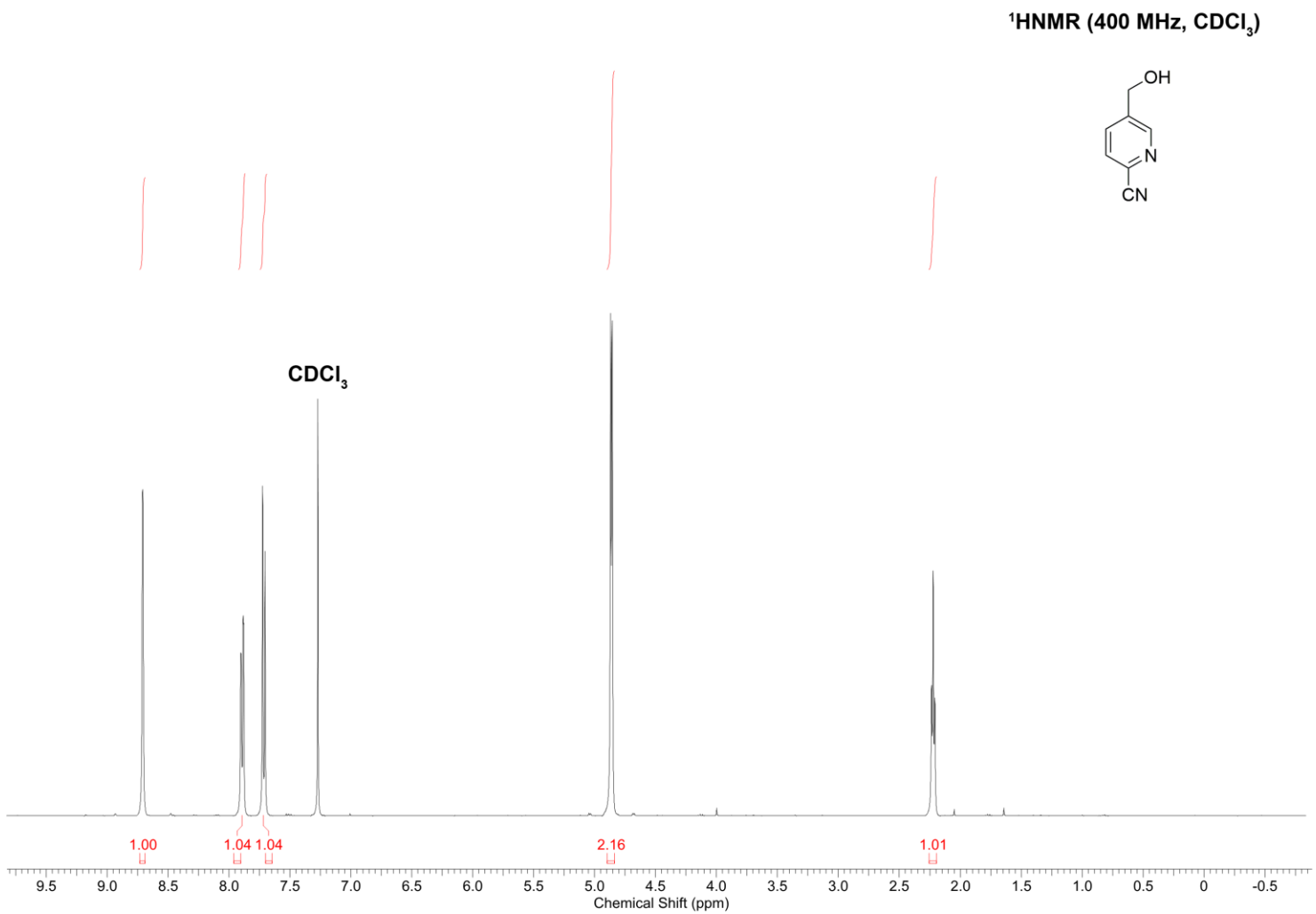
¹HNMR (400 MHz, CDCl3)
OH
N
CN
CDCl3
1.00
1.04
1.04
2.16
1.01
9.5
9.0
8.5
8.0
7.5
7.0
6.5
6.0
5.5
5.0
4.5
4.0
3.5
3.0
2.5
2.0
1.5
1.0
0.5
0
-0.5
Chemical Shift (ppm)

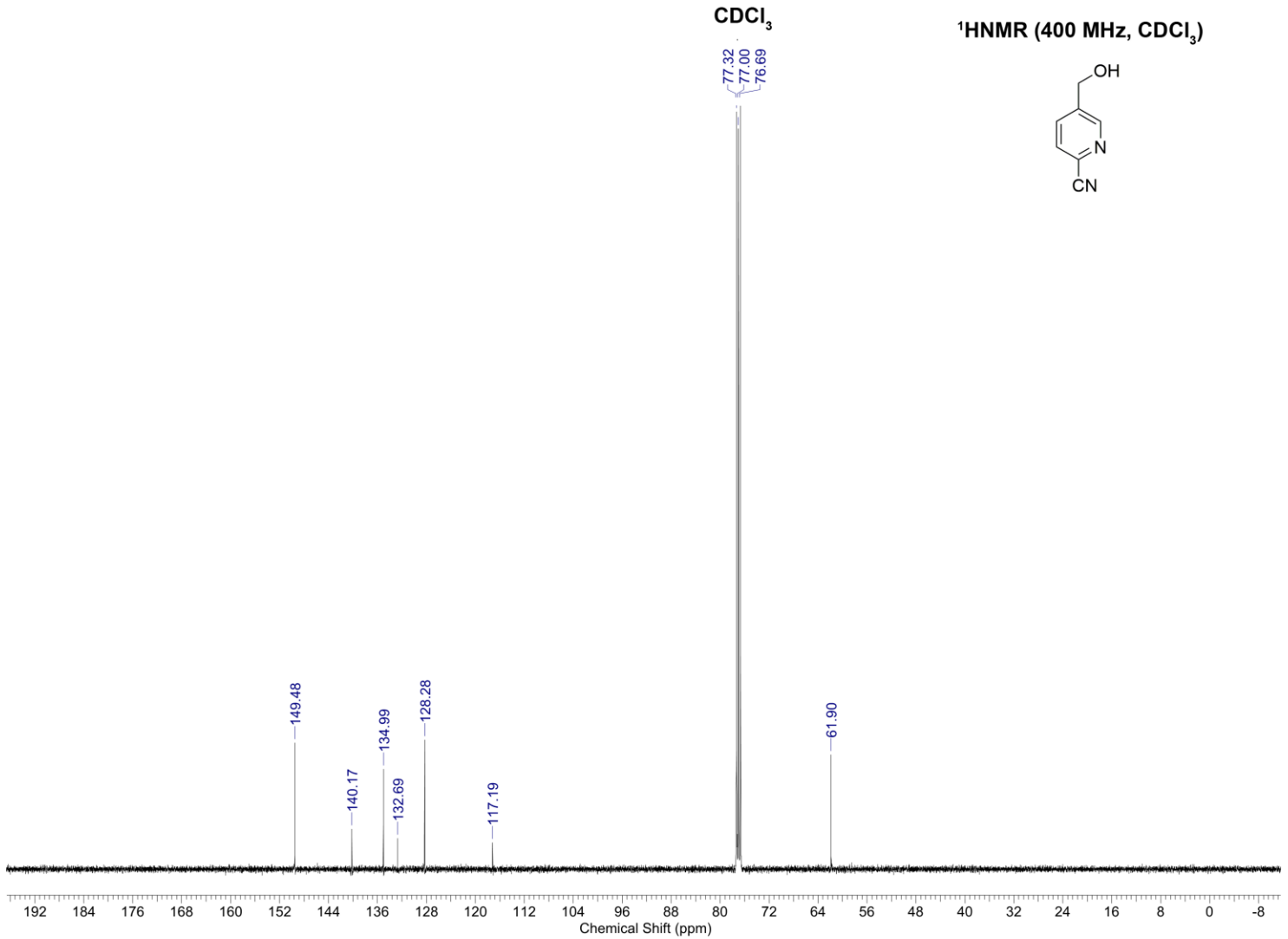
CDCl3
77.32
77.00
76.69
1HNMR (400 MHz, CDCl3)
OH
N
CN
149.48
140.17
134.99
132.69
128.28
117.19
61.90
192 184 176 168 160 152 144 136 128 120 112 104 96 88 80 72 64 56 48 40 32 24 16 8 0 -8
Chemical Shift (ppm)

^{1}HNMR (400 MHz, $CDCl_3$)

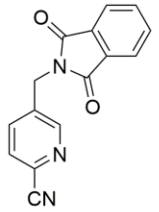

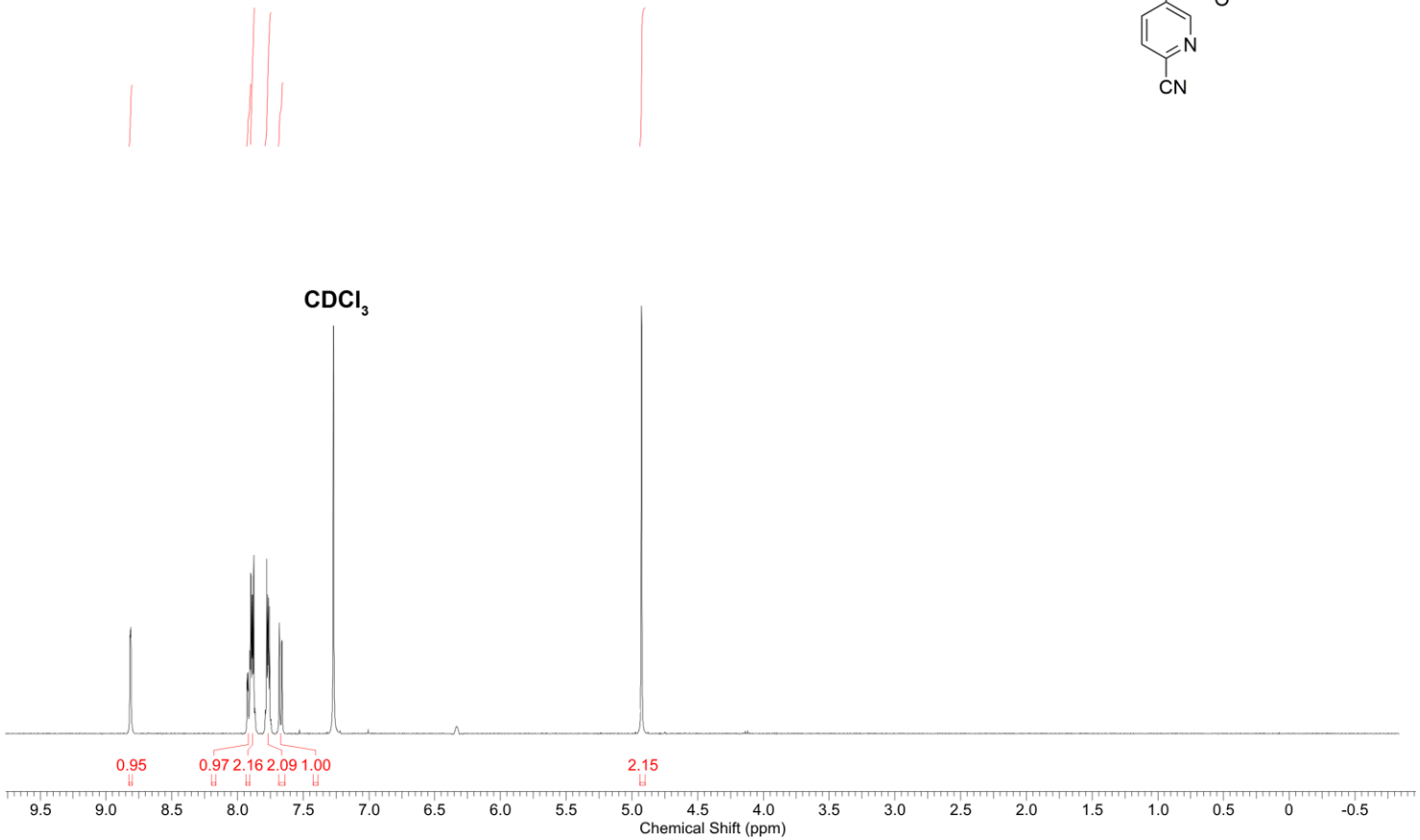

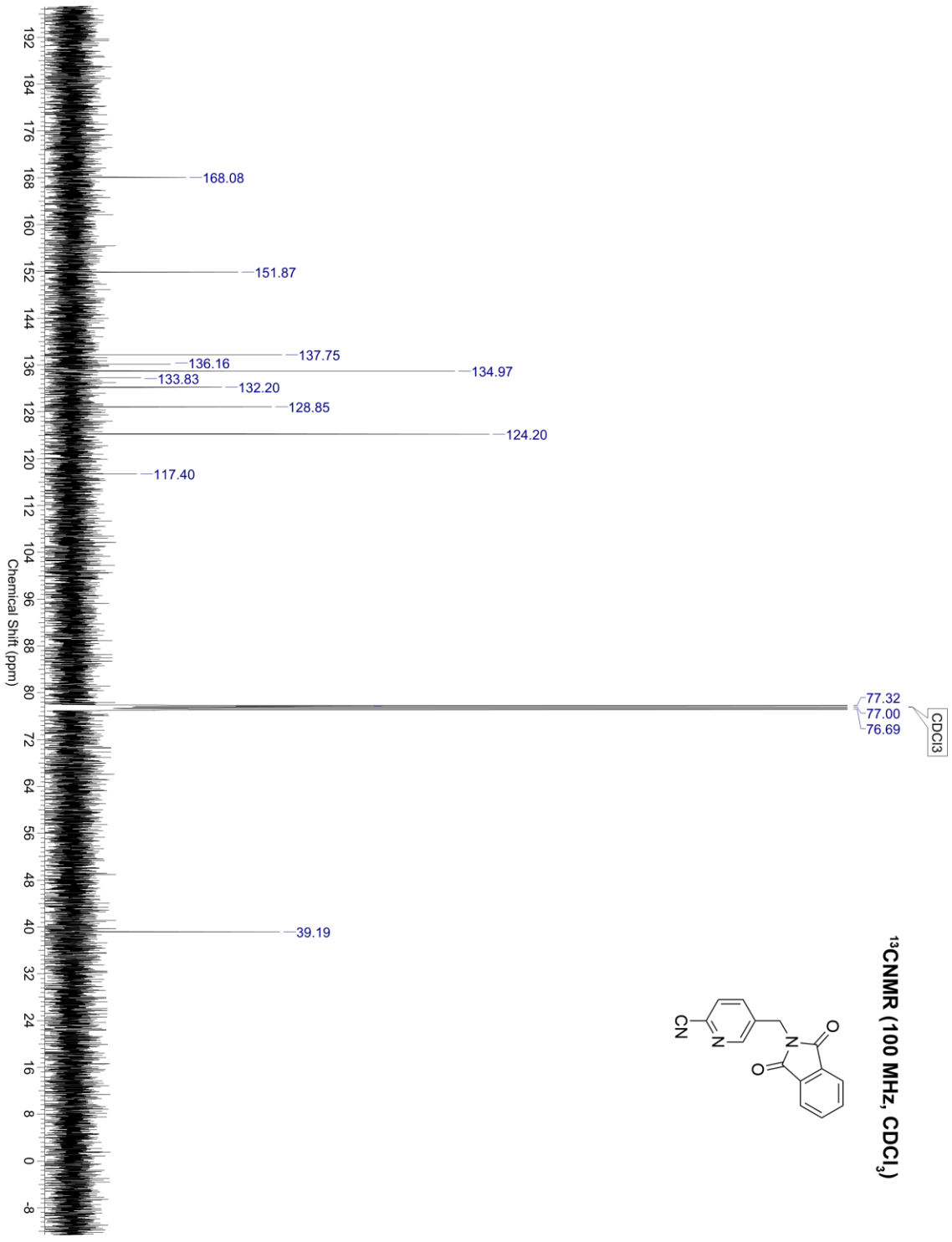

^{13}CNMR (100 MHz, $CDCl_3$)

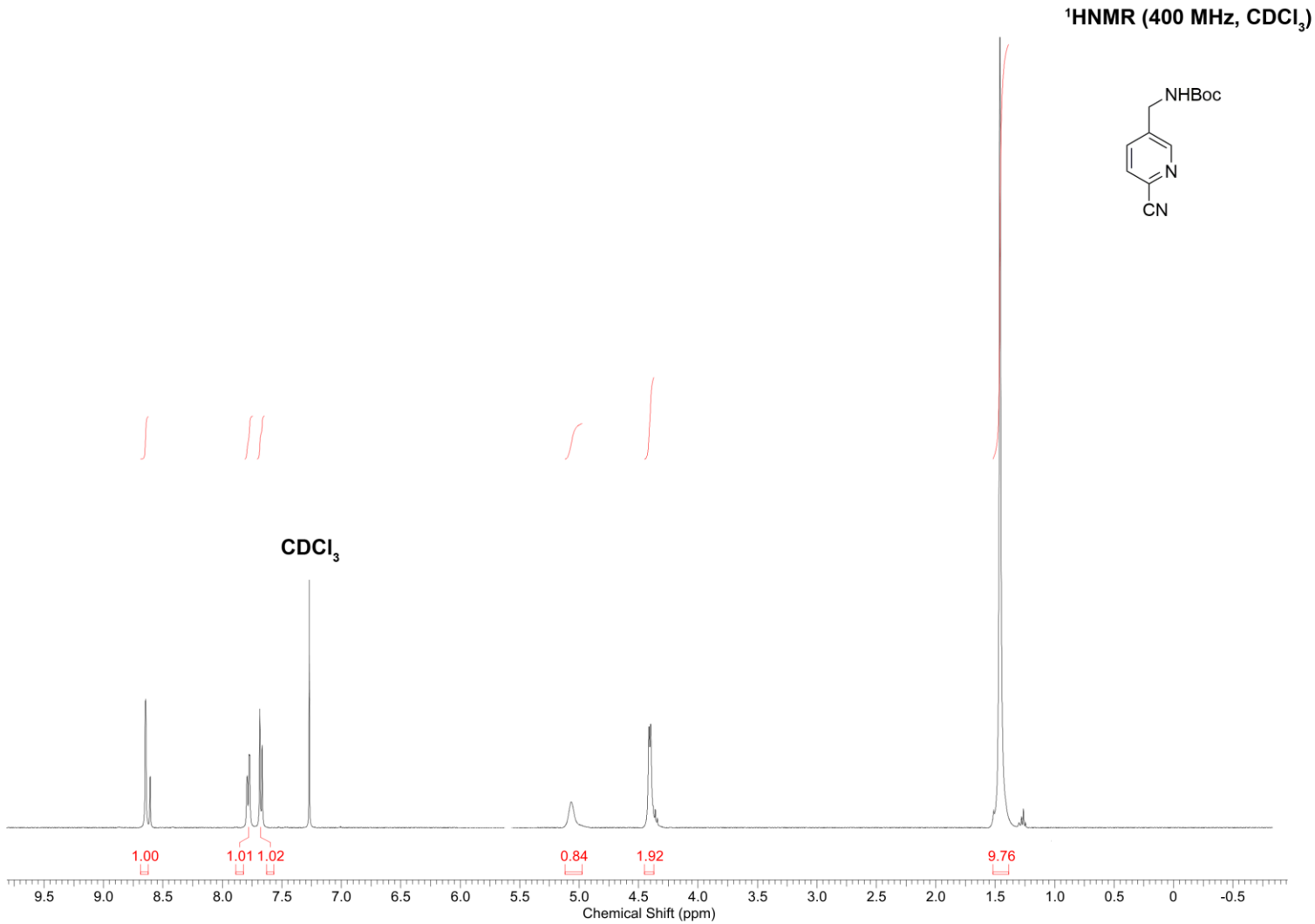
¹HNMR (400 MHz, CDCl3)
NHBoc
N
CN
CDCl3
1.00
1.01
1.02
0.84
1.92
9.76
9.5 9.0 8.5 8.0 7.5 7.0 6.5 6.0 5.5 5.0 4.5 4.0 3.5 3.0 2.5 2.0 1.5 1.0 0.5 0 -0.5
Chemical Shift (ppm)

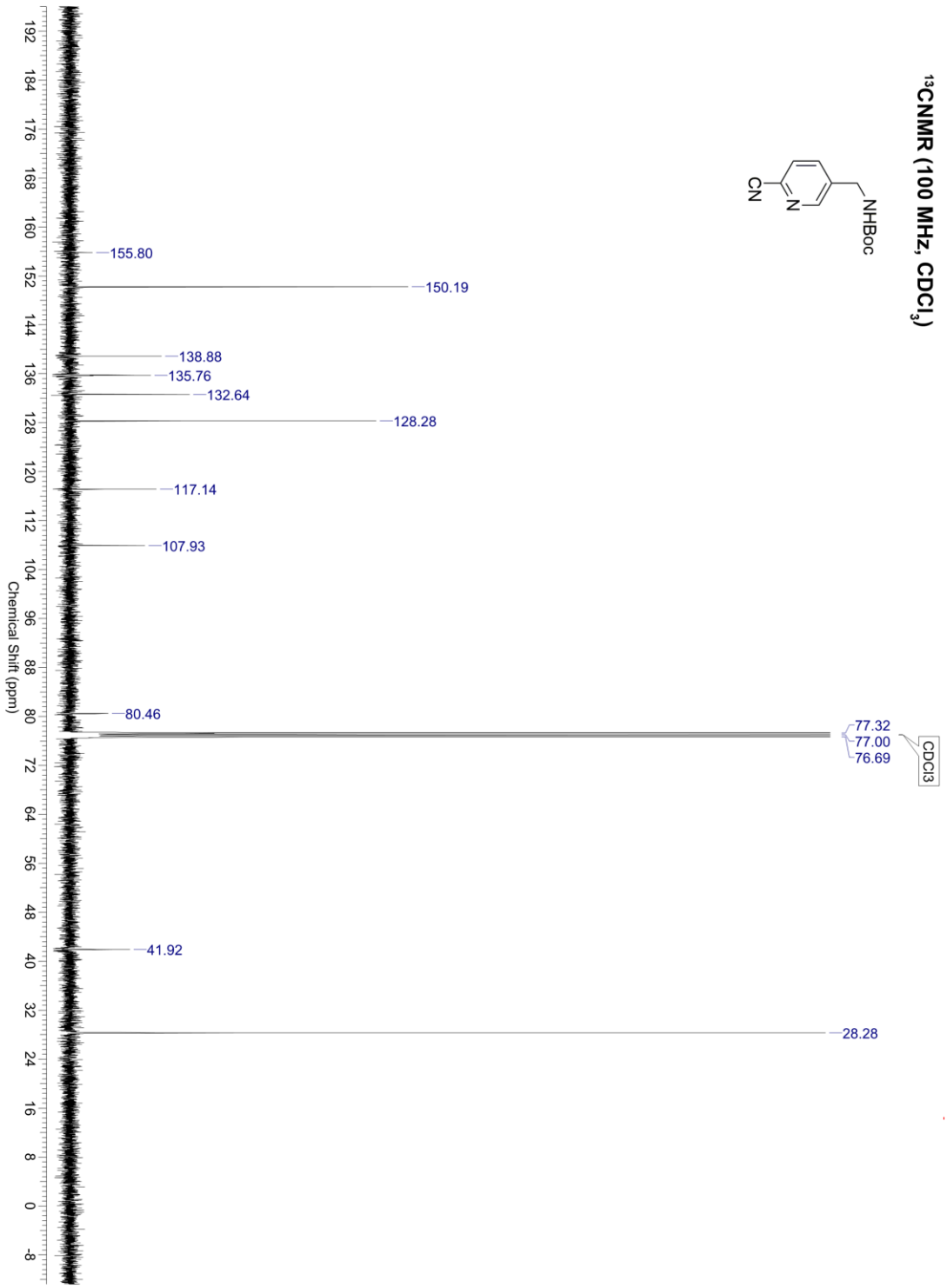
^{13}CNMR (100 MHz, $CDCl_3$)
CN
N
NHBoc
155.80
150.19
138.88
135.76
132.64
128.28
117.14
107.93
80.46
77.32
77.00
76.69
CDCl3
41.92
28.28
Chemical Shift (ppm)

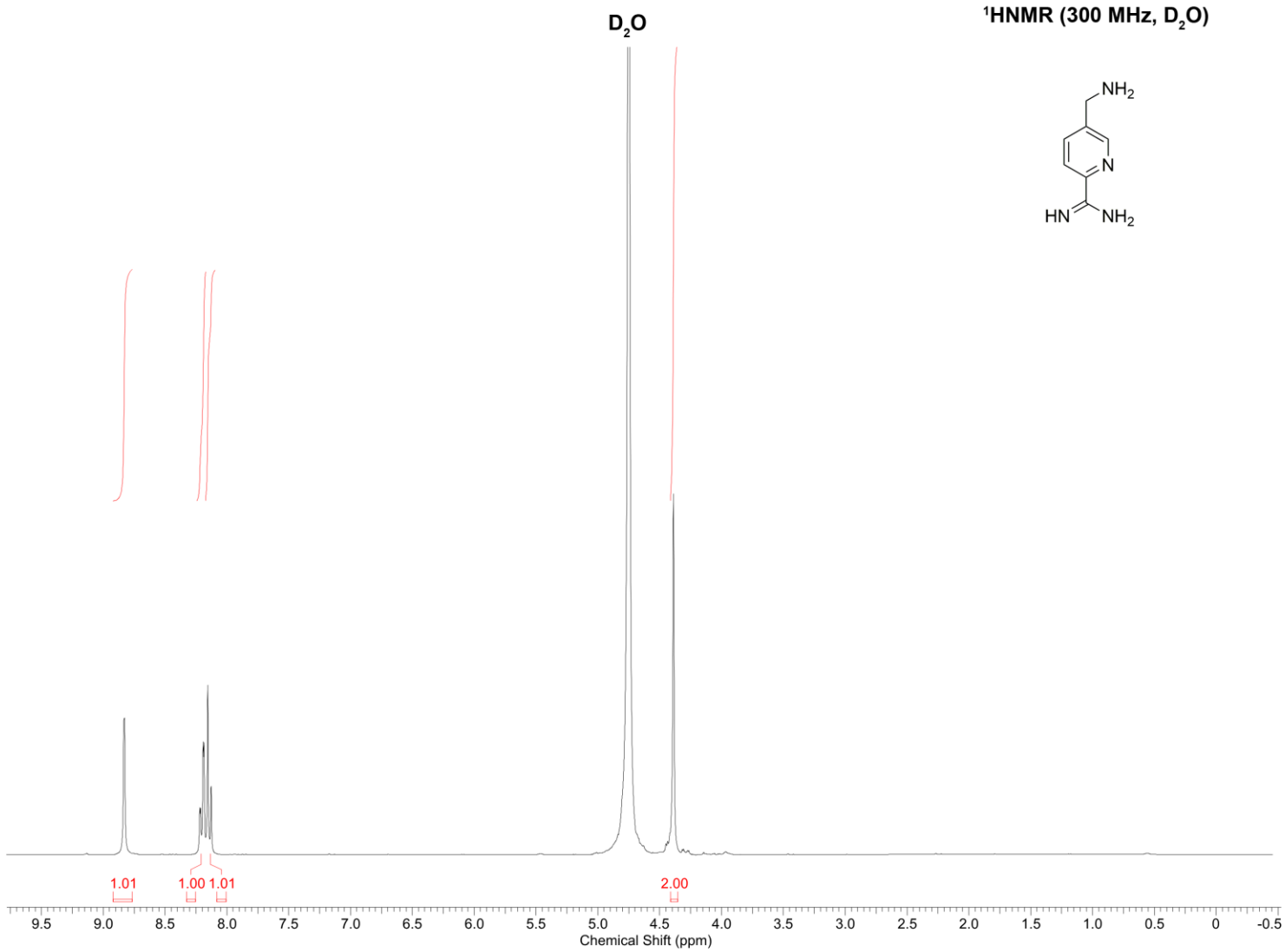
D2O
1HNMR (300 MHz, D2O)
NH2
N
HN
NH2
1.01
1.00
1.01
2.00
9.5
9.0
8.5
8.0
7.5
7.0
6.5
6.0
5.5
5.0
4.5
4.0
3.5
3.0
2.5
2.0
1.5
1.0
0.5
0
-0.5
Chemical Shift (ppm)

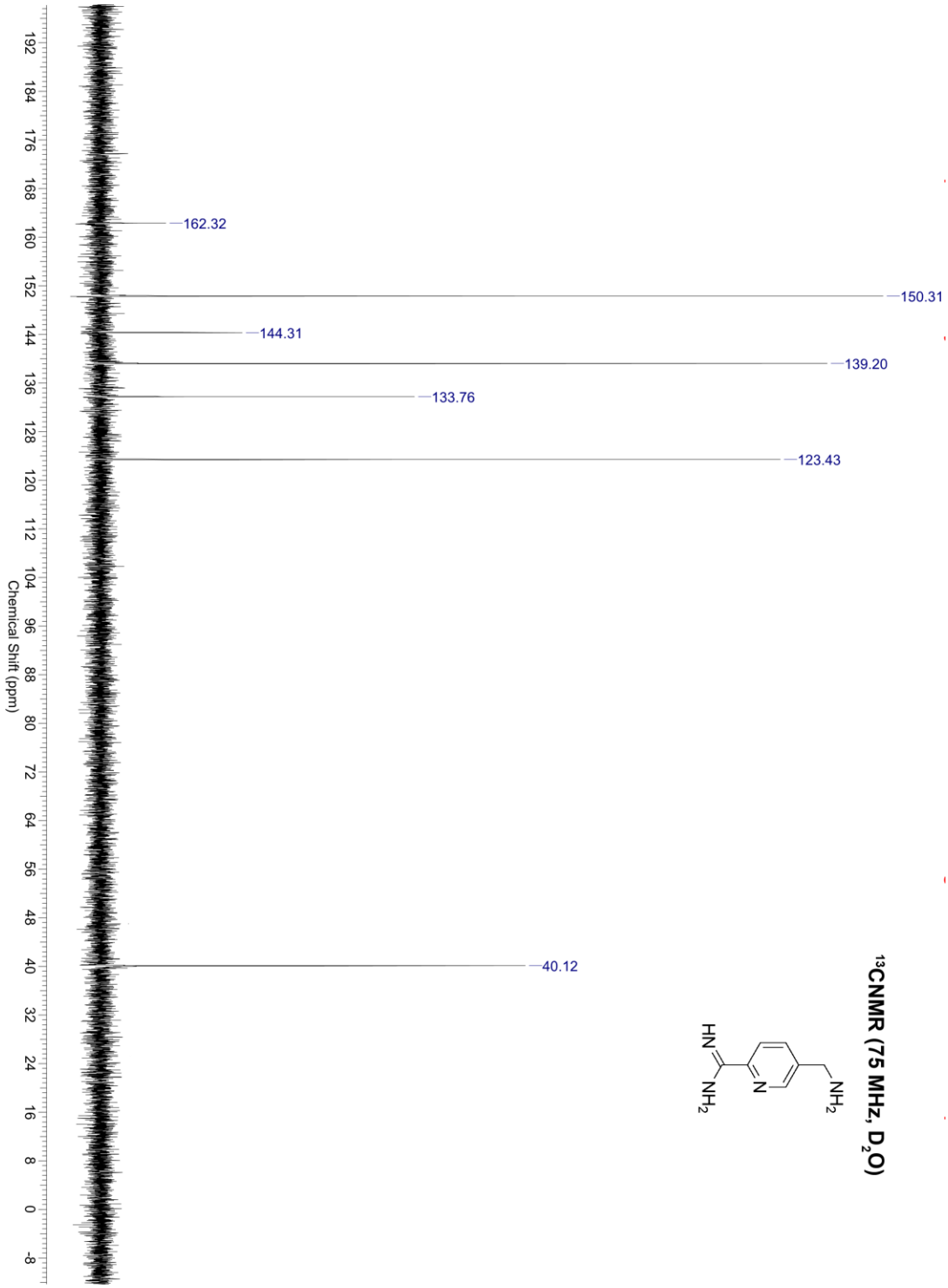
162.32
150.31
144.31
139.20
133.76
123.43
40.12
Chemical Shift (ppm)
192 184 176 168 160 152 144 136 128 120 112 104 96 88 80 72 64 56 48 40 32 24 16 8 0 -8
HN
NH2
N
NH2
13CNMR (75 MHz, D2O)

APPENDIX IV

All the HPLC chromatograms of peptides and NMR spectra for small molecule intermediates synthesized in chapter 3 is presented in this appendix.

HPLC chromatograms:

Compound **3**:

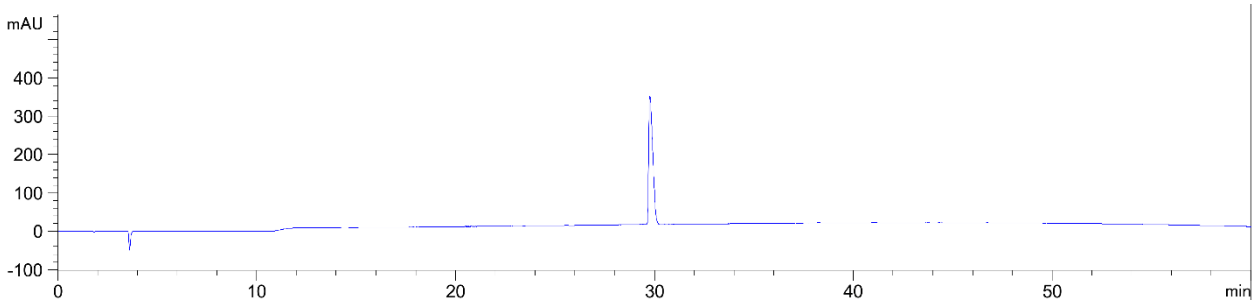

Compound **4**:

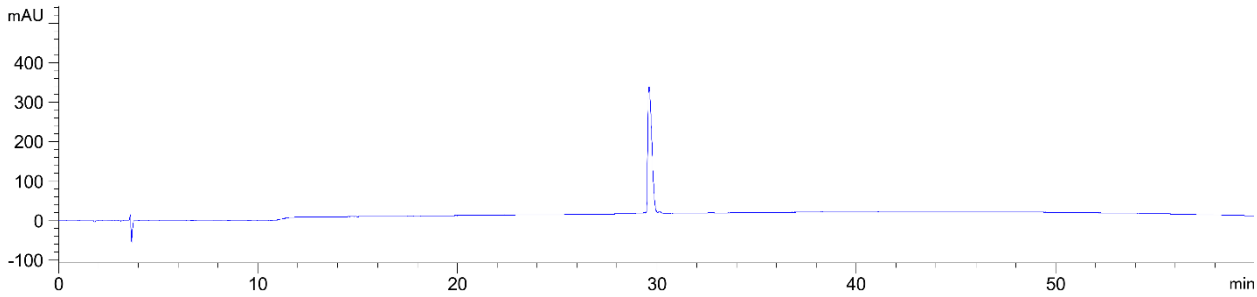

Compound **5**:

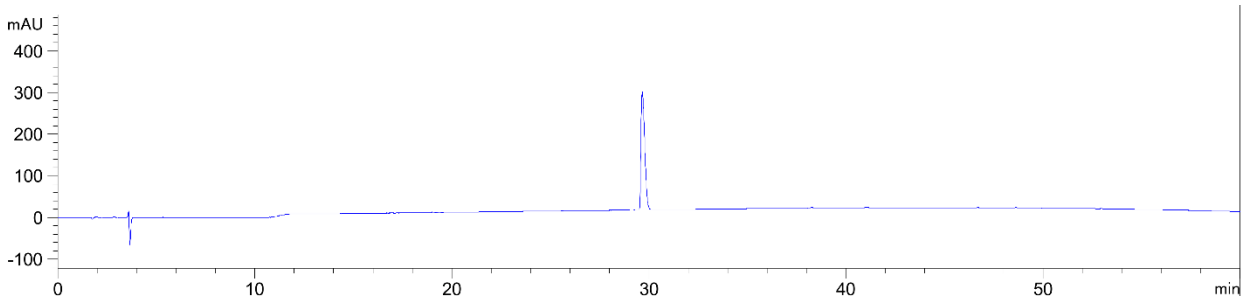

Compound **6**:

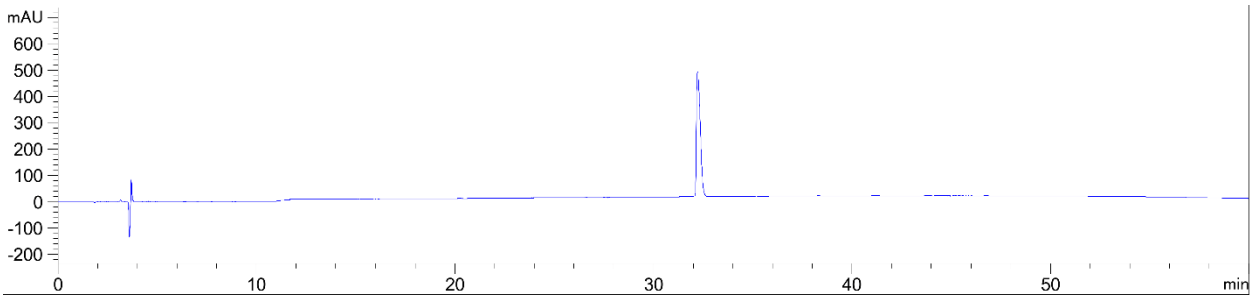

Compound **7**:

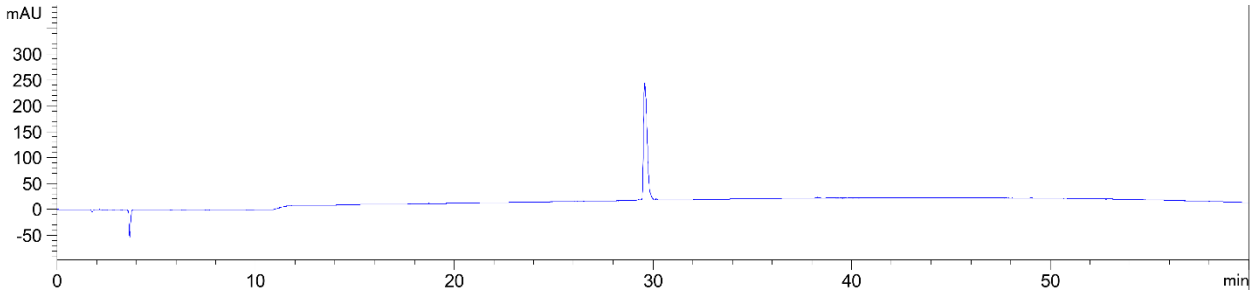

Compound **8**:

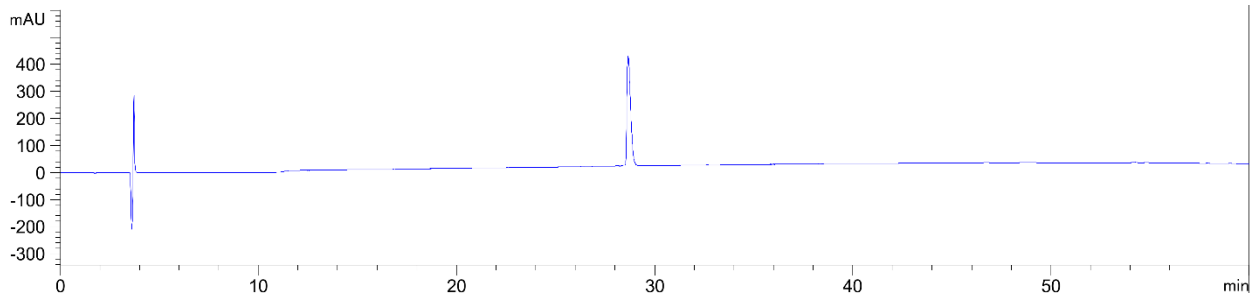

Compound **9**:

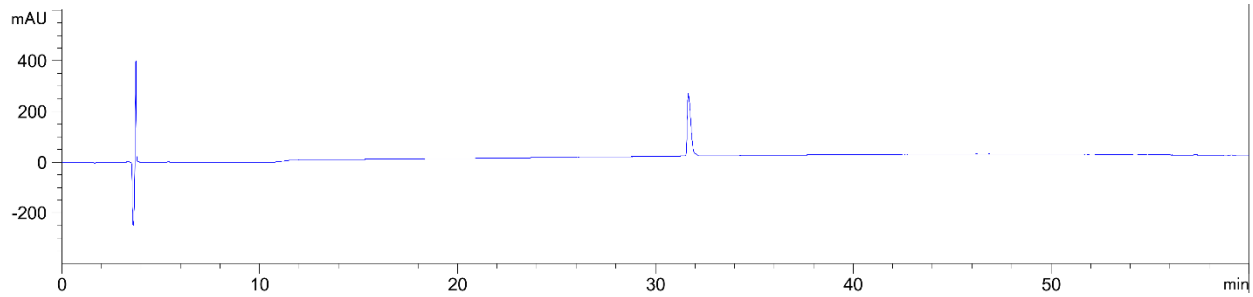

Compound **10**:

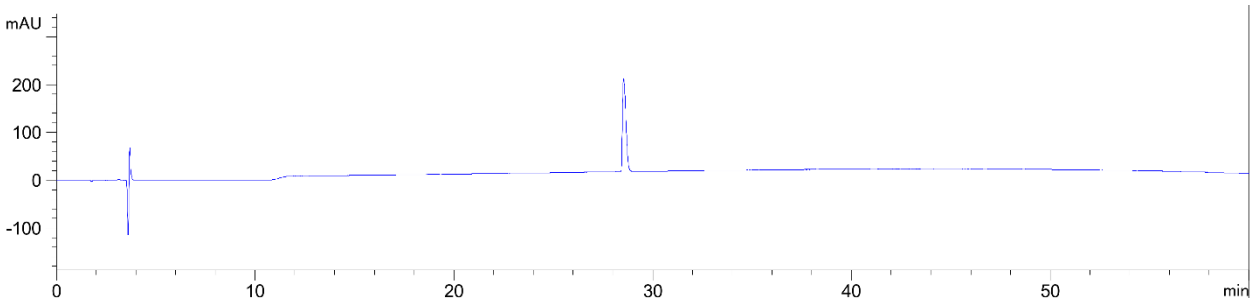

Compound **11**:

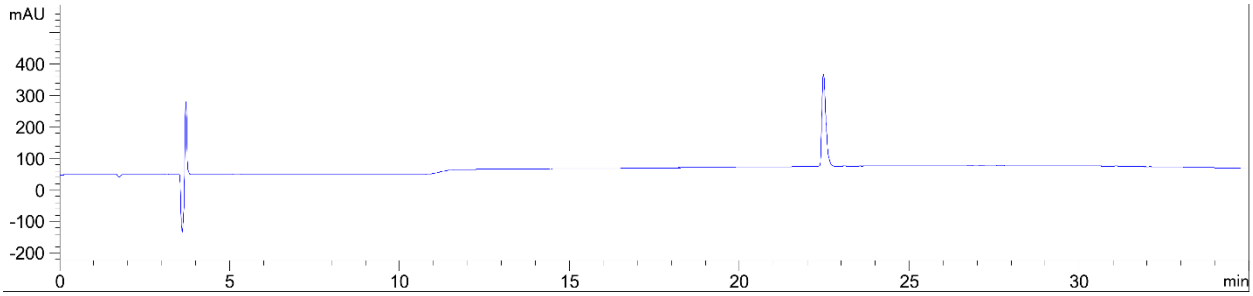

Compound **12**:

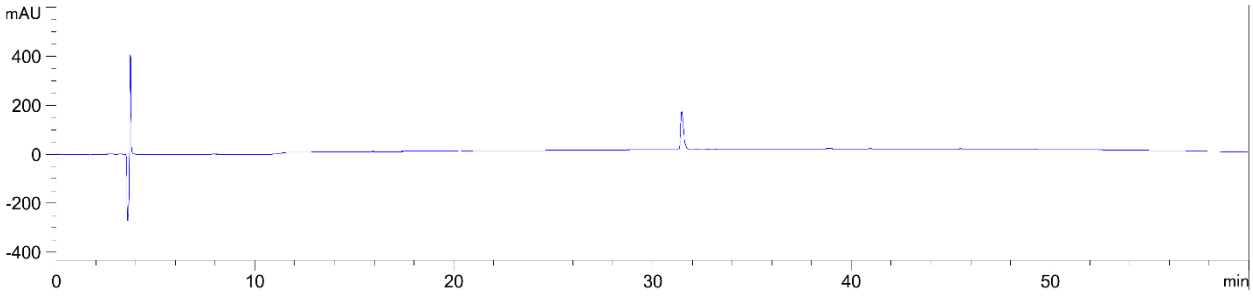

Compound 1**3**:

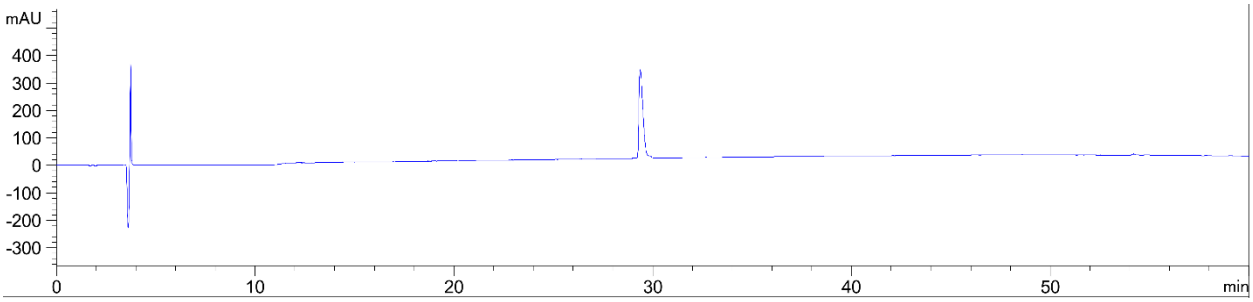

Compound **14**:

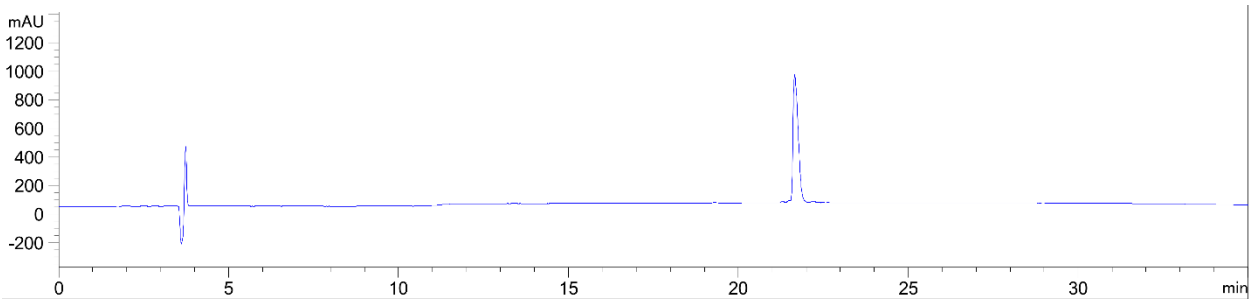

Compound **15**:

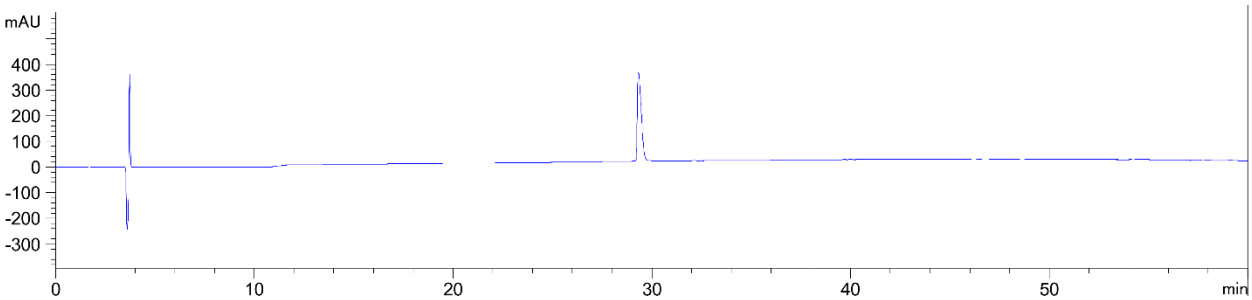

Compound **16**:

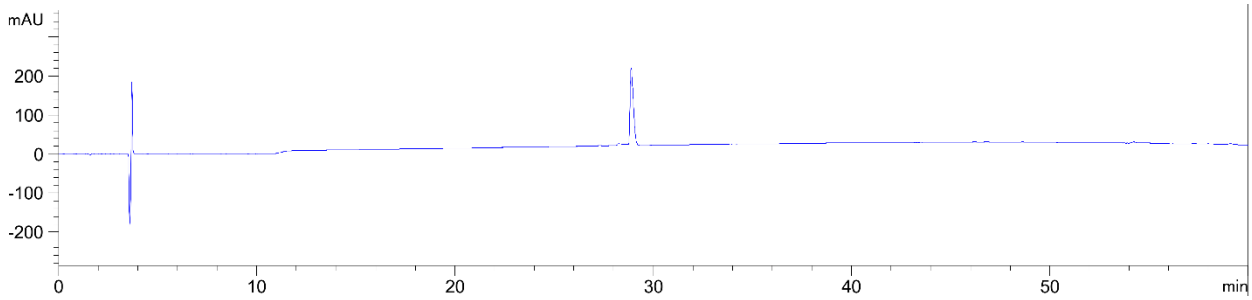

Compound **17**:

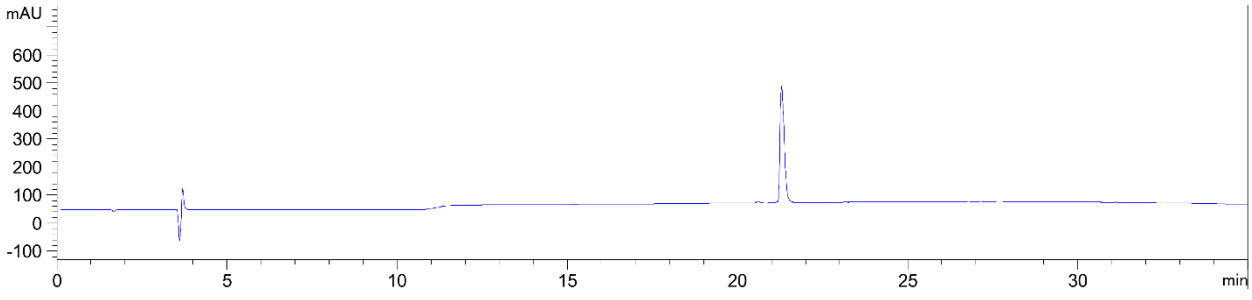

Compound **18**:

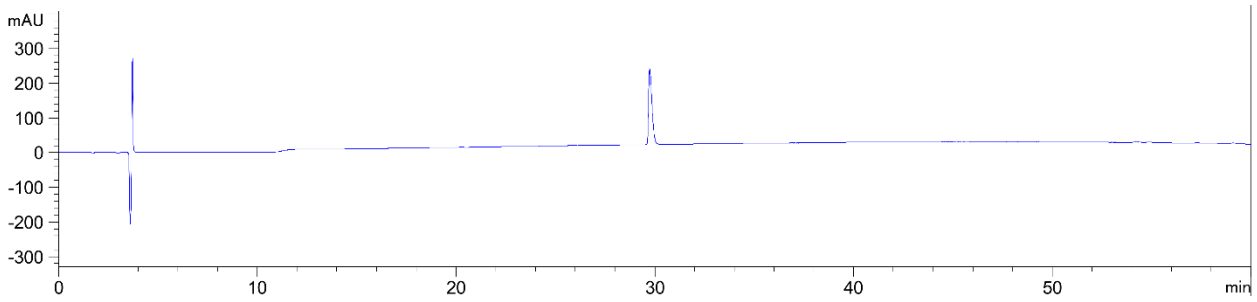

Compound **19**:

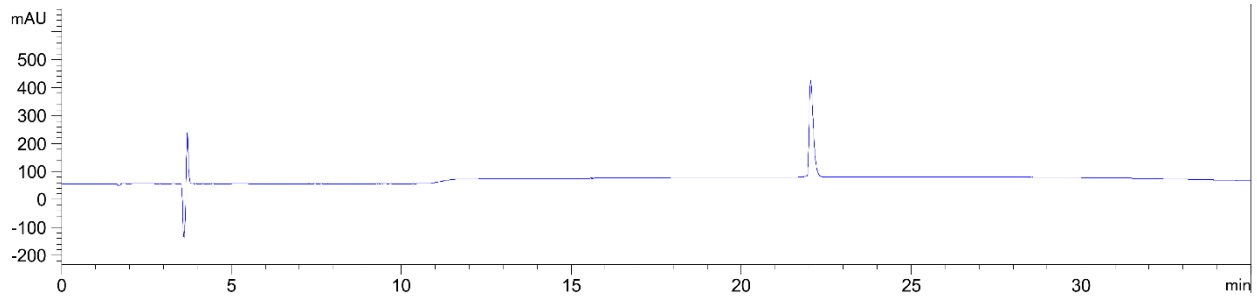

Compound **20**:

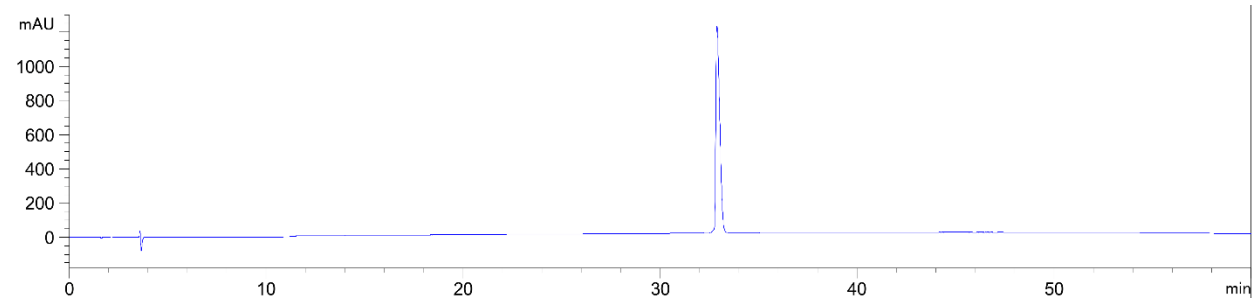

Compound **21**:

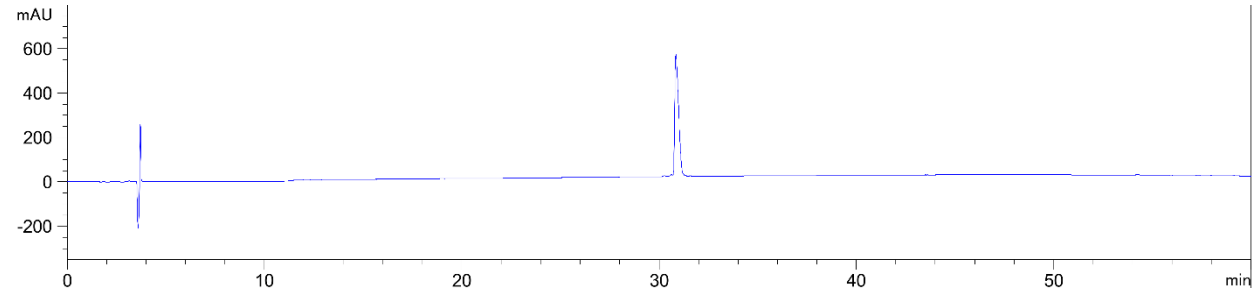

Compound **28**:

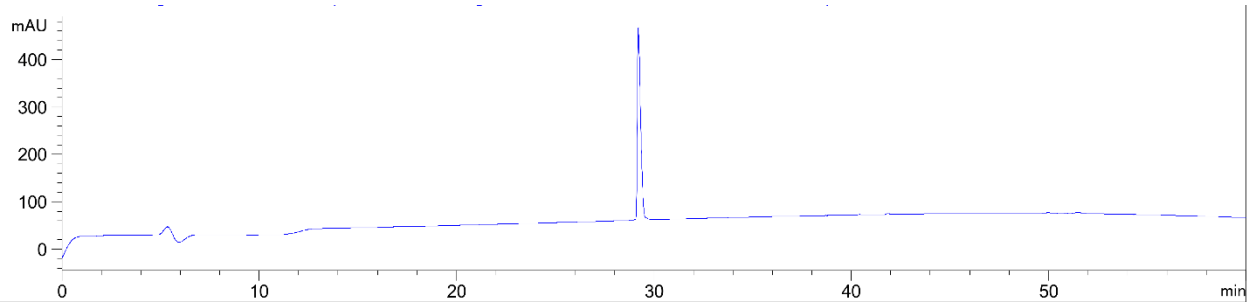

Compound **29**:

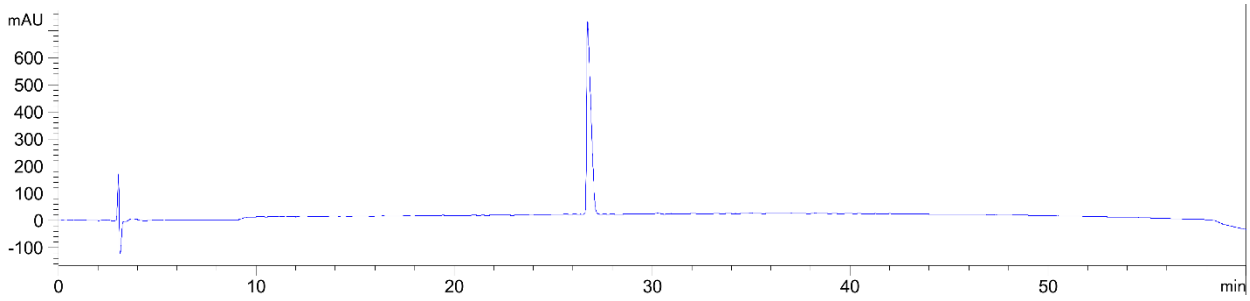

Compound **30**:

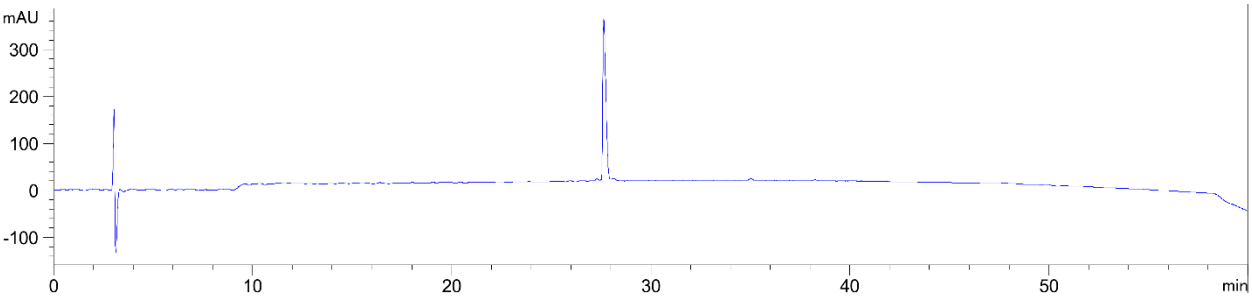

Compound **31**:

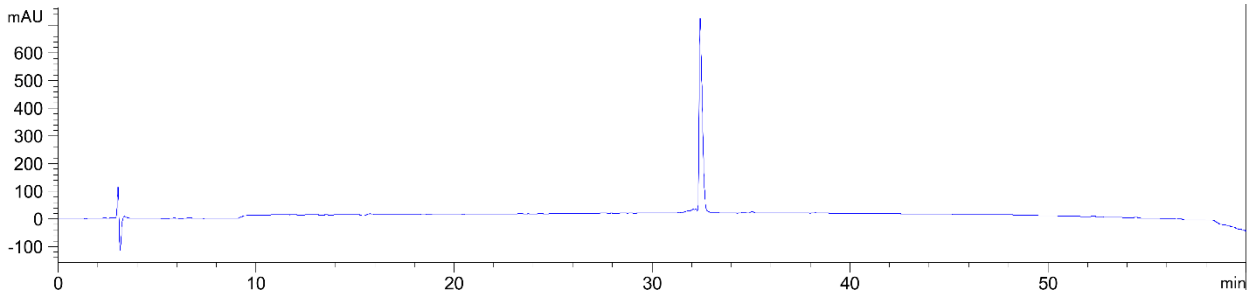

Compound **32**:

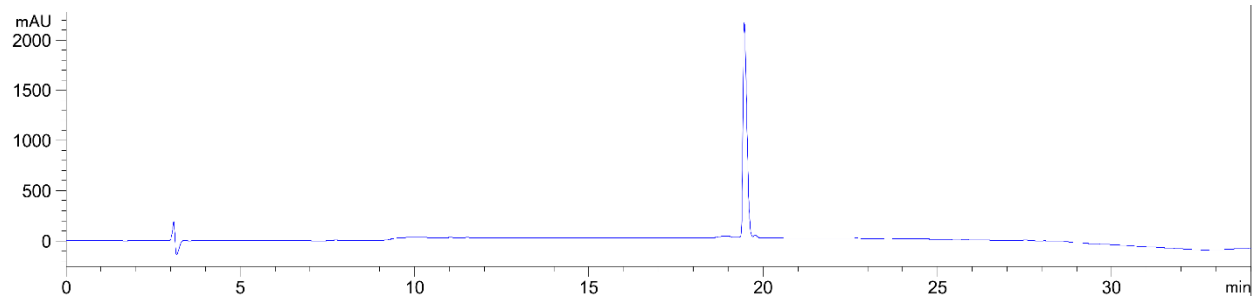

Compound **33**:

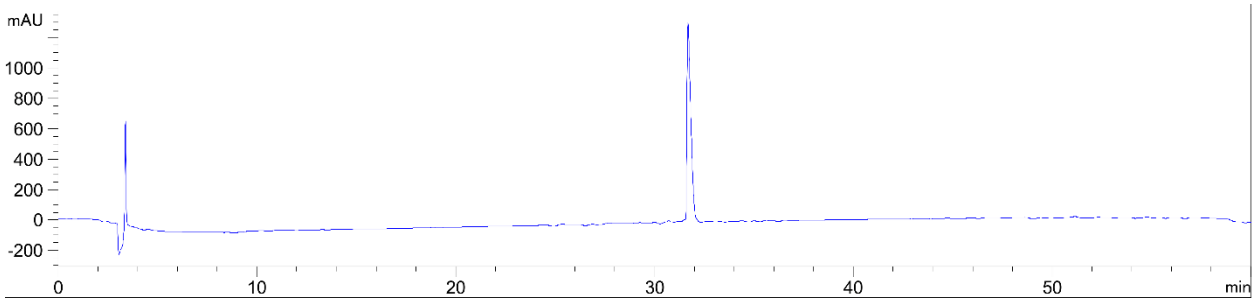

Compound **35**:

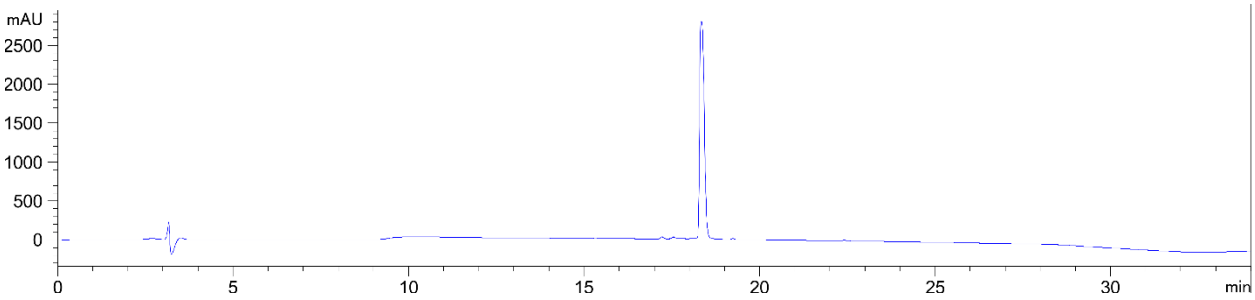

Compound **36**:

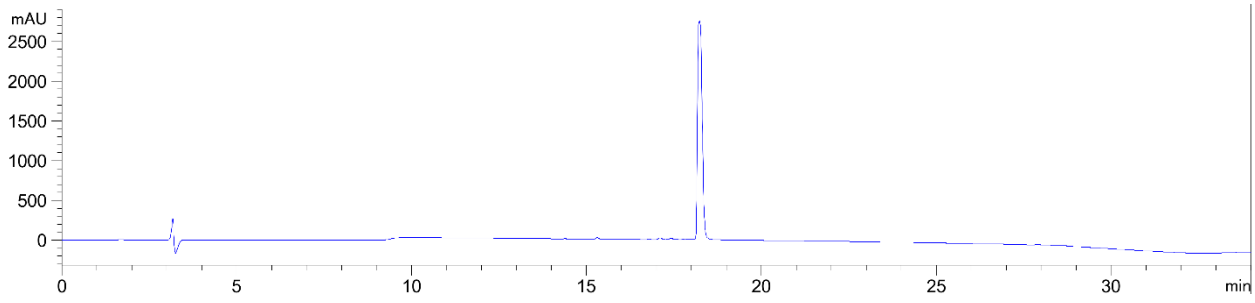

Compound **37**:

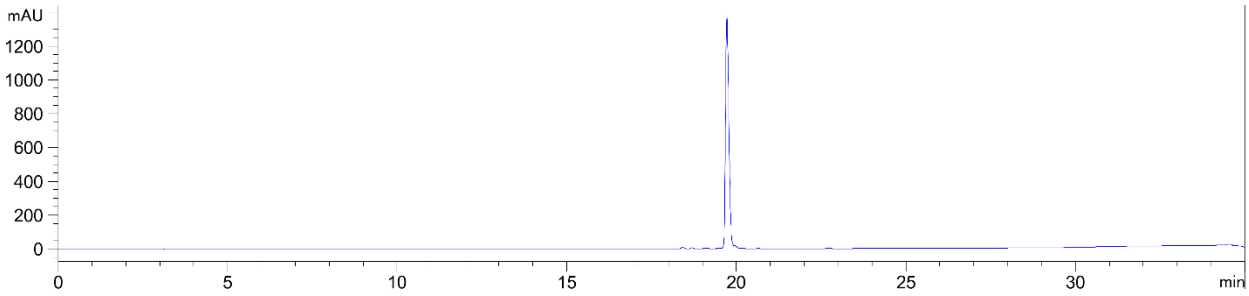

Compound **38**:

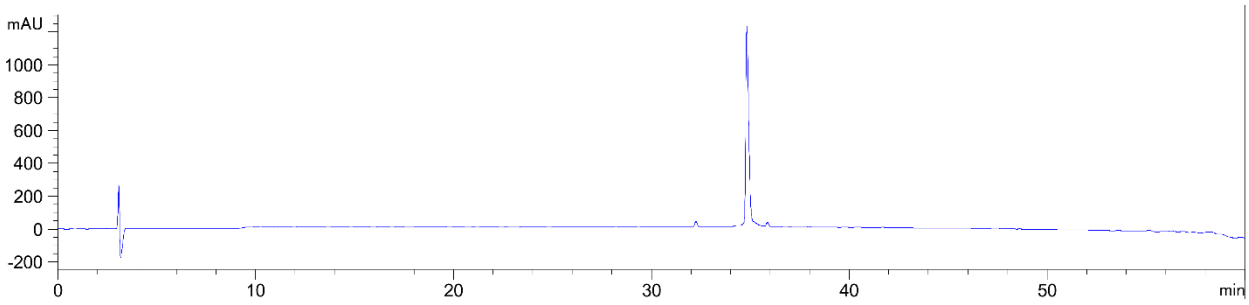

^{1}H NMR and ^{13}C NMR spectra:

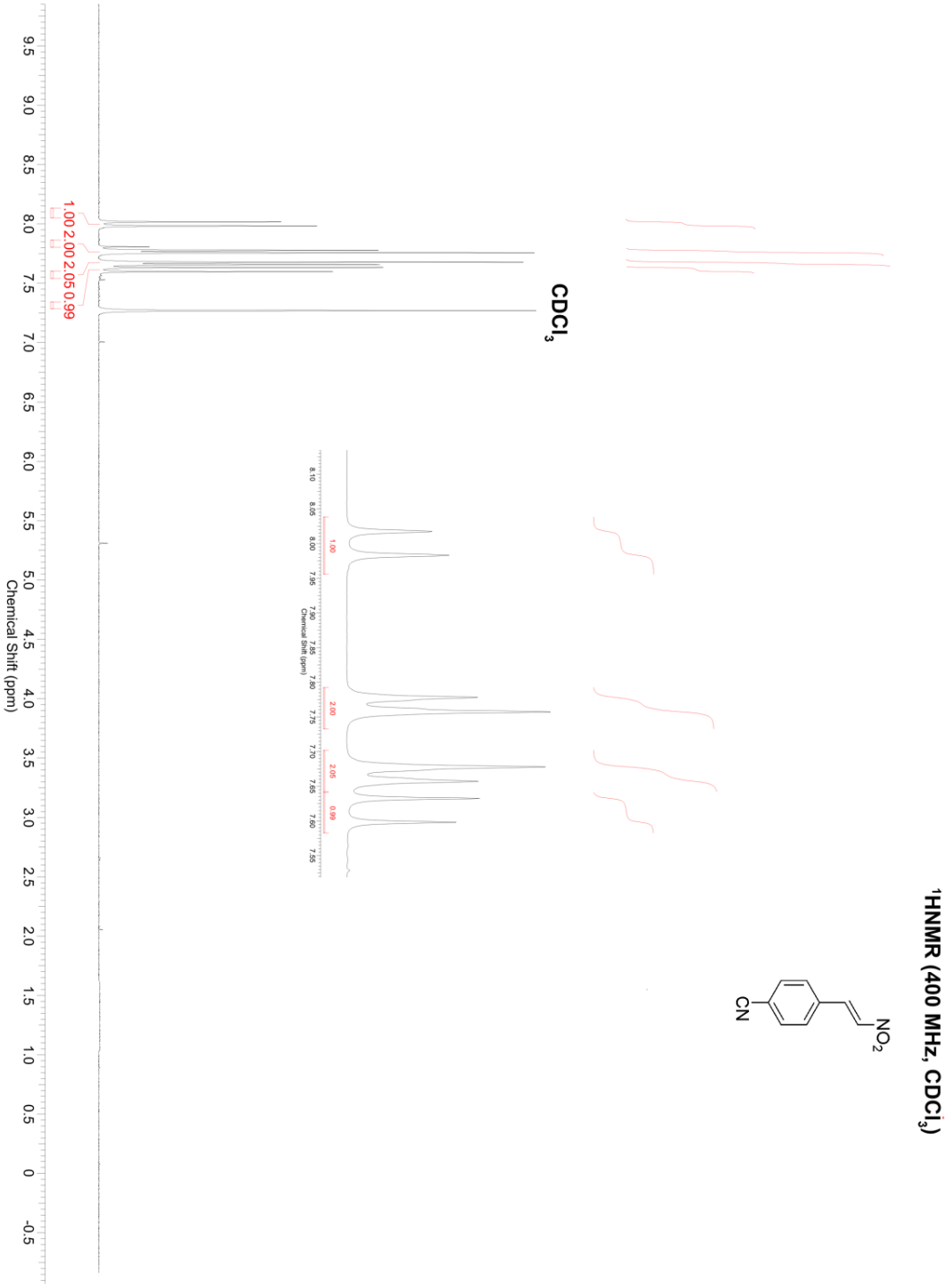

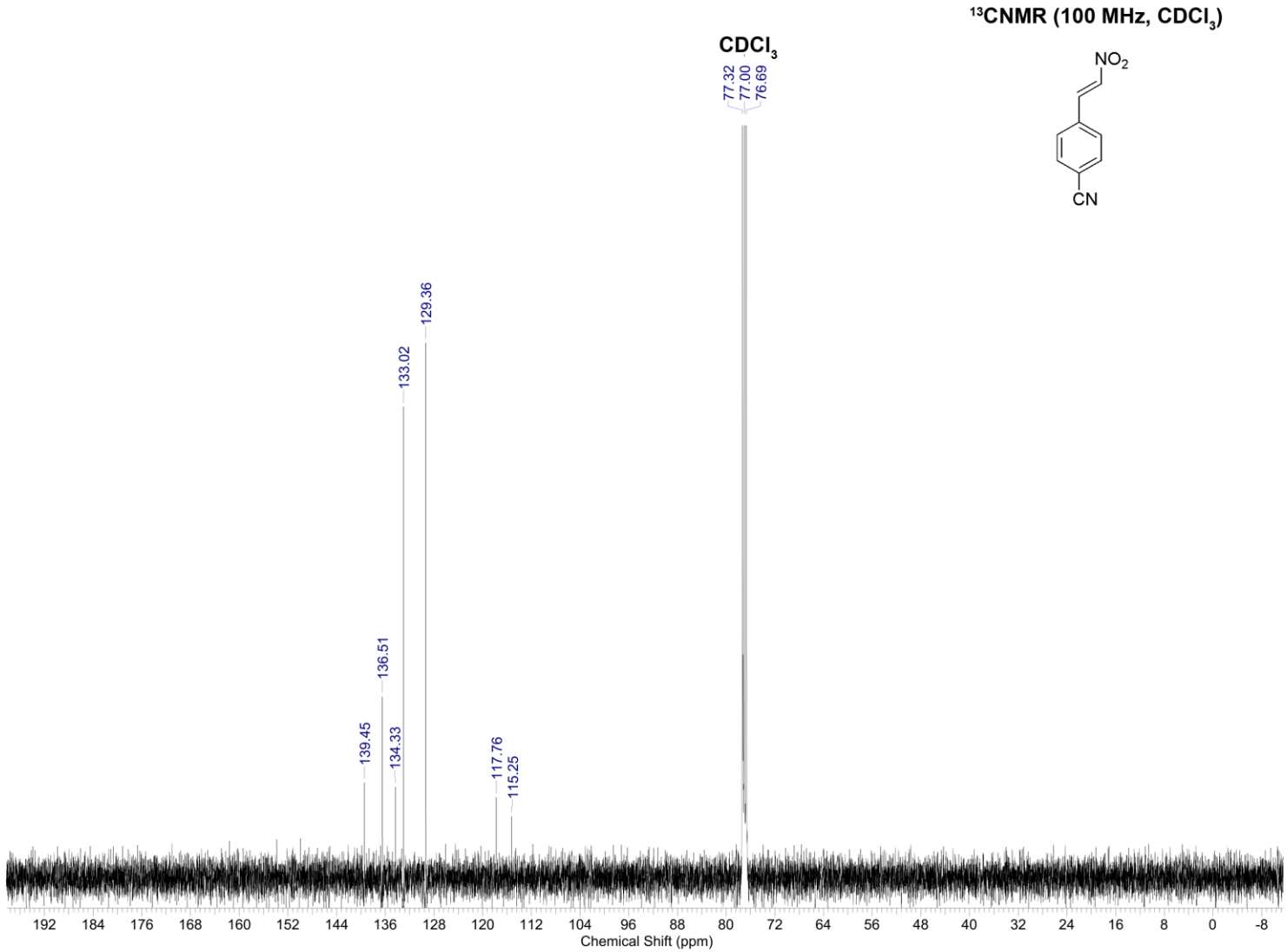
^{13}CNMR (100 MHz, $CDCl_3$)
$CDCl_3$
77.32
77.00
76.69
NO_2
CN
129.36
133.02
136.51
139.45
134.33
117.76
115.25
192 184 176 168 160 152 144 136 128 120 112 104 96 88 80 72 64 56 48 40 32 24 16 8 0 -8
Chemical Shift (ppm)

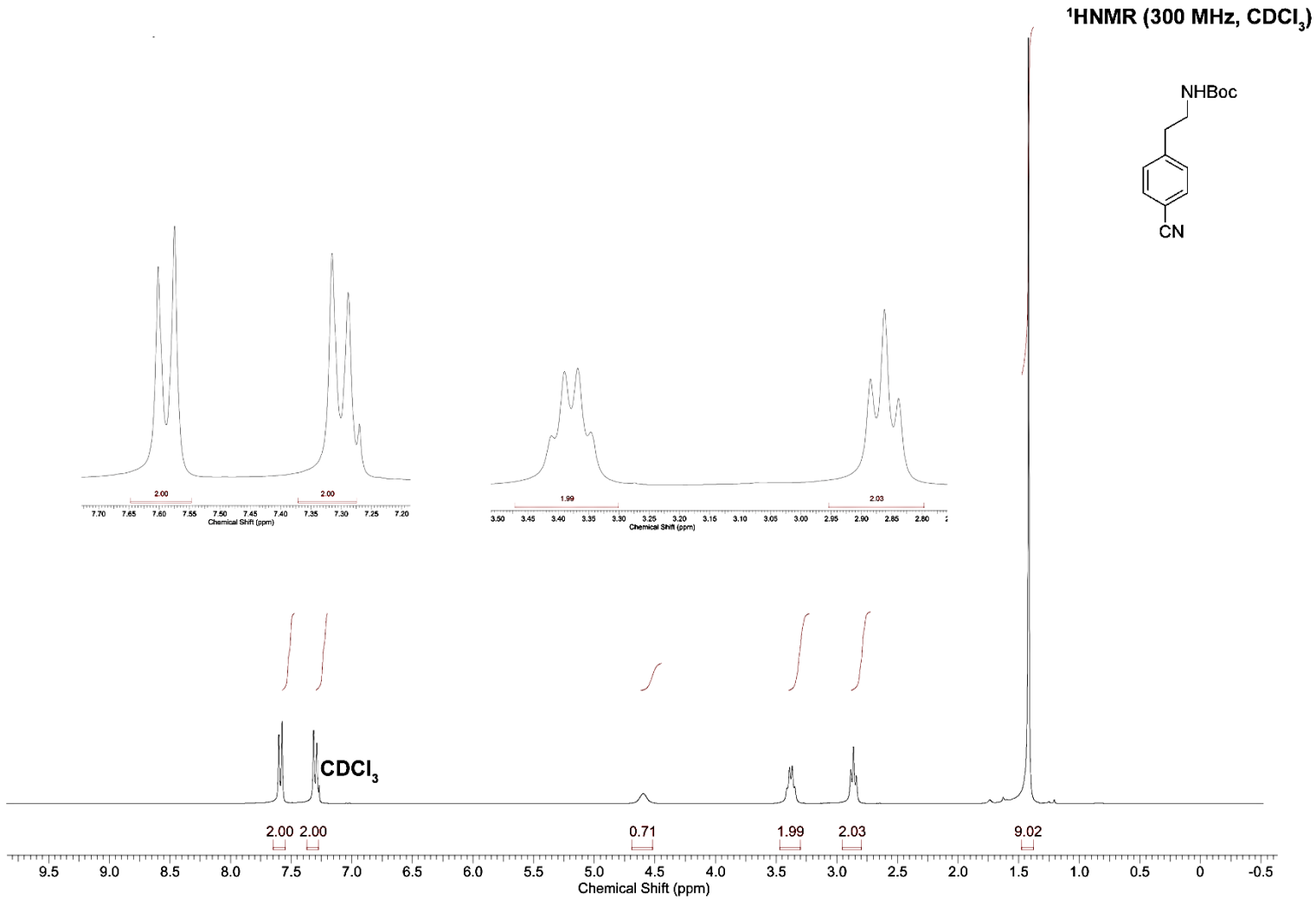
¹HNMR (300 MHz, CDCl3)
NHBoc
CN
CDCl3
2.00 2.00
0.71
1.99
2.03
9.02
Chemical Shift (ppm)

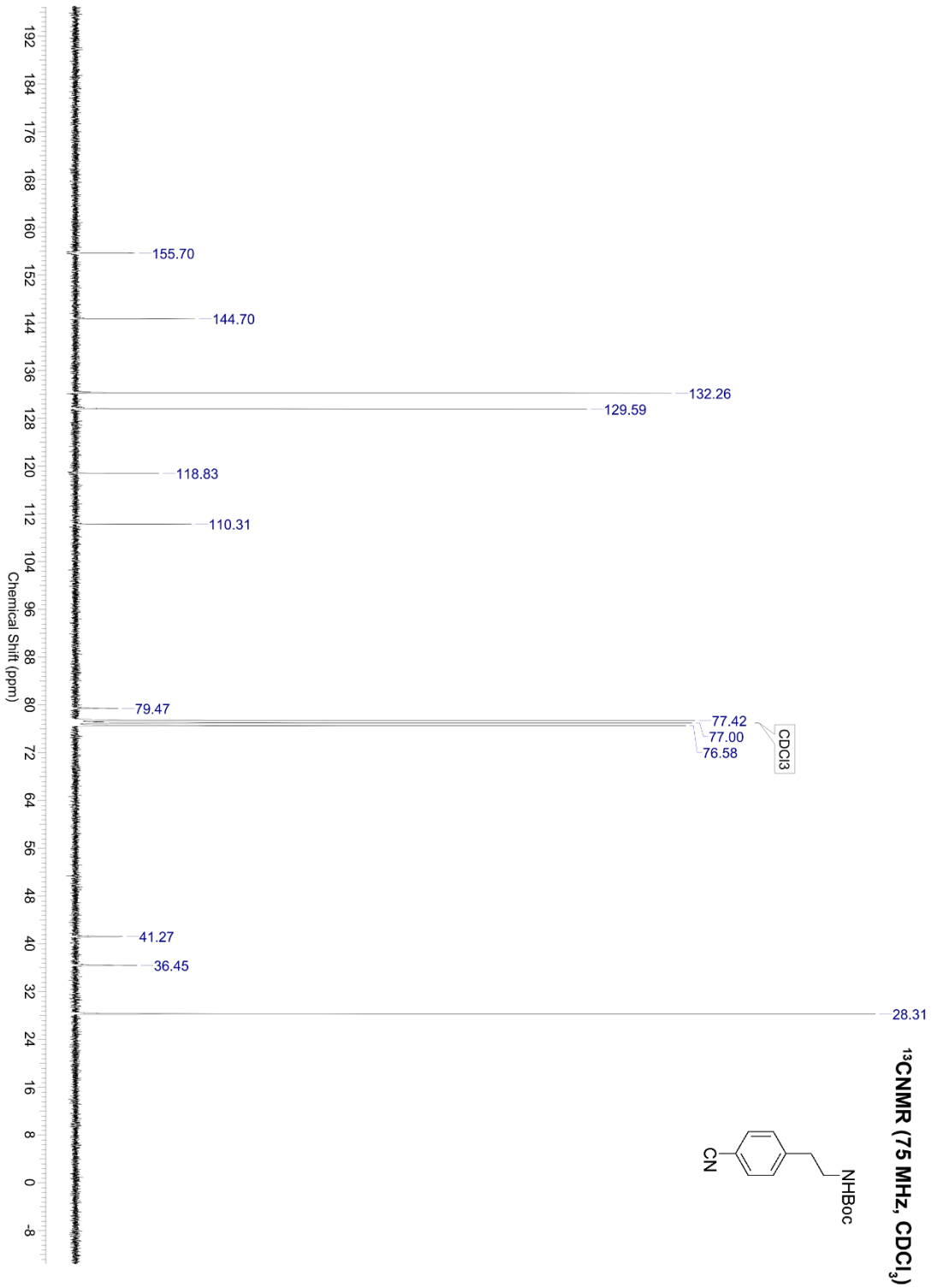
155.70
144.70
132.26
129.59
118.83
110.31
79.47
77.42
77.00
76.58
CDCl3
41.27
36.45
28.31
Chemical Shift (ppm)
192
184
176
168
160
152
144
136
128
120
112
104
96
88
80
72
64
56
48
40
32
24
16
8
0
-8
CN
NHBoc
13CNMR (75 MHz, CDCl3)

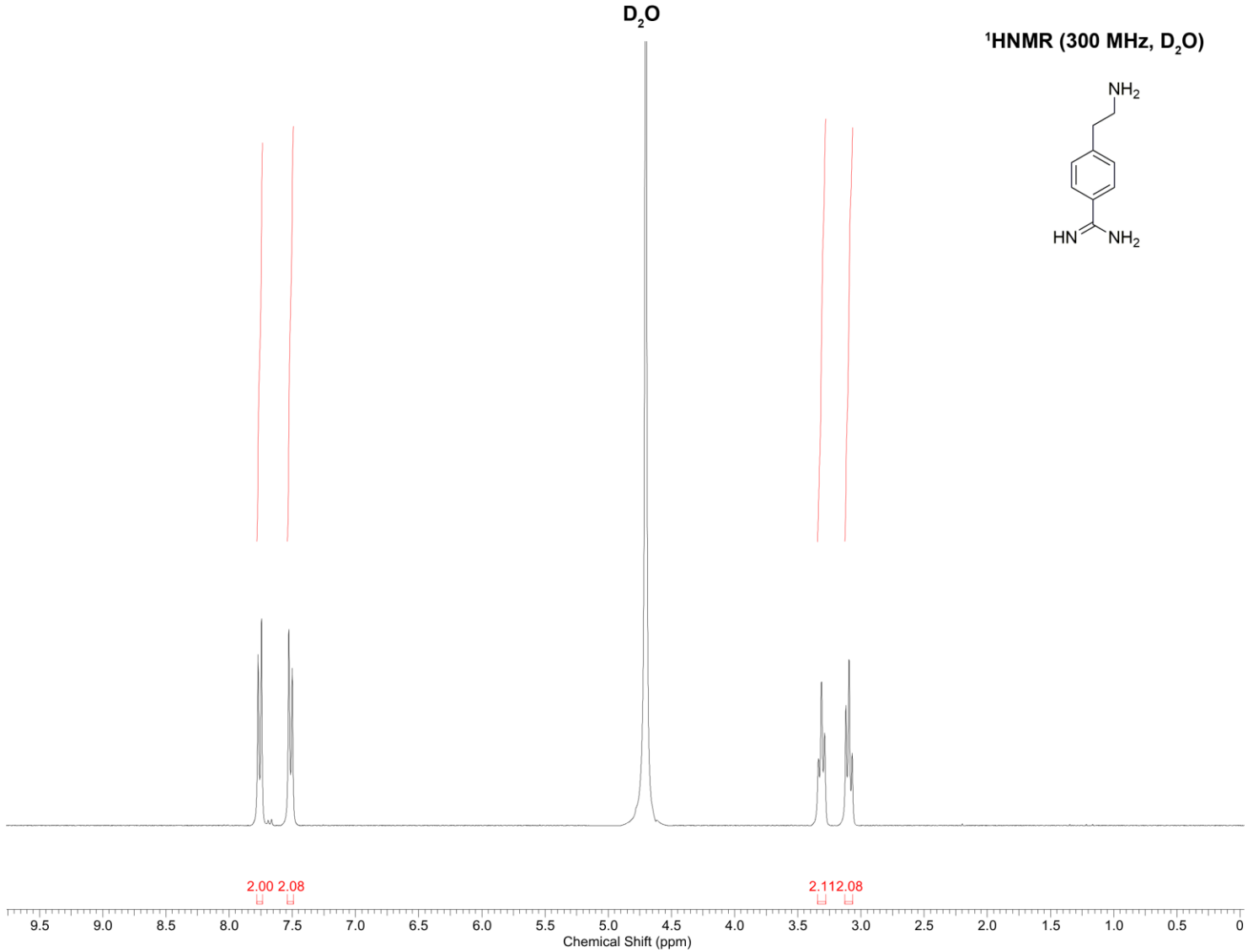
D2O
1HNMR (300 MHz, D2O)
NH2
HN
NH2
2.00 2.08
2.11 2.08
9.5 9.0 8.5 8.0 7.5 7.0 6.5 6.0 5.5 5.0 4.5 4.0 3.5 3.0 2.5 2.0 1.5 1.0 0.5 0
Chemical Shift (ppm)

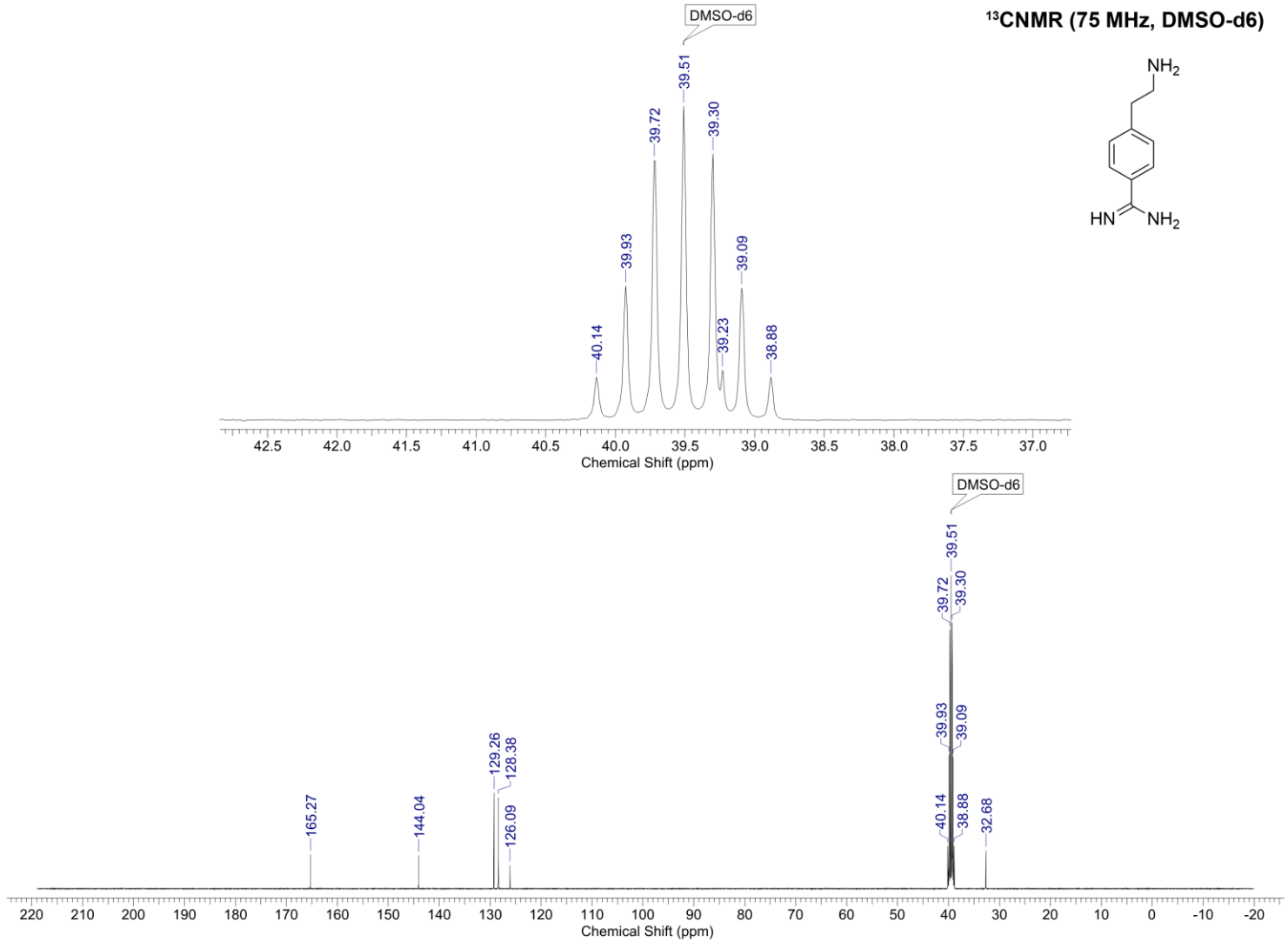
13CNMR (75 MHz, DMSO-d6)
NH2
HN
NH2
DMSO-d6
39.51
39.72
39.30
39.93
39.09
39.23
40.14
38.88
42.5 42.0 41.5 41.0 40.5 40.0 39.5 39.0 38.5 38.0 37.5 37.0
Chemical Shift (ppm)
DMSO-d6
39.51
39.72
39.30
39.93
39.09
129.26
128.38
165.27
144.04
126.09
40.14
38.88
32.68
220 210 200 190 180 170 160 150 140 130 120 110 100 90 80 70 60 50 40 30 20 10 0 -10 -20
Chemical Shift (ppm)

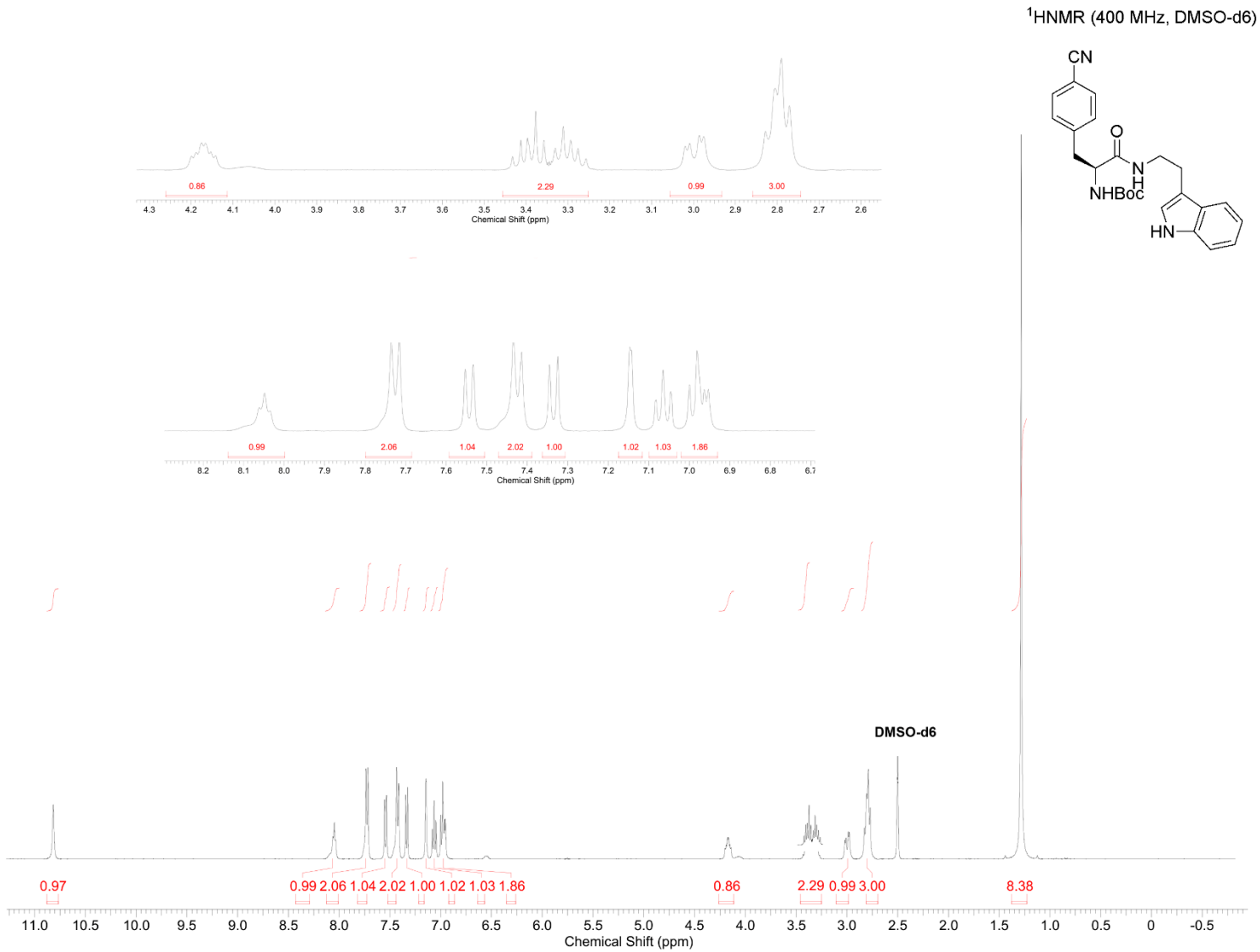
^{1}HNMR (400 MHz, DMSO-d6)
CN
O
N
H
NHBoc
HN
DMSO-d6
0.97
0.99 2.06 1.04 2.02 1.00 1.02 1.03 1.86
0.86
2.29 0.99 3.00
8.38
Chemical Shift (ppm)

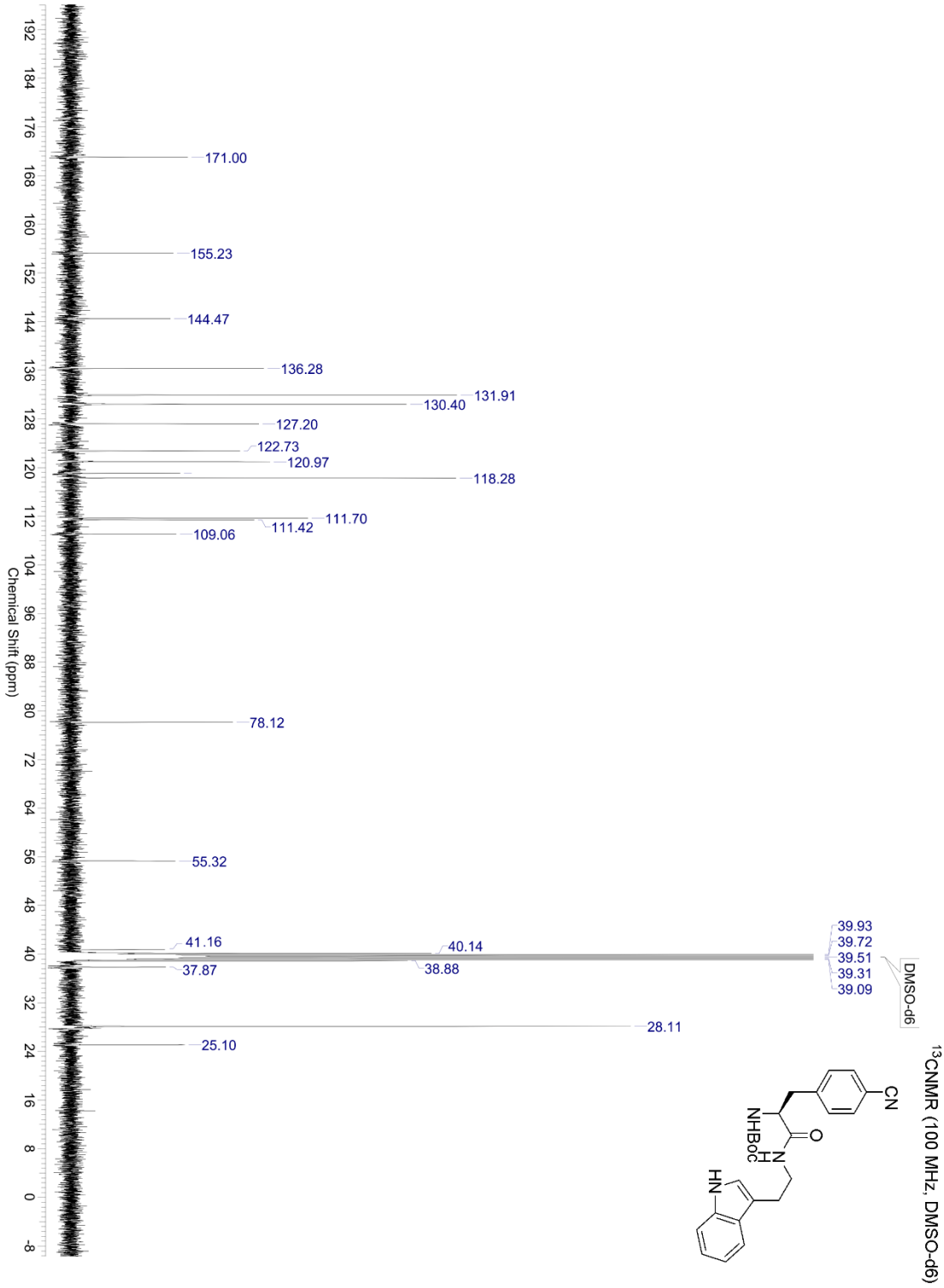
171.00
155.23
144.47
136.28
131.91
130.40
127.20
122.73
120.97
118.28
111.70
111.42
109.06
78.12
55.32
41.16
40.14
38.88
37.87
39.93
39.72
39.51
39.31
39.09
DMSO-d6
28.11
25.10
Chemical Shift (ppm)
192 184 176 168 160 152 144 136 128 120 112 104 96 88 80 72 64 56 48 40 32 24 16 8 0 -8
CN
NHBoc
O
N
H
HN
13CNMR (100 MHz, DMSO-d6)

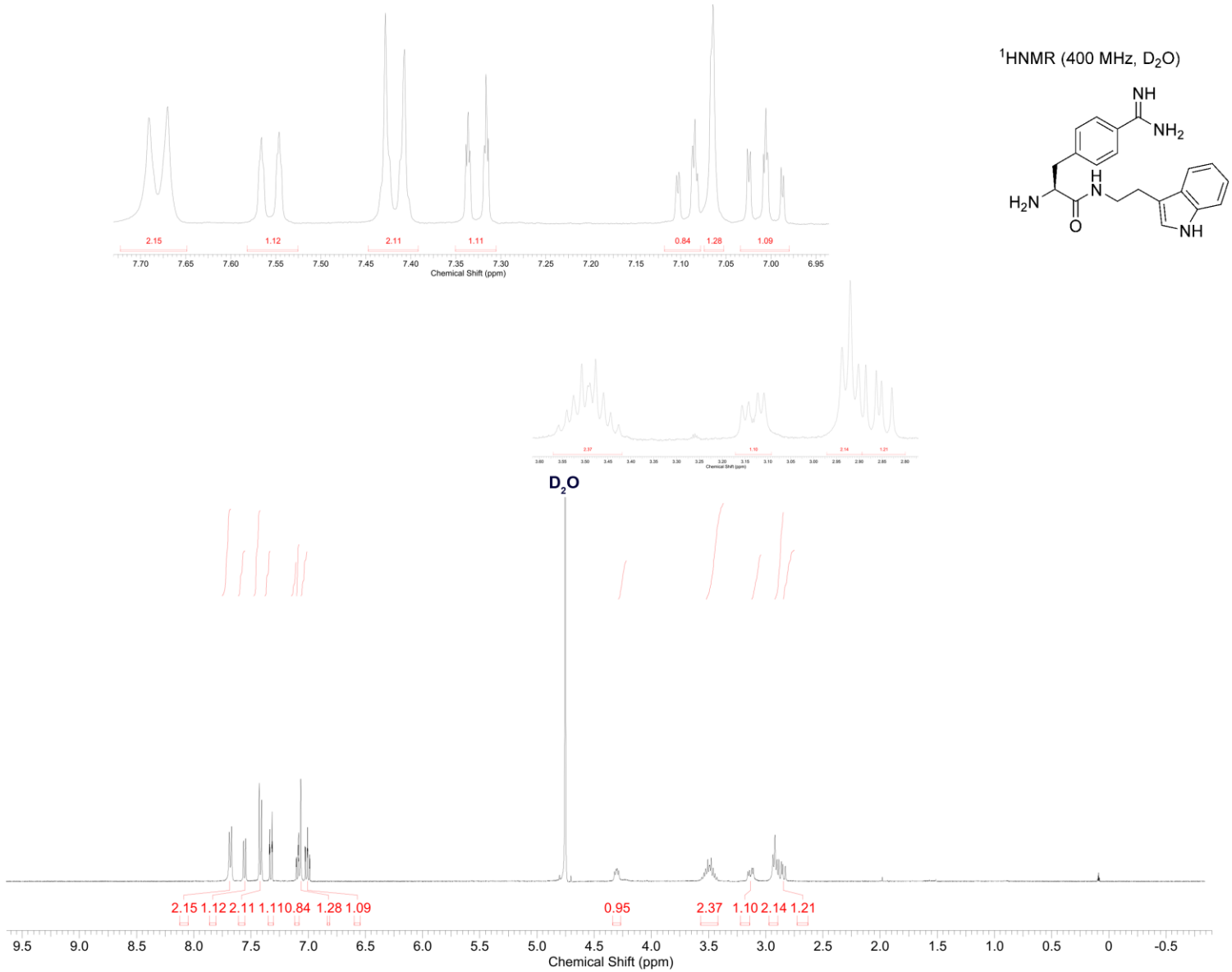
^{1}HNMR (400 MHz, D_2O)
NH
NH_2
H_2N
H
N
O
NH
D_2O
2.15 1.12 2.11 1.11 0.84 1.28 1.09
0.95
2.37 1.10 2.14 1.21
Chemical Shift (ppm)

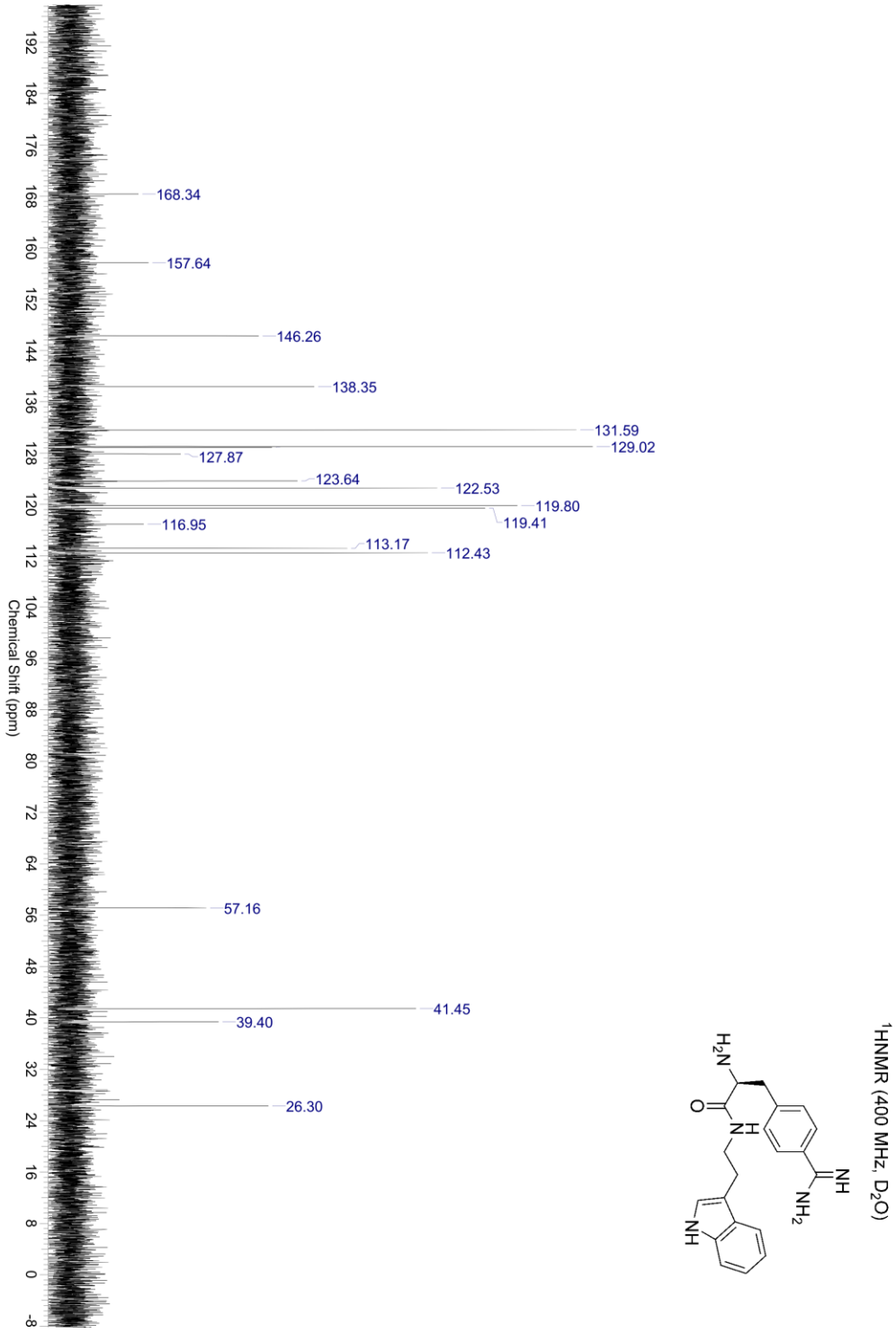
168.34
157.64
146.26
138.35
131.59
129.02
127.87
123.64
122.53
119.80
119.41
116.95
113.17
112.43
57.16
41.45
39.40
26.30
Chemical Shift (ppm)
192
184
176
168
160
152
144
136
128
120
112
104
96
88
80
72
64
56
48
40
32
24
16
8
0
-8
^{1}HNMR (400 MHz, D_2O)

^{1}HNMR (400 MHz, $CDCl_3$)

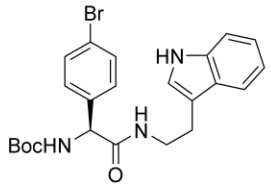

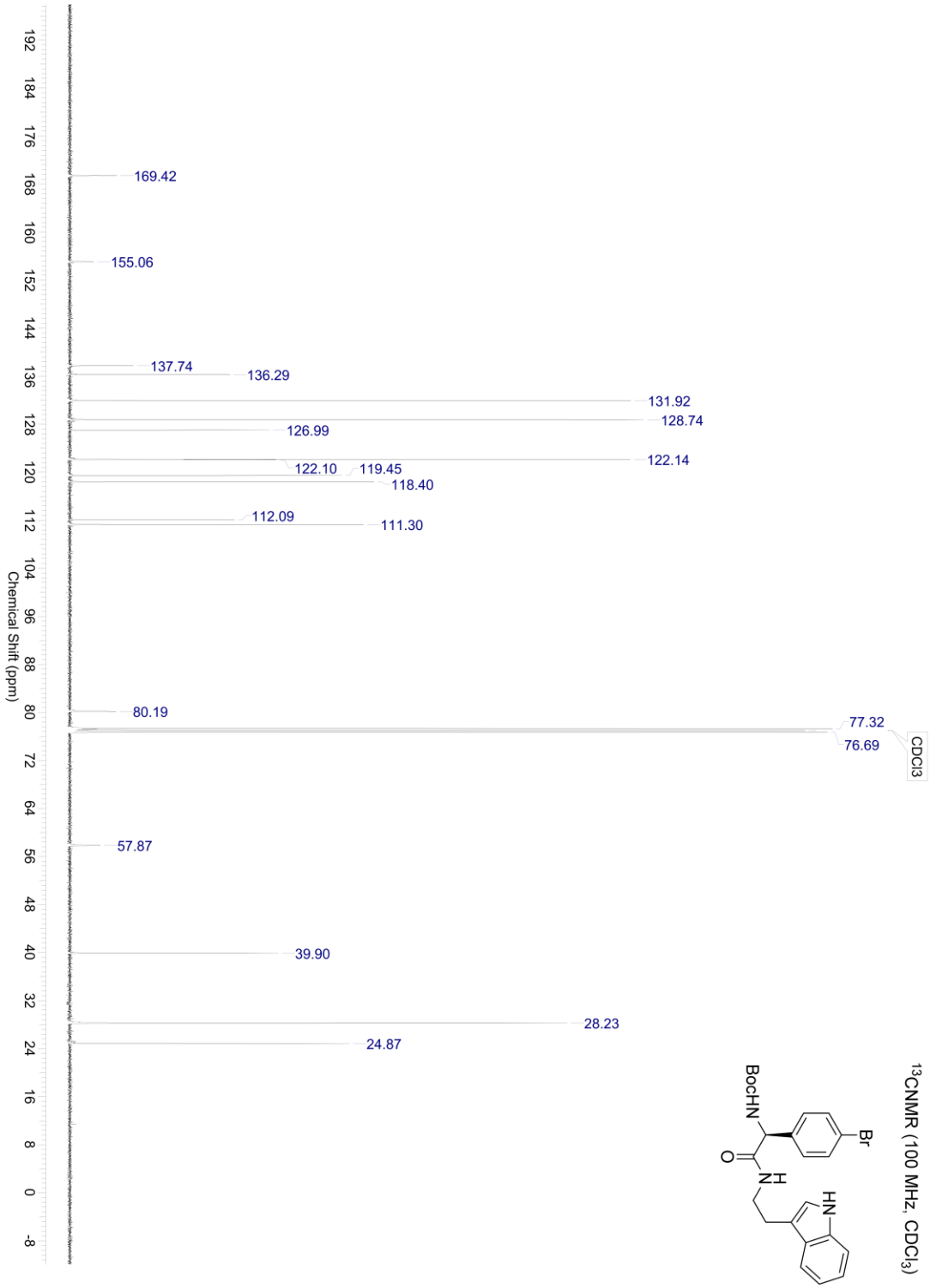
169.42
155.06
137.74
136.29
131.92
128.74
126.99
122.14
122.10
119.45
118.40
112.09
111.30
80.19
77.32
76.69
CDCl3
57.87
39.90
28.23
24.87
Chemical Shift (ppm)
192
184
176
168
160
152
144
136
128
120
112
104
96
88
80
72
64
56
48
40
32
24
16
8
0
-8
BocHN
O
H
N
Br
HN
^{13}CNMR (100 MHz, CDCl$_3$)

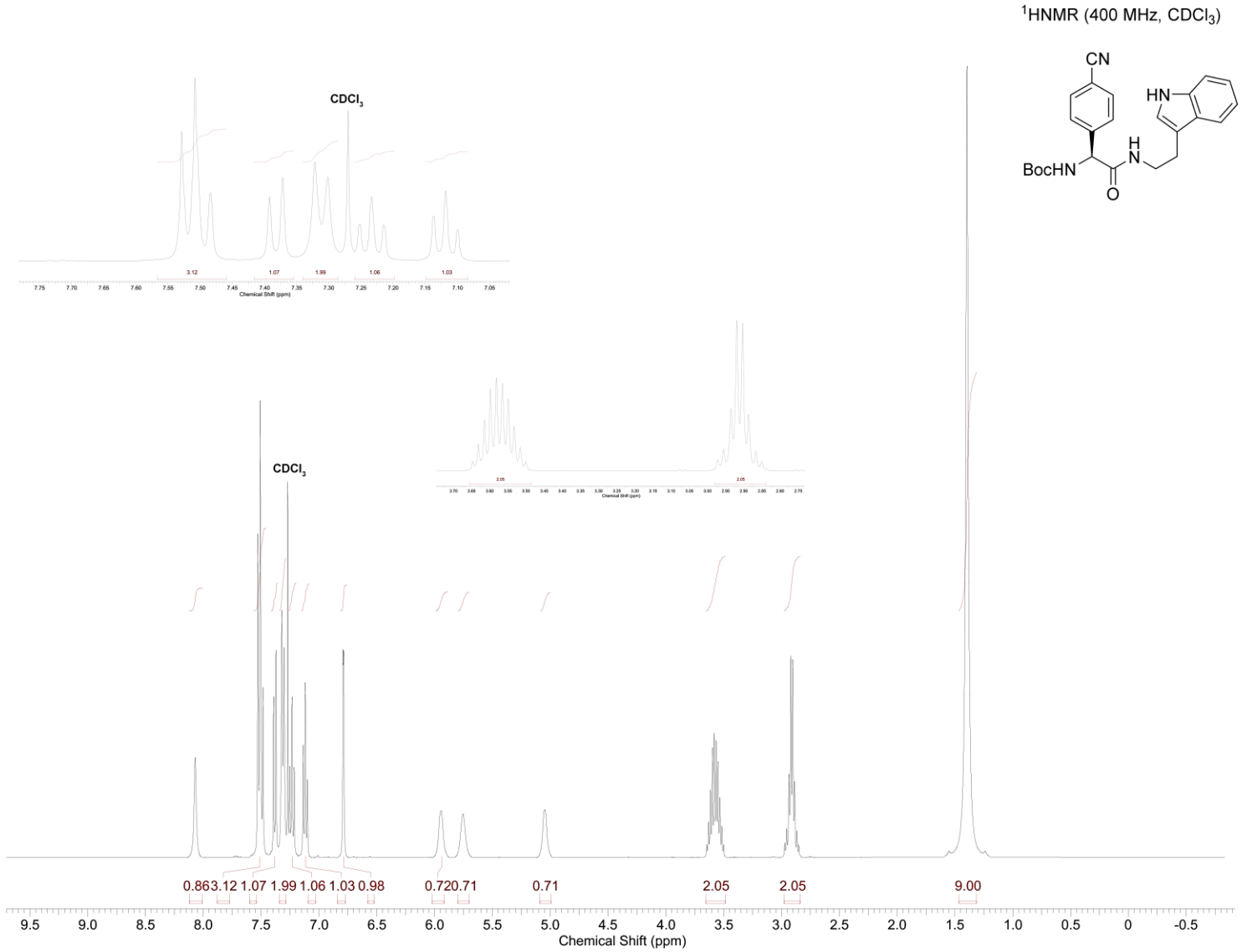
^{1}HNMR (400 MHz, $CDCl_3$)
CN
HN
H
N
BocHN
O
$CDCl_3$
$CDCl_3$
0.86 3.12 1.07 1.99 1.06 1.03 0.98
0.72 0.71
0.71
2.05
2.05
9.00
Chemical Shift (ppm)

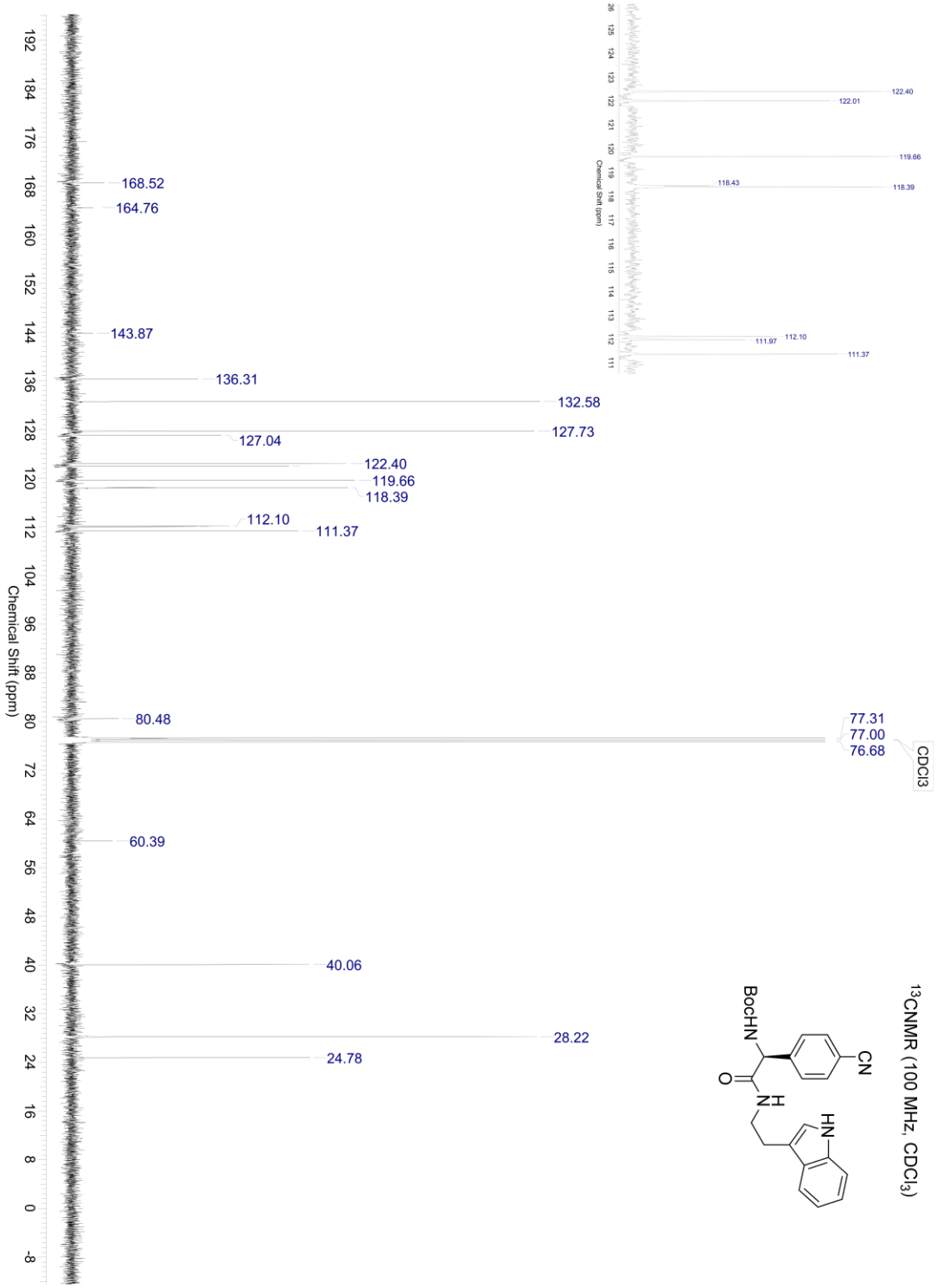
168.52
164.76
143.87
136.31
132.58
127.73
127.04
122.40
119.66
118.39
112.10
111.37
80.48
77.31
77.00
76.68
CDCl3
60.39
40.06
28.22
24.78
Chemical Shift (ppm)
122.40
122.01
119.66
118.43
118.39
111.97
112.10
111.37
BocHN
CN
O
H
N
HN
^{13}CNMR (100 MHz, CDCl$_3$)

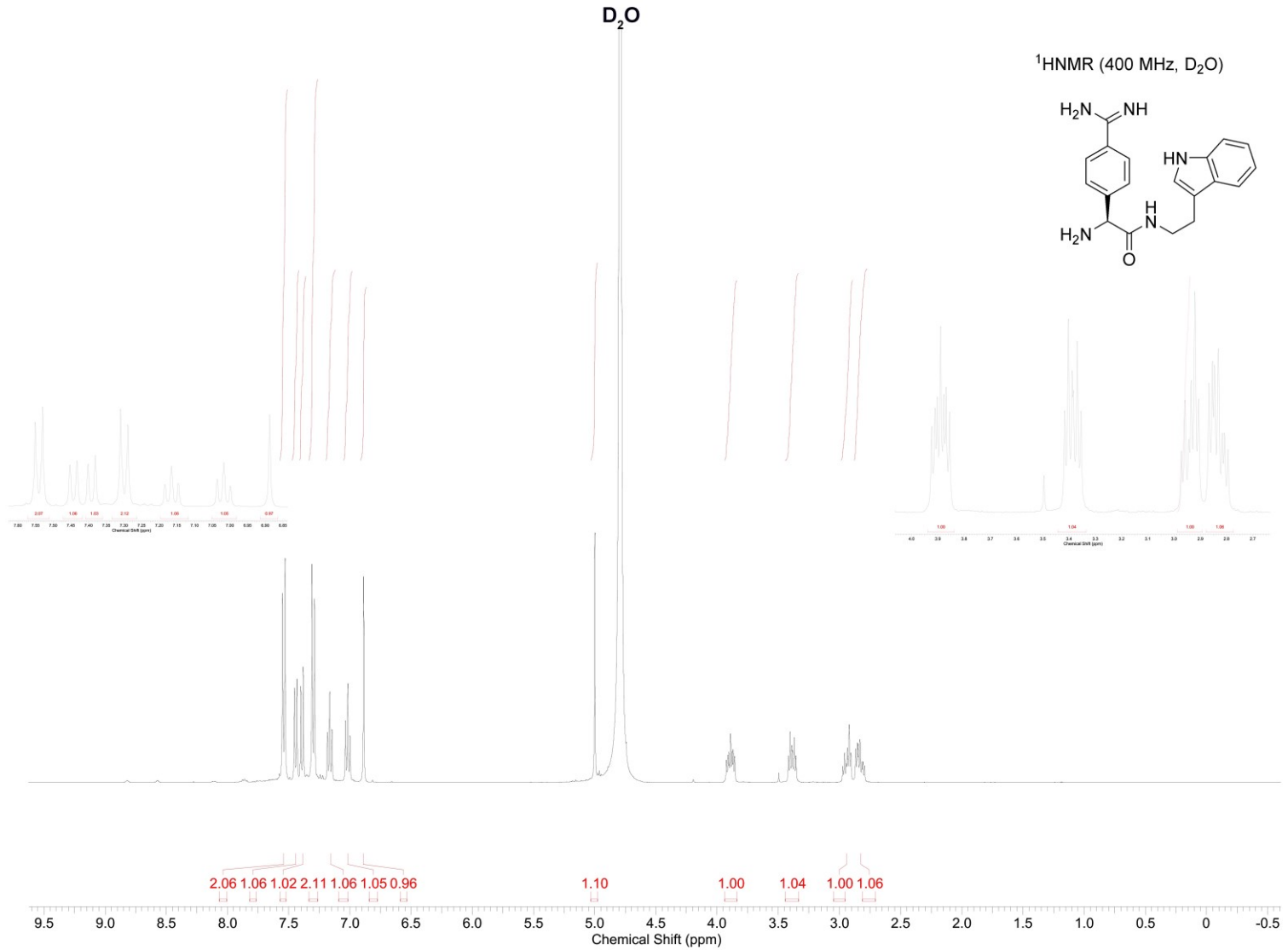
D2O
1HNMR (400 MHz, D2O)
H2N
NH
HN
H
N
H2N
O
2.06 1.06 1.02 2.11 1.06 1.05 0.96
1.10
1.00
1.04
1.00 1.06
9.5 9.0 8.5 8.0 7.5 7.0 6.5 6.0 5.5 5.0 4.5 4.0 3.5 3.0 2.5 2.0 1.5 1.0 0.5 0 -0.5
Chemical Shift (ppm)

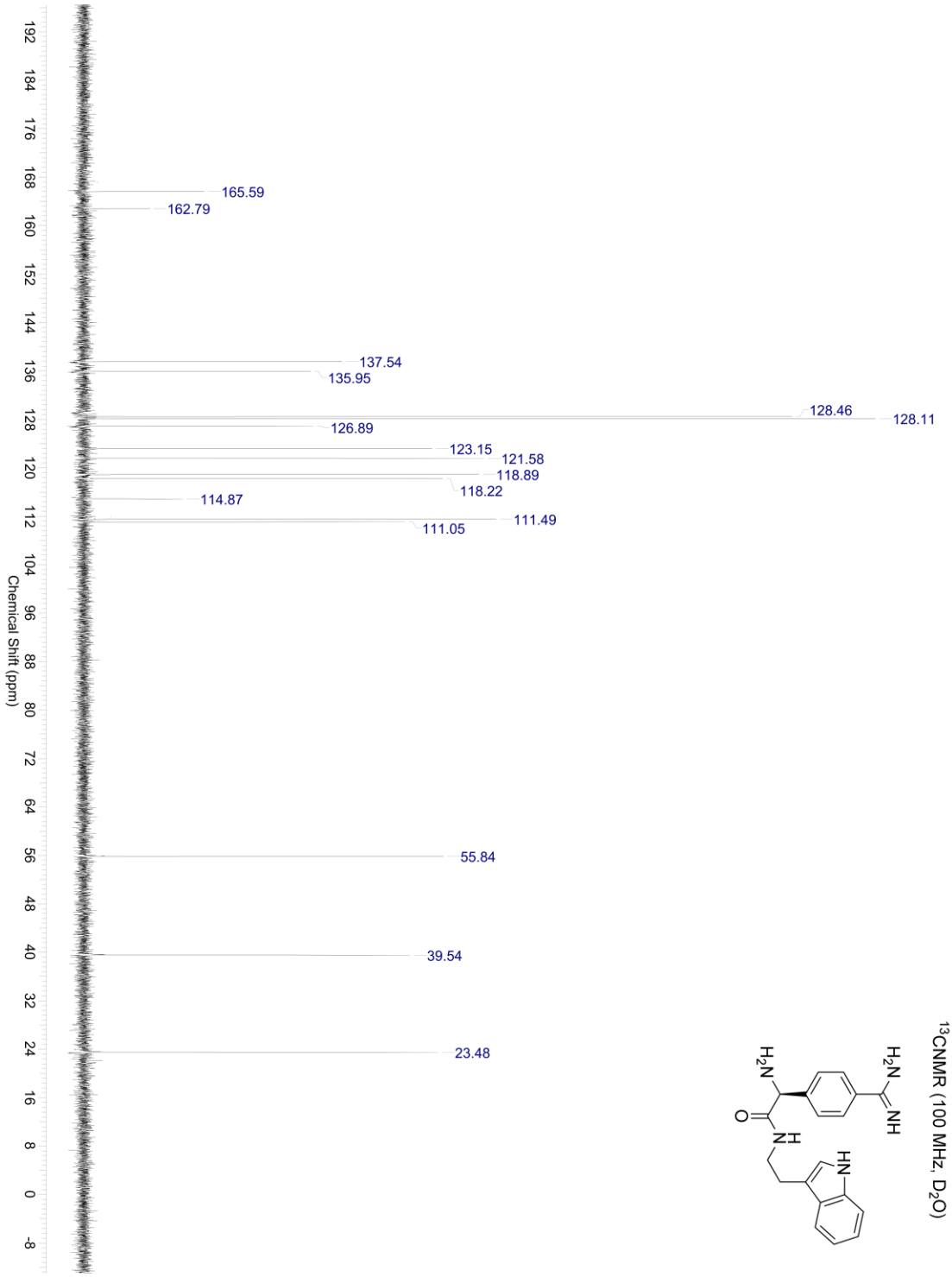

^{13}CNMR (100 MHz, D_2O)

REFERENCES AND NOTES

1. Salaverry, O., [Cancer Etymology and Its Historical Curious Course]. *Rev. Peru. Med. Exp. Salud Publica* **2013,** *30*, 137-141.

2. Weinberg, R. A., *The Biology of Cancer*. Second edition. ed.; Garland Science, Taylor & Francis Group: New York, 2014; p xx, 876, A 876, G 830, I 828 pages.

3. Kerr, J. F., A Histochemical Study of Hypertrophy and Ischaemic Injury of Rat Liver with Special Reference to Changes in Lysosomes. *J. Pathol. Bacteriol.* **1965,** *90*, 419-435.

4. Wang, W., Radiotherapy in the Management of Early Breast Cancer. *J. Med. Rad. Sci.* **2013,** *60*, 40-46.

5. Young, R. A.; Bast, C., Chapter 8 - Mustards and Vesicants A2 - Gupta, Ramesh C. In *Handbook of Toxicology of Chemical Warfare Agents*, Academic Press: San Diego, 2009; pp 93-108.

6. The Prostate. http://www.cancer.ca/en/cancer-information/cancer-type/prostate/prostate-cancer/the-prostate/?region=on (accessed 19 September).

7. Frenette, G.; Tremblay, R. R.; Dube, J. Y., Zinc Binding to Major Human Seminal Coagulum Proteins. *Arch. Androl.* **1989,** *23*, 155-163.

8. Lee, C.; Keefer, M.; Zhao Zhong, W. E. N.; Kroes, R.; Berg, L.; Liu, X.; Sensibar, J., Demonstration of the Role of Prostate-Specific Antigen in Semen Liquefaction by Two-Dimensional Electrophoresis. *J. Androl.* **1989,** *10*, 432-438.

9. Costello, L. C.; Franklin, R. B., Prostatic Fluid Electrolyte Composition for the Screening of Prostate Cancer: A Potential Solution to a Major Problem. *Prostate Cancer Prostatic Dis.* **2008,** *12*, 17-24.

10. Malm, J.; Hellman, J.; Hogg, P.; Lilja, H., Enzymatic Action of Prostate-Specific Antigen (Psa or Hk3): Substrate Specificity and Regulation by Zn2+, a Tight-Binding Inhibitor. *Prostate* **2000,** *45*, 132-139.

11. Canadian Cancer Society's Advisory Committee on Cancer Statistics. Canadian Cancer Statistics 2017. Toronto, ON: CanadianCancer Society; 2017

12. Packer, J. R.; Maitland, N. J., The Molecular and Cellular Origin of Human Prostate Cancer. *Biochim. Biophys. Acta* **2016,** *1863*, 1238-1260.

13. Martorana, E.; Micali, S.; Pirola, G. M.; Reggiani Bonetti, L.; Clò, V.; Ghaith, A.; Bianchi, G., Management and Therapeutic Response of a Prostate Ductal Adenocarcinoma: A Still Unknown Tumour? *Urologia Journal* **2016,** *83*, 163-167.

14. Cunningham, D.; You, Z., In Vitro and in Vivo Model Systems Used in Prostate Cancer Research. *J. Biol. Methods* **2015,** *2*, e17.

15. Parker, C. C.; Gospodarowicz, M.; Warde, P., Does Age Influence the Behaviour of Localized Prostate Cancer? *BJU Int.* **2002,** *87*, 629-637.

16. Albertsen, P. C.; Hanley, J. A.; Gleason, D. F.; Barry, M. J., Competing Risk Analysis of Men Aged 55 to 74 Years at Diagnosis Managed Conservatively for Clinically Localized Prostate Cancer. *JAMA* **1998,** *280*, 975-980.

17. Lecarpentier, J.; Silvestri, V.; Kuchenbaecker, K. B.; Barrowdale, D.; Dennis, J.; McGuffog, L.; Soucy, P.; Leslie, G.; Rizzolo, P.; Navazio, A. S.; Valentini, V.; Zelli, V.; Lee, A.; Amin Al Olama, A.; Tyrer, J. P.; Southey, M.; John, E. M.; Conner, T. A.; Goldgar, D. E.; Buys, S. S.; Janavicius, R.; Steele, L.; Ding, Y. C.; Neuhausen, S. L.; Hansen, T. V. O.; Osorio, A.; Weitzel, J. N.; Toss, A.; Medici, V.; Cortesi, L.; Zanna, I.; Palli, D.; Radice, P.; Manoukian, S.; Peissel, B.; Azzollini, J.; Viel, A.; Cini, G.; Damante, G.; Tommasi, S.; Peterlongo, P.; Fostira, F.; Hamann, U.; Evans, D. G.; Henderson, A.; Brewer, C.; Eccles, D.; Cook, J.; Ong, K.-r.; Walker, L.; Side, L. E.; Porteous, M. E.; Davidson, R.; Hodgson, S.; Frost, D.; Adlard, J.; Izatt, L.; Eeles, R.; Ellis, S.; Tischkowitz, M.; Godwin, A. K.; Meindl, A.; Gehrig, A.; Dworniczak, B.; Sutter, C.; Engel, C.; Niederacher, D.; Steinemann, D.; Hahnen, E.; Hauke, J.; Rhiem, K.; Kast, K.; Arnold, N.; Ditsch, N.; Wang-Gohrke, S.; Wappenschmidt, B.; Wand, D.; Lasset, C.; Stoppa-Lyonnet, D.; Belotti, M.; Damiola, F.; Barjhoux, L.; Mazoyer, S.; Van Heetvelde, M.; Poppe, B.; De Leeneer, K.; Claes, K. B. M.; de la Hoya, M.; Garcia-Barberan, V.; Caldes, T.; Perez Segura, P.; Kiiski, J. I.; Aittomäki, K.; Khan, S.; Nevanlinna, H.; van Asperen, C. J.; Vaszko, T.; Kasler, M.; Olah, E.; Balmaña, J.; Gutiérrez-Enríquez, S.; Diez, O.; Teulé, A.; Izquierdo, A.; Darder, E.; Brunet, J.; Del Valle, J.; Feliubadalo, L.; Pujana, M. A.; Lazaro, C.; Arason, A.; Agnarsson, B. A.; Johannsson, O. T.; Barkardottir, R. B.; Alducci, E.; Tognazzo, S.; Montagna, M.; Teixeira, M. R.; Pinto, P.; Spurdle, A. B.; Holland, H.; Lee, J. W.; Lee, M. H.; Lee, J.; Kim, S.-W.; Kang, E.; Kim, Z.; Sharma, P.; Rebbeck, T. R.; Vijai, J.; Robson, M.; Lincoln, A.; Musinsky, J.; Gaddam, P.; Tan, Y. Y.; Berger, A.; Singer, C. F.; Loud, J. T.; Greene, M. H.; Mulligan, A. M.; Glendon, G.; Andrulis, I. L.; Toland, A. E.; Senter, L.; Bojesen,

A.; Nielsen, H. R.; Skytte, A.-B.; Sunde, L.; Jensen, U. B.; Pedersen, I. S.; Krogh, L.; Kruse, T. A.; Caligo, M. A.; Yoon, S.-Y.; Teo, S.-H.; von Wachenfeldt, A.; Huo, D.; Nielsen, S. M.; Olopade, O. I.; Nathanson, K. L.; Domchek, S. M.; Lorenchick, C.; Jankowitz, R. C.; Campbell, I.; James, P.; Mitchell, G.; Orr, N.; Park, S. K.; Thomassen, M.; Offit, K.; Couch, F. J.; Simard, J.; Easton, D. F.; Chenevix-Trench, G.; Schmutzler, R. K.; Antoniou, A. C.; Ottini, L., Prediction of Breast and Prostate Cancer Risks in Male Brca1 and Brca2 Mutation Carriers Using Polygenic Risk Scores. *J. Clin. Oncol.* **2017,** *35*, 2240-2250.

18. Roach, M., III; Krall, J.; Keller, J. W.; Perez, C. A.; Sause, W. T.; Doggett, R. L. S.; Rotman, M.; Russ, H.; Pilepich, M. V.; Asbell, S. O.; Shipley, W., The Prognostic Significance of Race and Survival from Prostate Cancer Based on Patients Irradiated on Radiation Therapy Oncology Group Protocols (1976–1985). *Int. J. Radiat. Oncol. Biol. Phys.* **1992,** *24*, 441-449.

19. Plaskon, L. A.; Penson, D. F.; Vaughan, T. L.; Stanford, J. L., Cigarette Smoking and Risk of Prostate Cancer in Middle-Aged Men. *Cancer Epidemiol. Biomarkers Prev.* **2003,** *12*, 604-609.

20. Tantamango-Bartley, Y.; Knutsen, S. F.; Knutsen, R.; Jacobsen, B. K.; Fan, J.; Beeson, W. L.; Sabate, J.; Hadley, D.; Jaceldo-Siegl, K.; Penniecook, J.; Herring, P.; Butler, T.; Bennett, H.; Fraser, G., Are Strict Vegetarians Protected against Prostate Cancer? *Am. J. Clin. Nutr.* **2016,** *103*, 153-160.

21. Sp, I.; Ramona, I.; Sukesh, The Efficiency of the Serum Prostate Specific Antigen Levels in Diagnosing Prostatic Enlargements. *J. Clin. Diagn. Res.* **2013,** *7*, 82-84.

22. Mellinger, G. T.; Gleason, D.; Bailar, J., The Histology and Prognosis of Prostatic Cancer. *J. Urol.* **1967,** *97*, 331-337.

23. Humphrey, P. A., Gleason Grading and Prognostic Factors in Carcinoma of the Prostate. *Mod. Pathol.* **2004,** *17*, 292-306.

24. Andriole, G. L.; Crawford, E. D.; Grubb, R. L.; Buys, S. S.; Chia, D.; Church, T. R.; Fouad, M. N.; Gelmann, E. P.; Kvale, P. A.; Reding, D. J.; Weissfeld, J. L.; Yokochi, L. A.; O'Brien, B.; Clapp, J. D.; Rathmell, J. M.; Riley, T. L.; Hayes, R. B.; Kramer, B. S.; Izmirlian, G.; Miller, A. B.; Pinsky, P. F.; Prorok, P. C.; Gohagan, J. K.; Berg, C. D., Mortality Results from a Randomized Prostate-Cancer Screening Trial. *New Engl. J. Med.* **2009,** *360*, 1310-1319.

25. Schröder, F. H.; Hugosson, J.; Roobol, M. J.; Tammela, T. L. J.; Zappa, M.; Nelen, V.; Kwiatkowski, M.; Lujan, M.; Määttänen, L.; Lilja, H.; Denis, L. J.; Recker, F.; Paez, A.; Bangma, C. H.; Carlsson, S.;

Puliti, D.; Villers, A.; Rebillard, X.; Hakama, M.; Stenman, U.-H.; Kujala, P.; Taari, K.; Aus, G.; Huber, A.; van der Kwast, T.; van Schaik R, R. H. N.; de Koning, H. J.; Moss, S. M.; Auvinen, A.; for the, E. I., The European Randomized Study of Screening for Prostate Cancer – Prostate Cancer Mortality at 13 Years of Follow-Up. *Lancet* **2014,** *384*, 2027-2035.

26. Massard, C.; Fizazi, K., Targeting Continued Androgen Receptor Signaling in Prostate Cancer. *Clin. Cancer. Res.* **2011,** *17*, 3876-3883.

27. Askew, E. B.; Gampe, R. T.; Stanley, T. B.; Faggart, J. L.; Wilson, E. M., Modulation of Androgen Receptor Activation Function 2 by Testosterone and Dihydrotestosterone(). *J. Biol. Chem.* **2007,** *282*, 25801-25816.

28. Schröder, F.; Crawford, E. D.; Axcrona, K.; Payne, H.; Keane, T. E., Androgen Deprivation Therapy: Past, Present and Future. *BJU Int.* **2012,** *109*, 1-12.

29. Thompson, I. M., Flare Associated with Lhrh-Agonist Therapy. *Rev. Urol.* **2001,** *3*, S10-S14.

30. Schally, A. V., Luteinizing Hormone-Releasing Hormone Analogs: Their Impact on the Control of Tumorigenesis. *Peptides* **1999,** *20*, 1247-1262.

31. Orvieto, R.; Patrizio, P., Gnrh Agonist Versus Gnrh Antagonist in Ovarian Stimulation: An Ongoing Debate. *Reprod. Biomed. Online* **2013,** *26*, 4-8.

32. Nieschlag, E.; Nieschlag, S., Testosterone Deficiency: A Historical Perspective. *Asian J Androl* **2014,** *16*, 161-168.

33. Migliari, R.; Muscas, G.; Murru, M.; Verdacchi, T.; De Benedetto, G.; De Angelis, M., Antiandrogens: A Summary Review of Pharmacodynamic Properties and Tolerability in Prostate Cancer Therapy. *Arch. Ital. Urol. Androl.* **1999,** *71*, 293-302.

34. Thole, Z.; Manso, G.; Salgueiro, E.; Revuelta, P.; Hidalgo, A., Hepatotoxicity Induced by Antiandrogens: A Review of the Literature. *Urol. Int.* **2004,** *73*, 289-295.

35. Bennett, C. L.; Raisch, D. W.; Sartor, O., Pneumonitis Associated with Nonsteroidal Antiandrogens: Presumptive Evidence of a Class Effect. *Ann. Intern. Med.* **2002,** *137*, 625-635.

36. Potter, G. A.; Barrie, S. E.; Jarman, M.; Rowlands, M. G., Novel Steroidal Inhibitors of Human Cytochrome P45017 Alpha (17 Alpha-Hydroxylase-C17,20-Lyase): Potential Agents for the Treatment of Prostatic Cancer. *J. Med. Chem.* **1995,** *38*, 2463-2471.

37. de Bono, J. S.; Logothetis, C. J.; Molina, A.; Fizazi, K.; North, S.; Chu, L.; Chi, K. N.; Jones, R. J.; Goodman, O. B.; Saad, F.; Staffurth, J. N.; Mainwaring, P.; Harland, S.; Flaig, T. W.; Hutson, T. E.; Cheng, T.; Patterson, H.; Hainsworth, J. D.; Ryan, C. J.; Sternberg, C. N.; Ellard, S. L.; Fléhon, A.; Saleh, M.; Scholz, M.; Efstathiou, E.; Zivi, A.; Bianchini, D.; Loriot, Y.; Chieffo, N.; Kheoh, T.; Haqq, C. M.; Scher, H. I.; for the, C. O. U. A. A. I., Abiraterone and Increased Survival in Metastatic Prostate Cancer. *New Engl. J. Med.* **2011,** *364*, 1995-2005.

38. Princivalle, M.; Broqua, P.; White, R.; Meyer, J.; Mayer, G.; Elliott, L.; Bjarnason, K.; Haigh, R.; Yea, C., Rapid Suppression of Plasma Testosterone Levels and Tumor Growth in the Dunning Rat Model Treated with Degarelix, a New Gonadotropin-Releasing Hormone Antagonist. *J. Pharmacol. Exp. Ther.* **2007,** *320*, 1113-1118.

39. Samant, M. P.; White, R.; Hong, D. J.; Croston, G.; Conn, P. M.; Janovick, J. A.; Rivier, J., Structure−Activity Relationship Studies of Gonadotropin-Releasing Hormone Antagonists Containing S-Aryl/Alkyl Norcysteines and Their Oxidized Derivatives. *J. Med. Chem.* **2007,** *50*, 2067-2077.

40. Boccon-Gibod, L.; van der Meulen, E.; Persson, B.-E., An Update on the Use of Gonadotropin-Releasing Hormone Antagonists in Prostate Cancer. *Ther. Adv. Urol.* **2011,** *3*, 127-140.

41. Hegde, S.; Schmidt, M., Chapter 28 - to Market, to Market—2009. In *Annu. Rep. Med. Chem.*, Macor, J. E., Ed. Academic Press: 2010; Vol. 45, pp 466-537.

42. Jiang, G.; Stalewski, J.; Galyean, R.; Dykert, J.; Schteingart, C.; Broqua, P.; Aebi, A.; Aubert, M. L.; Semple, G.; Robson, P.; Akinsanya, K.; Haigh, R.; Riviere, P.; Trojnar, J.; Junien, J. L.; Rivier, J. E., Gnrh Antagonists: A New Generation of Long Acting Analogues Incorporating P-Ureido-Phenylalanines at Positions 5 and 6. *J. Med. Chem.* **2001,** *44*, 453-467.

43. Goodman, J.; Walsh, V., *The Story of Taxol : Nature and Politics in the Pursuit of an Anti-Cancer Drug*. Cambridge University Press: Cambridge ; New York, 2001; p 282 p.

44. Kingston, D. G. I., The Shape of Things to Come: Structural and Synthetic Studies of Taxol and Related Compounds. *Phytochemistry* **2007,** *68*, 1844-1854.

45. Ganem, B.; Franke, R. R., Paclitaxel from Primary Taxanes: A Perspective on Creative Invention in Organozirconium Chemistry. *J. Org. Chem.* **2007,** *72*, 3981-3987.

46. Geiduschek, E. P., „Reversible" DNA. *Proc. Natl. Acad. Sci. U.S.A.* **1961,** *47*, 950-955.

47. William Lown, J., Anthracycline and Anthraquinone Anticancer Agents: Current Status and Recent Developments. *Pharmacol. Ther.* **1993,** *60*, 185-214.

48. Dal Ben, D.; Palumbo, M.; Zagotto, G.; Capranico, G.; Moro, S., DNA Topoisomerase Ii Structures and Anthracycline Activity: Insights into Ternary Complex Formation. *Curr. Pharm. Des.* **2007,** *13*, 2766-2780.

49. Wu, X.; Hasinoff, B. B., The Antitumor Anthracyclines Doxorubicin and Daunorubicin Do Not Inhibit Cell Growth through the Formation of Iron-Mediated Reactive Oxygen Species. *Anticancer Drugs* **2005,** *16*, 93-99.

50. De Santis, M.; Saad, F., Practical Guidance on the Role of Corticosteroids in the Treatment of Metastatic Castration-Resistant Prostate Cancer. *Urology* **2016,** *96*, 156-164.

51. Nishimura, K.; Nonomura, N.; Satoh, E.; Harada, Y.; Nakayama, M.; Tokizane, T.; Fukui, T.; Ono, Y.; Inoue, H.; Shin, M.; Tsujimoto, Y.; Takayama, H.; Aozasa, K.; Okuyama, A., Potential Mechanism for the Effects of Dexamethasone on Growth of Androgen-Independent Prostate Cancer. *J. Natl. Cancer Inst.* **2001,** *93*, 1739-1746.

52. Shtivelman, E.; Beer, T. M.; Evans, C. P., Molecular Pathways and Targets in Prostate Cancer. *Oncotarget* **2014,** *5*, 7217-7259.

53. Ramakrishnan Geethakumari, P.; Schiewer, M. J.; Knudsen, K. E.; Kelly, W. K., Parp Inhibitors in Prostate Cancer. *Curr. Treat. Options Oncol.* **2017,** *18*, 37.

54. Brenner, J. C.; Ateeq, B.; Li, Y.; Yocum, A. K.; Cao, Q.; Asangani, I. A.; Patel, S.; Wang, X.; Liang, H.; Yu, J.; Palanisamy, N.; Siddiqui, J.; Yan, W.; Cao, X.; Mehra, R.; Sabolch, A.; Basrur, V.; Lonigro, R. J.; Yang, J.; Tomlins, S. A.; Maher, C. A.; Elenitoba-Johnson, K. S.; Hussain, M.; Navone, N. M.; Pienta, K. J.; Varambally, S.; Feng, F. Y.; Chinnaiyan, A. M., Mechanistic Rationale for Inhibition of Poly(Adp-Ribose) Polymerase in Ets Gene Fusion-Positive Prostate Cancer. *Cancer Cell* **2011,** *19*, 664-678.

55. Crumbaker, M.; Khoja, L.; Joshua, A. M., Ar Signaling and the Pi3k Pathway in Prostate Cancer. *Cancers (Basel)* **2017,** *9*, 34-49.

56. Faltermeier, C. M.; Drake, J. M.; Clark, P. M.; Smith, B. A.; Zong, Y.; Volpe, C.; Mathis, C.; Morrissey, C.; Castor, B.; Huang, J.; Witte, O. N., Functional Screen Identifies Kinases Driving Prostate Cancer Visceral and Bone Metastasis. *Proc. Natl. Acad. Sci. U.S.A.* **2016,** *113*, E172-E181.

57. Cai, H.; Smith, D. A.; Memarzadeh, S.; Lowell, C. A.; Cooper, J. A.; Witte, O. N., Differential Transformation Capacity of Src Family Kinases During the Initiation of Prostate Cancer. *Proc. Natl. Acad. Sci. U.S.A.* **2011,** *108*, 6579-6584.

58. Eckschlager, T.; Plch, J.; Stiborova, M.; Hrabeta, J., Histone Deacetylase Inhibitors as Anticancer Drugs. *Int. J. Mol. Sci.* **2017,** *18*, 1414-1439.

59. Hance, M. W.; Dole, K.; Gopal, U.; Bohonowych, J. E.; Jezierska-Drutel, A.; Neumann, C. A.; Liu, H.; Garraway, I. P.; Isaacs, J. S., Secreted Hsp90 Is a Novel Regulator of the Epithelial to Mesenchymal Transition (Emt) in Prostate Cancer. *J. Biol. Chem.* **2012,** *287*, 37732-37744.

60. Shiota, M.; Zardan, A.; Takeuchi, A.; Kumano, M.; Beraldi, E.; Naito, S.; Zoubeidi, A.; Gleave, M. E., Clusterin Mediates Tgf-Beta-Induced Epithelial-Mesenchymal Transition and Metastasis Via Twist1 in Prostate Cancer Cells. *Cancer Res.* **2012,** *72*, 5261-5272.

61. Dai, J.; Zhang, H.; Karatsinides, A.; Keller, J. M.; Kozloff, K. M.; Aftab, D. T.; Schimmoller, F.; Keller, E. T., Cabozantinib Inhibits Prostate Cancer Growth and Prevents Tumor-Induced Bone Lesions. *Clin. Cancer. Res.* **2014,** *20*, 617-630.

62. Shah, A. A.; Karzai, F.; Madan, R. A.; Figg, W. D.; Chau, C. H.; Gulley, J. L.; Chun, G.; Wright, J. J.; Apolo, A. B.; Parnes, H. L.; Dahut, W. L., A Phase Ii Study of Trebananib (Amg 386) and Abiraterone in Metastatic Castration Resistant Prostate Cancer. *J. Clin. Oncol.* **2013,** *31*, TPS5102-TPS5102.

63. Muller, J.-M.; Chevrier, L.; Cochaud, S.; Meunier, A.-C.; Chadeneau, C., Hedgehog, Notch and Wnt Developmental Pathways as Targets for Anti-Cancer Drugs. *Drug Discov. Today Dis. Mech.* **2007,** *4*, 285-291.

64. Sridhar, S. S.; Freedland, S. J.; Gleave, M. E.; Higano, C.; Mulders, P.; Parker, C.; Sartor, O.; Saad, F., Castration-Resistant Prostate Cancer: From New Pathophysiology to New Treatment. *Eur. Urol.* **2014,** *65*, 289-299.

65. Schwartzberg, L.; Kim, E. S.; Liu, D.; Schrag, D., Precision Oncology: Who, How, What, When, and When Not? *Am Soc Clin Oncol Educ Book* **2017,** *37*, 160-169.

66. Mann, M.; Jensen, O. N., Proteomic Analysis of Post-Translational Modifications. *Nat. Biotechnol.* **2003,** *21*, 255.

67. Steiner, D. F.; Oyer, P. E., The Biosynthesis of Insulin and a Probable Precursor of Insulin by a Human Islet Cell Adenoma. *Proc. Natl. Acad. Sci. U. S. A.* **1967,** *57*, 473-480.

68. Chretien, M.; Li, C. H., Isolation, Purification, and Characterization of Gamma-Lipotropic Hormone from Sheep Pituitary Glands. *Can. J. Biochem.* **1967,** *45*, 1163-1174.

69. Julius, D.; Brake, A.; Blair, L.; Kunisawa, R.; Thorner, J., Isolation of the Putative Structural Gene for the Lysine-Arginine-Cleaving Endopeptidase Required for Processing of Yeast Prepro-Alpha-Factor. *Cell* **1984,** *37*, 1075-1089.

70. Thomas, G.; Thorne, B. A.; Thomas, L.; Allen, R. G.; Hruby, D. E.; Fuller, R.; Thorner, J., Yeast Kex2 Endopeptidase Correctly Cleaves a Neuroendocrine Prohormone in Mammalian Cells. *Science* **1988,** *241*, 226-230.

71. Fuller, R. S.; Sterne, R. E.; Thorner, J., Enzymes Required for Yeast Prohormone Processing. *Annu. Rev. Physiol.* **1988,** *50*, 345-362.

72. Fuller, R. S.; Brake, A. J.; Thorner, J., Intracellular Targeting and Structural Conservation of a Prohormone-Processing Endoprotease. *Science* **1989,** *246*, 482-486.

73. Kiefer, M. C.; Tucker, J. E.; Joh, R.; Landsberg, K. E.; Saltman, D.; Barr, P. J., Identification of a Second Human Subtilisin-Like Protease Gene in the Fes/Fps Region of Chromosome 15. *DNA Cell Biol.* **1991,** *10*, 757-769.

74. Henrich, S.; Cameron, A.; Bourenkov, G. P.; Kiefersauer, R.; Huber, R.; Lindberg, I.; Bode, W.; Than, M. E., The Crystal Structure of the Proprotein Processing Proteinase Furin Explains Its Stringent Specificity. *Nat. Struct. Biol.* **2003,** *10*, 520-526.

75. Cunningham, D.; Danley, D. E.; Geoghegan, K. F.; Griffor, M. C.; Hawkins, J. L.; Subashi, T. A.; Varghese, A. H.; Ammirati, M. J.; Culp, J. S.; Hoth, L. R.; Mansour, M. N.; McGrath, K. M.; Seddon, A. P.; Shenolikar, S.; Stutzman-Engwall, K. J.; Warren, L. C.; Xia, D.; Qiu, X., Structural and Biophysical

Studies of Pcsk9 and Its Mutants Linked to Familial Hypercholesterolemia. *Nat. Struct. Mol. Biol.* **2007,** *14*, 413-419.

76. Chorba, J. S.; Shokat, K. M., The Proprotein Convertase Subtilisin/Kexin Type 9 (Pcsk9) Active Site and Cleavage Sequence Differentially Regulate Protein Secretion from Proteolysis. *J. Biol. Chem.* **2014,** *289*, 29030-29043.

77. Seidah, N. G.; Mowla, S. J.; Hamelin, J.; Mamarbachi, A. M.; Benjannet, S.; Touré, B. B.; Basak, A.; Munzer, J. S.; Marcinkiewicz, J.; Zhong, M.; Barale, J.-C.; Lazure, C.; Murphy, R. A.; Chrétien, M.; Marcinkiewicz, M., Mammalian Subtilisin/Kexin Isozyme Ski-1: A Widely Expressed Proprotein Convertase with a Unique Cleavage Specificity and Cellular Localization. *Proc. Natl. Acad. Sci. U. S. A.* **1999,** *96*, 1321-1326.

78. Ozawa, A.; Peinado, J. R.; Lindberg, I., Modulation of Prohormone Convertase 1/3 Properties Using Site-Directed Mutagenesis. *Endocrinology* **2010,** *151*, 4437-4445.

79. Anderson, E. D.; VanSlyke, J. K.; Thulin, C. D.; Jean, F.; Thomas, G., Activation of the Furin Endoprotease Is a Multiple-Step Process: Requirements for Acidification and Internal Propeptide Cleavage. *The EMBO Journal* **1997,** *16*, 1508-1518.

80. Fugere, M.; Limperis, P. C.; Beaulieu-Audy, V.; Gagnon, F.; Lavigne, P.; Klarskov, K.; Leduc, R.; Day, R., Inhibitory Potency and Specificity of Subtilase-Like Pro-Protein Convertase (Spc) Prodomains. *J. Biol. Chem.* **2002,** *277*, 7648-7456.

81. Kobayashi, H.; Utsunomiya, H.; Yamanaka, H.; Sei, Y.; Katunuma, N.; Okamoto, K.; Tsuge, H., Structural Basis for the Kexin-Like Serine Protease from Aeromonas Sobria as Sepsis-Causing Factor. *J. Biol. Chem.* **2009,** *284*, 27655-27663.

82. Zhou, A.; Martin, S.; Lipkind, G.; LaMendola, J.; Steiner, D. F., Regulatory Roles of the P Domain of the Subtilisin-Like Prohormone Convertases. *J. Biol. Chem.* **1998,** *273*, 11107-11114.

83. Molloy, S. S.; Anderson, E. D.; Jean, F.; Thomas, G., Bi-Cycling the Furin Pathway: From Tgn Localization to Pathogen Activation and Embryogenesis. *Trends Cell Biol.* **1999,** *9*, 28-35.

84. Lusson, J.; Benjannet, S.; Hamelin, J.; Savaria, D.; Chrétien, M.; Seidah, N. G., The Integrity of the Rrgdl Sequence of the Proprotein Convertase Pc1 Is Critical for Its Zymogen and C-Terminal Processing and for Its Cellular Trafficking. *Biochem. J* **1997,** *326 (Pt 3)*, 737-744.

85. Rovère, C.; Luis, J.; Lissitzky, J. C.; Basak, A.; Marvaldi, J.; Chrétien, M.; Seidah, N. G., The Rgd Motif and the C-Terminal Segment of Proprotein Convertase 1 Are Critical for Its Cellular Trafficking but Not for Its Intracellular Binding to Integrin Alpha5beta1. *J. Biol. Chem.* **1999,** *274*, 12461-12467.

86. Seidah, N. G.; Prat, A., The Biology and Therapeutic Targeting of the Proprotein Convertases. *Nat. Rev. Drug Discov.* **2012,** *11*, 367-383.

87. Henrich, S.; Lindberg, I.; Bode, W.; Than, M. E., Proprotein Convertase Models Based on the Crystal Structures of Furin and Kexin: Explanation of Their Specificity. *J. Mol. Biol.* **2005,** *345*, 211-227.

88. Seidah, N. G.; Day, R.; Chrétien, M., The Family of Pro-Hormone and Pro-Protein Convertases. *Biochem. Soc. Trans.* **1993,** *21 (Pt 3)*, 685-691.

89. Seidah, N. G.; Chretien, M.; Day, R., The Family of Subtilisin/Kexin Like Pro-Protein and Pro-Hormone Convertases: Divergent or Shared Functions. *Biochimie* **1994,** *76*, 197-209.

90. Luo, Y.; Warren, L.; Xia, D.; Jensen, H.; Sand, T.; Petras, S.; Qin, W.; Miller, K. S.; Hawkins, J., Function and Distribution of Circulating Human Pcsk9 Expressed Extrahepatically in Transgenic Mice. *J. Lipid Res.* **2009,** *50*, 1581-1588.

91. Couture, F.; Sabbagh, R.; Kwiatkowska, A.; Desjardins, R.; Guay, S.-P.; Bouchard, L.; Day, R., Pace4 Undergoes an Oncogenic Alternative Splicing Switch in Cancer. *Cancer Res.* **2017,** *77*, 6863-6879.

92. Zhong, M.; Benjannet, S.; Lazure, C.; Munzer, S.; Seidah, N. G., Functional Analysis of Human Pace4-a and Pace4-C Isoforms: Identification of a New Pace4-Cs Isoform. *FEBS Lett.* **1996,** *396*, 31-36.

93. Essalmani, R.; Hamelin, J.; Marcinkiewicz, J.; Chamberland, A.; Mbikay, M.; Chretien, M.; Seidah, N. G.; Prat, A., Deletion of the Gene Encoding Proprotein Convertase 5/6 Causes Early Embryonic Lethality in the Mouse. *Mol. Cell. Biol.* **2006,** *26*, 354-361.

94. Khatib, A.-M.; Siegfried, G.; Chrétien, M.; Metrakos, P.; Seidah, N. G., Proprotein Convertases in Tumor Progression and Malignancy: Novel Targets in Cancer Therapy. *Am. J. Pathol.* **2002,** *160*, 1921-1935.

95. Takumi, I.; Steiner, D. F.; Sanno, N.; Teramoto, A.; Osamura, R. Y., Localization of Prohormone Convertases 1/3 and 2 in the Human Pituitary Gland and Pituitary Adenomas: Analysis by Immunohistochemistry, Immunoelectron Microscopy, and Laser Scanning Microscopy. *Mod. Pathol.* **1998,** *11*, 232-238.

96. Jin, L.; Kulig, E.; Qian, X.; Scheithauer, B. W.; Young, W. F., Jr.; Davis, D. H.; Seidah, N. G.; Chretien, M.; Lloyd, R. V., Distribution and Regulation of Proconvertases Pc1 and Pc2 in Human Pituitary Adenomas. *Pituitary* **1999,** *1*, 187-195.

97. Tzimas, G. N.; Chevet, E.; Jenna, S.; Nguyên, D. T.; Khatib, A. M.; Marcus, V.; Zhang, Y.; Chrétien, M.; Seidah, N.; Metrakos, P., Abnormal Expression and Processing of the Proprotein Convertases Pc1 and Pc2 in Human Colorectal Liver Metastases. *BMC Cancer* **2005,** *5*, 149-160.

98. Mbikay, M.; Seidah, N. G.; Chrétien, M., Neuroendocrine Secretory Protein 7b2: Structure, Expression and Functions. *Biochem. J* **2001,** *357*, 329-342.

99. Mbikay, M.; Sirois, F.; Yao, J.; Seidah, N. G.; Chretien, M., Comparative Analysis of Expression of the Proprotein Convertases Furin, Pace4, Pc1 and Pc2 in Human Lung Tumours. *Br. J. Cancer* **1997,** *75*, 1509-1514.

100. Jaaks, P.; Bernasconi, M., The Proprotein Convertase Furin in Tumour Progression. *Int. J. Cancer* **2017,** *141*, 654-663.

101. E., B. D.; Jian, F.; Ricardo, L. d. C.; J.P., K.-S. A., Proprotein Convertases: "Master Switches" in the Regulation of Tumor Growth and Progression. *Mol. Carcinog.* **2005,** *44*, 151-161.

102. Lehmann, M.; Rigot, V.; Seidah, N. G.; Marvaldi, J.; Lissitzky, J. C., Lack of Integrin Alpha-Chain Endoproteolytic Cleavage in Furin-Deficient Human Colon Adenocarcinoma Cells Lovo. *Biochem. J* **1996,** *317 (Pt 3)*, 803-809.

103. Lissitzky, J. C.; Luis, J.; Munzer, J. S.; Benjannet, S.; Parat, F.; Chretien, M.; Marvaldi, J.; Seidah, N. G., Endoproteolytic Processing of Integrin Pro-Alpha Subunits Involves the Redundant Function of Furin and Proprotein Convertase (Pc) 5a, but Not Paired Basic Amino Acid Converting Enzyme (Pace) 4, Pc5b or Pc7. *Biochem. J* **2000,** *346 Pt 1*, 133-138.

104. Posthaus, H.; Dubois, C. M.; Laprise, M. H.; Grondin, F.; Suter, M. M.; Muller, E., Proprotein Cleavage of E-Cadherin by Furin in Baculovirus over-Expression System: Potential Role of Other Convertases in Mammalian Cells. *FEBS Lett.* **1998,** *438*, 306-310.

105. Maret, D.; Sadr, M. S.; Sadr, E. S.; Colman, D. R.; Del Maestro, R. F.; Seidah, N. G., Opposite Roles of Furin and Pc5a in N-Cadherin Processing. *Neoplasia* **2012,** *14*, 880-892.

106. Bassi, D. E.; Mahloogi, H.; Klein-Szanto, A. J. P., The Proprotein Convertases Furin and Pace4 Play a Significant Role in Tumor Progression. *Mol. Carcinog.* **2000,** *28*, 63-69.

107. Wang, F.; Wang, L.; Pan, J., Pace4 Regulates Proliferation, Migration and Invasion in Human Breast Cancer Mda-Mb-231 Cells. *Mol Med Rep* **2015,** *11*, 698-704.

108. Panet, F.; Couture, F.; Kwiatkowska, A.; Desjardins, R.; Guérin, B.; Day, R., Pace4 Is an Important Driver of Zr-75-1 Estrogen Receptor-Positive Breast Cancer Proliferation and Tumor Progression. *Eur. J. Cell Biol.* **2017,** *96*, 469-475.

109. Bassi, D. E.; Lopez De Cicco, R.; Cenna, J.; Litwin, S.; Cukierman, E.; Klein-Szanto, A. J., Pace4 Expression in Mouse Basal Keratinocytes Results in Basement Membrane Disruption and Acceleration of Tumor Progression. *Cancer Res.* **2005,** *65*, 7310-7319.

110. Bassi, D. E.; Cenna, J.; Zhang, J.; Cukierman, E.; Klein-Szanto, A. J., Enhanced Aggressiveness of Benzopyrene-Induced Squamous Carcinomas in Transgenic Mice Overexpressing the Proprotein Convertase Pace4 (Pcsk6). *Mol. Carcinog.* **2015,** *54*, 1122-1131.

111. Longuespée, R.; Couture, F.; Levesque, C.; Kwiatkowska, A.; Desjardins, R.; Gagnon, S.; Vergara, D.; Maffia, M.; Fournier, I.; Salzet, M.; Day, R., Implications of Proprotein Convertases in Ovarian Cancer Cell Proliferation and Tumor Progression: Insights for Pace4 as a Therapeutic Target. *Transl. Oncol.* **2014,** *7*, 410-419.

112. Lin, Y.-E.; Wu, Q.-N.; Lin, X.-D.; Li, G.-Q.; Zhang, Y.-J., Expression of Paired Basic Amino Acid-Cleaving Enzyme 4 (Pace4) Correlated with Prognosis in Non-Small Cell Lung Cancer (Nsclc) Patients. *J. Thorac. Dis.* **2015,** *7*, 850-860.

113. Fu, Y.; Campbell, E. J.; Shepherd, T. G.; Nachtigal, M. W., Epigenetic Regulation of Proprotein Convertase Pace4 Gene Expression in Human Ovarian Cancer Cells. *Mol. Cancer Res.* **2003,** *1*, 569-576.

114. D'Anjou, F.; Routhier, S.; Perreault, J. P.; Latil, A.; Bonnel, D.; Fournier, I.; Salzet, M.; Day, R., Molecular Validation of Pace4 as a Target in Prostate Cancer. *Transl. Oncol.* **2011,** *4*, 157-172.

115. Klee, E. W.; Bondar, O. P.; Goodmanson, M. K.; Dyer, R. B.; Erdogan, S.; Bergstralh, E. J.; Bergen, H. R.; Sebo, T. J.; Klee, G. G., Candidate Serum Biomarkers for Prostate Adenocarcinoma Identified by Mrna Differences in Prostate Tissue and Verified with Protein Measurements in Tissue and Blood. *Clin. Chem.* **2012,** *58*, 599-609.

116. Kang, S.; Zhao, Y.; Hu, K.; Xu, C.; Wang, L.; Liu, J.; Yao, A.; Zhang, H.; Cao, F., Mir-124 Exhibits Antiproliferative and Antiaggressive Effects on Prostate Cancer Cells through Pace4 Pathway. *Prostate* **2014,** *74*, 1095-1106.

117. Couture, F.; D'Anjou, F.; Desjardins, R.; Boudreau, F.; Day, R., Role of Proprotein Convertases in Prostate Cancer Progression. *Neoplasia* **2012,** *14*, 1032-1042.

118. Krem, M. M.; Di Cera, E., Molecular Markers of Serine Protease Evolution. *EMBO J.* **2001,** *20*, 3036-3045.

119. Brenner, S., The Molecular Evolution of Genes and Proteins: A Tale of Two Serines. *Nature* **1988,** *334*, 528-530.

120. Garten, W.; Hallenberger, S.; Ortmann, D.; Schäfer, W.; Vey, M.; Angliker, H.; Shaw, E.; Klenk, H. D., Processing of Viral Glycoproteins by the Subtilisin-Like Endoprotease Furin and Its Inhibition by Specific Peptidylchloroalkylketones. *Biochimie* **1994,** *76*, 217-225.

121. Jean, F.; Basak, A.; DiMaio, J.; Seidah, N. G.; Lazure, C., An Internally Quenched Fluorogenic Substrate of Prohormone Convertase 1 and Furin Leads to a Potent Prohormone Convertase Inhibitor. *Biochem. J* **1995,** *307 (Pt 3)*, 689-695.

122. Remacle, A. G.; Gawlik, K.; Golubkov, V. S.; Cadwell, G. W.; Liddington, R. C.; Cieplak, P.; Millis, S. Z.; Desjardins, R.; Routhier, S.; Yuan, X. W.; Neugebauer, W. A.; Day, R.; Strongin, A. Y., Selective and Potent Furin Inhibitors Protect Cells from Anthrax without Significant Toxicity. *Int. J. Biochem. Cell Biol.* **2010,** *42*, 987-995.

123. Cheng, Y.; Prusoff, W. H., Relationship between the Inhibition Constant (Ki) and the Concentration of Inhibitor Which Causes 50 Percent Inhibition (I50) of an Enzymatic Reaction. *Biochem. Pharmacol.* **1973,** *22*, 3099-3108.

124. Murphy, D. J., Determination of Accurate Ki Values for Tight-Binding Enzyme Inhibitors: An in Silico Study of Experimental Error and Assay Design. *Anal. Biochem.* **2004,** *327*, 61-67.

125. Angliker, H., Synthesis of Tight Binding Inhibitors and Their Action on the Proprotein-Processing Enzyme Furin. *J. Med. Chem.* **1995,** *38*, 4014-4018.

126. Fugere, M.; Appel, J.; Houghten, R. A.; Lindberg, I.; Day, R., Short Polybasic Peptide Sequences Are Potent Inhibitors of Pc5/6 and Pc7: Use of Positional Scanning-Synthetic Peptide Combinatorial Libraries as a Tool for the Optimization of Inhibitory Sequences. *Mol. Pharmacol.* **2007,** *71*, 323-332.

127. Ramos-Molina, B.; Lick, A. N.; Nasrolahi Shirazi, A.; Oh, D.; Tiwari, R.; El-Sayed, N. S.; Parang, K.; Lindberg, I., Cationic Cell-Penetrating Peptides Are Potent Furin Inhibitors. *PLoS One* **2015,** *10*, e0130417.

128. Gu, M.; Rappaport, J.; Leppla, S. H., Furin Is Important but Not Essential for the Proteolytic Maturation of Gp160 of Hiv-1. *FEBS Lett.* **1995,** *365*, 95-97.

129. Bassi, D. E.; Lopez De Cicco, R.; Mahloogi, H.; Zucker, S.; Thomas, G.; Klein-Szanto, A. J. P., Furin Inhibition Results in Absent or Decreased Invasiveness and Tumorigenicity of Human Cancer Cells. *Proc. Natl. Acad. Sci. U.S.A.* **2001,** *98*, 10326-10331.

130. Stieneke-Grober, A.; Vey, M.; Angliker, H.; Shaw, E.; Thomas, G.; Roberts, C.; Klenk, H. D.; Garten, W., Influenza Virus Hemagglutinin with Multibasic Cleavage Site Is Activated by Furin, a Subtilisin-Like Endoprotease. *EMBO J.* **1992,** *11*, 2407-2414.

131. Shiryaev, S. A.; Remacle, A. G.; Ratnikov, B. I.; Nelson, N. A.; Savinov, A. Y.; Wei, G.; Bottini, M.; Rega, M. F.; Parent, A.; Desjardins, R.; Fugere, M.; Day, R.; Sabet, M.; Pellecchia, M.; Liddington, R. C.; Smith, J. W.; Mustelin, T.; Guiney, D. G.; Lebl, M.; Strongin, A. Y., Targeting Host Cell Furin Proprotein Convertases as a Therapeutic Strategy against Bacterial Toxins and Viral Pathogens. *J. Biol. Chem.* **2007,** *282*, 20847-20853.

132. Pang, Y. J.; Tan, X. J.; Li, D. M.; Zheng, Z. H.; Lei, R. X.; Peng, X. M., Therapeutic Potential of Furin Inhibitors for the Chronic Infection of Hepatitis B Virus. *Liver Int.* **2013,** *33*, 1230-1238.

133. Cameron, A.; Appel, J.; Houghten, R. A.; Lindberg, I., Polyarginines Are Potent Furin Inhibitors. *J. Biol. Chem.* **2000,** *275*, 36741-36749.

134. Karicherla, P.; Hobden, J. A., Nona-D-Arginine Therapy for Pseudomonas Aeruginosa Keratitis. *Invest. Ophthalmol. Vis. Sci.* **2009,** *50*, 256-262.

135. Karicherla, P.; Hobden, J. A., Nona-D-Arginine Amide for Prophylaxis and Treatment of Experimental Pseudomonas Aeruginosa Keratitis. *Curr. Eye Res.* **2010,** *35*, 220-224.

136. Basak, A.; Lazure, C., Synthetic Peptides Derived from the Prosegments of Proprotein Convertase 1/3 and Furin Are Potent Inhibitors of Both Enzymes. *Biochem Journal* **2003,** *373*, 231-239.

137. Basak, A.; Ernst, B.; Brewer, D.; Seidah, N. G.; Munzer, J. S.; Lazure, C.; Lajoie, G. A., Histidine-Rich Human Salivary Peptides Are Inhibitors of Proprotein Convertases Furin and Pc7 but Act as Substrates for Pc1. *J. Pept. Res.* **1997,** *49*, 596-603.

138. Basak, A.; Koch, P.; Dupelle, M.; Fricker, L. D.; Devi, L. A.; Chretien, M.; Seidah, N. G., Inhibitory Specificity and Potency of Prosaas-Derived Peptides toward Proprotein Convertase 1. *J. Biol. Chem.* **2001,** *276*, 32720-32728.

139. Basak, A.; Schmidt, C.; Ismail, A. A.; Seidah, N. G.; Chretien, M.; Lazcre, C., Peptidyl Substrates Containing Unnatural Amino Acid at the P′1 Position Are Potent Inhibitors of Prohormone Convertases. *Int. J. Pept. Protein Res.* **1995,** *46*, 228-237.

140. Apletalina, E.; Appel, J.; Lamango, N. S.; Houghten, R. A.; Lindberg, I., Identification of Inhibitors of Prohormone Convertases 1 and 2 Using a Peptide Combinatorial Library. *J. Biol. Chem.* **1998,** *273*, 26589-26595.

141. Fittler, H.; Depp, A.; Avrutina, O.; Dahms, S. O.; Than, M. E.; Empting, M.; Kolmar, H., Engineering a Constrained Peptidic Scaffold Towards Potent and Selective Furin Inhibitors. *ChemBioChem* **2015,** *16*, 2441-2444.

142. Jean, F.; Stella, K.; Thomas, L.; Liu, G.; Xiang, Y.; Reason, A. J.; Thomas, G., A(1)-Antitrypsin Portland, a Bioengineered Serpin Highly Selective for Furin: Application as an Antipathogenic Agent. *Proc. Natl. Acad. Sci. U. S. A.* **1998,** *95*, 7293-7298.

143. Dufour, E. K.; Denault, J. B.; Bissonnette, L.; Hopkins, P. C.; Lavigne, P.; Leduc, R., The Contribution of Arginine Residues within the P6-P1 Region of Alpha 1-Antitrypsin to Its Reaction with Furin. *J. Biol. Chem.* **2001,** *276*, 38971-38979.

144. Lu, W.; Zhang, W.; Molloy, S. S.; Thomas, G.; Ryan, K.; Chiang, Y.; Anderson, S.; Laskowski, M., Jr., Arg15-Lys17-Arg18 Turkey Ovomucoid Third Domain Inhibits Human Furin. *J. Biol. Chem.* **1993,** *268*, 14583-14585.

145. VAN ROMPAEY, L.; Ayoubi, T.; VAN DE VEN, W.; Marynen, P., Inhibition of Intracellular Proteolytic Processing of Soluble Proproteins by an Engineered A2-Macroglobulin Containing a Furin Recognition Sequence in the Bait Region. *Biochem. J* **1997,** *326*, 507-514.

146. Komiyama, T.; Swanson, J. A.; Fuller, R. S., Protection from Anthrax Toxin-Mediated Killing of Macrophages by the Combined Effects of Furin Inhibitors and Chloroquine. *Antimicrob. Agents Chemother.* **2005,** *49*, 3875-3882.

147. Liu, Z.-x.; Fei, H.; Chi, C.-w., Two Engineered Eglin C Mutants Potently and Selectively Inhibiting Kexin or Furin. *FEBS Lett.* **2004,** *556*, 116-120.

148. Komiyama, T.; VanderLugt, B.; Fugère, M.; Day, R.; Kaufman, R. J.; Fuller, R. S., Optimization of Protease-Inhibitor Interactions by Randomizing Adventitious Contacts. *Proc. Natl. Acad. Sci. U.S.A.* **2003,** *100*, 8205-8210.

149. Lindberg, I.; van den Hurk, W. H.; Bui, C.; Batie, C. J., Enzymic Characterization of Immunopurified Prohormone Convertase 2: Potent Inhibition by a 7b2 Peptide Fragment. *Biochemistry* **1995,** *34*, 5486-5493.

150. Apletalina, E. V.; Juliano, M. A.; Juliano, L.; Lindberg, I., Structure–Function Analysis of the 7b2 Ct Peptide. *Biochem. Biophys. Res. Commun.* **2000,** *267*, 940-942.

151. Basak, A.; Khatib, A.-M.; Mohottalage, D.; Basak, S.; Kolajova, M.; Bag, S. S.; Basak, A., A Novel Enediynyl Peptide Inhibitor of Furin That Blocks Processing of Propdgf-a, B and Provegf-C. *PLoS One* **2009,** *4*, 1-14.

152. Podsiadlo, P.; Komiyama, T.; Fuller, R. S.; Blum, O., Furin Inhibition by Compounds of Copper and Zinc. *J. Biol. Chem.* **2004,** *279*, 36219-36227.

153. Basak, A.; Cooper, S.; Roberge, A. G.; Banik, U. K.; Chrétien, M.; Seidah, N. G., Inhibition of Proprotein Convertases-1, -7 and Furin by Diterpines of Andrographis Paniculata and Their Succinoyl Esters. *Biochem. J* **1999,** *338*, 107-113.

154. Jiao, G.-S.; Cregar, L.; Wang, J.; Millis, S. Z.; Tang, C.; O'Malley, S.; Johnson, A. T.; Sareth, S.; Larson, J.; Thomas, G., Synthetic Small Molecule Furin Inhibitors Derived from 2,5-Dideoxystreptamine. *Proc. Natl. Acad. Sci. U.S.A.* **2006,** *103*, 19707-19712.

155. Ramos-Molina, B.; Lick, A. N.; Blanco, E. H.; Posada-Salgado, J. A.; Martinez-Mayorga, K.; Johnson, A. T.; Jiao, G.-S.; Lindberg, I., Identification of Potent and Compartment-Selective Small Molecule Furin Inhibitors Using Cell-Based Assays. *Biochem. Pharmacol.* **2015,** *96*, 107-118.

156. Dahms, S. O.; Jiao, G.-S.; Than, M. E., Structural Studies Revealed Active Site Distortions of Human Furin by a Small Molecule Inhibitor. *ACS Chem. Biol.* **2017,** *12*, 1211-1216.

157. Becker, G. L.; Sielaff, F.; Than, M. E.; Lindberg, I.; Routhier, S.; Day, R.; Lu, Y.; Garten, W.; Steinmetzer, T., Potent Inhibitors of Furin and Furin-Like Proprotein Convertases Containing Decarboxylated P1 Arginine Mimetics. *J. Med. Chem.* **2010,** *53*, 1067-1075.

158. Becker, G. L.; Lu, Y.; Hardes, K.; Strehlow, B.; Levesque, C.; Lindberg, I.; Sandvig, K.; Bakowsky, U.; Day, R.; Garten, W.; Steinmetzer, T., Highly Potent Inhibitors of Proprotein Convertase Furin as Potential Drugs for Treatment of Infectious Diseases. *J. Biol. Chem.* **2012,** *287*, 21992-22003.

159. Dahms, S. O.; Hardes, K.; Becker, G. L.; Steinmetzer, T.; Brandstetter, H.; Than, M. E., X-Ray Structures of Human Furin in Complex with Competitive Inhibitors. *ACS Chem. Biol.* **2014,** *9*, 1113-1118.

160. Hardes, K.; Becker, G. L.; Lu, Y.; Dahms, S. O.; Kohler, S.; Beyer, W.; Sandvig, K.; Yamamoto, H.; Lindberg, I.; Walz, L.; von Messling, V.; Than, M. E.; Garten, W.; Steinmetzer, T., Novel Furin Inhibitors with Potent Anti-Infectious Activity. *ChemMedChem* **2015,** *10*, 1218-1231.

161. Ivanova, T.; Hardes, K.; Kallis, S.; Dahms, S. O.; Than, M. E.; Künzel, S.; Böttcher-Friebertshäuser, E.; Lindberg, I.; Jiao, G.-S.; Bartenschlager, R.; Steinmetzer, T., Optimization of Substrate-Analogue Furin Inhibitors. *ChemMedChem* **2017,** *12*, 1953-1968.

162. Dahms, S. O.; Arciniega, M.; Steinmetzer, T.; Huber, R.; Than, M. E., Structure of the Unliganded Form of the Proprotein Convertase Furin Suggests Activation by a Substrate-Induced Mechanism. *Proc. Natl. Acad. Sci. U.S.A.* **2016,** *113*, 11196-11201.

163. Loughlin, W. A.; Tyndall, J. D. A.; Glenn, M. P.; Hill, T. A.; Fairlie, D. P., Update 1 Of: Beta-Strand Mimetics. *Chem. Rev.* **2010,** *110*, PR32-PR69.

164. Couture, F.; D'Anjou, F.; Day, R., On the Cutting Edge of Proprotein Convertase Pharmacology: From Molecular Concepts to Clinical Applications. *Biomol. Concepts* **2011,** *2*, 421-438.

165. Dahms, S. O.; Hardes, K.; Steinmetzer, T.; Than, M. E., X-Ray Structures of the Proprotein Convertase Furin Bound with Substrate Analogue Inhibitors Reveal Substrate Specificity Determinants Beyond the S4 Pocket. *Biochemistry* **2018,** *57*, 925-934.

166. Levesque, C.; Fugere, M.; Kwiatkowska, A.; Couture, F.; Desjardins, R.; Routhier, S.; Moussette, P.; Prahl, A.; Lammek, B.; Appel, J. R.; Houghten, R. A.; D'Anjou, F.; Dory, Y. L.; Neugebauer, W.; Day, R., The Multi-Leu Peptide Inhibitor Discriminates between Pace4 and Furin and Exhibits Antiproliferative Effects on Prostate Cancer Cells. *J. Med. Chem.* **2012,** *55*, 10501-10511.

167. Kwiatkowska, A.; Couture, F.; Levesque, C.; Ly, K.; Desjardins, R.; Beauchemin, S.; Prahl, A.; Lammek, B.; Neugebauer, W.; Dory, Y. L.; Day, R., Design, Synthesis, and Structure-Activity Relationship Studies of a Potent Pace4 Inhibitor. *J. Med. Chem.* **2014,** *57*, 98-109.

168. Kwiatkowska, A.; Couture, F.; Levesque, C.; Ly, K.; Beauchemin, S.; Desjardins, R.; Neugebauer, W.; Dory, Y. L.; Day, R., Novel Insights into Structure-Activity Relationships of N-Terminally Modified Pace4 Inhibitors. *ChemMedChem* **2016,** *11*, 289-301.

169. Lepek, T.; Kwiatkowska, A.; Couture, F.; Ly, K.; Desjardins, R.; Dory, Y.; Prahl, A.; Day, R., Macrocyclization of a Potent Pace4 Inhibitor: Benefits and Limitations. *Eur. J. Cell Biol.* **2017,** *96*, 476-485.

170. Levesque, C.; Couture, F.; Kwiatkowska, A.; Desjardins, R.; Guerin, B.; Neugebauer, W. A.; Day, R., Pace4 Inhibitors and Their Peptidomimetic Analogs Block Prostate Cancer Tumor Progression through Quiescence Induction, Increased Apoptosis and Impaired Neovascularisation. *Oncotarget* **2015,** *6*, 3680-3693.

171. Maluch, I.; Levesque, C.; Kwiatkowska, A.; Couture, F.; Ly, K.; Desjardins, R.; Neugebauer, W. A.; Prahl, A.; Day, R., Positional Scanning Identifies the Molecular Determinants of a High Affinity Multi-Leucine Inhibitor for Furin and Pace4. *J. Med. Chem.* **2017,** *60*, 2732-2744.

172. Guérin, B.; Ait-Mohand, S.; Tremblay, M.-C.; Dumulon-Perreault, V.; Fournier, P.; Bénard, F., Total Solid-Phase Synthesis of Nota-Functionalized Peptides for Pet Imaging. *Org. Lett.* **2010,** *12*, 280-283.

173. Couture, F.; Ly, K.; Levesque, C.; Kwiatkowska, A.; Ait-Mohand, S.; Desjardins, R.; Guérin, B.; Day, R., Multi-Leu Pace4 Inhibitor Retention within Cells Is Pace4 Dependent and a Prerequisite for Antiproliferative Activity. *Biomed Res. Int.* **2015,** *2015*, 1-9.

174. Madala, P. K.; Tyndall, J. D. A.; Nall, T.; Fairlie, D. P., Update 1 Of: Proteases Universally Recognize Beta Strands in Their Active Sites. *Chem. Rev.* **2010,** *110*, PR1-PR31.

175. Ghosh, A. K.; Anderson, D. D.; Weber, I. T.; Mitsuya, H., Enhancing Protein Backbone Binding—a Fruitful Concept for Combating Drug-Resistant Hiv. *Angew. Chem. Int. Ed.* **2012,** *51*, 1778-1802.

176. Chou, P. Y.; Fasman, G. D., Secondary Structural Prediction of Proteins from Their Amino Acid Sequence. *Trends Biochem. Sci* **1977,** *2*, 128-131.

177. Swindells, M. B.; MacArthur, M. W.; Thornton, J. M., Intrinsic Φ,Ψ Propensities of Amino Acids, Derived from the Coil Regions of Known Structures. *Nat. Struct. Biol.* **1995,** *2*, 596-603.

178. Minor, D. L., Jr.; Kim, P. S., Measurement of the Beta-Sheet-Forming Propensities of Amino Acids. *Nature* **1994,** *367*, 660-663.

179. Street, A. G.; Mayo, S. L., Intrinsic Beta-Sheet Propensities Result from Van Der Waals Interactions between Side Chains and the Local Backbone. *Proc. Natl. Acad. Sci. U.S.A.* **1999,** *96*, 9074-9076.

180. Pal, D.; Chakrabarti, P., Beta-Sheet Propensity and Its Correlation with Parameters Based on Conformation. *Acta Crystallogr. D Biol. Crystallogr.* **2000,** *56*, 589-594.

181. Bai, Y.; Englander, S. W., Hydrogen Bond Strength and Beta-Sheet Propensities: The Role of a Side Chain Blocking Effect. *Proteins* **1994,** *18*, 262-266.

182. Kempf, D. J.; Marsh, K. C.; Denissen, J. F.; McDonald, E.; Vasavanonda, S.; Flentge, C. A.; Green, B. E.; Fino, L.; Park, C. H.; Kong, X. P.; et al., Abt-538 Is a Potent Inhibitor of Human Immunodeficiency Virus Protease and Has High Oral Bioavailability in Humans. *Proc. Natl. Acad. Sci. U.S.A.* **1995,** *92*, 2484-2488.

183. Clements, J. M.; Beckett, R. P.; Brown, A.; Catlin, G.; Lobell, M.; Palan, S.; Thomas, W.; Whittaker, M.; Wood, S.; Salama, S.; Baker, P. J.; Rodgers, H. F.; Barynin, V.; Rice, D. W.; Hunter, M. G., Antibiotic Activity and Characterization of Bb-3497, a Novel Peptide Deformylase Inhibitor. *Antimicrob. Agents Chemother.* **2001,** *45*, 563-570.

184. Yamamoto, A.; Tomoo, K.; Hara, T.; Murata, M.; Kitamura, K.; Ishida, T., Substrate Specificity of Bovine Cathepsin B and Its Inhibition by Ca074, Based on Crystal Structure Refinement of the Complex. *J. Biochem.* **2000,** *127*, 635-643.

185. Kuo, L. H.; Li, J. H.; Kuo, H. T.; Hung, C. Y.; Tsai, H. Y.; Chiu, W. C.; Wu, C. H.; Wang, W. R.; Yang, P. A.; Yao, Y. C.; Wong, T. W.; Huang, S. J.; Huang, S. L.; Cheng, R. P., Effect of Charged Amino

Acid Side Chain Length at Non-Hydrogen Bonded Strand Positions on Beta-Hairpin Stability. *Biochemistry* **2013,** *52*, 7785-7797.

186. Syud, F. A.; Stanger, H. E.; Gellman, S. H., Interstrand Side Chain--Side Chain Interactions in a Designed Beta-Hairpin: Significance of Both Lateral and Diagonal Pairings. *J. Am. Chem. Soc.* **2001,** *123*, 8667-8677.

187. Riemen, A. J.; Waters, M. L., Design of Highly Stabilized Beta-Hairpin Peptides through Cation-Pi Interactions of Lysine and N-Methyllysine with an Aromatic Pocket. *Biochemistry* **2009,** *48*, 1525-1531.

188. Wu, L.; McElheny, D.; Huang, R.; Keiderling, T. A., Role of Tryptophan-Tryptophan Interactions in Trpzip Beta-Hairpin Formation, Structure, and Stability. *Biochemistry* **2009,** *48*, 10362-10371.

189. Almeida, A. M.; Li, R.; Gellman, S. H., Parallel Beta-Sheet Secondary Structure Is Stabilized and Terminated by Interstrand Disulfide Cross-Linking. *J. Am. Chem. Soc.* **2012,** *134*, 75-78.

190. Maynard, S. J.; Almeida, A. M.; Yoshimi, Y.; Gellman, S. H., New Charge-Bearing Amino Acid Residues That Promote Beta-Sheet Secondary Structure. *J. Am. Chem. Soc.* **2014,** *136*, 16683-16688.

191. Longuespee, R.; Couture, F.; Levesque, C.; Kwiatkowska, A.; Desjardins, R.; Gagnon, S.; Vergara, D.; Maffia, M.; Fournier, I.; Salzet, M.; Day, R., Implications of Proprotein Convertases in Ovarian Cancer Cell Proliferation and Tumor Progression: Insights for Pace4 as a Therapeutic Target. *Transl. Oncol.* **2014,** *7*, 410-419.

192. Becker, G. L.; Hardes, K.; Steinmetzer, T., New Substrate Analogue Furin Inhibitors Derived from 4-Amidinobenzylamide. *Bioorg. Med. Chem. Lett.* **2011,** *21*, 4695-4697.

193. Dunbrack, R. L.; Karplus, M., Backbone-Dependent Rotamer Library for Proteins Application to Side-Chain Prediction. *J. Mol. Biol.* **1993,** *230*, 543-574.

194. Baker, E. N.; Hubbard, R. E., Hydrogen Bonding in Globular Proteins. *Prog. Biophys. Mol. Biol.* **1984,** *44*, 97-179.

195. Izzo, I.; Acosta, G. A.; Tulla-Puche, J.; Cupido, T.; Martin-Lopez, M. J.; Cuevas, C.; Albericio, F., Solid-Phase Synthesis of Aza-Kahalalide F Analogues: (2r,3r)-2-Amino-3-Azidobutanoic Acid as Precursor of the Aza-Threonine. *Eur. J. Org. Chem.* **2010**, 2536-2543.

196. Feichtinger, K.; Zapf, C.; Sings, H. L.; Goodman, M., Diprotected Triflylguanidines: A New Class of Guanidinylation Reagents. *J. Org. Chem.* **1998,** *63*, 3804-3805.

197. Bernatowicz, M. S.; Wu, Y.; Matsueda, G. R., 1h-Pyrazole-1-Carboxamidine Hydrochloride an Attractive Reagent for Guanylation of Amines and Its Application to Peptide Synthesis. *J. Org. Chem.* **1992,** *57*, 2497-2502.

198. Cohrt, A. E.; Nielsen, T. E., Solid-Phase Synthesis of Peptide Thioureas and Thiazole-Containing Macrocycles through Ru-Catalyzed Ring-Closing Metathesis. *ACS Comb. Sci.* **2014,** *16*, 71-77.

199. Kuo, H.-T.; Liu, S.-L.; Chiu, W.-C.; Fang, C.-J.; Chang, H.-C.; Wang, W.-R.; Yang, P.-A.; Li, J.-H.; Huang, S.-J.; Huang, S.-L.; Cheng, R. P., Effect of Charged Amino Acid Side Chain Length on Lateral Cross-Strand Interactions between Carboxylate- and Guanidinium-Containing Residues in a B-Hairpin. *Amino Acids* **2015,** *47*, 885-898.

200. Cheng, Y.; Prusoff, W. H., Relationship between the Inhibition Constant (K1) and the Concentration of Inhibitor Which Causes 50 Per Cent Inhibition (I50) of an Enzymatic Reaction. *Biochem. Pharmacol.* **1973,** *22*, 3099-3108.

201. Morrison, J. F., Kinetics of the Reversible Inhibition of Enzyme-Catalysed Reactions by Tight-Binding Inhibitors. *Biochim. Biophys. Acta* **1969,** *185*, 269-286.

202. Madhavi Sastry, G.; Adzhigirey, M.; Day, T.; Annabhimoju, R.; Sherman, W., Protein and Ligand Preparation: Parameters, Protocols, and Influence on Virtual Screening Enrichments. *J. Comput. Aided Mol. Des.* **2013,** *27*, 221-234.

203. Berendsen, H. J. C.; van der Spoel, D.; van Drunen, R., Gromacs: A Message-Passing Parallel Molecular Dynamics Implementation. *Comput. Phys. Commun.* **1995,** *91*, 43-56.

204. Lindahl, E.; Hess, B.; van der Spoel, D., Gromacs 3.0: A Package for Molecular Simulation and Trajectory Analysis. *J. Mol. Model.* **2001,** *7*, 306-317.

205. Van Der Spoel, D.; Lindahl, E.; Hess, B.; Groenhof, G.; Mark, A. E.; Berendsen, H. J. C., Gromacs: Fast, Flexible, and Free. *J. Comput. Chem.* **2005,** *26*, 1701-1718.

206. Pronk, S.; Pall, S.; Schulz, R.; Larsson, P.; Bjelkmar, P.; Apostolov, R.; Shirts, M. R.; Smith, J. C.; Kasson, P. M.; van der Spoel, D.; Hess, B.; Lindahl, E., Gromacs 4.5: A High-Throughput and Highly Parallel Open Source Molecular Simulation Toolkit. *Bioinformatics* **2013,** *29*, 845-854.

207. Páll, S.; Abraham, M. J.; Kutzner, C.; Hess, B.; Lindahl, E., Tackling Exascale Software Challenges in Molecular Dynamics Simulations with Gromacs. In *Solving Software Challenges for Exascale: International Conference on Exascale Applications and Software, Easc 2014, Stockholm, Sweden, April 2-3, 2014, Revised Selected Papers*, Markidis, S.; Laure, E., Eds. Springer International Publishing: Cham, 2015; pp 3-27.

208. Abraham, M. J.; Murtola, T.; Schulz, R.; Páll, S.; Smith, J. C.; Hess, B.; Lindahl, E., Gromacs: High Performance Molecular Simulations through Multi-Level Parallelism from Laptops to Supercomputers. *SoftwareX* **2015,** *1*, 19-25.

209. Garcia, A. E.; Sanbonmatsu, K. Y., Alpha-Helical Stabilization by Side Chain Shielding of Backbone Hydrogen Bonds. *Proc. Natl. Acad. Sci. U.S.A.* **2002,** *99*, 2782-3787.

210. Klein-Szanto, A. J.; Bassi, D. E., Proprotein Convertase Inhibition: Paralyzing the Cell's Master Switches. *Biochem. Pharmacol.* **2017,** *140*, 8-15.

211. Fugère, M.; Day, R., Cutting Back on Pro-Protein Convertases: The Latest Approaches to Pharmacological Inhibition. *Trends Pharmacol. Sci.* **2005,** *26*, 294-301.

212. Dianati, V.; Shamloo, A.; Kwiatkowska, A.; Desjardins, R.; Soldera, A.; Day, R.; Dory, Y. L., Rational Design of a Highly Potent and Selective Peptide Inhibitor of Pace4 by Salt Bridge Interaction with D160 at Position P3. *ChemMedChem* **2017,** *12*, 1169-1172.

213. Huggins, D. J.; Sherman, W.; Tidor, B., Rational Approaches to Improving Selectivity in Drug Design. *J. Med. Chem.* **2012,** *55*, 1424-1444.

214. Lynas, J.; Walker, B., Peptidyl Inverse Esters of P-Methoxybenzoic Acid: A Novel Class of Potent Inactivator of the Serine Proteases. *Biochem. J* **1997,** *325*, 609-616.

215. Thompson, R. C., Use of Peptide Aldehydes to Generate Transition-State Analogs of Elastase. *Biochemistry* **1973,** *12*, 47-51.

216. MarvinSketch (version 18.1.0 , calculation module developed by ChemAxon, http://www.chemaxon.com/products/marvin/marvinsketch/, 2018.

217. Tailhades, J.; Gidel, M.-A.; Grossi, B.; Lécaillon, J.; Brunel, L.; Subra, G.; Martinez, J.; Amblard, M., Synthesis of Peptide Alcohols on the Basis of an O–N Acyl-Transfer Reaction. *Angew. Chem. Int. Ed.* **2010,** *49*, 117-120.

218. Judkins, B. D.; Allen, D. G.; Cook, T. A.; Evans, B.; Sardharwala, T. E., A Versatile Synthesis of Amidines from Nitriles Via Amidoximes. *Synth. Commun.* **1996,** *26*, 4351-4367.

219. Bondebjerg, J.; Xiang, Z.; Bauzo, R. M.; Haskell-Luevano, C.; Meldal, M., A Solid-Phase Approach to Mouse Melanocortin Receptor Agonists Derived from a Novel Thioether Cyclized Peptidomimetic Scaffold. *J. Am. Chem. Soc.* **2002,** *124*, 11046-11055.

220. Thomson, D. W.; Commeureuc, A. G. J.; Berlin, S.; Murphy, J. A., Efficient Route to the Pineal Hormone Melatonin by Radical-Based Indole Synthesis. *Synth. Commun.* **2003,** *33*, 3631-3641.

221. Xu, Z.; Xiao, Y.; Ding, H.; Cao, C.; Li, H.; Pang, G.; Shi, Y., Palladium/N-Heterocyclic Carbene Catalyzed Mono- and Double-Cyanation of Aryl Halides Using Potassium Ferrocyanide Trihydrate under Aerobic Conditions. *Synthesis* **2015,** *47*, 1560-1566.

222. Cioslowski, J.; Barański, A.; Juška, T., A Simple Algorithm for the Calculation of the Π Ionization Energies of Substituted Benzenes. *Tetrahedron* **1986,** *42*, 4549-4555.

223. Cai, S.; Zhang, S.; Zhao, Y.; Wang, D. Z., New Approach to Oximes through Reduction of Nitro Compounds Enabled by Visible Light Photoredox Catalysis. *Org. Lett.* **2013,** *15*, 2660-2663.

224. Day, J. I.; Weaver, J. D., Selective and Scalable Perfluoroarylation of Nitroalkanes. *The Journal of Organic Chemistry* **2017,** *82*, 6801-6810.

225. Badgujar, S.; Kaur, K.; Malpani, Y.; Kanjilal, P. R., Practical and Chemoselective Reduction of Acyl Chloride to Alcohol by Borohydride in Aqueous Dichloromethane Au - Rajan, Ramya. *Synth. Commun.* **2010,** *40*, 2897-2907.

226. Ashimori, A.; Ono, T.; Uchida, T.; Ohtaki, Y.; Fukaya, C.; Watanabe, M.; Yokoyama, K., Novel 1, 4-Dihydropyridine Calcium Antagonists. I. : Synthesis and Hypotensive Activity of 4-(Substituted Pyridyl)-1, 4-Dihydropyridine Derivatives. *Chem. Pharm. Bull. (Tokyo)* **1990,** *38*, 2446-2458.

227. Kohn, W.; Becke, A. D.; Parr, R. G., Density Functional Theory of Electronic Structure. *The Journal of Physical Chemistry* **1996,** *100*, 12974-12980.

228. Valdes, H.; Pluháčková, K.; Pitonák, M.; Řezáč, J.; Hobza, P., Benchmark Database on Isolated Small Peptides Containing an Aromatic Side Chain: Comparison between Wave Function and Density Functional Theory Methods and Empirical Force Field. *PCCP* **2008,** *10*, 2747-2757.

229. Zhao, Y.; Truhlar, D. G., Density Functionals with Broad Applicability in Chemistry. *Acc. Chem. Res.* **2008,** *41*, 157-167.

230. Schmidt, M. W.; Baldridge, K. K.; Boatz, J. A.; Elbert, S. T.; Gordon, M. S.; Jensen, J. H.; Koseki, S.; Matsunaga, N.; Nguyen, K. A.; Su, S.; Windus, T. L.; Dupuis, M.; Montgomery Jr, J. A., General Atomic and Molecular Electronic Structure System. *J. Comput. Chem.* **1993,** *14*, 1347-1363.

231. Molecular Operating Environment (MOE), 2013.08; Chemical Computing Group ULC: 1010 Sherbooke St. West, Suite #910, Montreal, QC, Canada, H3A 2R7, 2018.

232. Murphy, D. J., Determination of Accurate Ki Values for Tight-Binding Enzyme Inhibitors: An in Silico Study of Experimental Error and Assay Design. *Anal. Biochem.* **2004,** *327*, 61-67.

233. Mains, R. E.; Berard, C. A.; Denault, J. B.; Zhou, A.; Johnson, R. C.; Leduc, R., Pace4: A Subtilisin-Like Endoprotease with Unique Properties. *Biochem. J* **1997,** *321*, 587-593.

234. Kwiatkowska et. al. unpublished results. It is important to mention that in our previous studies half time values were reported based on a method using 0.50 g/Lconcentrations of peptides, which could potentially inhibit some proteases and/or compete for the degradation. In the present study, we utilized a more sensitive method based on UPLC-MS detection, which allows us to reduce the final concentration of peptides to 50 μg/L thus obtaining more reliable half times. Obviously, the obtained results for two methods are incomparable.

235. Wimley, W. C.; White, S. H., Experimentally Determined Hydrophobicity Scale for Proteins at Membrane Interfaces. *Nat. Struct. Biol.* **1996,** *3*, 842-848.

236. White, S. H.; Wimley, W. C., Hydrophobic Interactions of Peptides with Membrane Interfaces. *Biochimica et Biophysica Acta (BBA) - Reviews on Biomembranes* **1998,** *1376*, 339-352.

237. Futaki, S.; Nakase, I., Cell-Surface Interactions on Arginine-Rich Cell-Penetrating Peptides Allow for Multiplex Modes of Internalization. *Acc. Chem. Res.* **2017,** *50*, 2449-2456.

238. Bechara, C.; Sagan, S., Cell-Penetrating Peptides: 20years Later, Where Do We Stand? *FEBS Lett.* **2013,** *587*, 1693-1702.

239. Rydberg, H. A.; Matson, M.; Åmand, H. L.; Esbjörner, E. K.; Nordén, B., Effects of Tryptophan Content and Backbone Spacing on the Uptake Efficiency of Cell-Penetrating Peptides. *Biochemistry* **2012,** *51*, 5531-5539.

240. Maiolo, J. R.; Ferrer, M.; Ottinger, E. A., Effects of Cargo Molecules on the Cellular Uptake of Arginine-Rich Cell-Penetrating Peptides. *Biochim. Biophys. Acta* **2005,** *1712*, 161-172.

241. Eksteen, J. J.; Ausbacher, D.; Simon-Santamaria, J.; Stiberg, T.; Cavalcanti-Jacobsen, C.; Wushur, I.; Svendsen, J. S.; Rekdal, Ø., Iterative Design and in Vivo Evaluation of an Oncolytic Antilymphoma Peptide. *J. Med. Chem.* **2017,** *60*, 146-156.

242. Hung, L.-C.; Jiang, I.; Chen, C.-J.; Lu, J.-Y.; Hsieh, Y.-F.; Kuo, P.-H.; Hung, Y.-L.; Wang, L. H.-C.; Chang, M. D.-T.; Sue, S.-C., Heparin-Promoted Cellular Uptake of the Cell-Penetrating Glycosaminoglycan Binding Peptide, Gbpecp, Depends on a Single Tryptophan. *ACS Chem. Biol.* **2017,** *12*, 398-406.

243. Jafari, M.; Karunaratne, D. N.; Sweeting, C. M.; Chen, P., Modification of a Designed Amphipathic Cell-Penetrating Peptide and Its Effect on Solubility, Secondary Structure, and Uptake Efficiency. *Biochemistry* **2013,** *52*, 3428-3435.

244. Bechara, C.; Pallerla, M.; Zaltsman, Y.; Burlina, F.; Alves, I. D.; Lequin, O.; Sagan, S., Tryptophan within Basic Peptide Sequences Triggers Glycosaminoglycan-Dependent Endocytosis. *FASEB J.* **2013,** *27*, 738-749.

245. Mascotti, D. P.; Lohman, T. M., Thermodynamics of Charged Oligopeptide-Heparin Interactions. *Biochemistry* **1995,** *34*, 2908-2915.

246. Luca, G.; Rossella De, M.; Lucia, C., Chemical Modifications Designed to Improve Peptide Stability: Incorporation of Non-Natural Amino Acids, Pseudo-Peptide Bonds, and Cyclization. *Curr. Pharm. Des.* **2010,** *16*, 3185-3203.

247. Kouretova, J.; Hammamy, M. Z.; Epp, A.; Hardes, K.; Kallis, S.; Zhang, L.; Hilgenfeld, R.; Bartenschlager, R.; Steinmetzer, T., Effects of Ns2b-Ns3 Protease and Furin Inhibition on West Nile and Dengue Virus Replication. *J. Enzyme Inhib. Med. Chem.* **2017,** *32*, 712-721.

248. Weigel, L. F.; Nitsche, C.; Graf, D.; Bartenschlager, R.; Klein, C. D., Phenylalanine and Phenylglycine Analogues as Arginine Mimetics in Dengue Protease Inhibitors. *J. Med. Chem.* **2015,** *58*, 7719-7733.

249. Stoermer, M. J.; Chappell, K. J.; Liebscher, S.; Jensen, C. M.; Gan, C. H.; Gupta, P. K.; Xu, W.-J.; Young, P. R.; Fairlie, D. P., Potent Cationic Inhibitors of West Nile Virus Ns2b/Ns3 Protease with Serum Stability, Cell Permeability and Antiviral Activity. *J. Med. Chem.* **2008,** *51*, 5714-5721.

250. Adamczyk, M.; Akireddy, S. R.; Reddy, R. E., Enantioselective Synthesis of (2-Pyridyl)Alanines Via Catalytic Hydrogenation and Application to the Synthesis of L-Azatyrosine. *Org. Lett.* **2001,** *3*, 3157-3159.

251. Ahmed, S. T.; Parmeggiani, F.; Weise, N. J.; Flitsch, S. L.; Turner, N. J., Synthesis of Enantiomerically Pure Ring-Substituted L-Pyridylalanines by Biocatalytic Hydroamination. *Org. Lett.* **2016,** *18*, 5468-5471.